WNK Kinases: Novel Regulators of Electrolyte Balance and Blood Pressure

Michelle O'Reilly

A thesis submitted in partial fulfilment of the requirements of the Degree of Doctor of Philosophy awarded by the University of Edinburgh

2006

EDINBURGH UNIV. BIOL.

Declaration

I hereby declare that this thesis and the work presented herein are entirely the result of my own independent investigation except where otherwise stated. This work has not been and is not concurrently submitted for any other degree.

Acknowledgements

I would like to thank my supervisors Dr. Roger W. Brown and Professor Jean Beggs for their guidance, encouragement and support throughout my PhD. I am indebted to everyone in the Department of Endocrinology for their unrelenting patience, advice, scientific input and continuous support, in particular Elaine Marshall, Chris J. Kenyon, Julie Nixon, Karen Chapman, June Noble, Lynne Ramage, Karen French, Manish Mittal, and Wei Xue. I am particularly grateful for the administrative support of Elaine Smith, Lisa Mills and Heather Laing. I would like to acknowledge Angie Fawkes and Thomas MacGillivray from the Wellcome Trust Clinical Research Facility for their assistance with real-time PCR and image analysis, respectively, and the staff at the BRF particularly William Mungan and Sharon Rossitor, for their assistance and advice.

I am also particularly indebted to the Welcome Trust for funding and supporting me over the course of my PhD studies.

Finally I would like to thank my family and friends, especially my parents for their continual support and belief in my ability.

Table of Contents

Abstract

In 2001 mutations in WNK1 (With-No-K, lysine) and WNK4 were linked to the dominant, hypertensive, hyperkalemic disorder, Gordon syndrome. Although a mystery for many years, the basis of this unusual disorder, having concurrent Na^+ and K^+ retention, promised to yield valuable insights into the causes of essential hypertension (thiazide diuretics are first-line treatments for both). The association of mutations in WNK1 and WNK4 with Gordon syndrome was a major breakthrough also implicating these novel serine/threonine kinases in the regulation of electrolyte balance and blood pressure (BP). Thus, elucidation of the novel pathway in which these WNK kinases participate should lead to fundamental advances in our understanding of these phenomena.

When the studies of this thesis began only very limited findings were reported about WNK1 and WNK4, and so to begin to understand how this pathway might function, particularly *in vivo*, it was important to examine the expression of the genes involved. *In situ* hybridization and PCR studies revealed tissue-specific splicing for WNK1 and widespread, intricate regulation of WNK1 and WNK4 expression during development involving both epithelial and non-epithelial tissues. The importance of this expression is highlighted by the WNK1-/- mouse which is embryonic lethal by mid-gestation. A survey of the distribution of WNK1 and WNK4 across adult mouse tissues by Northern blot strikingly highlighted the unique qualities of how the WNK pathway is expressed in kidney. Thus, kidney has by far the strongest expression of WNK4 of any major organ. Moreover, whilst WNK1 is widely expressed, the kidney has an additional kidney-specific smaller WNK1 transcript. Thus, the high levels of WNK4 and this smaller WNK1 transcript seemed likely to be linked to how mutations in this pathway have crucial consequences in kidney altering electrolyte handling and BP. Accordingly, detailed studies of the nature and expression of these WNK gene transcripts were undertaken. These showed that rather than merely being a polyA-tail variant the short kidney-specific WNK1 transcript (WNK1-S) actually differed from the longer widely distributed transcript (WNK1-L) in a much more functionally significant way. It lacked the first four coding exons yielding a predicted protein missing the kinase domain. Establishing that in kidney, transcription of the

WNK1 gene differed from elsewhere and a kinase deficient WNK1 product would predominate, demanded a revision of ideas as to how mutations of this gene might cause autosomal dominant disease. Thus, it became apparent that the WNK pathway at least in kidney may involve features beyond a simple kinase cascade, shifting the focus of research on this pathway.

Reports of *in vitro* interactions between WNK4 and/or WNK1 and a number of renal electrolyte transporters have been flooding into the literature implying a surprising diversity of possible regulatory roles of these genes in electrolyte balance. Detailed localization studies, undertaken as part of this thesis, show that WNK1-S and WNK4 are highly expressed in distal convoluted tubule (DCT) and connecting tubule (CNT), adjacent distal nephron segments known to play key roles in electrolyte balance and BP control. Additional novel domains of substantial WNK4 expression were found in thick ascending limb (TAL; including *macula densa*), while WNK1-L was uniformly expressed at low-level throughout kidney. These findings indicate that the spectrum of WNK interacting partners may be determined largely by their local renal distributions, a factor which is frequently overlooked at present.

Having established the steady-state expression of this pathway in kidney, work then extended to investigating how the WNK pathway, and genes likely linked to it, respond to dynamic changes in renal K^+, Na^+ and Cl^- load and aldosterone level. This work has revealed key dietary electrolyte and aldosterone driven transcriptional regulation of elements of the WNK pathway and the renal outer medullary K^+ channel (ROMK), leading to better understanding of how this pathway may participate in the *in vivo* regulation of electrolyte balance and BP. Specifically, upregulation of WNK1-S and WNK4 was found with high K^+ intake, which via inhibition of the thiazide sensitive NaCl cotransporter (NCC) and enhanced distal Na^+ delivery would facilitate enhanced K^+-excretion needed in response to high K^+ intake. As K^+ intake drops, the WNK pathway modulation of K^+ balance coordinates with H^+/K^+-ATPase and striking reciprocal ROMK isoform-specific expression changes in a way which would allow fine regulation of K^+ and acid-base balance. As chronic NaCl intake drops to low levels there may be regulation of WNK gene

expression limiting NaCl excretion. These *in vivo* findings, in conjunction with clues from reported *in vitro* functional studies, allow the development of a model of how the WNK pathway may function in an integrated way which fits well with normal renal electrolyte handling and also how this is altered in treatment with thiazide diuretics or when mutated in Gordon syndrome.

List of Figures

List of Tables

List of Abbreviations

11βHSD	11β-hydroxysteroid dehydrogenase
ACE	Angiotensin converting enzyme
ADP	Adenosine diphosphate
Adx	Adrenalectomy
Aldo	Aldosterone
AME	Apparent mineralocorticoid excess
Ang	Angiotensin
ANOVA	Analysis of variance
ATP	Adenosine triphosphate
BNX	Bilateral nephrectomy
BP	Blood pressure
BSA	Bovine serum albumin
CCD	Cortical CD
CCT	Cortical collecting tubule
CD	Collecting duct
cDNA	Complementary deoxyribonucleic acid
CFEX	Cl^-/Formate (anion) exchanger
cHKA	Colonic H^+/K^+-ATPase pump
CLCKB	Chloride channel kidney B
CNS	Central nervous system
CNT	Connecting tubule
Cort	Corticosterone
Cre	Creatinine
cTAL	Cortical TAL
C-ter	C-terminus
CTP	Cytosine triphosphate
Ctrl	Control
DAB	Diaminobenzidine tetrahydrochloride
DBP	Diastolic BP
DCT	Distal convoluted tubule
DEPC	Diethylpyrocarbonate
DTT	Dithiothreitol
ECF	Extracellular fluid volume
eGFP	Enhanced green fluorescent protein
ELISA	Enzyme linked immunosorbent assay
ENaC	(Amiloride sensitive) Epithelial Na^+ channel
EST	Expressed sequence tag
FAM	6-carboxyfluorescin
FHHt	Familial hyperkalaemic hypertension
GFR	Glomerular filtration rate
GRH	Glucocorticoid remediable hypertension
GTP	Guanidine triphosphate
HA	High aldosterone
HEK293 cells	Human embryonic kidney 293 cells
HK	High K^+
HNa	High Na^+

HRP	Horseradish peroxidase
iCCT	Initial CCT
Ig	Immunoglobulin
IGF	Insulin growth factor
IMCD	Inner medullary CD
ISH	*In situ* hybridisation
KLH	Keyhole limpet hemacyanin
LA	Low aldosterone
LK	Low K^+
LNa	Low Na^+
MCD	Medullary CD
MDCK cells	Madin-Darby kidney cells
MP	Mini-pump
MR	Mineralocorticoid receptor
mRNA	messenger RNA
mTAL	Medullary TAL
NCC	(Thiazide sensitive) NaCl cotransporter
Nedd4-2	Neural precursor cell expressed developmentally downregulated 4-2
NH	Northern hybridisation
NK	Normal K^+
NKCC1	$Na^+/K^+/2Cl^-$ cotransporter-1 (basolateral)
NKCC2	$Na^+/K^+/2Cl^-$ cotransporter-2 (apical)
NNa	Normal Na^+
NS	Non-significant
OMCD	Outer medullary CD
OMIM	Online mendelian inheritance in man
ORF	Open reading frame
OSR1	Oxidative stress responsive1
PAGE	Polyacrylamide gel electrophoresis
PBS	Phosphate buffered saline
PCR	Polymerase chain reaction
PDK	Phosphoinositide-dependent kinase
PDZ domain	Domain present in PSD-95, Dlg, and ZO-1/2
PHA	Pseudohypoaldosteronism
PI-3-kinase	Phosphatidylinositol-3-kinase
PKB	Protein kinase B
polyA	Polyadenylation
PRA	Plasma renin activity
PRC	Plasma renin concentration
QTL	Quantitative trait locus
RAAS	Renin angiotensin aldosterone system
RIA	Radioimmunoassay
RNA	Ribonucleic acid
ROMK	Renal outer medullary K^+ channel
ROMK-T	ROMK-total
RT	Reverse transcription
RT-PCR	Reverse transcriptase PCR

SBP	Systolic BP
SDS	Sequence detection systems
SDS	Sodium dodecyl sulphate
SGK	Serum glucocorticoid kinase
SH3	Src homology 3
SHR	Spontaneously hypertensive rat
SNP	Single nucleotide polymorphism
SPA	Scintillation proximity assay
SPAK	Ste-20-related praline-alanine-rich kinase
SPF	Specific pathogen free
SRE	Steroid response element
SSC	Saline sodium citrate
Syt	Synaptotagmin
TAL	Thick ascending limb of the loop of *Henlé*
TAMRA	6-carboxytetramethyrhodamine
TBE	Tris borate EDTA
TBP	TATA-box binding protein
TBS	Tris buffered saline
TE	Tris EDTA
TER	Transepithelial resistance
tRNA	transfer RNA
TRPV4	Transient receptor potential vanilloid 4
UTP	Uridine triphosphate
WF	Wingful
WNK	With No K (lysine)
WNK1-L	WNK1-long
WNK1-S	WNK1-short
WNK1-T	WNK1-total

Publications from this Thesis

O'Reilly M, Marshall E, MacGillivray T, Mittal M, Xue W, Kenyon CJ, and Brown RW: "Dietary electrolyte driven responses in the renal WNK kinase pathway in vivo". *J Am Soc Nephrol.* 2006 Sept;17(9):2402-13.

O'Reilly M, Marshall E, Speirs HJ, and Brown RW: "WNK1, a gene within a novel blood pressure control pathway, tissue-specifically generates radically different isoforms with and without a kinase domain." *J Am Soc Nephrol.* 2003 Oct;14(10):2447-56.

Chapter 1 Introduction.

1.1 Electrolyte Balance and BP Control

1.1.1 Epithelial Transport: Transcellular and Paracellular Pathways

The primary function of epithelial cells in all organs of higher organisms is to partition extracellular compartments of different composition. The flux of electrolytes across a polarised epithelium is a highly regulated process (Figure 1.1(a)), with permeating species traversing by either the transcellular route through cells or the paracellular route between cells (reviewed in[130]). Transcellular transport is mediated by specialised channels, exchangers, cotransporters and pumps typically found differentially expressed between the apical and basolateral surfaces of polarised epithelial cells (Figure 1.1(b)). Transport between cells is more obscure but it is well established that tight junctions between epithelial cells form the major barriers regulating diffusion through the paracellular pathway. The tight junction also prevents the lateral diffusion of integral membrane proteins, including those involved in the transcellular pathway, thereby functionally dividing the apical and basolateral membrane domains. Tight junctions of different epithelia vary in tightness and show charge and size selectivity in their permeability. Recent work has demonstrated the key role of the Claudin family of tight junction proteins in determining paracellular permeability (reviewed in[120;136]). Transepithelial transport is particularly important in the kidney where it regulates whole body fluid, electrolyte homeostasis and BP.

1.1.2 BP Control in Kidney

High BP or hypertension affects 20-25% of the adult population in industrialized countries, contributing to morbidity and mortality from stroke, myocardial infarction, congestive heart failure, and renal failure[98]. Despite its major importance, very little is understood about the causes of essential hypertension. Over 30 years ago, Guyton hypothesised that control of BP in the steady-state and on a long-term basis is critically dependent on renal mechanisms[44;45]. It is now well established that the normal regulation of electrolyte handling in the distal nephron of kidney (importantly Na^+, Cl^- and K^+ ions) is required for normal long-term BP control.

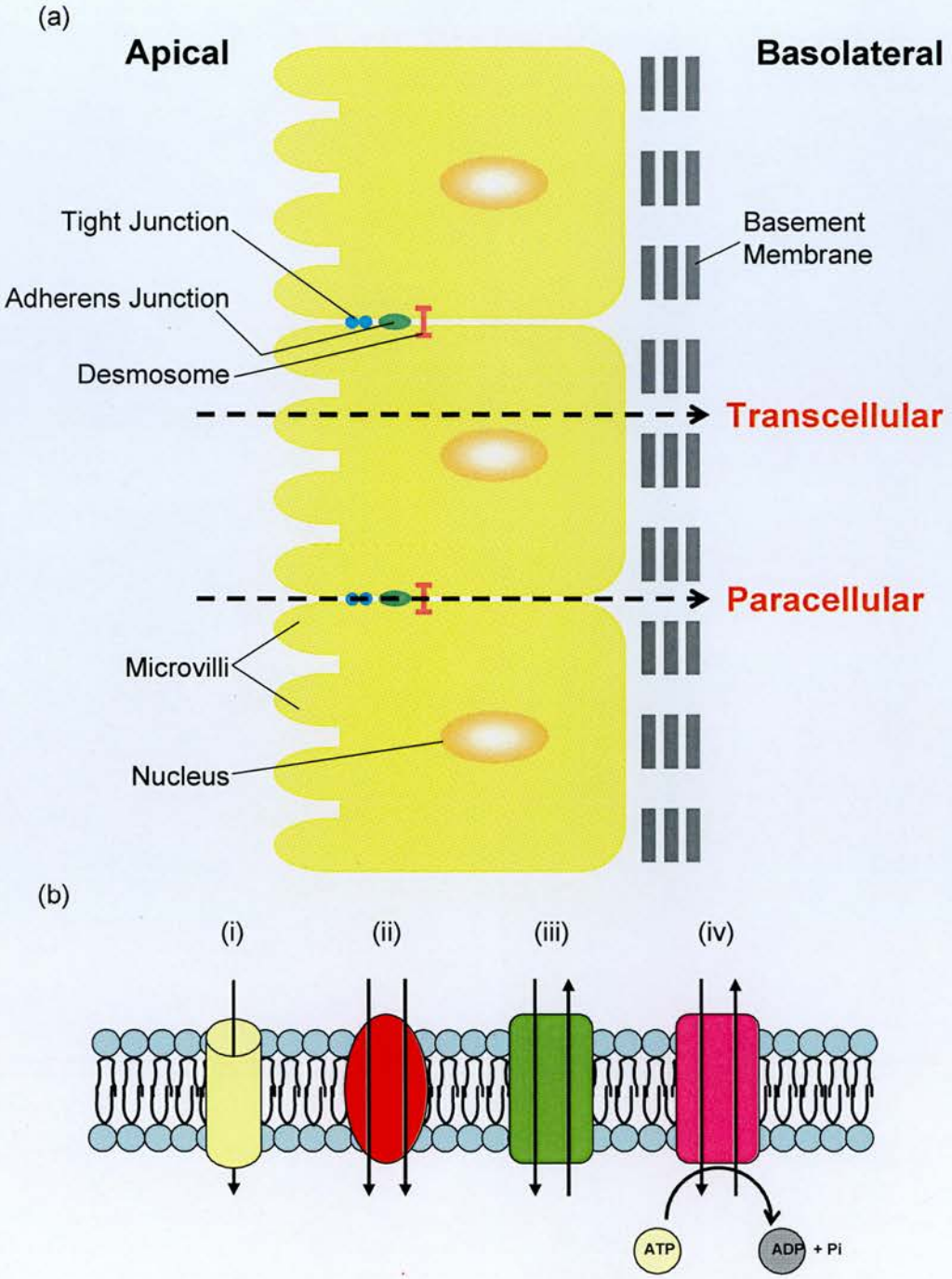

Figure 1.1: Schematic representation of transepithelial transport. (a)Epithelial cells establish apical contacts with neighbouring epithelial cells through a tripartite junctional complex to form an epithelium. This tripartite junctional complex consists of the tight junction, the adherens junction, and the desmosome. Electrolyte transport across a polarised epithelium occurs by either the transcellular route through cells or the paracellular route between cells. The tight junction forms the major barrier to the paracellular transport of electrolytes. (b)Transcellular transport is mediated by (i)specialised channels, (ii)cotransporters, (iii)exchangers, and (iv)energy-coupled pumps found on the apical and basolateral surfaces of epithelial cells.

1.1.3 Electrolyte Balance in Distal Nephron

The kidney filters ~170 litres of plasma daily containing ~23 mol salt. More than 99.5% of this filtered salt must be reabsorbed to maintain homeostasis. The bulk (~60%) of the filtered Na^+ is reabsorbed in the proximal tubule and a further 30% is reabsorbed in TAL. The remainder is recovered in DCT, CNT and the collecting duct (CD; Figure 1.2). NaCl reabsorption in DCT-CD is driven by basolateral Na^+/K^+-ATPase in conjunction with two major apical pathways. Firstly, electroneutral cotransport by NCC (encoded by SLC12A3; Figure 1.3(a)), a member of the cation-chloride cotransporter gene family (SLC12), which mediates the reabsorption of 3-7% of the total filtered NaCl across the apical surface of epithelial cells of DCT. The second pathway involves electrogenic Na^+ reabsorption in the late DCT (DCT2), CNT and CD through the amiloride-sensitive epithelial Na^+ channel (ENaC; a tetrameric ($\alpha_2\beta\gamma$) channel composed of α, β, and γ subunits encoded by SCNN1A, SCNN1B, and SCNN1G, respectively) accompanied by largely paracellular Cl^- flux (Figure 1.3(b))[95].

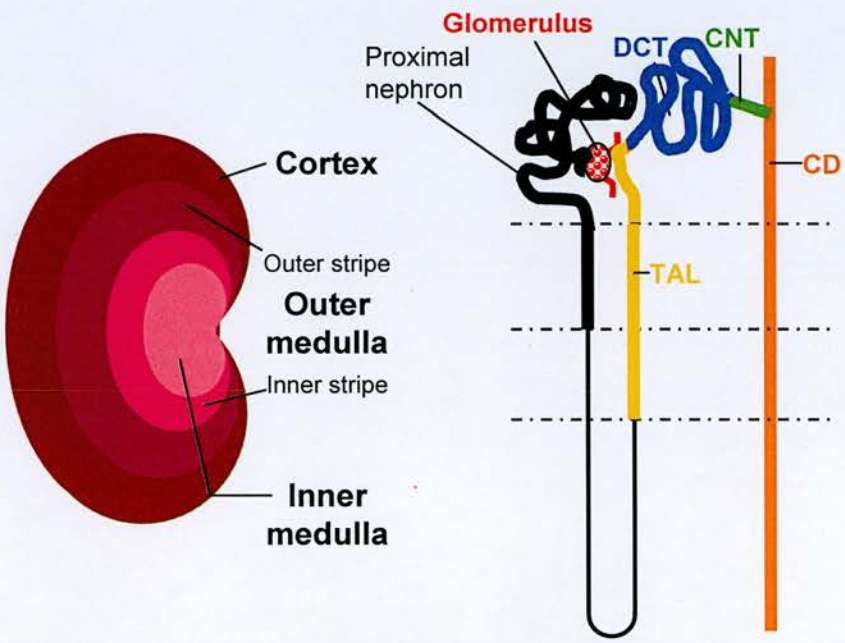

Figure 1.2: Schematic depiction of kidney and nephron structure. (a) Saggital section through the kidney illustrating the cortical, outer medullary (subdivided into outer stripe and inner stripe) and inner medullary regions. (b) The nephron (functional unit of the kidney) is illustrated, highlighting the distal nephron segments: TAL (yellow), DCT (blue), CNT (green) and CD (yellow).

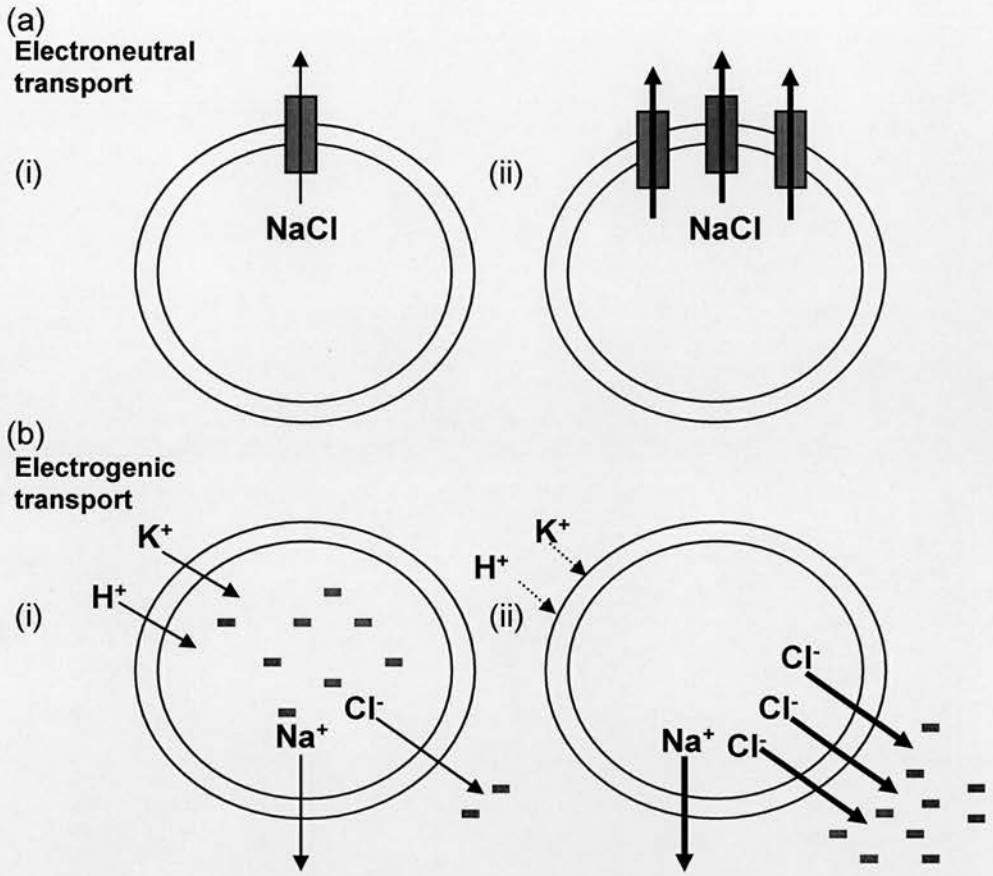

Figure 1.3: Schematic depiction of electroneutral and electrogenic transport. (a)(i)Electroneutral transport occurs in DCT whereby NaCl is reabsorbed from the tubular lumen via NCC. (ii)Overactivity of NCC would create a transcellular shunt in DCT, resulting in excess NaCl reabsorption in this segment and reduced distal Na^+ delivery. (b)(i)Electrogenic reabsorption occurs in DCT2-CD, whereby Na^+ is reabsorbed via ENaC, in association with a paracellular Cl^- flux. This generates a lumen negative charge which facilitates K^+ and H^+ excretion. (ii)Excessive or "leaky" paracellular Cl^- transport ("paracellular Cl^- shunt") would deplete the lumen negative charge, thereby diminishing the electrochemical driving force for K^+ and H^+ excretion.

Maintenance of the body's unequal distribution of K^+ between the intra- and extracellular compartments is essential for many fundamental cellular functions and is critical to normal electrical polarization of the cell. Mechanisms regulating the transport of K^+ (and NaCl) between intracellular and extracellular compartments play an important role at times in smoothing and damping short-term swings in electrolyte and fluid balance which naturally occur on occasions such as after ingesting a meal. However these mechanisms are of relatively short-term importance and it is the kidney which is principally responsible for determining K^+ balance over hours, days and in the longer-term. In the kidney the bulk of filtered K^+ is reabsorbed in proximal

nephron segments, with tightly regulated K^+ secretion, occurring in DCT2-CD (principally in the CNT and CCD), largely determining K^+ balance[82]. Electrogenic Na^+ reabsorption by ENaC provides a "lumen negative" driving force for K^+ secretion (Figure 1.3(b)), occurring primarily via the inwardly rectifying ROMK channel (Kir1.1; encoded by KCNJ1). Remarkably, during K^+ depletion, the CNT-CD switches from a largely K^+ secreting segment to a site of K^+ reabsorption. In severe K^+ restriction several attendant processes assist in renal function with minimal K^+, including the production and recycling of NH_4^+, an ion which can substitute for K^+ to maintain key transport of NaCl by NKCC2 ($Na^+/K^+/2Cl^-$ cotransporter-2) and Na^+/K^+-ATPase[41;141]. The role of NH_4^+ in electrolyte homeostasis, particularly K^+ and acid-base balance, is discussed in greater detail in Chapter 9.

Although in quantitative terms the DCT-CD distal nephron segments make a minority contribution to renal NaCl reabsorption (≤10%), they nonetheless normally have the primary role in determining net NaCl and K^+ balance as Na^+ reabsorption and K^+ secretion are closely regulated in the distal nephron and this is the major determinant of the final excretion of these electrolytes from the body.

1.1.3.1 Renin Angiotensin Aldosterone System (RAAS)

In health, the renin-angiotensin-aldosterone system (RAAS; Figure 1.4) powerfully assists in the maintenance of circulatory homeostasis with key effects on vascular tone and in determining renal NaCl and K^+ handling, with a major influence on distal nephron. Lower circulatory filling and pressure are sensed through: higher autonomic (baroreceptor) reflex stimulation; reduced renal afferent arteriolar stretch and/or altered NaCl delivery to the *macula densa*. These specific physiological stimuli signal to trigger secretion of the aspartyl protease renin from specialised afferent arteriole cells forming part of the juxtaglomerular apparatus. Renin cleaves circulating angiotensinogen releasing a decapeptide, angiotensin I. This is converted to an octapeptide, angiotensin II, in the lung by angiotensin converting enzyme (ACE). This potent short peptide has several important actions including binding to its receptor in the *zona glomerulosa* of the adrenal cortex and inducing the secretion of the mineralocorticoid hormone, aldosterone. Binding of aldosterone to the

mineralocorticoid receptor (MR), a nuclear hormone receptor found in principal cells of the distal nephron, initiates a sequence of events leading to increased activity of ENaC, thereby upregulating salt reabsorption (Figure 1.5)[95].

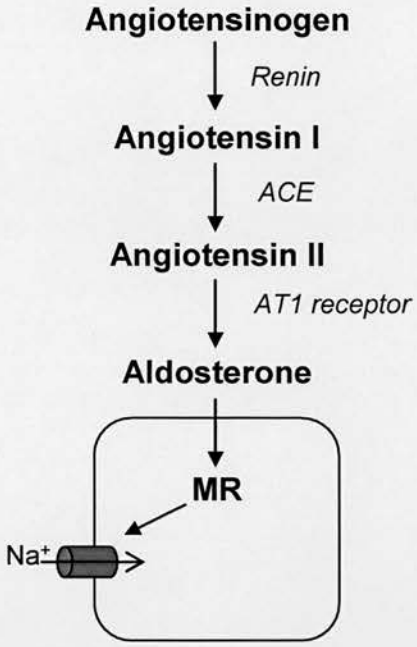

Figure 1.4: Overview of the Renin-Angiotensin-Aldosterone System.
The aspartyl protease renin is released from the juxtaglomerular apparatus (cells of the afferent and efferent arterioles of the glomerulus) in response to specific signals. Renin cleaves circulating angiotensinogen releasing a decapeptide, angiotensin I. This is converted to an octapeptide, angiotensin II, in the lung by ACE. This short peptide hormone binds to its AT1 receptor in the *zona glomerulosa* of the adrenal cortex and induces the secretion of the mineralocorticoid hormone, aldosterone. Binding of aldosterone to MR, found in particular in late DCT, CNT and principal cells of the distal nephron, initiates a sequence of events leading to increased activity of ENaC, thereby upregulating salt reabsorption.

Aldosterone secretion is stimulated in two different physiological states: hypovolemia, triggering increased renin secretion and angiotensin II action as just described; and hyperkalaemia, directly stimulating adrenal aldosterone secretion, thereby promoting increased K^+ secretion. How the kidney differentiates between these two high aldosterone states so that in the first there is powerful stimulation principally of NaCl reabsorption, but in the second potassium secretion is strongly augmented remains poorly understood[14].

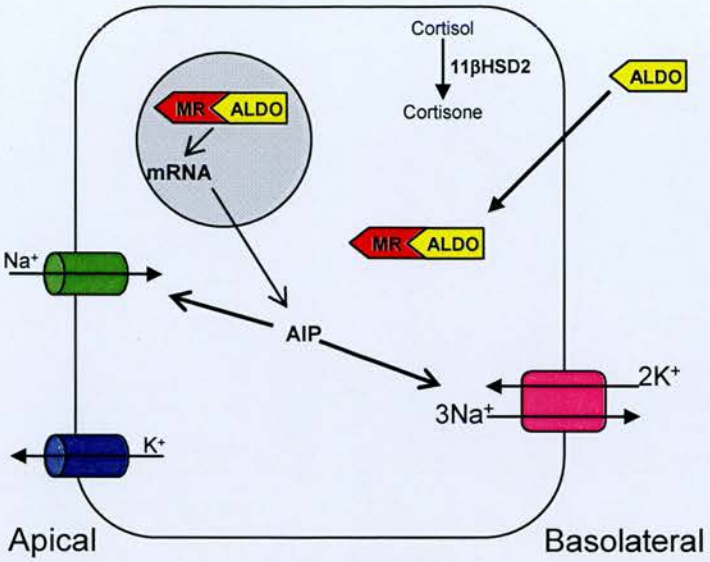

Figure 1.5: Mechanism of aldosterone action. Aldosterone (ALDO) traverses the plasma membrane and binds to its cytosolic receptor, MR. The receptor-hormone complex translocates to the nucleus, where it interacts with steroid response elements (SREs) within the promoter region of target genes activating or repressing their transcriptional activity. Aldosterone-induced or –repressed proteins (AIPs or ARPs) mediate an increase in transepithelial sodium transport by increasing the activity and/or number of transport proteins (e.g. ENaC, Na/K-ATPase) in the plasma membrane. 11β-Hydroxysteroid Dehydrogenase 2 (11β-HSD2) converts cortisol to cortisone, thus preventing occupancy of MR by cortisol.

1.1.4 Single gene disorders of electrolyte balance and BP

Inappropriate transepithelial transport can lead to disease and this is particularly evident in kidney disorders. Molecular genetic studies have recently identified a number of rare Mendelian disorders of both electrolyte balance and BP, in which single gene mutations alter normal transepithelial transport in the distal nephron[67;77]. Although rare these disorders have been disproportionately valuable in our understanding of electrolyte balance and hypertension. Most of these disorders have a related phenotype, having either hypertension with hypokalaemia or the opposite, hypotension with hyperkalaemia. The gradual cloning and characterisation of the genes associated with these disorders revealed they function in a common pathway in kidney, the RAAS pathway, explaining the related phenotype in these disorders (Figure 1.6 and Table 1.1) and highlighting the importance of the nephron segments in which they are expressed in Na^+ and K^+ balance.

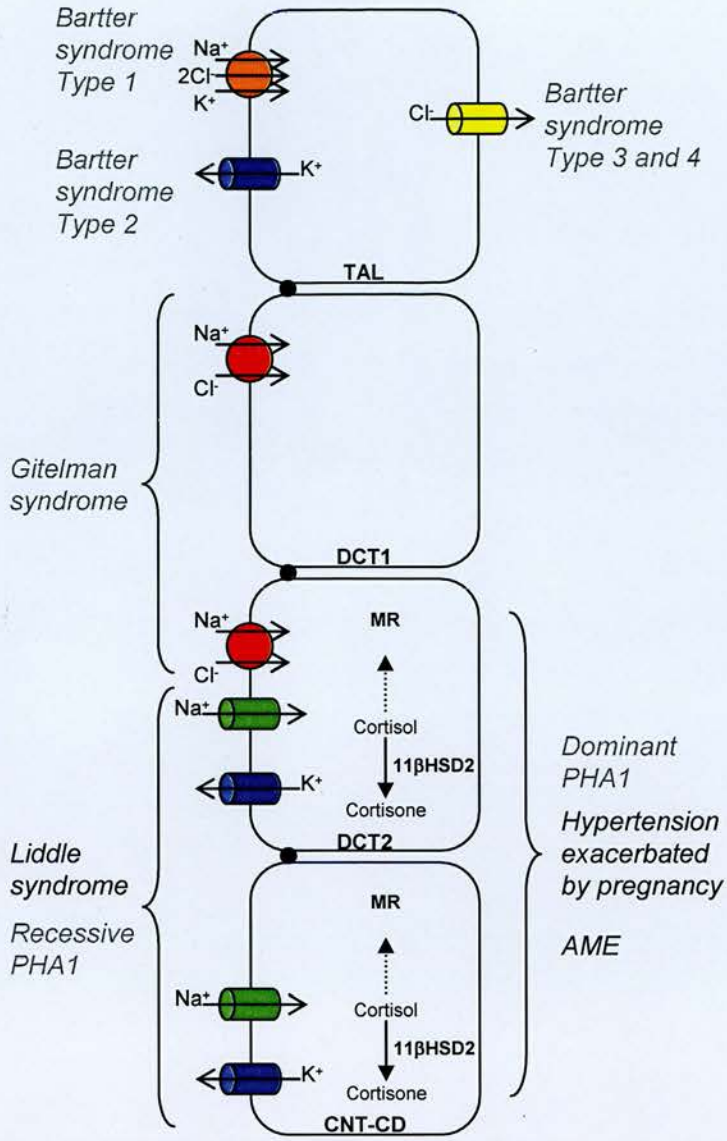

Figure 1.6: Single gene disorders of BP associated with the distal nephron. Loss-of-function mutations in NCC in DCT cause Gitelman's syndrome[128]; loss-of-function mutations in either NKCC2[126], ROMK[127], or CLCkb[125] in TAL cause Bartter syndrome; gain of function mutations in β or γENaC in DCT2-CD cause Liddle syndrome[46;123], while loss-of–function mutations in α, β, or γENaC cause Pseudohypoaldosteronism Type 1 (PHA 1, recessive); loss-of-function mutations in 11β-HSD2 in DCT2-CD cause Apparent Mineralocorticoid Excess (AME)[99]; loss-of-function mutations in MR in DCT2-CD cause PHA1 (autosomal dominant)[39], while gain-of-function mutations in MR cause Hypertension Exacerbated in Pregnancy[38].

A number of these genes have also been modified in transgenic mouse models, reproducing the human disease phenotype and further highlighting the importance of these distal nephron segments in electrolyte balance[72;115;132]. In addition, some of the most powerful and effective BP treatments target these nephron segments, for example, loop and thiazide diuretics act in TAL and DCT, respectively;

spironalactone and amiloride act in DCT2-CCD (cortical collecting duct). A study by Majid *et al.* also identified regulation of Na^+ reabsorption by NCC in DCT, as the major contributor to BP[81]. Thus, the adjacent distal nephron segments, TAL-CD, play a powerful role in long-term regulation of electrolyte balance, extracellular fluid (ECF) volume and BP.

Table 1.1: Single gene disorders of electrolyte balance and BP.

DISORDER	PHENOTYPE	SITE	CAUSE
GRH	↑BP ↓K^+	CD	Aldo Synthase
Liddle syndrome	↑BP ↓K^+	CD	ENaC
AME	↑BP ↓K^+	CD	11βHSD2
Gordon syndrome	↑BP ↑K^+	?DCT?	WNK1, WNK4
PHA I	↓BP ↑K^+	CD	ENaC

1.2 Gordon syndrome

1.2.1 Features of Gordon syndrome

The study of such rare inherited diseases has led to the identification of novel components of important regulatory networks maintaining normal electrolyte balance and BP. Gordon syndrome (pseudohypoaldosteronism type II (PHA II); familial hyperkalaemia and hypertension (FHHt); Online Mendelian Inheritance in Man, OMIM, #145260), one such rare disorder, is an autosomal dominant disease featuring hypertension (attributed to increased renal NaCl reabsorption) with hyperkalaemia (due to impaired renal K^+ excretion) despite a normal glomerular filtration rate (GFR)[42;43;112]. Thus the Gordon syndrome phenotype is quite distinct from other Mendelian hypertensive disorders in which serum potassium is either normal or low (Table 1.1). This unusual feature suggests combined K^+ and NaCl retention in Gordon syndrome. This also indicates that a novel pathway distinct from the aldosterone pathway may be involved, as classically changes in aldosterone affect BP (NaCl) and K^+ in a reciprocal manner.

Hyperchloremic metabolic acidosis is a variable associated finding, and is due to a significant decrease in urinary H^+ excretion. In addition, patients have suppressed plasma renin activity. Plasma aldosterone varies from low normal to high normal (reviewed by[42]), but is often referred to as inappropriately low with respect to the observed high level of plasma potassium, a strong stimulus of aldosterone secretion. Additional features, including retarded growth, intellectual impairment, and muscle weakness (reviewed by[42]), have been associated with some cases of Gordon syndrome. The clinical manifestations of Gordon syndrome are chloride dependent (corrected when infusion of sodium sulphate or sodium bicarbonate is substituted for sodium chloride), and are largely treated with low doses of thiazide diuretics (also a first-line treatment in essential hypertension), specific antagonists of NCC, in DCT[13;43;119].

1.2.2 Proposed Mechanisms Underlying Gordon syndrome

Based on clinical studies in affected patients, two major pathophysiological mechanisms have been proposed to explain Gordon syndrome (reviewed in[37]). The first potential mechanism is based on increased paracellular reabsorption of Cl^-, also known as the "paracellular chloride shunt" hypothesis (Figure 1.3(b)). This chloride shunt plays a major role in NaCl and K^+ homeostasis in CNT and CD, where it has been suggested that 70% of Cl^- reabsorption may occur via the paracellular pathway[122]. However, until recently, a lack of understanding of the molecular architecture of the tight junction, the barrier to paracellular flux, has slowed down the advancement of this hypothesis. The second proposed mechanism is based on overactivity of the thiazide-sensitive NCC (Figure 1.3(a)). Despite this, genome-wide analysis of linkage in Gordon syndrome families revealed no linkage with SLC12A3 encoding NCC, but instead demonstrated locus heterogeneity; mapping three disease loci, to chromosomes 1q31-42[85], 17p11-q21[85] and 12p13[26]. This underscores the heterogeneity of the clinical phenotype[42]. Three families have also been reported that are not linked to any of these loci, suggesting a fourth unidentified locus[27]. A breakthrough by Wilson *et al.* in 2001 identified the genes encoding for two members of a novel protein kinase family, WNK1 and WNK4, as the two genes underlying Gordon syndrome linked to chromosomes 12 and 17, respectively[148].

1.2.3 Identification of Mutations Underlying Gordon syndrome

1.2.3.1 Intronic Deletions in WNK1

In 2001, Wilson *et al.* showed that a Gordon syndrome kindred with complete linkage to the chromosome 12p13 region co-segregated with a 41kb deletion within the large first intron of a recently described novel kinase, WNK1[148]. Analysis of a second Gordon syndrome kindred revealed a 21kb deletion contained within the same intronic region of WNK1. No mutations in WNK1 coding sequence were detected in these or sixteen other Gordon syndrome kindreds.

Wilson and colleagues reported a 5-fold increase in the level of WNK1 transcripts, measured by real-time RT-PCR analysis, of peripheral leukocyte RNA in Gordon syndrome patients compared to unaffected controls, providing evidence that the intronic deletion alters WNK1 gene expression. Based on these findings it was postulated that Gordon syndrome could result from "gain-of-function" WNK1 mutations that increase WNK1 activity[148]. In keeping with this, a gene trap study in 2003 demonstrated that heterozygote WNK1 deficient mice suffered a reduction in BP of ~12 mmHg, with no notable pathological changes in kidney. Interestingly, blood chemistry and urinalysis results demonstrated normal kidney function, and a three week low salt diet (0.01% NaCl) treatment failed to induce a significant difference in water and food intake or urinary output between heterozygote and wild-type animals. These results demonstrate that WNK1 is a regulator of BP but also suggest that WNK1 haploinsufficiency may not affect the ability of mice to conserve electrolytes in response to a low salt diet[165].

1.2.3.2 Missense Mutations in WNK4

Subsequent genomic sequence and EST database searches revealed that a WNK1 paralog, WNK4, localised to the genetic interval containing the Gordon syndrome locus on chromosome 17. Examination of WNK4 in Gordon syndrome kindreds identified four charge-altering missense mutations, all of which co-segregated with the disease. Three of these mutations cluster in a span of four amino acids just distal to the first of two putative coiled-coil domains, within a ten amino acid stretch that is

highly conserved among all members of the WNK kinase family. The fourth mutation lies just distal to the second putative coiled coil domain. These findings implicate WNK1 and WNK4 in a previously unrecognised signalling pathway that regulates the balance between NaCl reabsorption versus K^+ and H^+ secretion[148]. Intriguingly, no WNK or WNK-like gene is located on human chromosome 1q31-42, suggesting that a completely different protein is involved.

1.3 With No K (Lysine) Kinases

1.3.1 Discovery of WNK Kinases

WNK kinases comprise a novel family of ser/thr kinases, which show greatest similarity (approximately 30% sequence identity within the catalytic domain) to sterile-20 (STE-20) kinases. Xu *et al.* cloned and characterised the first WNK kinase, rat WNK1, isolating a 7.2 kb cDNA, encoding a 2126 amino acid protein, from a rat brain cDNA library[151]. The acronym reflects the unusual character of its catalytic domain which lacks an otherwise conserved lysine residue, hence With No K=lysine (WNK). Verissimo and Jordan went on to clone and characterise WNK1 in human, a 251 kDa protein composed of 2382 amino acid encoded in an open reading frame (ORF) of 7149 bp[137]. The degree of identity between human and rat WNK1 is ~86%. Four members of the WNK kinase family, WNK1-4, have been identified so far in humans, located on chromosomes 12, 9, X and 17 respectively[137;148]. It is now believed that WNKs are present exclusively in multicellular eukaryotes, with homologs identified in *Drosophila melanogaster* and *Caenorhabditis elegans*[137] and at least eight homologs identified in *Arabidopsis thaliana*, some of which are believed to contribute to circadian rhythms[100;102].

1.3.2 Atypical WNK Kinase Domain

Protein kinases comprise an important superfamily of enzymes (genome-wide this has been termed a kinome, and has several major branches; see http://198.202.68.14/human/kinome/) that participate in complex signalling networks, regulating many cellular processes ranging from cell cycle control to differentiation. The human protein kinome was recently estimated to possess just over 500 members[84]. Structurally these proteins are extremely heterogeneous but

share high homology over their catalytic core, a region of approximately 250-300 residues organised in twelve subdomains, with several residues that are strictly conserved.

The WNK family is characterised by the replacement of the conserved catalytic lysine residue, found in β strand 3 of subdomain II of almost all known protein kinases, by a cysteine. This specific lysine residue is involved in orientating ATP to facilitate phosphoryl transfer, which is essential for catalytic function. In WNKs the catalytic lysine is located further N-terminally within the glycine-rich string (replacing the third glycine in the GXGXXG motif) in β strand 2 of subdomain I[151]. This was recently confirmed by the crystallisation of the WNK1 kinase domain[94]. Sequence alignment of the catalytic domains of WNK1-4 reveals variations from typical kinase subdomains I and II, similar to WNK1. The overall degree of amino acid sequence identity between the catalytic domains of WNK2, 3 and 4 and that of WNK1 is ~79% [37].

1.3.3 WNK Protein Domains

Besides the highly homologous N-terminal kinase domain, the WNK kinase family also features two conserved coiled-coil domains and a cluster of conserved charged amino acid residues in which mutations in WNK4 have been identified in Gordon syndrome patients. In addition, WNK kinases contain several PXXP motifs, which could potentially interact with SH3 domains of other proteins (described further in Chapter 3)[109;137;148;151].

1.3.4 WNK Protein Kinase Activity

Upon activation by an upstream signal or sometimes a specific combination of signals, protein kinases positively or negatively regulate the activity of downstream target proteins via phosphorylation. Consequently protein kinases are often thought of as molecular switches, rapidly and reversibly responding to specific signals, simultaneously integrating multiple signalling pathways and thereby mediating the appropriate cellular responses.

Most of the initial biochemical knowledge of the WNK kinase family has come through work with WNK1. Initial findings described rWNK1 as a ser/thr kinase[151] whose kinase activity is regulated by two serine residues, located within the WNK activation loop, serine 378 and 382, which have been proposed to be part of an autophosphorylation domain[152]. Furthermore, it has been reported that NaCl enhances WNK1 autophosphorylation[151], suggesting a role in osmosensing pathways.

The WNK4 kinase domain is highly homologous to that of WNK1 but studies on WNK4 kinase activity are more limited. Expressing the kinase domain as a small GST fusion protein produced no kinase activity when transfected into HEK293 cells[147]. However, kinase-dependent and independent functions have been identified for WNK4 in the regulation of renal electrolyte transporters [56;149;161] (see section 1.4). In addition, Yamauchi identified Claudins (tight junction proteins) as molecular targets of WNK4 kinase activity *in vitro*[53;159] (see section 1.4.3).

1.3.4.1 Upstream Signalling and Downstream Targets

Recently, WNK1 was shown to be a novel substrate for protein kinase B/Akt. Vitari *et al.* provide pharmacological and genetic evidence that WNK1 is phosphorylated by PKB on Thr58[51;138]. This upstream pathway was, more recently, linked to ENaC regulation via SGK and Nedd4-2[153;154] (Table 1.3). The downstream target pathways of WNK1 kinase activity are still under investigation but Xu *et al.* also report evidence that WNK1 activates the ERK5 MAPK pathway through MEKK2/3 (MAP3K)[155]. WNK1 phosphorylation of Synaptotagmin proteins (involved in vesicle trafficking) has also been reported[64] (Table 1.3). Interestingly some of these studies indicate that WNK1 function may not be based on its catalytic activity alone, but may involve a scaffolding role, whereby WNK1 allows the complex assembly of interacting proteins[154;155].

1.3.5 WNK Kinase Expression

When the studies in this thesis began only very limited information regarding the expression of WNK1 and WNK4 was available. RNA and protein analysis revealed

WNK1 expression in virtually all tissues examined, but predominantly in kidney, heart, and muscle[24;137;148]. In contrast, WNK4 expression was reportedly restricted to kidney. Immunohistochemistry studies investigating the nephron segment and subcellular distributions of these proteins, report cytoplasmic WNK1 expression in DCT and CD, whereas WNK4 expression was reported in tight junctions of DCT, and in both the cytoplasm and tight junctions of CCD [148].

Table 1.2: WNK expression.

	Tissue	Cytoplasm	Lateral membrane	Tight Junction	Ref
WNK1	DCT & CD	✓			147
	Epidermis	✓			18
	Eccrine sweat glands (skin)	✓			18
	Gall bladder epithelium	✓			18
	Colonic crypt epithelium	✓			18
	Oesophagus	✓			18
	Hepatic bilary ducts		✓		18
	Pancreatic ducts		✓		18
	Epididymis		✓		18
WNK4	DCT			✓	147
	CCD	✓		✓	147
	Pancreatic ducts		✓	✓	52
	Hepatic bilary ducts		✓	✓	52
	Colonic crypts	✓		✓	52
	Eccrine sweat glands (skin)	✓		✓	52
	Epidiymis		✓	✓	52
	Blood-brain barrier epithelium		✓	✓	52

Over the last two years further evidence of WNK expression has been reported (Table 1.2) and it has subsequently become apparent that WNK4 is discreetly expressed in a wider range of tissues (Chapter 4). Studies submitted as part of this

thesis have also made a significant contribution to the current understanding of WNK1 gene expression[109] and are discussed in detail in Chapters 3 and 9.

1.4 WNK Kinase Regulation of Ion Transport Processes

Mutations in either WNK1 or WNK4 cause Gordon syndrome, a disorder featuring a Na^+ and K^+ imbalance. The clinical features of Gordon syndrome can be explained by distal nephron defects in ion transport processes that are corrected by treatment with thiazide diuretics. WNK1 and WNK4 are expressed in adjacent distal nephron segments which ultimately regulate net salt reabsorption as well as net K^+ and H^+ secretion. All of these considerations prompted the investigation of potential roles for WNK kinases in distal nephron ion transport processes.

During the course of the studies reported in this thesis, a mass of *in vitro* functional data has been reported, predominantly from *Xenopus* oocyte studies, proposing diverse regulatory roles for WNK1 and particularly WNK4 in electrolyte transport, both within and outside kidney (summarised in Table 1.3). These include extensive interactions with Na^+, K^+ and Cl^- transporting systems, including NCC[148;161-163], ROMK[56], ENaC[153;154], the basolateral isoform of the Na^+-K^+-$2Cl^-$ cotransporter, NKCC1, the apical Cl^-/anion exchanger, CFEX[52], the basolateral Ca^{2+} channel, TRPV4[34], and also Claudin (tight junction) proteins[53;160]. WNK signalling has also been associated with Ste-20-related Proline-Alanine-rich Kinase, SPAK[35;36;97;113;139], and synaptotagmins [64], further suggesting a role for this pathway in membrane trafficking (Table 1.3).

However, the physiological relevance of phenomena observed in experimental systems must be queried as the genes under study are often overexpressed, or expressed at inappropriate ratios in relation to each other. Also, normal protein function may not be observed due to the absence of (or inappropriate presence of) upstream signals, downstream targets, or other regulatory factors. So although informative these *in vitro* findings require further validation particularly in an *in vivo* model, before these phenomena can be accepted. While many of these studies will be discussed at greater length in Chapter 9, interactions forming the basis of currently

Table 1.3: Potential WNK1 and/or WNK4 interacting candidate proteins.

PROTEIN	THEORY	EVIDENCE	SYSTEM	REF	RATING
NCC	WNK4 inhibits NCC by reducing NCC surface expression; WNK1-L may prevent this inhibition.	•WNK4 ↓NCC-mediated activity by ↓NCC surface expression possibly by ↑NCC removal from plasma membrane (section 1.4.1) •Controversey over involvement of WNK4 kinase activity (section 1.4.1) •Effect of GS mutations controversial (section 1.4.1.1) •WNK1-L suppresses WNK4-induced inhibition of NCC (section 1.4.1.2)	Xenopus oocytes	149;161 149;161;162 148;161-163 161	✓✓✓ ✓
SPAK	WNK1 & WNK4 interact with SPAK to regulate cation-chloride-coupled transporters.	•WNK4 interacts with SPAK/OSR1 •WNK4 binds to SPAK (C-ter) activating NKCC1 & deactivating KCC2 via phosphorylation regardless of external osmolarity or cell volume •SPAK immunoprecipitates with WNK1; WNK1 phosphorylates SPAK/OSR1; low Cl^- hypotonic stress ↑WNK1 kinase activity, activated SPAK/OSR1, ↑phosphorylation of conserved OSR1 ser residue & ↑NCC phosphorylation •WNK1 associates with SPAK in testis; both WNK1 & WNK4 activate SPAK/OSR1 via phosphorylation of T-loop (catalytic domain) leading to phosphorlyation of NKCC1	Yeast 2-hybrid screen of mouse brain Xenopus oocytes MDCK cells HEK293 cells Rat testis HEK293 cells *E.coli* cells	113 35;36 97 139	✓✓✓ ✓
NKCC1	WNK4 inhibits basolateral NKCC1 activity & surface expression.	•WNK4 ↓NKCC1-mediated-^{86}Rb-influx by ↓NKCC1 surface expression •Conflicting study reports WNK4 does not interact directly with NKCC1 but involves SPAK (see above)	Xenopus oocytes Yeast 2-hybrid screen of mouse brain	52 35	✓✓✓ ✓ (see SPAK above)
ROMK	WNK4 inhibits ROMK activity & surface expression.	•WNK4 ↓ROMK activity (kinase-independent) by ↓surface expression possibly by ↑ROMK clearance from membrane via clathrin-dependent endocytosis •Coimmunoprecitation following transient transfection •GS mutations (Q562E and E559K) ↑ROMK inhibition (section 1.4.2). •GS mutation (D564A) does not alter ROMK localisation	Xenopus oocytes HEK 293 cells *In vivo* mouse model	56 56 159	✓✓✓

PROTEIN	THEORY	EVIDENCE	SYSTEM	REF	RATING
Claudins (tight junction)	WNK4 ↑paracellular Cl^- flux via Claudin phosphorylation.	•WNK4 ↓TER & ↑paracellular Cl^- permeability (kinase-dependent) •WNK4 phosphorylates Claudins 1-4 and WNK4-Claudin interaction occurs via YV motif in Claudin C-terminus •WNK4 GS mutants (D564A, Q562E and E559K) showed ↑inhibition (section 1.4.3) •WNK4 tight junction expression	MDCKII cells Mouse kidney	53 159 53;159 148	✓✓✓
PI 3-K PKB/Akt	Upstream activator of WNK1	•IGF-1 stimulates WNK1 phosphorylation on Thr58 by PKB/Akt (see SGK below)	HEK293 cells 3T3-L1 adipocytes	138 51	✓✓
SGK-Nedd4-2-ENaC	WNK1-L positively regulates ENaC via SGK1 phosphorylation of Nedd4-2 and may involve a scaffolding role for WNK1.	•WNK1 interacts with SGK1; promotes SGK1 activation via ↑phosphorylation of its activation loop (WNK1 does not phosphorylate SGK1) which increases ENaC activity •SGK1 activation by WNK1 is PI 3-kinase-dependent & requires Akt catalytic activity; N-terminus of WNK1 (phosphorylated on T58) activates SGK1 & ENaC independently of catalytic activity.	Yeast 2 hybrid screen of rat brain HEK293 cells Xenopus oocytes HEK293 cells	153 154	✓✓
CFEX	WNK4 inhibits CFEX activity.	WNK4 ↓CFEX-mediated-[^{14}C] formate uptake	Xenopus oocytes	52	✓
TRPV4	WNK1 & WNK4 inhibit TRPV4 activity & surface expression.	•WNK1 & WNK4 inhibit Ca^{2+} entry via TRPV4 by ↓TRPV4 surface expression •Kinase-dead WNK4 (D318A) had no effect suggesting kinase dependent function but N-terminal truncated WNK4 is functional; C-ter WNK4 essential •WNK4 (E559K) & (Q562E) less effective •Kinase-dead WNK1 mutants (K233M & D382A) less effective	HEK293 cells	34	✓
Syts	WNK1 phosphorylates Syts affecting membrane trafficking & vesicle fusion.	•WNK1 binds Syt 1, 2, 3 and 9; WNK1 & Syt2 coimmunoprecipitate & colocalize on a subset of secretory granules in INS-1cells; WNK1 phosphorylation of Syt2 ↑Ca^{2+} requirement for Syt2 binding to phospholipids vesicles	Yeast 2-hybrid screen of mouse brain Neuronal & neuroendocrine cells	64	✓
MEKK2/3	WNK1 stimulates MEKK2/3	•WNK1 activates ERK5 via MEKK2/3; coimmunoprecipates with MEKK2/3 •Phosphorylates MEKK2/3; is required for EGF activation of ERK5 •May form a scaffold allowing assembly of an ERK5 activation complex.	HEK293 cells HeLa cells	155	✓

held theories, which are regularly referred to in the chapters to follow, are introduced here in detail.

1.4.1 WNK4 Inhibits NCC

Recently, two independent studies based in the *Xenopus laevis* oocyte expression system examined the regulation of NCC by WNK kinases. It was observed that coinjection of oocytes with NCC and wild-type WNK4 reduced ^{22}Na influx, compared with NCC injection alone[149;161]. The C-terminus of WNK4 mediates this NCC inhibition and Yang *et al.* have demonstrated that the C-terminal 200 amino acids of NCC interact with WNK4 in HEK293 cells[162]. Additional experiments utilizing either eGFP-tagged NCC[149] or immunoprecipitation of surface-biotinylated NCC[161], indicated that WNK4 inhibits NCC function by reducing the amount of NCC present in the plasma membrane, possibly by increasing the removal of NCC from the plasma membrane. Wilson *et al.* performed similar studies with a kinase-dead WNK4 (D318A) which showed no inhibition of NCC-mediated ^{22}Na influx, suggesting that WNK4 inhibition of NCC is kinase-dependent[149]. This conflicts with findings by Yang *et al.* showing that catalytically inactive WNK4 maintains the ability to inhibit NCC suggesting that this inhibition occurs largely through protein-protein interactions rather than by phosphorylation[161].

1.4.1.1 Mutant WNK4 and NCC Inhibition

Intriguingly, Wilson *et al.*[149] showed total loss, while Yang *et al.*[161] showed only 50% loss, of NCC inhibition with WNK4 harbouring the Gordon syndrome-causing missense mutation Q562E (Q565E in hWNK4). However, WNK4 Q562E retained its ability to form a complex with NCC. Although Wilson *et al.* also indicate that another Gordon syndrome mutation, WNK4 E559K, had also lost effect on NCC activity, Yang *et al.* failed to show any loss of inhibiting capacity for either WNK4 E559K or D561A (E562K and D564A in hWNK4). More recently, Yang *et al.* demonstrated that WNK4 harbouring the most distal of the Gordon syndrome mutations, R1164C, was as effective as wild-type WNK4 in its ability to inhibit NCC[162]. Adding to this controversy, a recent study showed that while WNK4 expression disrupted apical localisation of NCC in polarised MDCK II epithelial

cells, this inhibitory effect was also observed with coexpression of mutant WNK4 D564A[163]. Furthermore, the activity and/or localisation of electrolyte transporters unrelated to Gordon syndrome (CFEX and NKCC1) was also decreased by both wild-type and mutant WNK4 expression. Further work will be needed to clarify discrepancies between these studies and to accurately determine the physiological relevance of the WNK4-NCC interaction.

1.4.1.2 Causal Chain: WNK1 Regulation of WNK4-Mediated NCC Inhibition

Mutations in WNK1 or WNK4 cause a broadly similar phenotype, suggesting that these proteins participate in the same pathway, or in parallel pathways on similar downstream targets. Interestingly, similar expression studies involving WNK1 showed that although WNK1 alone had no effect on NCC activity, WNK1 suppresses WNK4-induced inhibition of NCC, thereby restoring cotransporter activity to near base-line levels[161]. WNK1 physically associates with WNK4 in a protein complex involving their highly homologous N-terminal kinase domains. Catalytically active full-length WNK1 is required to suppress WNK4-mediated NCC inhibition, possibly explained by WNK1 tetramer formation[162].

1.4.1.3 Potential Mechanism

Based on these studies it is hypothesised that wild-type WNK4 is an inhibitor of NCC activity and that this inhibition may be lost due to inactivating WNK4 mutations in Gordon syndrome. Thus, as suggested by the mirror image between Gordon syndrome and Gitelman's disease, as well as effective treatment of Gordon syndrome with thiazide diuretics, increased activity of NCC could cause a transcellular chloride shunt just as hypothesised in the past in explaining features characteristic of Gordon syndrome. Increased Na^+ reabsorption in DCT would expand plasma volume and raise cardiac output causing hypertension. It would also reduce the amount of Na^+ reabsorption via the electrogenic channel, ENaC, impairing the development of the lumen-negative potential that is required for normal secretion of K^+ and H^+ in the distal nephron. Gain of function mutations causing an increase in WNK1 expression, as has been reported at least in leukocytes in Gordon syndrome

patients[148], would suppress WNK4 activity, activating NCC, and could also lead to the Gordon syndrome phenotype.

In keeping with WNK4 as a regulator of Na^+ flux, a recent clinical study suggests that WNK4 modulates Na^+ transport in airways and that this may be the result of regulation of ENaC or a K^+ channel[31].

1.4.2 WNK4 Inhibits ROMK

ROMK channels are located in TAL where they mediate apical K^+ recycling to facilitate Na^+ reabsorption through the apical Na^+-K^+-$2Cl^-$ cotransporter (NKCC2), and more distally in DCT-CNT-CD where at least from late DCT (DCT2) distally ROMK is regarded as forming the major K^+ secretory pathway driven by colocalised electrogenic Na^+ reabsorption via ENaC. As one of the prominent features of Gordon syndrome is hyperkalaemia and WNK4 is expressed in DCT2-CD segments as well as DCT1, the possibility of a direct role for WNK4 in the regulation of K^+ secretion was examined by Kahle *et al.* in *Xenopus* oocytes[56]. Expression of eGFP-tagged ROMK2 produced a large K^+ current that was markedly inhibited (68% reduction) by coexpression of WNK4. Further experiments indicated that WNK4 inhibits ROMK by increasing its clearance from the cell surface (by up to 87%) through clathrin-dependent endocytosis. Co-immunoprecipitation of a WNK4 fragment (extending from the end of the kinase domain to the normal C terminus) with the cytoplasmic C terminus of ROMK, implies that WNK4 and ROMK interact physically. One possibility proposed by the authors is that WNK4 serves as a scaffold to bring together ROMK and other factors that target ROMK for endocytosis. Kinase-dead WNK4 (D318A) also fully inhibited ROMK, indicating that inhibition of ROMK by WNK4 is not dependent on WNK4 kinase activity.

1.4.2.1 Mutant WNK4 and ROMK Inhibition

The Gordon syndrome mutation Q562E was shown to increase the inhibition of K^+ current by 80% and caused a further 87% reduction in ROMK surface expression compared with wild-type WNK4. Similar results were obtained with WNK4 E559K. From this study the authors propose that WNK4 inhibits K^+ secretion via ROMK in a

kinase-independent manner by increasing its clearance from the plasma membrane via clathrin-dependent endocytosis and that the Gordon syndrome missense mutations appear to increase ROMK inhibition, potentially explaining the impaired K^+ secretion characteristic of this disease. Thus WNK4 appears to inhibit NCC and ROMK by different mechanisms.

1.4.3 WNK4 Regulates Paracellular Permeability via Claudins

The conspicuous localization of WNK4 in the tight junction complex[148] and the "paracellular chloride shunt" hypothesis proposed to explain Gordon syndrome (section 1.2.2) prompted both Yamauchi *et al.* and Kahle *et al.* to investigate the possibility that WNK4 regulates paracellular Cl^- flux. These studies were based in MDCKII cells which form tight (high transepithelial resistance (TER)), electrolyte transporting epithelia regarded as having distal tubule/CD characteristics. Although controversy exists between the two studies over the effect of wild-type WNK4[53;159], overall they demonstrate that WNK4 increases paracellular Cl^- permeability by reducing TER through phosphorylation of Claudin proteins[159], and that Gordon syndrome WNK4 mutants (D564A[159], Q562E and E559K[53]) further enhance this effect. Thus, Claudin proteins may be downstream molecular targets of WNK4, suggesting that WNK4 may function as a specific regulator of the paracellular pathway, and that mutations in this respect behave as gain-of-function mutations.

1.5 Summary: Roles of WNKs in Integrated Physiology

1.5.1 Molecular Switch Hypothesis

As discussed in section 1.2.2, two models have been proposed to explain Gordon syndrome, both effectively involving a Cl^- shunt, routing either transcellularly (through NCC overactivity) or paracellulary (across "leaky" tight junctions). Findings from the *in vitro* studies described above provide evidence for both these possibilities.

Kahle and colleagues propose a transcellular model whereby in normal physiology WNK4 acts as a molecular switch simultaneously controlling reciprocal fluxes in Na^+ and K^+ (via inhibition of NCC and ROMK, respectively; Figure 1.7). Gordon

syndrome mutations are proposed to disrupt inhibition of NCC (increasing NaCl reabsorption) and enhance ROMK inhibition (proposed to reduce K^+ secretion). However, it is unclear from these *in vitro* based studies, where in the nephron this putative effect on ROMK would occur as it is a broadly expressed gene (TAL-CD). Controversial findings from a more recent study also question whether this ROMK effect occurs *in vivo*[160]. It is tempting to speculate that loss of WNK4 regulation of NCC alone (resulting in increased electroneutral NaCl reabsorption in DCT and reducing the potential for K^+ secretion via electrogenic transport further distally) might provide a sufficient explanation for Gordon syndrome, fitting with the long established overactive NCC hypothesis (Figure 1.3(a))[10;56].

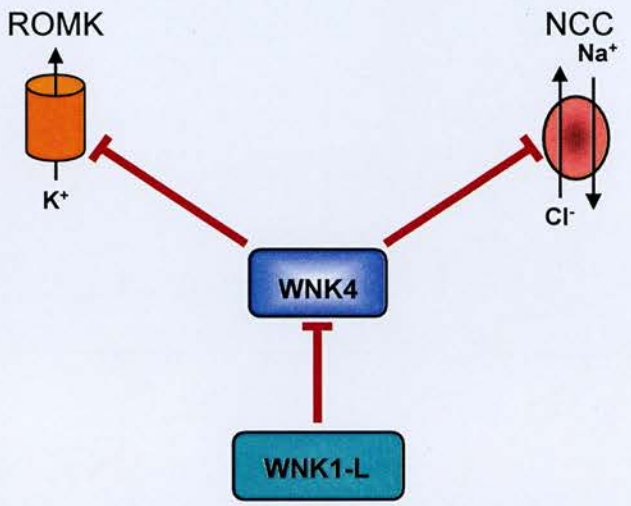

Figure 1.7: WNK4 molecular switch hypothesis. WNK4 serves as a molecular switch simultaneously regulating NaCl reabsorption via NCC and K^+ secretion via ROMK. Kahle *et al.* propose that at low aldosterone levels, WNK4 inhibits the surface expression of NCC and ROMK. In hypovolemic states, WNK4-inhibition of NCC is relieved allowing increased NaCl reabsorption, whereas the routing of ROMK to the plasma membrane is suppressed. In hyperkalemic states, WNK4-inhibition of ROMK is relieved, whereas the routing of NCC is suppressed. Yang *et al.* show that WNK1-L can inhibit WNK4-mediated inhibition of NCC.

WNK4 regulation of paracellular Cl^- flux adds an additional possibility to this molecular switch hypothesis. The Gordon syndrome mutations increase paracellular Cl^- reabsorption, depleting the lumen negative charge, and thereby reducing the driving force for K^+ and H^+ secretion. Overall, this would enhance NaCl reabsorption and diminish K^+ and H^+ secretion (Figure 1.3(b)). This is an alternative or additional mechanism, by which the Gordon syndrome mutants could lock the switch in a mode

that expands plasma volume by increasing NaCl reabsorption, while retaining plasma K^+.

Overall these studies demonstrate that in a normal physiological setting WNK signalling could potentially coordinate transcellular and paracellular flux to achieve NaCl and K^+ homeostasis[53;159], and may play a pivotal role in electrolyte balance, propagating the appropriate renal response to aldosterone signalling. Thus, these *in vitro* functional studies provide evidence for both the overactive NCC hypothesis and the paracellular Cl^- shunt hypothesis proposed to explain Gordon syndrome and indeed both could exist in parallel.

1.5.2 Drug targets

The WNK pathway represents an attractive target for development of novel antihypertensive agents at least as powerful as thiazide diuretics and without the adverse metabolic effects currently raising concerns about first line use of certain antihypertensives including thiazides and β-blockers. That they may be free of thiazide-like metabolic side effects gains support from the lack of such problems affecting patients with Gordon syndrome.

The studies described above identify WNK1 and WNK4 as strong candidates possibly involved in contributing to the pathogenesis of essential hypertension. Interestingly, WNK4 lies within a region of the genome which has been reported to show a human quantitative trait locus (QTL) for essential hypertension on a genome scan, and moreover this area is syntenic to a region in the genome of the spontaneously hypertensive rat (SHR) strain[169], harbouring a long known major QTL for hypertension in this animal model of essential hypertension. A number of case-control and population based studies have been very recently carried out to look for association between various single nucleotide polymorphisms (SNPs) in WNK1 and WNK4 and BP variation. Although WNK4 variants have been identified in hypertensive patients, results have been inconsistent and the physiological importance of these genetic variations remains to be determined[58;59;169].

Until very recently there was very little evidence of an association between WNK1 polymorphisms and BP variation. Kokubo *et al.* found no association between WNK1 SNPs and clinic SBP or DBP in a large Japanese population[59]. Whilst overall the BRIGHT study found no association of WNK1 with essential hypertension, this important study shows nominal evidence of an association between one WNK1 SNP near the promoter region and the severity of hypertension[107]. Interestingly, a study published by Tobin and colleagues is the first to report an association between common genetic WNK1 variants and BP in a white European population[135;166]. Although, these findings will need to be confirmed by other epidemiological studies and also functional studies, they raise the possibility that milder variations than seen in Gordon syndrome within the WNK pathway may be contributing to human variations in BP and influence salt sensitivity and the response to antihypertensive drugs. Whether such genetic markers are of use in predicting the incidence of hypertension and cardiovascular morbidity and mortality or the response to salt restriction or particular classes of antihypertensives would require clarification through further studies.

1.5.3 Concluding remarks

Genetic and physiologic evidence suggests WNK1 and WNK4 as molecular switches regulating Na^+, K^+, and Cl^- balance in the distal nephron. Clearly our perception of the respective physiological roles of WNK1 and WNK4 is largely in its infancy. A number of interactions of interest have been reported in *in vitro* studies often in single non-polarised cells such as *Xenopus* oocytes. Whilst these early studies are valuable it still remains to be established if such phenomena apply *in vivo* in mammalian kidney to importantly affect electrolyte transport and BP. Unravelling the mechanisms of these regulatory pathways within kidney has the potential to deepen our understanding of the integrated physiology of electrolyte balance and promises to yield insights into new mechanisms involved in essential hypertension.

Aims

The primary aim of this thesis was to investigate the WNK pathway in kidney and elucidate its role in electrolyte balance and BP control by addressing the following aims:

1. To examine the distribution and alternative splicing of WNK1 and WNK4 gene expression in mouse kidney.
2. To produce anti-WNK antisera specific for mouse WNK1 and WNK4.
3. To assess the impact of stimuli, known to affect electrolyte balance and BP, on WNK pathway gene expression *in vivo*.

Chapter 2 Materials and Methods

2.1 Materials

Unless otherwise stated all chemicals and reagents were purchased from ***Sigma-Aldrich Company Ltd., Poole, Dorset, UK.***

2.1.1 General Chemicals

BDH-Merck, Poole, Dorset, UK:

Acetone, DPX Mountant, Formaldehyde, Glacial Acetic Acid, Hydrochloric Acid, Xylene, and any other organic solvents.

Bright, UK:

Cryo-m-bed-embedding compound

Fisher Scientific, Loughborough, Leicester, UK:

Duolite Mixed Resin.

Fluka Chemicals Ltd., Gillingham, Dorset, UK:

Acetic Anhydride, Triethanolamine.

Hayman Ltd., Witham, Essex, UK:

Ethanol.

VWR International, Lutterworth, Leicester, UK:

SuperFrost Plus Slides, Paraformaldehyde.

Whatman® International Ltd., Maidstone, England:

Whatman 3mm Chromatography Paper, Whatman Filter Paper.

2.1.2 Molecular Biology Reagents

Applied Biosystems, Applera, Warrington, Cheshire, UK:

TaqMan™ primers and probes, TaqMan™ PCR core reagent kit.

Amersham Pharmacia Biotech, Little Chalfont, Buckinghamshire, UK:

Anti Rabbit Scintillation Proximity Assay (SPA) reagent, ^{14}C Microscales, ECL™ Western Blotting Detection Reagents, Horseradish-peroxidase linked anti-rabbit antibody, Hybond ECL™ Nitrocellulose Membrane, Hybond-N^+ Membrane, Hyperfilm ECL™, Rediprime® II Random Prime Labeling System, NICK sephadex G-50 DNA column.

Anachem Ltd., Luton, Bedfordshire, UK:

NTB-2 photographic emulsion.

Biowhittaker Molecular Applications, Wokingham, Surrey, UK:

SeaKem® LE Agarose (For Electrophoresis).

Canberra Packard, UK:

PicoFluor 40 Scintillant fluid.

H.A. West, Edinburgh, UK:

Amfix high speed fixer.

Invitrogen Life Technologies/Gibco BRL, Paisley, UK:

Custom Primers, 1kb DNA Ladder, 100bp DNA Ladder, Low DNA Mass Ladder, Low Melting Point Agarose, TRIzol®, Yeast tRNA.

Promega Ltd., Southhampton, Hants, UK:

Nuclease-free Water, Nucleotides, Reverse Transcription System, RNase Inhibitor (RNasin), RQ1 DNase (RNase-free), Transcription optimised buffer (5x), RNA polymerases (T3 and T7), Taq DNA Polymerase and buffer.

Qiagen Ltd., Crawley, West Sussex,UK:

QIAquick Gel Extraction Kit, QIAquick PCR Purification Kit.

Sigma-Aldrich Company Ltd., Poole, Dorset, UK:

Kodak Biomax MS film, Kodak Biomax MR film.

Roche Diagnostics Ltd., Lewes, East Sussex, UK:

RNase A.

2.1.3 Protein Reagents

Bio-Rad Laboratories Ltd., Hamel Hampstead, UK:

Blotting Grade Blocker Non-Fat Dry Milk, Bradford Protein Assay Reagent, Precision Plus Protein Standards Dual Color, Tween.

Roche Diagnostics Ltd., Lewes, East Sussex, UK:

Complete Protease Inhibitor Cocktail.

2.1.3.1 Antibodies

Alomone Labs Ltd., Jerusalem, Israel:

Anti-ROMK.

Gift from Jan Loffing, University of Freiburg:

Anti-NCC.

2.1.4 Radioisotopes

Amersham Pharmacia Biotech, Little Chalfont, Buckinghamshire, UK:

[1,2,6,7-^{3}H]-corticosterone (2.8-3.9 TBq/mmol), [α-^{32}P]-dCTP (111 TBq/mmol), ^{35}S-UTP (30 TBq/mmol).

2.1.5 Animals

Charles River Laboratories, UK:

C57BL/6J Mice.

DURECT Corporation, Cupertino, CA, US:

Alzet® Mini-Osmotic Pump (Model 2004).

Sigma-Aldrich Company Ltd., Poole, Dorset, UK:

Dexamethasone.

Special Diet Services (SDS), Witham, Essex, UK:

Standard Chow (61.9% carbohydrate, 18.8% protein, 3.4% oil and 0.6% salt), Specially formulated diets.

Steraloids, Newport, US:

Aldosterone.

2.1.6 Materials for plasma assays

Bachem, Merseyside, England, UK:

Angiotensin I.

Diagnostic Products Corporation, LA, USA:

Count-A-Coat Aldosterone Radioimmunoassay (including ^{125}I-Aldosterone).

Gift from Dr. JJ Morton, Glasgow:

Anti-Angiotensin I.

Reagent of Dr. CJ Kenyon, Edinburgh:

Anti-Corticosterone.

2.1.7 Equipment

Amersham Pharmacia Biotech, Little Chalfont, UK:

GeneQuant RNA/DNA Calculator, Hyper-processor.

Applied Biosystems, Applera, Warrington, Cheshire, UK:

TaqMan™ ABI Prism 7900 Sequence Detector™.

Berthold Technology Ltd., St. Albans, Hertfordshire, UK:

Berthold LB 2111 γ-counter.

Bio-Rad Laboratories Ltd., Hamel Hampstead, UK.

Electrophoresis Power Pac 300, Mini-Protean 3 Cell, Mini Trans-Blot Electrophoretic Transfer Cell.

Bio-Tek Instruments Inc., Winooski, Vermont, USA:

EL 312e Bio-Kinetics Microplate Reader.

Dage Inc., Michigan City, Indiana, USA:

Dage MTI CCD72S imaging camera.

Eppendorf AG, Hamburg, Germany:

Eppendorf Mastercycler gradient
(PCRs, RTs and denaturation).

FSA Laboratory Supplies, Fissons plc., UK:

Whirlimixer.

Fuji Photo Film Company Ltd., Tokyo, Japan:

Phosphoimager FLA-2000, Phosphoimager screens.

Gallenkamp, UK:

Fan Incubator.

Jouan Inc., Winchester, Virginia, USA:

Jouan A-14 Centrifuge (Ultracentrifuge rpm < 14000).

Hybaid, UK:

Hybaid Omni Slide Wash Module.

Ika, Labortechnik, Staufen, Germany:

Ultra-Turrax T8 auto-homogeniser.

Jencons-PLS, Bedfordshire, UK:

Techne Hybridiser HBID, Hybridisation Bottles.

Leica Microsystems, UK:

Leica Cryostat.

Savant Instruments Inc., USA:

DNA Speed Vac® DNA110.

Stuart Scientific, Staffordshire, UK:

Stuart Gyro-rocker SSL3.

Techniplast, Kettering, Northamptonshire, UK:

Mouse Metabolic Cages.

Wallac Oy:

1450 Microbeta Plus Liquid Scintillation Counter.
(utilised for standard cpm counting)

2.1.8 Software

Applied Biosystems, Applera, Warrington, Cheshire, UK:

Sequence Detection Systems (SDS).

Mathworks, Natick, MA, USA:

MATLAB® v7 Technical Computing Environment and Imaging Processing Toolbot.

Raytest Scientific Ltd., Sheffield, UK:

Fujifilm Fluorescent Image Analyser FLA-200 V.1.0, Aida 2.0 Auto Image Data Analyser.

Statsoft, Tulsa, Oklahoma, USA:

Statistica v.5.0.

Wallac Oy:

Multicalc Advanced v2.0.

Zeiss:

Zeiss Contron KS400 software.

2.1.9 Buffers and Solutions

1.2% Agarose Formaldehyde Denaturing Gel: 17ml formaldehyde *(BDH, 101134A)* added to 1.2g of agarose, pre-melted in DEPC-treated water (73ml) and 10X MOPS buffer (10ml).

Box Buffer:

A - 20ml 20xSSC buffer, 50ml deionised formamide *(Sigma, F7503)* made up to 100ml in DEPC-treated water (see below).

B - 0.5M NaCl, 10mM Tris, 1mM EDTA in dH_2O.

Blocking Solution (Western blot): 25g powdered milk *(Bio-Rad, 170-6404)*, 500µl Tween *(Bio-Rad, 170-6531)*, 50mls 10xTBS (see below) made up to 500mls with dH_2O.

Deionised Formamide (for use in box buffer): 150ml formamide *(Sigma, F7503)* mixed with 15g mixed bed ion-exchange resin *(Duolite, MB-6113)* for >1 hr, filtered twice through Whatman filter paper *(Whatman, 1001150)* and stored protected from light using sterile glassware.

DEPC-Treated Water: dH_2O mixed with diethylpyrocarbonate (DEPC; 1 drop/ 100ml), shaken and left for 1-24 hr prior to autoclaving.

1xDiluent Buffer: 8.25g boric acid, 2.7g NaOH, and 3.5ml conc. HCl (10M) made up to litre with distilled water (dH_2O), (pH 7.4; containing 0.5% bovine serum albumin (BSA), 1% methanol and 0.1% ethylene glycol). Stored at -20°C and thawed at room temperature immediately before use.

250mM EDTA (pH 8.0): 80mls water was added to 9.3g $Na_2EDTA.2H_2O$. pH adjusted with NaOH and volume adjusted to 100mls.

Ethanol in Ammonium Acetate:

50% - 11.55g Ammonium Acetate dissolved in 250ml ethanol, made up to 500ml with dH_2O.

70% - 11.55g Ammonium Acetate dissolved in 350ml ethanol, made up to 500ml with dH_2O.

90% - 11.55g Ammonium Acetate dissolved in 450ml ethanol, made up to 500ml with dH_2O.

2xHybridisation Buffer: 1.2M NaCl, 20mM Tris-HCl (pH 7.5), 2x Denhardt's solution *(Sigma, D2532)*, 2mM EDTA (pH 8.0), 0.2mg salmon sperm DNA (11mg/ml; *Sigma, D9156*), 0.2mg yeast tRNA (50 mg/ml; *Invitrogen, 15401-029*) and 2g dextran sulphate *(Sigma, D8906)* made up to 10ml in DEPC-treated water, stored at -20°C.

4x Laemmli Buffer: 4% SDS, 20% glycerol, 2mM DTT, 125mM Tris (pH 6.8), 16% β-mercaptoethanol, bromophenol blue.

Loading Buffer:

A - 0.35% w/v orange G, 40% glycerol in dH_2O.

B - 40% sucrose w/ v, 0.25% bromophenol blue (w/v) in dH_2O.

(filter-sterilised before use)

Lysis Buffer (Tissue Protein Homogenate Preparation): 50mM Tris (pH 7.5), 0.25M sucrose, 5mM EDTA, 1x stock cocktail protease inhibitors (Complete

Protease Inhibitor Cocktail Tablets, *Roche, 11 836 153 001*; inhibition of serine, cysteine and metalloproteases), made up in dH_2O.

10x MOPS Buffer (pH 7): 42g MOPS, 16.6ml 3M sodium acetate (pH5.2) and 20ml 0.5M EDTA dissolved in 1L dH_2O; adjusted to pH 7. Autoclaved before use.

4% Paraformaldehyde in 0.1M Phosphate Buffer (pH7.5): 20mM NaH_2PO_4, 80mM Na_2HPO_4 in 1L DEPC-treated water, heated to 80°C prior to addition of 40g paraformaldehyde using sterile glassware. Stirred for 1 hr to dissolve and stored at 4°C.

Phosphate Buffer: 0.2M NaH_2PO_4 0.6M Na_2HPO_4, 5mM EDTA. Autoclaved before use.

PBS (Phosphate Buffered Saline; pH 7.4): 0.1M phosphate buffer with 137mM NaCl, 2.7mM KCl in dH_2O. Autoclaved before use.

0.1% Ponceau Stain: 100mg Ponceau in 100ml of 1% acetic acid.

2xPre-hybridisation Buffer: 1.2M NaCl, 20mM Tris-HCl (pH 7.5), 2x Denhardt's solution *(Sigma, D2532)*, 2mM EDTA (pH 8.0), 10mg salmon sperm DNA (11mg/ml; *Sigma, D9156*), 0.2mg yeast tRNA (50 mg/ml; *Invitrogen, 15401-029*) made up to 10ml in DEPC-treated water, stored at -20°C.

Resolving Gel (5%; Western Blot): 9.075ml dH_2O, 1.875ml Acrylamide/bis-acrylamide (40% stock solution mixture; *Sigma, A2917*), 3.75ml 1M Tris (pH 8.8), 0.15ml 10% SDS, 112.5µl 10% ammonium persulphate and 15µl TEMED.

RNA Sample Buffer: 50% deionised formamide *(Sigma, F9037)*, 18% formaldehyde *(BDH, 101134A)*, 1xMOPS buffer.

RNase A Solution: 25mg RNase A *(Roche, 10109 142 001)* dissolved in 1mM Tris, 15mM NaCl made up to 2.5ml with dH_2O (10mg/ml). Heated to 100°C for 15 min then cooled to room temperature and stored at -20°C. RNase A (10mg/ml) added to box buffer B (3µl/ml).

20x SSC (Saline Sodium Citrate Buffer; pH7.0): 3M NaCl, 0.3M Na citrate in 1L DEPC-treated water, pH 7.0. Autoclaved before use.

5M Sodium Chloride: 29.55g added to 100ml DEPC-water.

Stacking Gel (4%; Western Blot): 11.3475ml dH_2O, 1.875ml 1M Tris (pH 6.8), 1.5ml Acrylamide/bis-acrylamide (40% stock solution mixture; *Sigma, A2917*), 0.15ml 10% SDS, 112.5µl 10% ammonium persulphate and 15µl TEMED.

10xTBE Buffer: 0.9M Tris, 0.9M Boric acid, 20mM EDTA (pH 8.0) in dH_2O. Autoclaved before use.

10xTBS (Tris Buffered Saline; pH 7.6): 0.2M Tris, 1.4M NaCl in dH_2O.

TE Buffer (pH8.0): 10mM Tris-HCl (pH 8.0), 1mM EDTA (pH 8.0). Autoclaved before use.

Transfer Buffer (pH8.3; Western blot): 50mM Tris, 0.38M Glycine, 20% Methanol in dH_2O.

0.1M Triethanolamine (pH8.0): 13.3ml Triethanolamine *(Fluka, 90280)* dissolved in 800ml DEPC-water, volume adjust to 1L, using sterile glassware.

1xTris/Glycine/SDS Running Buffer (pH8.3; Western Blot): 50mM Tris, 0.38M Glycine, 0.1% SDS in dH_2O.

Type III Loading Buffer (6x): 0.25% (w/v) Bromophenol Blue, 0.25% (w/v) Xylene Cyanol FF, 30% (v/v) Glycerol in H2O. Filter-sterilised before use.

Urea-5.3% Acrylamide Gel: 3.6g urea, 1.32ml Acrylamide/bis-acrylamide (40% stock solution mixture; *Sigma, A2917*), 0.1% ammonium persulphate (v/v), 10µl TEMED in 1x TBE.

Wash Buffer A (Low Stringency): 50mM $NaPO_4$ (pH 7.2), 1% SDS.

Wash Buffer B (High Stringency): 25mM $NaPO_4$ (pH 7.2), 1% SDS.

Wash Buffer C (Highest Stringency): 25mM $NaPO_4$ (pH 7.2), 0.1% SDS.

Western Stripping Buffer: 1M Glycine (pH 2), 0.1% SDS, 0.1% Tween made in dH_2O.

2.2 Methods

2.2.1 Animal Maintenance

Male C57BL/6J mice were obtained from Charles River Laboratories at ~7 weeks of age. Mice were maintained under controlled conditions of light (lights on 0800 h – 2000 h) and temperature (21-22°C), and allowed free access to standard chow (61.9% carbohydrate, 18.8% protein, 3.4% oil and 0.6% salt) and drinking water. Mice were housed two per cage.

2.2.1.1 Animal Experimental Treatments

All treatments were carried out under the terms of the UK Home Office Animals (Scientific Procedures) Act, 1986. During treatment periods, mice were principally under my care, with assistance from the staff of the Biomedical Research Facility, Western General Hospital[†]. Treatments involved variations in dietary composition, adrenalectomy (Adx), corticosteroid replacement via subcutaneous mini-pump (MP) and mild restraint in metabolic cages. Animals were observed regularly for changes

[†] Surgical procedures were carried out by Dr. Chris J. Kenyon.

in bodyweight, food and fluid intake, and in some experiments urinary and faecal output were also measured. Daily urine and faecal samples were stored at -20°C until required for electrolyte analysis.

2.2.1.2 Killing and Harvesting of Tissues

At the conclusion of experiments, blood samples were collected by cardiac puncture rapidly after initiation of terminal halothane-induced anaesthesia by Dr. Chris J. Kenyon. Blood samples were centrifuged, plasma was removed, put on ice and rapidly stored at –20°C. Tissues were removed by dissection and quickly frozen on dry ice. Tissue samples were stored thereafter at -80°C.

Non-treatment animals were killed by cervical dislocation and tissues harvested as before.

2.2.2 Assays

2.2.2.1 Aldosterone Radioimmunoassay

Aldosterone RIA was performed using a commercially available kit (Coat-A-Count Aldosterone, DPC, USA). A range of concentrations of aldosterone was prepared (0-3,300 pmol/l) to allow the construction of a standard curve. Standards and samples were incubated in duplicate in aldosterone-specific antibody coated polypropylene tubes with ^{125}I Aldosterone (1ml per sample) at room temperature for 18 hr. Two tubes were prepared with only ^{125}I Aldosterone solution to document the total counts used per incubation, and two with a mixture of ^{125}I Aldosterone and steroid free buffer to estimate non-specific binding. The tubes were decanted thoroughly before being counted in a γ-counter and the concentration of aldosterone in the samples estimated by comparison with the standard curve (γ counts/min vs. pmol/L aldosterone). The inter- and intra-assay coefficients of variation were <15% and <10% respectively.

2.2.2.2 Corticosterone Radioimmunoassay[‡]

Plasma samples were diluted tenfold with diluent buffer. A range of corticosterone concentrations (0-320nM) was prepared to allow construction of a standard curve.

[‡] Corticosterone and renin assays were carried out by Dr. Chris J. Kenyon.

After heating samples at 80°C for 30 min to denature corticosterone binding globulin, aliquots (25µl) of diluted plasma were incubated with the rabbit RIA antibody to corticosterone (final dilution 1:40,000), [1,2,6,7-^{3}H]-corticosterone (specific activity 2.8-3.9 TBq/mmol; final concentration 1.5nM) and scintillation proximity assay (SPA; anti rabbit) reagent (25µl diluted suspension) in a final volume of 100µl diluent buffer. After incubation overnight at room temperature, samples and standards were counted in a β-counter (LKB Wallac Microbeta counter) and the concentration of corticosterone in each sample was determined from the standard curve (β-counts/min vs. nmol/L corticosterone). Intra- and inter-assay coefficients of variation were 9.4 and 9.2% respectively. In this assay, in comparison with corticosterone (100%), the cross-reactivities for progesterone, deoxycorticosterone and cortisol are 7.7, 6.5 and 5.3 %, respectively[80].

2.2.2.3 Renin Radioimmunoassay

Plasma for assay of renin was aliqouted (to avoid excessive freeze-thawing) and treated with great care to avoid protein degradation or unwanted enzyme activity on endogenous substrate.

Plasma renin concentration (PRC) measures the generation of Angiotensin I (Ang I) when plasma is incubated with excess angiotensinogen, derived from rat plasma where angiotensinogen is high and renin absent (after bilateral nephrectomy: BNX (plasma)). A typical Ang I generating system for measuring PRC involves 9ul BNX to which 1ul of plasma sample is added (which may be prediluted five-fold to ensure the assay has angiotensin in clear excess).

Plasma renin activity (PRA) measures Ang I generated from endogenous renin and endogenous angiotensinogen. The Ang I generating system is simply the undiluted sample plasma.

A range of concentrations of Ang I standards (0-400pg/10µl) prepared with Tris buffer allowed the construction of a standard curve. 10µl of Ang I generating system or standards was then added to 10µl of anti-Angiotensin I in RIA cups in

quadruplicate at 0°C and centrifuged at 2000rpm for 1min. Two of the four cups were incubated and shaken for 30 min at 0°C ('cold' standards and samples), whilst the remaining two cups were incubated and shaken at 37°C ('hot' standards and samples). All cups were subsequently placed on ice, and 150µl of Tris, containing approximately 4000-5000 cpm ^{125}I-Angiotensin I, was added to each cup. All cups were briefly shaken and incubated at 2°C for 18h. 250µl of charcoal suspension was then added to each cup and centrifuged at 3000rpm for 15 min at 4°C. The supernatant was aspirated fully and the free charcoal pellet was counted in a γ-counter. A standard curve converting γ-count rate to AngI concentration was constructed using values obtained for the standards and the concentration of Ang I in the 'hot' and 'cold' samples were determined by comparison with this curve (γ-counts/min vs. ng/ml AngI). To calculate sample renin level (whether PRA or PRC), the average 'hot-cold' AngI generated was determined for each sample and expressed as ng AngI/ml plasma/hr.

2.2.2.4 Protein Estimation Assay

The protein concentrations of tissue homogenates were determined colorimetrically using a Bradford Protein Assay Reagent (Bio-Rad, UK). A range of protein standards (0.05–0.5mg/ml) was prepared in duplicate in lysis buffer from the provided protein standard (BSA). Bradford Protein Assay Reagent was diluted 1:5 in dH_2O. Diluted Bradford Protein Assay Reagent (200µl) was added to protein standard (10µl) or appropriately diluted tissue homogenate/lysate in a 96-well plate, mixed and left at room temperature for 20 min to allow colour development. Absorbance of samples at λ570nm (A570) was measured using an ELISA (Enzyme linked immunosorbent assay) plate reader, and the concentration of protein in each sample was estimated by comparison with the standard curve (A570 vs. mg/ml protein concentration).

2.2.3 RNA Extraction

Total RNA was extracted from tissues using TRIzol® Reagent (Invitrogen) - a mono-phasic solution containing phenol and guanidine isothiocyanate. This reagent maintains RNA integrity whilst disrupting cells and dissolving cell components.

2.2.3.1 Tissue Homogenisation

Immediately prior to RNA extraction, tissues were fragmented, whilst still deep frozen, on dry ice to increase the surface area of tissue exposed to TRIzol® and aid homogenisation. 1ml TRIzol® was added per 50mg tissue whilst frozen and samples were homogenised on ice using a mechanical homogeniser; homogenising intermittently to avoid any sample heating.

2.2.3.2 Phase Separation

Following homogenisation, samples were allowed to equilibrate to RT then left for 5 min to allow complete dissociation of the nucleoprotein complexes. 0.2ml Chloroform per ml TRIzol® used in original homogenisation was added to each sample. Samples were mixed by repeated inversion for 15 sec then incubated at RT for 3 min. Samples were centrifuged at 12,000g for 15 min at 4°C resulting in a lower red phenol-containing phase (containing proteins), an interphase (containing DNA and denatured proteins) and an upper aqueous phase containing RNA.

2.2.3.3 RNA Precipitation

The upper aqueous phase from each sample was transferred into a fresh Eppendorf and the RNA was precipitated by addition of an equal volume of isopropanol. Following addition of isopropanol, samples were incubated at RT for 10 min prior to centrifugation at 12,000g for 10 min at 4°C. The RNA precipitate forms a visible gel-like pellet on the side of the tube.

2.2.3.4 RNA Wash

Following centrifugation the supernatant was removed and the RNA pellet was washed with 1ml 75% ethanol (per ml TRIzol® in original homogenisation). Pellets were vortexed and centrifuged at 7000g for 5 min at 4°C.

2.2.3.5 RNA Resuspension

Following the RNA wash, the ethanol was removed and the pellets were briefly air-dried on ice for 5 min, being careful not to completely dry out the RNA, which greatly reduces solubility. RNA pellets were resuspended in 200-500µl DEPC-

treated water (volume depending on pellet size). RNA was then ethanol-precipitated by adding 3M sodium acetate pH 5.2 (0.1 x sample volume) and 100% ethanol (2.5 x sample volume). Ethanol-precipitated RNA was stored at -20°C until required.

2.2.3.6 RNA Quantification

Before use, RNA was quantified using a GeneQuant RNA/DNA Calculator. 10µl of each RNA sample was precipitated by centrifugation at 12,000g for 10 min at 4°C. Supernatant was removed and the RNA pellet was washed with 100µl 75% ethanol. The pellet was vortexed and centrifuged at 12,000g for 5 min. Following the RNA wash, the ethanol was removed, the pellet was briefly air-dried on ice and resuspended in 100µl TE buffer (pH8.0). The absorbance at λ260nm (A260) and λ280nm (A280) was determined to assess concentration and purity. Only RNA with a A260/A280 of 1.8-2.0 was used.

2.2.4 Reverse Transcriptase Polymerase Chain Reaction (RT-PCR)

2.2.4.1 Reverse Transcriptase Reaction

First strand cDNA synthesis was performed using a Reverse Transcription System *(Promega, A3500)*. 1µg of total RNA was precipitated by centrifugation at 12,000g for 10 min at 4°C. Supernatant was removed and the RNA pellet was washed with 100µl 75% ethanol. The pellet was vortexed and centrifuged at 12,000g for 5 min. Following the RNA wash, the ethanol was removed, the pellet was briefly air-dried on ice and resuspended in 7.4µl DEPC-treated water. This RNA sample was then denatured at 75°C for 3 min in a reaction mixture containing 1x reverse transcription buffer, 8U RNasin and 0.2µg random primers, and then immediately snap-cooled on ice. A second mixture containing 1x reverse transcription buffer, 5mM $MgCl_2$, 16U RNasin, 1mM each of dATP, dCTP, dGTP and dTTP, and 15U AMV-reverse transcriptase, was added to the denatured RNA sample. This was then reverse transcribed by incubating at 28°C for 15 min, followed by 42°C for 60 min.

2.2.4.2 PCR Reaction

Forward and reverse oligonucleotide primers were designed to target mouse mRNA sequences of interest, based upon published sequences made available through the nonredundant Genbank/EMBL, EST and mammalian genome databases all publicly accessible via websites such as that of NCBI (National Centre for Biotechnology Information, National Library of Medicine, Bethesda, MD, USA.) and former HGMP (Human Genome Mapping Project, Hinxton, UK) with their useful sequence analysis and BLAST search facilities.

5µl of cDNA template (diluted 1:20 in DEPC-treated water) was used in each PCR reaction containing 1x DNA polymerase Reaction Buffer (containing 2.5mM $MgCl_2$) and made up to a final volume of 25µl with DEPC-treated water. A second mixture containing 1x DNA polymerase Reaction Buffer (containing 2.5mM $MgCl_2$), 100µM dNTP (dATP, dCTP, dGTP and dTTP; *Promega U1420*), 15pmol forward primer, 15pmol reverse primer and 1.25 U *Taq* DNA Polymerase (5U/µl; *Promega, M2865*) was made up to 25µl in DEPC-treated water. A negative control reaction containing DEPC-treated water rather than cDNA template was performed in parallel to detect any contamination of PCR reagents generating PCR products.

PCRs were performed on an Eppendorf Mastercycler Gradient with a heated lid (set to 110°C). The templates in the first 25µl PCR buffer mixture were heated to 95°C for 3 min for initial denaturation, incubated on ice for 1 min before the addition of the remaining 25 µl containing *Taq* polymerase. All samples then underwent 30-40 cycles of PCR amplification (denaturation at 95°C for 1 min, primer annealing at 60°C (unless otherwise specified) for 1 min and elongation at 72°C for 2 min). Upon completion of the PCR programme, samples were incubated at 72°C for a further 10 min to ensure elongation of products to full length and chilled to 4°C prior to gel electrophoresis.

2.2.4.3 Gel Electrophoresis

RT-PCR products were analysed by agarose gel electrophoresis. Gels were prepared by melting 0.8-1.2% (w/v) agarose in 0.5x TBE and adding 1µl/100ml of ethidium

bromide (10 mg/ml). After pouring into a gel mould with appropriately sized combs in place, gels were allowed to set at room temperature then placed in 0.5x TBE in a gel tank.

1µl DNA ladder (Invitrogen, 15615-016 (1Kb) or 15628-019 (100bp)) was mixed with 2µl loading buffer (loading buffer A was most commonly used; the use of loading buffer A or B was determined by the size of the expected PCR product) and 9µl DEPC-treated water and loaded into the first well on each gel to allow determination of PCR product size. 10µl of each RT-PCR product was mixed with 2µl loading buffer and loaded into individual wells in the gel. Gels were electrophoresed at 100V until the loading buffer band was approximately ¾ of the way down the gel and were then photographed under UV light at λ254nm.

2.2.5 Real-time PCR

Real-time PCR exploits the 5'-3' exonuclease activity of *Taq* DNA Polymerase to cleave a probe during the PCR reaction. The *Taq*man® probes used in our studies incorporate 6-carboxyfluorescin (FAM) reporter dye covalently attached at the 5' end and 6-carboxytetramethyrhodamine (TAMRA) quencher dye attached via a linker arm at the 3' end. When the probe is intact, the proximity of the reporter dye to the quencher dye results in suppression of the reporter fluorescence. During the PCR reaction, if the target of interest is present the probe specifically anneals between the forward and reverse primer sites. The 5'-3' exonuclease activity of *Taq* DNA Polymerase then cleaves the probe separating the reporter dye and the quencher dye, which results in increased fluorescence of the reporter. Accumulation of PCR products is detected directly using the ABI PRISM 7900 Sequence Detection System, which monitors the increase in fluorescence of the reporter dye. The cleaved probe fragments are displaced from the target, and polymerisation of the strand continues. This process occurs in every cycle and does not interfere with the exponential accumulation of product. The increase in fluorescence signal is detected only if the target sequence is complimentary to the probe and is amplified during PCR. Because of these requirements, any non-specific amplification is not detected.

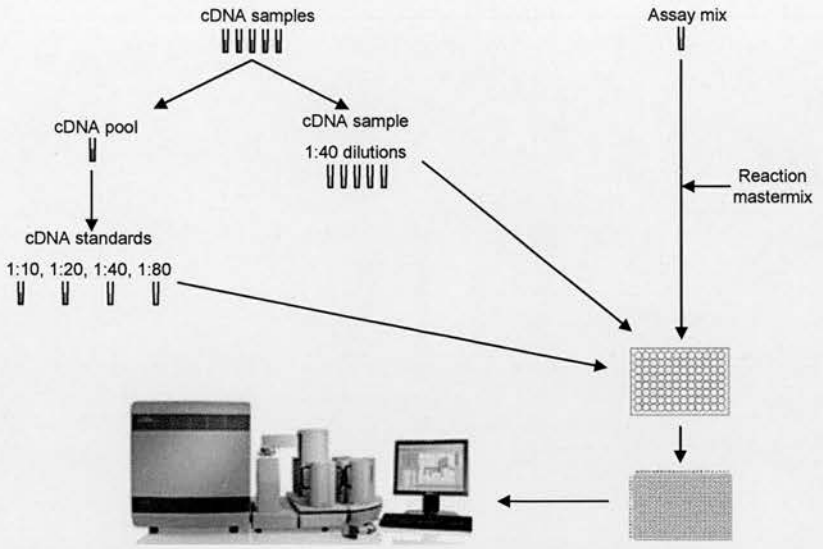

Figure 2.1: Schematic representation of real-time PCR set-up. cDNA standards were prepared from a pooled aliquot of all cDNA samples. cDNA (standards and samples) and assay mastermix were transferred to a 96-well plate from which they were aliquoted into a 374-well reaction plate using a multichannel pipette.

Data analysis was carried out using Sequence Detection Systems (SDS) software. Before analysing data the baseline and threshold values are adjusted. The baseline is a range of cycles before genuine amplification of PCR product is detected and is set so that the initial amplification curve begins at a cycle that is greater than the maximum value of the baseline. SDS software uses a default range of cycles 3-15 to establish the baseline, which may be adjusted if necessary. Once the baseline range is determined, the threshold value is automatically set at 10 standard deviations above the mean baseline fluorescence within the exponential phase of the logarithmic scale amplification plots. The threshold can be adjusted manually if necessary. The cycle number at which a PCR amplification plot crosses this threshold is known as the C_T value for the sample. The C_T value is predictive of the quantity of input cDNA. The more of the target gene present in the sample the earlier it will be detected in the PCR cycles and the lower the C_T. A standard curve is constructed using serial dilutions of cDNA. Relative target gene mRNA abundance in samples is extrapolated from the standard curve (CT value vs. target gene abundance) and expressed in arbitrary units. Target gene data are then normalised to an endogenous control, TATA-box binding protein (TBP), and calibrated to the control group in the study. Details of the real-time PCR assays used in this study are described in Table 2.1 and 2.2. PCR cycling conditions are outlined below.

PCR was performed in a 10µl reaction mixture containing 5.0µl of *Taq*Man Universal PCR Master Mix (Applied Biosystems, Foster City, CA), 200nM of each primer, 5nM probe, 4.5µl of template (1:40 dilution of cDNA synthesised as described in section 2.2.4.1) in 384 well plates (Figure 2.1). In order to generate a standard curve; an aliquot of cDNA from each sample was collected and used to form stock cDNA. Serial 1:10 dilutions of the stock cDNA were included as standard samples on the plate in a similar manner to test samples. Non-template negative controls were also constructed by substitution of nuclease-free water for cDNA. Each sample was assayed in duplicate or triplicate. Thermal cycling conditions comprised an initial denaturation step at 95°C for 10 min and 40 cycles of; 95°C for 15 sec and 60°C for 1 min.

Table 2.1: Primer and probe sequences for real-time assays by design.

GENE	FORWARD PRIMER (5'-3')	REVERSE PRIMER (5'-3')	PROBE (5'-3')
WNK1-T	GGGATGTACCAGAAGATGTTGCT	CCATGGTCTTGTGATCACCTTCA	CCAGACTCAACCATTTCT
WNK1-S	TGCTGCTGTTCTCAAAAGGATTGTA	TTCAGGAATTGCTACTTTGTCAAAACTG	CTGGCTTCACTCCCTCATT
WNK1-L	TGCATGCTTGAGATGGCTACAT	CTTTGTCAAAACTGGCTGGCTT	CACTCCACTGGTCACTCG
WNK4	GCGGAGGAGGTGGCT	GCCACTGGCTGGTAGTCA	CCAAGGCTACCATCTCC
WF	CGGAGCCATGGAGATGTTACTATG	CGAAAAGCCATTGGAAAACGAAAAG	CCACTTTGAAAACTCCG
ROMK1	CGGAGGTGTATGTGCAGAGT	GCCCAAATATGTGAGTGACAAACC	CAGTGCCCTGATCATC
ROMK2	GGACCAAGAAAATGAACGTTTGTCT	GCCCAAATATGTGAGTGACAAACC	CCTGATCTCATGGATTGC

Table 2.2: Real-time assays on demand.

GENE	ASSAY	Accession No.	Exon boundary	Assay position
cHKA	Mm00446786_m1	NM_138652.1	15-16	2410
NCC	Mm00490213_m1	NM_019415.1	19-20	2370
OSR1	Mm01351757_m1	BC046453.1	1-2	316
ROMK-T	Mm00444727_s1	NM_019659.2	2-2	931
SPAK	Mm00444101_m1	NM_016866.2	1-2	352
TBP	Mm00446973_m1	NM_013684.1	3-4	523

2.2.5.1 Evaluation of TBP as an Endogenous Control in Kidney.

An endogenous control is used to normalise the expression levels of target genes by correcting for potential differences in starting amounts of cDNA, in techniques such

as real-time PCR. It is important to demonstrate that while expression levels of the target may range widely, that of the endogenous control remains constant. Thus, when conducting this test, it is crucial to load identical amounts of cDNA for each test sample.

In order to confirm the uniformity of TBP expression in our samples, we introduced a known concentration of a specific RNA transcript into each of our RNA samples prior to reverse transcription, to act as an exogenous control using the following method. The Drosophila gene, Wingful (WF; NM_079995/AY078993), was selected as our RNA spike to avoid any sequence homology with mammalian transcripts (confirmed by a series of BLAST searches).

A fly homogenate was prepared by homogenising 10 flies in 500µl TRIzol® Reagent. A further 500µl TRIzol® Reagent was added to the homogenate prior to RNA extraction as outlined in section 2.2.3. To collect a pure aqueous RNA phase free from exoskeletal components, the phase separation step was performed twice. Drosophila cDNA was synthesised as described in section 2.2.4.1 and a WF transcript was amplified by PCR (conditions as outlined in section 2.2.4.2). Flanking T3 and T7 phage polymerase consensus sites were introduced by nested PCR (conditions as outlined in section 2.2.7.3.1; see Table 2.3 for primer sequences). The resulting WF PCR fragment was purified using a QIAquick PCR Purification Kit and concentrated in a DNA speed vac. Recovery of the DNA fragment was assessed by electrophoresis of 1µl of the DNA solution through an agarose gel as described in section 2.2.4.3 and a Low DNA Mass Ladder *(Invitrogen, 10068-013)* was used to determine approximate DNA concentration. WF RNA was transcribed *in vitro* at 37°C for 2 hr in a reaction containing ~1.2–1.6 µg cDNA, 2mM ATP, CTP, GTP and UTP, 10mM dithiothreitol (DTT), 2.5µl RNasin, and 2.35µl T3 RNA polymerase (40 units) in a total volume of 100µl 1x transcription optimised buffer. Following incubation, 2µl RQ1 DNase (RNase free; *Promega, P118B*) was added and reactions incubated at 37°C for a further 15 min to degrade the DNA template, after which reactions were placed on ice and purified using NICK columns. The column was prepared by washing through with 3ml TE buffer (pH 8.0). The transcribed RNA

mixture was then applied to the column. The column was washed with 400µl TE buffer and the initial elutant discarded. The transcribed RNA was eluted in an additional 400µl TE buffer, aliquoted and stored at -80°C until required. RNA concentration was quantified (0.014pg/µl) using a GeneQuant RNA/DNA Calculator. WF RNA was introduced into experimental RNA samples prior to reverse transcription (described in section 2.2.4.1) by spiking the H_2O used in this reaction with WF RNA (1:10,000 dilution, ~1pg Wingful RNA per reverse transcription reaction). As the concentration of WF present in each sample was constant, we were able to assess the uniformity of TBP gene expression by real-time PCR, by comparing it to that of WF.

Preliminary work showed TBP to be an excellent control for gene expression in kidney, showing no significant variation over a range of relevant and comparable treatments (dietary and induced hormone changes).

2.2.6 Northern Analysis of RNA

2.2.6.1 RNA Electrophoresis and Capillary Transfer

Total RNA was separated by electrophoresis on a 1.2% agarose formaldehyde denaturing gel. A 100ml gel was prepared by melting 1.2g of agarose in 73ml DEPC-treated water and 10x MOPS buffer (10ml), and adding 17ml formaldehyde before pouring into a gel mould with appropriately sized combs in place. RNA was prepared for electrophoresis by precipitating 15µg of RNA by centrifugation at 12,000g for 20 min at 4°C. Supernatant was removed and the RNA pellet was washed with 100µl 75% ethanol. The pellet was vortexed and centrifuged at 12,000g for 10 min. Following the RNA wash, the ethanol was removed, the pellet was briefly air-dried on ice and resuspended in 15µl RNA sample buffer. The RNA sample was denatured by incubation at 65°C for 10 min and snap-cooled on ice for a further 10 min. 4µl sterile Type III loading buffer and 0.5µl ethidium bromide (10 mg/ml) was added to each sample of denatured RNA. The RNA was loaded into the wells on the gel and electrophoresed in 1x MOPS buffer in a gel tank at 90V for 4-6 hr, until the front band of the loading buffer was ¾ of the way down the gel. The gel was photographed under UV light (λ = 254nm) with as little exposure as possible to minimise RNA

damage. The presence of intact 28S, 18S and 5S Ribosomal RNA bands indicated that the integrity of the RNA was intact. The gel was soaked for two 10 min intervals in 10x SSC buffer for 10 min before blotting onto a nylon membrane. A wick of Whatman 3MM chromatography paper was placed over an upturned gel mould in a plastic tray containing 10x SSC buffer and the gel placed on top (upside down). A piece of nylon membrane cut to the same size (prewetted) was smoothed on top of the gel and this was covered with 3 layers of 3MM filter paper and approximately 10cm of paper towels. A glass plate and light weight was placed on the top to secure the apparatus, and a builder's spirit level was utilised to ensure "evenness" of the tower. Capillary transfer was allowed to take place overnight at room temperature. The following day, the membrane was removed and washed in 2x SSC to remove any gel fragments and the efficiency of transfer checked by photographing both the gel and the membrane under UV light (λ = 254nm). The membrane was air-dried for ~15 min and cross-linked by baking for 2 hr at 80°C between two sheets of 3MM Chromatography paper. Membranes were stored at 4°C until required.

2.2.6.2 Hybridisation to ^{32}P-labelled cDNA

The membrane was placed in a Techne hybridisation bottle containing 20ml hybridisation buffer (0.5M $NaPO_4$/7% SDS) that had been pre-heated to 65°C (Techne Hybridiser HBID). Denatured Salmon testes DNA (10mg/ml; 200µl) and denatured yeast tRNA (50 mg/ml; 8µl) was then added to this. The membrane was prehybridised in a Hybaid hybridisation oven at 65°C for a minimum of 2 hr. The ^{32}P-labelled cDNA probe (prepared as described in section 2.2.6.3) was denatured before use by heating to 100°C for 10 min, followed by snap-cooling on ice for 10 min. Denatured probe was added directly to the hybridisation buffer ($1.5x10^6$counts/ml hybridisation buffer) and the membrane was hybridised with the probe overnight at 65°C. The probe was then disposed of and the membrane was rinsed with wash buffer A. This was followed by a further two washes in the same wash buffer at 65°C for 10 min. The level of radioactive signal remaining on the membrane was checked and if this was too high the membrane was washed 1-2 times in wash buffer B at 65°C for 10 min. If necessary, a super high stringency wash was carried out 1-2 times in wash buffer C at 68°C for 10 min. The membrane was

MRC UNIV. EDINBURGH

wrapped in parafilm and exposed to a Fujifilm imaging screen for between 5 min-24 hr and the level of hybridised probe quantified using a Fuji FLA2000 phosphoimager. Membranes were also exposed to Kodak Biomax MS film at -70°C for 1-7 days.

Membranes were stripped after probing by a 20 min wash with boiling 0.1% SDS. Stripping was confirmed by exposing the membrane to Kodak Biomax MS film at -70°C overnight.

2.2.6.3 Preparation of ^{32}P-labelled probes

2.2.6.3.1 Preparation of cDNA templates by PCR

cDNA templates were prepared by PCR (as described in section 2.2.4.2) for various genes of interest, to be used subsequently for the synthesis of DNA probes for use in Northern hybridisations. Prior to use as cDNA templates for probe generation, all PCR products were purified using either a QIAquick PCR Purification Kit or a QIAquick Gel Extraction Kit (Qiagen, Crawley, UK). Using the second purification method, the sample was first electrophoresed on a low melting point agarose gel (made as in section 2.2.4.3 but using low melting point agarose). The DNA fragment was visualised under UV light, excised from the gel using a scalpel, purified from the gel using the QIAquick Gel Extraction Kit and resuspended in 50µl DEPC-treated water. DNA fragments were concentrated in a DNA speed vac. Recovery of the DNA fragment was assessed by electrophoresis of 1µl of the DNA solution through an agarose gel as described in section 2.2.4.3.

2.2.6.3.2 ^{32}P-Labelling of cDNA

Rediprime® II *(RPN1633/4, Amersham)* random primed DNA labelling kit was used to label the DNA fragments. Approximately 20ng of DNA template was aliquoted into an Eppendorf, made up to 45µl with sterile TE buffer and denatured at 100°C for 10 min, and snap-cooled on ice for a further 10 min. In the meantime, 5µl [α^{32}P]-dCTP was added to the Rediprime® pre-mix to allow maximum rehydration of the lyophilised mix, and incubated at room temperature. The denatured probe was added to the rehydrated Rediprime® mix by pipetting ~12 times and incubated at 37°C for

30 min. Unincorporated radioactivity was removed by passing the mixture through a NICK column. The NICK column was prepared by washing with 3ml TE buffer (pH8.0) before application of the mixture. The column was washed with 400µl TE, the elutant discarded and the labelled DNA eluted from the column with a further 400µl TE. The probe was precipitated by adding 2µl tRNA (50 mg/ml), 40µl 3M sodium acetate pH5.2 and 1126µl 100% ethanol (cold), and centrifuging at 12,000g for 15 min. Supernatant was removed and the pellet was washed with 100µl 75% ethanol. The pellet was vortexed and centrifuged at 12,000g for 5 min. The ethanol was then removed, the pellet was briefly air-dried and resuspended in 400µl TE buffer (pH8.0). The activity of the probe was assessed by mixing 4µl of probe with 400µl of PicoFluor 40 scintillant fluid and counting in a β-counter. The probe was used if the specific activity was greater than 15,000cpm/µl.

2.2.7 ^{35}S *In Situ* Hybridisation

In situ hybridisation (ISH) allows the visualisation of the exact cellular and/or structural location of specific mRNAs (indicating transcription of the corresponding gene) by hybridisation of a ^{35}S-labelled 'antisense' RNA probe to the mRNA of interest. ^{35}S-UTP labelled RNA 'sense' probes of similar length, nucleotide content and specific activity were included in experiments in order to assess the specificity of the hybridisation seen.

Only RNase free, sterile solutions and equipment were used for ISH experiments in order to prevent degradation of target mRNA by exogenous RNases.

2.2.7.1 Slide Preparation

Prior to use, glass microscope slides were coated in 3-aminopropyltriethoxysilane in order to prevent section dehiscence. Slides were racked and washed in the following series of solutions; 0.2M HCl for 3 min, DEPC-treated water for 3 min, 2% 3-aminopropyltriethoxysilane in acetone (*Sigma, A3648;* dehydrated by filtering through $NaSO_4$) for 10 sec, acetone for 3 min (twice), and finally DEPC-treated water for 3 min. Slides were air-dried for 30-60 min before baking at 50°C for 4-16 hr. Dried slides were wrapped in aluminium foil and stored for up to 3 months.

2.2.7.2 Tissue Section Preparation

Tissues were routinely frozen on dry ice immediately after dissection from the animal and stored at -80°C until required.

Frozen tissue sections were cut using a Leica cryostat. Tissues frozen at -80°C were placed in the cryostat chamber at -20°C and allowed to equilibrate for approximately 30 min. Following equilibration, tissues were embedded in Cryo-m-bed embedding compound and positioned in the correct orientation for sectioning. 10μm thick sections of tissue were transferred to aminopropyltriethoxysilane-coated slides, and stored at -80°C until required.

2.2.7.3 Synthesis of ^{35}S-UTP Labelled Ribo-Probes

2.2.7.3.1 Preparation of cDNA templates by PCR

cDNA templates were prepared for various genes of interest, to be used subsequently for the synthesis of RNA probes for ISH analysis, using a nested PCR method. Firstly, the standard PCR method outlined in section 2.2.4.2, was used to generate an initial PCR product. When abundant clean product of expected size was generated, 1/400 and 1/8000 dilutions were made and used as templates in a second 'floppy' PCR where primers included 5' extensions containing phage polymerase consensus sites, with sense and antisense primer pairs incorporating T3 (TCTAGATTAACCCTCACTAAAGGGA) and T7 (GGATCCTAATACGACTCACTATAGGG) sites, respectively. The 'floppy' PCR program used 5 cycles of [45 s at 95°C, 45 s at 55°C, 120 s at 72°C], followed by 30 cycles of [45 s at 95°C, 45 s at 69°C, and 120 s at 72°C], and finally 10 min at 72°C. The dilution (1/400 or 1/8000) that produced the cleanest 'floppy' PCR product was used to generate a probe template stock.

Prior to use as cDNA templates for probe generation, all PCR products were purified using either a QIAquick PCR Purification Kit or a QIAquick Gel Extraction Kit (Qiagen, Crawley, UK). Using the second purification method, the sample was first electrophoresed on a low melting point agarose gel (as in section 2.2.4.3 but using

low melting point agarose). The DNA fragment was visualised under UV light, excised from the gel using a scalpel, purified from the gel using the QIAquick Gel Extraction Kit and resuspended in 50µl DEPC-treated water. Recovery of the DNA fragment was assessed by electrophoresis of 1µl of the DNA solution through an agarose gel as described in section 2.2.4.3.

2.2.7.3.2 ^{35}S-UTP-Labelling of cDNA

0.5-1µg of cDNA template (prepared as described in section 2.2.4.1) was transcribed by incubation at 37°C for 60-90 min in a reaction mixture containing 1mM ATP, CTP and GTP, 4µl ^{35}S-UTP (1.48 MBq/µl), 10mM dithiothreitol (DTT; *Sigma, D9779*), 0.4µl RNasin (40U/µl; *Promega, N211A*), and 1µl appropriate RNA polymerase (T3, sense (17U/µl; *Promega, P208C*); T7, antisense (20U/µl; *Promega, P207C*)) in a total volume of 10µl 1x transcription optimised buffer. Following incubation, 1µl DNase 1 (RNase free) was added and reactions incubated at 37°C for a further 10-15 min to degrade the DNA template, after which probes were placed on ice for 1-5 min and purified using NICK columns, to remove unincorporated radioactivity. The column was prepared by washing through with 3ml TE buffer (pH 8.0). The probe mixture was then applied to the column. The column was washed with 400µl TE buffer and the initial elutant discarded. Labelled probe was eluted in an additional 400µl TE buffer.

For each probe, the total activity was estimated by counting 1µl of probe in 1ml PicoFluor 40 scintillant fluid in a β-counter (minimum activity required $2x10^5$ cpm/ µl). The purity of each probe was determined by running an aliquot (typically 0.5–$1x10^6$ counts) on a urea-5.3% acrylamide gel and exposing the gel to Kodak Biomax-MR film (HA West Ltd, Edinburgh, UK). High quality probes should produce a single black band on the developed film. Probes were stored at -20°C until required, for up to 3-4 weeks.

2.2.7.4 Fixation Protocol

Slides were removed from the -80°C freezer and kept on dry ice until the start of the fixation procedure. Slides were fixed in ice cold 4% paraformaldehyde in 0.1M phosphate buffer for 10 min (maintains tissue morphology and inhibits endogenous ribonucleases). Slides were rinsed twice in 1x PBS for 5 min, acetylated in 0.1M triethanolamine with 0.25% acetic anhydride for 10 min (reduces non-specific binding of the probe to positively charged amino groups in tissues) and rinsed in 1x PBS for 3 min. Following dehydration through a series of ethanol solutions (70, 80 and 95% ethanol in DEPC-treated water) slides were air dried for 30 min.

2.2.7.5 Prehybridisation and Hybridisation Steps

Following fixation, slides were pre-hybridised with 200µl/slide of 2x pre-hybridisation buffer diluted 1:1 with deionised formamide, at 50°C for 2 hr. Dampening two layers of Whatman 3MM chromatography paper with box buffer A humidified the slide boxes, hence preventing tissue sections from drying out.

Sense and antisense probes were thawed and added to 2x hybridisation buffer diluted 1:1 in deionised formamide to give a final probe concentration of $10x10^6$ cpm/ml. Probes were denatured at 75°C for 10 min and snap-cooled on ice before addition of 10mM DTT. Pre-hybridisation buffer was drained from slides and 200µl appropriate probe in hybridisation buffer was applied to slides. Slides were hybridised in sealed, humidified boxes at 50°C for an optimum of 16 hr.

2.2.7.6 RNase Treatment and Washes

Following hybridisation, slides were washed three times in 2x SSC for 5 min and carefully wiped dry around the sections with lens tissue. 200µl of RNase A (30µg/ml in box buffer B) were applied to each slide and slides were incubated at 37°C for 1 hr in humidified boxes (1 layer of Whatman 3MM chromatography paper dampened with box buffer B) to remove unhybridised probe.

Following RNase treatment, slides were washed in 2x SSC at room temperature for 1 hr, then in 0.1x SSC at 60°C for 1 hr, and finally in 0.1x SSC heated to 60°C and

allowed to cool to room temperature for the duration of the wash (1 hr). After washes, slides were dehydrated through a series of ethanol solutions containing 0.3M ammonium acetate (2 min in each of 50, 70 and 90% ethanol) and air-dried.

2.2.7.7 Visualisation of Hybridisation

Slides were exposed to Kodak Biomax-MR film for 1-10 days. ^{14}C-microscales were included with each exposure to calibrate autoradiograph greyscales in the image analysis process. Afterwards, slides were individually dipped in NTB-2 photographic emulsion (diluted 1:1 with water at 42°C) and exposed in light-tight boxes for a period of 1 day to 5 weeks at 4°C. Slides were developed in D19 solution (diluted 1:1 with water) at 15°C and fixed in Amfix solution (diluted 1:5 with water at 15°C) and rinsed in water.

2.2.7.8 Image Analysis

For image analysis autoradiographic films were scanned on a high resolution flatbed scanner and any damaged or inadequate sections were excluded. Dipped slides were visualized using a Zeiss microscope and images were captured using a Dage MTI CCD72S imaging camera and Zeiss Contron KS400 software. Digital image analysis was performed using custom-written applications within the environment of the Image Processing Toolkit of MATLAB® version 7 (The Mathworks.Inc. MA) using 16-bit grayscale TIFF images, and scaling across an intensity range from 0(black)-65535(white). This allows semi-quantitative image analysis of autoradiographic films and dipped emulsion slides from ISH studies measuring the areas and grayscale intensities (or silver grain densities) as an index of expression level. Measured grayscale levels are converted to equivalent dpm of bound radioactive probe by calibrating from co-exposed ^{14}C-microscales specifically designed for this purpose (*RPA511* [10 levels between 3.7-3635MBq/g] and *RPA504* [8 levels between 1110-31890MBq/g]; *Amersham*). Alignment of consecutive sections involved systematic rotation and linear displacement of one image relative to the next calculating their normalized cross-correlation and iteratively proceeding to find the optimal alignment, where this value is a maximum. The aligned images could then be displayed as different red and green channels of a single overlaid merged image. The

software was useful in facilitating selection of regions (typically complex shapes delineated by an expression threshold contours) showing expression highly significantly above background levels. The threshold expression levels (or level) above which expression was to be included for analysis were entered on graphical sliding scales, each of which plotted an expression contour line at the threshold value. Regions within the contour (having expression above threshold) were analysed to calculate area, average expression in grayscale and Bq/g derived from scaling units via automatic calibration using the microscales. Background was low with sense section backgrounds having a greyscale level not significantly different to zero.

2.2.8 Western blotting

Antisera were tested for the ability to detect WNK1 and WNK4 by western blotting. Soluble and insoluble protein fractions were prepared from kidney homogenate as described below and the protein concentration estimated using the protein estimation assay described in section 2.2.2.4.

2.2.8.1 Preparation of tissue homogenates

Kidneys were removed from storage at -80°C, roughly dissected while frozen, added directly to lysis buffer (~0.5mg tissue per 1ml buffer) and mechanically homogenised. Homogenates were centrifuged at 1000rpm for 1 min at 4°C to spin down insoluble tissue debris. The supernatant was removed and centrifuged for 1 hr at 14,000rpm at 4°C to separate the soluble protein fraction (supernatant) from the insoluble protein fraction (pellet). Soluble protein was aliquoted and stored at -80°C until required. Insoluble protein was resuspended in homogenising buffer (~1/5 original volume) supplemented with 0.1% Triton X-100. Laemmli buffer (4x) was added to aid resuspension. Pipetting and denaturing at 100°C for ~10 min with intermittent vortexing resuspended the pellet. This insoluble protein fraction was aliquoted and stored at -80°C until required.

2.2.8.2 Separation and transfer of proteins by SDS-PAGE

1mm thick SDS-PAGE gels were prepared in the vertical electrophoresis system *(Mini-Protean 3 Cell, Bio-Rad).* 5% resolving gel was poured between glass plates to

two-thirds of their height. The surface was covered with water-saturated butanol until the gel set. The butanol was then washed out and a 4% stacking gel poured on top, and a comb added and allowed to set.

Samples of 30μg of protein were diluted 1:4 in 4x Laemmli buffer and denatured for 5 min by heating to 99°C, snap-cooled on ice for 5 min and immediately loaded into separate wells on the SDS-PAGE gel. Samples were electrophoresed in 1xLaemmli (Tris-Glycine) running buffer at 20mA along with molecular weight markers *(Bio-Rad, 161-0374)* until the 75kDa marker reached the base of the gel. Proteins are separated according to their weight, with smaller species migrating further over the same period. The stacking gel was removed and the resolving gel was pre-soaked in cold transfer buffer, along with Hybond ECL™ Nitrocellulose Membrane, for 15 min. Proteins were then transferred to the membranes by electroblotting *(Mini Trans-Blot Electrophoretic Transfer Cell, Bio-Rad)* in cold transfer buffer at 250mA for 3 hr at 4-7°C. Complete transfer was verified by the loss of marker dyes from the gel.

2.2.8.3 Membrane staining

Membranes were stained in 0.1% Ponceau for ~1 minute (until clear bands were visible) and washed briefly in dH2O to remove excess stain. Membranes were then placed on a glass plate and cut into strips as required, and destained in 400μM NaOH for ~1 minute (until stain disappears), washed by dipping briefly in dH2O and neutralised in 1xPBS.

2.2.8.4 Blocking membranes & antibody preparations

Membranes were transferred to dishes containing blocking solution and left overnight at 4°C (or 1 hr at room temperature) on an orbital shaker (Stuart Gyro-rocker SSL3) to reduce non-specific binding. Primary antibody dilutions in blocking solution were added to the membrane for 2 hr at room temperature, followed by 5x 5 min washes in blocking solution on the orbital shaker. Secondary antibody dilutions in blocking solution were applied to the membrane for 1 hr at room temperature. This was followed by 3x 10 min washes in 1x TBS to remove unbound antibody before

proceeding to bound antigen visualisation using the Amersham ECL system (see below).

A second antibody application could be made to the same membrane after the existing antibody complex had been stripped. Blots were incubated for 1 hr with stripping buffer on the orbital shaker, washed 3x 5 min in 1x TBS, then blocked as before. Stripping was usually confirmed by ECL™ detection (see below) prior to re-use. ECL™ reagents were washed off in 1xTBS and stored at -4°C until required.

2.2.8.5 Protein detection and quantification

The antibody complex bound to the membrane was visualised using ECL™ (enhanced chemoluminescence) Western Blotting Detection Reagents *(Amersham Biosciences, RPN106)*. Secondary antibodies are attached to a horseradish-peroxidase molecule which catalyses the oxidation reaction of luminol in the presence of hydrogen peroxide and light is emitted. The light produced exposes chemiluminescence-sensitive film in areas corresponding to the specific antigenic protein bands on the membrane. Following the application of secondary antibody and subsequent 3 washes in 1xTBS, 1:1 mixtures of ECL™ Reagent 1 and 2 were applied to the membrane for 1 min, which was then drained (excess carefully blotted off), wrapped in transparent film, and placed under Hyperfilm ECL™ for a period of time sufficient to obtain visible bands. The film was developed using a hyper-processor.

2.2.9 Immunohistochemistry

Immunohistochemistry involves the binding of specific antibodies to target proteins in tissues, then attaching a visualisation system typically involving a secondary antibody and a system locally generating an amplified colour reaction (e.g. involving horseradish peroxidase) which enables their precise cellular localisation.

2.2.9.1 Sectioning

5μm sections were cut using a microtome, floated on a 42°C water bath and recovered onto SuperFrost Plus slides. Slides were dried at 40°C to heat fix tissue to

the slides. For fresh-frozen tissue sections were cut and mounted as described in section 2.2.7.2, and stored at -80°C.

2.2.9.2 Rehydration

To enable the antibody to penetrate the tissue effectively, paraffin section slides were dewaxed by 2x 5min treatments in xylene, rehydrating through an ethanol series (100%-95%-70%; 20 sec each), washing in dH_2O 2x5min and then in 1xPBS 2x5min.

2.2.9.3 Antigen Retrieval

Some antibodies require an extra step termed "antigen retrieval" which assists in ensuring adequate exposure of the target epitope and enhances immunodetection. For this purpose rehydrated slides were placed in a pressure cooker, containing either 0.01M sodium citrate buffer or 0.05M glycine/EDTA buffer, boiled under pressure for 5 min and left to rest in hot buffer for 20 min[21]. Following antigen retrieval, slides were washed in 1x PBS 3x3min.

2.2.9.4 Antibody Additions

The protocol used involved the sequential application of (1) a primary antibody, (2) a biotinylated secondary antibody, (3) an avidin horseradish peroxidase (HRP) complex and (4) a visualisation process whereby colourless DAB (diaminobenzidine tetrahydrochloride) and H_2O_2 allow local generation of a brown colour (oxidised DAB) by HRP revealing when the antigen is within the tissue.

Endogenous peroxidase was blocked in 3% H_2O_2 in Methanol for 10min, followed by washes in 1xPBS 3x3min. If a HRP detection system was not used this blocking step was omitted from the protocol. Endogenous avidin and biotin was blocked using an avidin/biotin blocking kit (Vector Laboratories, Peterborough, UK). Tissues were incubated with avidin for 15min, washed in 1x PBS for 2min, then incubated with biotin for 15min and washed in 1xPBS for 2min. Non-specific binding between the tissue and the antibody was blocked by incubating tissues in 1:5goat serum/5%BSA for 4hr.

Primary antibodies were diluted in 1:5goat serum/5%BSA, added to each slide and incubated at 4°C overnight. Slides were then washed in 1x PBST 3x3min.

Biotinylated secondary antibodies were diluted in 1:5goat serum/5%BSA and incubated at room temperature for 1hr. Following this incubation, slides were washed in 1x PBST for 3x3min.

A fresh Avidin-Biotin-HRP complex (ABC Elite, Vector Laboratories, Peterborough, UK) was then added to each slide for 1 hour at room temperature. This ABC complex was prepared 30min prior to use by adding 9µl of ABC Elite reagents A and B to 1ml 1x PBS ensuring binding between avidin and HRP.

Slides were then rinsed in 1x PBST 3x3min and DAB added following the kit instructions (Vector Laboratories, Peterborough, UK). This was incubated until a satisfactory level of brown immunohistochemical stain developed, and then finally slides were transferred to a dH_2O wash for 30-60 sec to stop the reaction.

The ABC technique enables the visualisation of the target protein location. The complex binds to biotin on the secondary antibody and when hydrogen peroxide (enzyme substrate) is added, the chemical reaction causes the enzyme to transfer hydrogen from DAB to the peroxide. The oxidised DAB forms a dark brown precipitate at the site of enzyme activity.

2.2.9.5 Tissue Staining

Sections were counterstained in haematoxylin (H_20 based) and then dehydrated through a series of ethanol washes (70, 80, 95, 100, 100% ethanol – 20 sec each) ending finally with 2x5min xylene treatments. Sections then were coverslip DPX mounted.

2.2.9.6 Immunohistochemistry on fresh-frozen sections

Fresh frozen sections are fixed directly from frozen in 10% Neutral Buffer Formalin for 10 min and washed in 1xPBS 2x5min. Fresh frozen sections do not require an antigen retrieval step. Endogenous peroxidase is blocked in 0.3%H_2O_2 in dH_20 for 30 min, followed by washing in 1xPBS for 10min. From this stage onwards frozen sections are treated similarly to paraffin sections.

2.2.10 Statistics

Data are expressed as mean±SEM, $P<0.05$ was considered significant, and comparisons between groups analyzed by one-way ANOVA and Neuman-Keuls post-hoc testing, unless otherwise stated. Least significant difference post-hoc test for planned comparisons ($ANOVA_{LSD}$) was also used if Neuman-Keuls testing was borderline non-significant. Changes are routinely expressed as % change (mean±SEM) relative to control values. Where changes are of a larger scale, they are expressed as fold change (mean±SEM), again relative to control values, and 95% confidence intervals are quoted.

Table 2.3: Primer sequences.

TARGET	SEQUENCE (5'-3')	ORIENTATION	PCR	USE
γENaC	GCCCGTCACAAACATCTACAATGCTGC	Sense	S	-
γENaC	CTTGGCCAGGTCAGTCTTGTTGAGC	Antisense	S	-
γENaC	tctagattaaccctcactaaagggaTCAGGAACATCTACAACGCTGC	Sense	N	ISH
γENaC	ggatcctaatacgactcactatagggCCAGGTCAGTCTTGTTGG	Antisense	N	ISH
cHKA	CAGCAGGGGCTCTTCAGAAAC	Sense	S	-
cHKA	TTGTCCCACCAGCTTCCAGG	Antisense	S	-
cHKA	tctagattaaccctcactaaagggaGCTCTTCAGAAACAAAGTCATC	Sense	N	ISH
cHKA	ggatcctaatacgactcactatagggGGACCAGCTTCCAGGGTAG	Antisense	N	ISH
NCC	GCATTCATTCCTCAAGCAGGAAGGTAG	Sense	S	-
NCC	GGTGTGCCATACTCCTGCAGTAGG	Antisense	S	-
NCC	tctagattaaccctcactaaagggaTTCCTCAAGCAGGAAGGTAGC	Sense	N	ISH
NCC	ggatcctaatacgactcactatagggTGCCACCCGACTTGACCTTG	Antisense	N	ISH
NKCC2	AAGATGTCGGTCAGCATCCCTTCC	Sense	S	-
NKCC2	CCATCATTGAATCGCTCTCCTTAAGAAGA	Antisense	S	-
NKCC2	tctagattaaccctcactaaagggaCAGTCGCTTTCAGGTCCATG	Sense	N	ISH
NKCC2	ggatcctaatacgactcactatagggCATCGCACCAGCACACCTTTC	Antisense	N	ISH
ROMK1	CACACAACTCCACTCTTGAGTTAACC	Sense	S	-
ROMK1 (Core)	GATGTTTGAACATCCTTTCTGTCAGTGC	Antisense	S	-
ROMK1	tctagattaaccctcactaaagggaAGCAAGCATCATTGTGAGGC	Sense	N	ISH
ROMK1	ggatcctaatacgactcactatagggATCAGCACTCTGCACATACAC	Antisense	N	ISH
ROMK2	GCATCCAAACTCTCGAATCAAAGGTG	Sense	S	-
ROMK2 (Core)	GATGTTTGAACATCCTTTCTGTCAGTGC	Antisense	S	-
ROMK2	tctagattaaccctcactaaagggaGAATCAAAGGTGCAAGGGAC	Sense	N	ISH
ROMK2	ggatcctaatacgactcactatagggTCATGGATTGCTGGGGTAAAC	Antisense	N	ISH
ROMK3	AGGAAGCTCCATGAAGTGCACC	Sense	S	-

TARGET	SEQUENCE (5'-3')	ORIENTATION	PCR	USE
ROMK3 (Core)	GATGTTTGAACATCCTTTCTGTCAGTGC	Antisense	S	-
ROMK3	tctagattaaccctcactaaagggaCACCCTTGACAGGGCTC	Sense	N	ISH
ROMK3	ggatcctaatacgactcactatagggCCTGATCCTTACCGAGTC	Antisense	N	ISH
ROMK-T	TCCACRTTTACCCCAGCAATCCATGAG	Sense	S	-
ROMK-T	CCCACACATGAAAGAATTGATTATAACTCC	Antisense	S	-
ROMK-T	tctagattaaccctcactaaagggaTCAGGGCACTGACAGAAAG	Sense	N	ISH
ROMK-T	ggatcctaatacgactcactatagggCCACACAAGGAGTRCGGTTG	Antisense	N	ISH
WNK1-L (EX1)	CTTGTCAGTGCTGAGTGGGAGTC	Sense	S	NH
WNK1-L (EX1)	CAGATTTTGTTAACTTTCGATCCTGCAATTC	Antisense	S	NH
WNK1-L (EX1)	tctagattaaccctcactaaagggaGCAACCTAGTGTACCTGC	Sense	N	ISH
WNK1-L (EX1)	ggatcctaatacgactcactatagggTCCACAGTGGTTTCGGTG	Antisense	N	ISH
WNK1-S (EX4a)	AGAAACTACTAGTAGCAAAATCCCTGTC	Sense	S	NH
WNK1-S (EX4a)	GCTTCACTCCCTCATTTATACAATCC	Antisense	S	NH
WNK1-S (EX4a)	tctagattaaccctcactaaagggaGCCAAGCTAAATAGATTGTTG	Sense	N	ISH
WNK1-S (EX4a)	ggatcctaatacgactcactatagggCATTTATACAATCCTTTTGAGAAC	Antisense	N	ISH
WNK1-T (EX6-9)	GTATCCGACAAAACAAAGATGAAAGATATTCC	Sense	S	NH
WNK1-T (EX6-9)	CTGTATTCCCTGCTGCTGAGGATG	Antisense	S	NH
WNK1-T (EX6-9)	tctagattaaccctcactaaagggaGTTGCTCAAGAAATGGTTGA	Sense	N	ISH
WNK1-T (EX6-9)	ggatcctaatacgactcactatagggATGTTGGATAGGTTGTGAAG	Antisense	N	ISH
WNK1 (EX4b)	TTATGGAAGGTGCAGCCACTAGTGG	Sense	S	-
WNK1 (EX4b)	CTCAACCATTTCTTGAGCAACATCTTCTG	Antisense	S	-
WNK1 (EX4b)	tctagattaaccctcactaaagggaAGGTGCAGCCACTAG	Sense	N	ISH
WNK1 (EX4b)	ggatcctaatacgactcactatagggCCACTGTTGCACCAG	Antisense	N	ISH
WNK1 (EX8)	CTAGTATATCTGTGTTGTCTGATGGAACC	Sense	S	Splicing
WNK1 (EX15)	GTCATTGTTCACCATAATTGTTGCTATCTC	Antisense	S	Splicing
WNK1 (EX11)	CAACATCCTCAGCAGCAGGGAATAC	Sense	S	-
WNK1 (EX11)	GAGATGGGAAGCCCTGGTACAAAAC	Antisense	S	-
WNK1 (EX11)	tctagattaaccctcactaaagggaCTTCCAGTTTCCCAGACAG	Sense	N	ISH, NH
WNK1 (EX11)	ggatcctaatacgactcactatagggTACAAAACATCTCCAGAGG	Antisense	N	ISH, NH
WNK1 (EX12)	GATGTTTTGTACCAGGGCTTCCCATC	Sense	S	-
WNK1 (EX12)	CGTCTGAATGTGCACTGTCTGCAG	Antisense	S	-
WNK1 (EX12)	tctagattaaccctcactaaagggaGCTTCCCATCTCGACTG	Sense	N	ISH, NH
WNK1 (EX12)	ggatcctaatacgactcactatagggCTCCAGAACTGCTTGCTG	Antisense	N	ISH, NH
WNK1 (EX1)	CCAAGGCAGTGGGAATGTCCAATG	Sense	S	-
WNK1 (EX7)	CGTTTTCTCTTAATTAAGGACACCCTATC	Antisense	S	-
WNK1 (EX1)	GTCGCTTTCTCAAATTTGACATCGAAATC	Sense	N	-
WNK1 (EX7)	CTTTGATAGCTTTAGCCATGGTCTTGTG	Antisense	N	-
WNK1 (EX2)	GCAGGATCGAAAGTTAACAAAATCTGAAAG	Sense	N	NH
WNK1 (EX2)	ACGTCTTAAGTGTTCCAGATGTCATTAG	Antisense	N	NH
WNK1 (EX3)	GAAAATCAAAGTTTTAAGAAGCTGGTGTC	Sense	N	NH
WNK1 (EX3)	TCTTGGCAAAAGAAGCCCGCTTTAGAG	Antisense	N	NH

TARGET	SEQUENCE (5'-3')	ORIENTATION	PCR	USE
WNK1 (EX4)	ACCCCAGAGTTTATGGCTCCTGAG	Sense	N	NH
WNK1 (EX4)	CACTCCACTGGTCACTCGAC	Antisense	N	NH
WNK1 (EX5)	GTGGAGTGAAGCCAGCCAGTTTTG	Sense	N	NH
WNK1 (EX5)	GAATATCTTTCATCTTTGTTTTGTCGGATAC	Antisense	N	NH
WNK1 (EX6)	GACCTTTTGAACCATGCCTTTTTCCAG	Sense	N	NH
WNK1 (EX6)	CTCAACCATTTCTTGAGCAACATCTTCTG	Antisense	N	NH
WNK1 (polyA)	GTTGTGAGCTGTGTGTGAAAGATAAGG	Sense	S	NH
WNK1 (polyA)	CAGACCTCACTCAGAATGACTAAACC	Antisense	S	NH
WNK4 (EX6-9)	GAACGAGAGGTTCACCATCCAGG	Sense	S	NH
WNK4 (EX6-9)	CATCTGAGGCGTAGCTATCCCCAG	Antisense	S	NH
WNK4 (EX6-9)	tctagattaaccctcactaaagggaCAGGAGATGGTAGCCTTG	Sense	N	ISH
WNK4 (EX6-9)	ggatcctaatacgactcactatagggTAGCTATCCCCAGGAG	Antisense	N	ISH
WNK4 (EX1)	CTTCCCATGCTAGCACCTCGAAATAC	Sense	S	-
WNK4 (EX1)	ACGTTGCCACAGCCTGGGTTTC	Antisense	S	-
WNK4 (EX1)	tctagattaaccctcactaaagggaCCTCGAAATACGGAGACTG	Sense	N	ISH
WNK4 (EX1)	ggatcctaatacgactcactatagggCTGGGTTTCTGTGTCCTC	Antisense	N	ISH
WNK4 (EX10)	GGATAGCTACGCCTCAGATGC	Sense	S	-
WNK4 (EX10)	GCTCTGGTCTGAGACACTAGTGAC	Antisense	S	-
WNK4 (EX10)	tctagattaaccctcactaaagggaCTCAGATGCGGCATCAG	Sense	N	ISH
WNK4 (EX10)	ggatcctaatacgactcactatagggACTAGTGACCCGGAGC	Antisense	N	ISH
WNK4 (EX12-13)	GAAATTGCAGCTGCCATGGTATACAATG	Sense	S	-
WNK4 (EX12-13)	CTTCTCTGGGGCTCTGCATTGG	Antisense	S	-
WNK4 (EX12-13)	tctagattaaccctcactaaagggaGCGAGATGGATTCC	Sense	N	ISH
WNK4 (EX12-13)	ggatcctaatacgactcactatagggCATTGGGTGGGCCTG	Antisense	N	ISH
WNK4 (EX14-15)	CTTCTCTCTGGCTGTGATGACTGTG	Sense	S	-
WNK4 (EX14-15)	AAGCTGGGGCTTTCCCTCTTCAG	Antisense	S	-
WNK4 (EX14-15)	tctagattaaccctcactaaagggaTTTCCCTTGCTTCTTGTGAC	Sense	N	ISH
WNK4 (EX14-15)	ggatcctaatacgactcactatagggCTTCAGATATAGGTGCCAG	Antisense	N	ISH
WF	CATGCCGGTTTCTATCTGCGCAAG	Sense	S	-
WF	GTTGTCCTTCTTATTGCGATGCTCC	Antisense	S	-
WF	tctagattaaccctcactaaagggaCTGATTCCCGTGGGATTG	Sense	N	SPIKE
WF	ggatcctaatacgactcactatagggCGTCGATCTTGATATTGACC	Antisense	N	SPIKE

Nucleotide sequence in lowercase indicates T3 (sense) and T7 (antisense) RNA polymerase footprints incorporated into primer sequences. Northern hybridisation probes were typically generated by straight PCR (S; section 2.2.6.3.1), whereas ISH probes involved an additional nested PCR (N; section 2.2.7.3.1) reaction to incorporate T3 and T7 RNA polymerase binding sites. Both Northern hybridisation and ISH to exons 11 and 12 of WNK1 used the nested PCR product. Nested PCR was also used to produce Northern hybridisation probes against exons 2, 3, 4, 5, and 6 of WNK1 to ensure amplification of WNK1 cDNA only (confirmed by sequencing) across the highly conserved kinase domain region.

Chapter 3 WNK1 mRNA distribution and alternative splicing in mouse.

3.1 Introduction

Following the identification of a causal link between mutations in the WNK1 gene and Gordon syndrome[148] it has become of key importance to establish the role played by this unusual protein kinase in electrolyte balance and BP control. Although the underlying genetic cause of Gordon syndrome remained a mystery for several years it was widely accepted that the novel phenotype, featuring hypertension accompanied by hyperkalaemia[42;43], meant that a novel BP control pathway distinct from the aldosterone pathway could be involved. The effective treatment of Gordon syndrome patients with thiazide diuretics[13;43;119], a first-line treatment for essential hypertension, also emphasises that understanding the genes and pathway involved in Gordon syndrome is particularly valuable as it might yield some clues as to the causes of essential hypertension.

Intriguingly, cases attributed to WNK1 mutations in this autosomal dominant disorder are due to intronic deletions and are not recognised as directly affecting WNK1 coding sequence[148]. It is of great interest how such WNK1 mutations, in a widely expressed gene, cause an autosomal dominant disease, with a mechanism seemingly explicable by a distal nephron–limited ion transport defect[43;92]. One possibility sees the intronic region involved in transcriptional regulation, and some preliminary evidence maintains this as a reasonable explanation. Alternatively, this apparently "silent" mutation may alter the complement of spliced products transcribed from the gene. Such superficially "silent" mutations have been shown on closer investigation to cause dominant diseases by altering splicing, for example, in the fibrillin-1 gene, causing Marfan syndrome[71]. Thus, evidence relating to promoter use or alternative splicing of WNK1, especially selectively relating to kidney, is likely to be of particular value in understanding the role of this gene and how it is disrupted to cause hypertension and electrolyte imbalance in Gordon syndrome.

To elucidate the novel WNK1 BP control pathway active in distal nephron we have examined WNK1 expression in detail in mouse. The studies presented here describe and detail, several isoforms produced from the WNK1 gene, some of which show strikingly different tissue-specific distributions, including one showing abundant

expression in kidney that is seen at low level, if at all, in other tissues. Such modifications, generating this transcriptional diversity, also produce predicted proteins of very different structure and will radically affect function. The findings reported thus help elucidate not only probable mechanisms by which the WNK1 intronic deletions cause disease, but also further clarify the novel WNK1 BP control pathway.

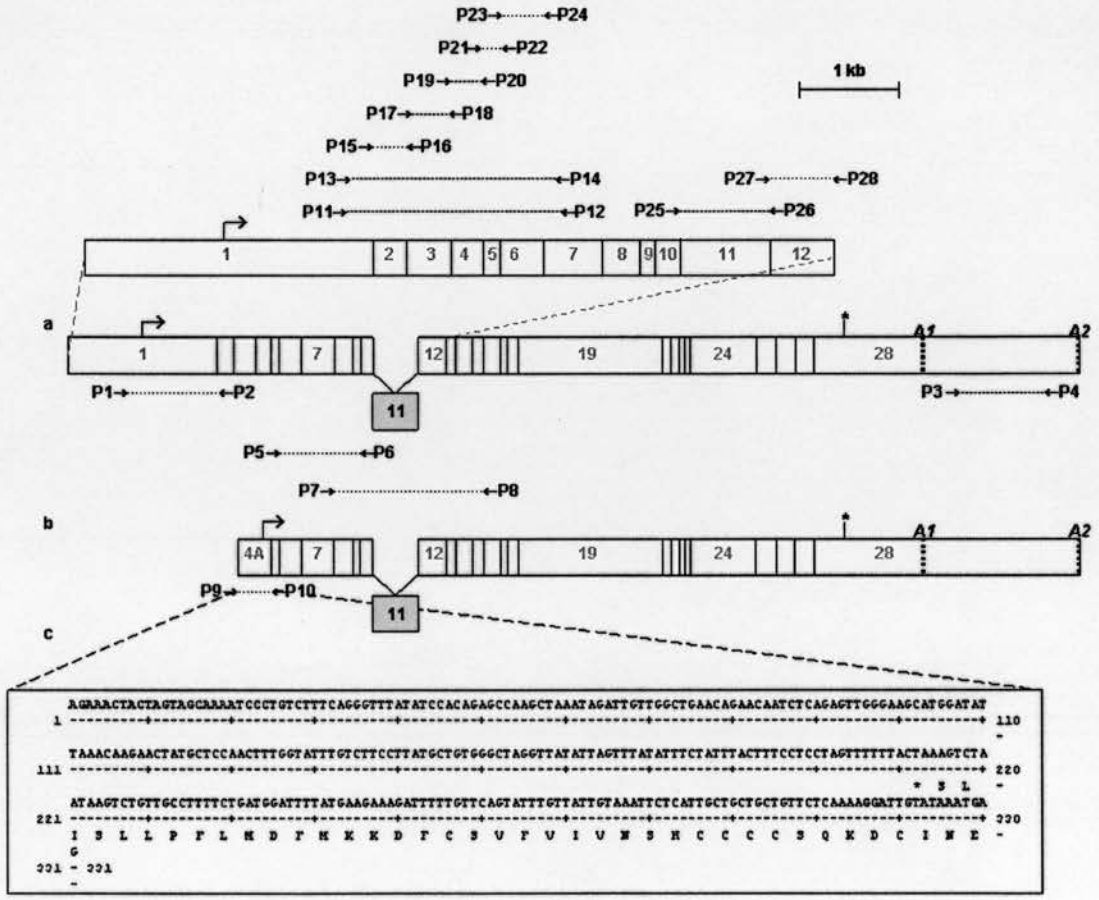

Figure 3.1: Schematic representation of WNK1 cDNA structure showing primer positions. (a and b) denote the cDNA structure of WNK1 and kidney-specific WNK1 containing exon 4A, respectively, with vertical bars representing splice junctions and dashed vertical bars indicating 3'-polyadenylation sites, *A1* and *A2*. Numbers within rectangles refer to exon numbers. Primers are represented by arrows (→) and numbered P1-P28. Additional primer details are given in Table 2.3. Horizontal dashed lines specify the cDNA region amplified by PCR using the corresponding primer pairs. (c) shows the cDNA sequence of exon 4A. The predicted amino acid sequence also shown would continue in frame across the splice site to exon 5.

3.2 Materials & Methods

Materials and common molecular biology methods are described in Chapter 2.

3.2.1 Northern Hybridisation Analysis

mWNK1 northern probes used in this study were constructed against: exons 6-9, P5/P6 (860 bp); poly-A, P3/P4 (875 bp); exon1, P1/P2 (928 bp); exon 2, P15/P16 (180 bp); exon 3, P17/P18 (187 bp); exon 4, P19/P20 (161 bp); exon 4A, P9/P10 (340 bp); exon 5, P21/P22 (96 bp); exon 6, P23/P24 (212 bp); exon 11, P25/P26 (462 bp); exon 12, P27/P28 (278 bp). cDNA templates for Northern probe production were PCR amplified (section 2.2.6.3.1) using the primer pairs detailed in Table 2.3. The primer numbering system used here refers to Figure 3.1 which illustrates relative primer/probe positions.

3.2.2 *ISH* Analysis

mWNK1 ISH probes used in this study were constructed against: exon 1 (434 bp); exon 4A (280 bp); exons 6-9 (552 bp); exon 11 (460 bp); exon 12 (283 bp); exon 4B (108 bp). cDNA templates for ISH probe production were PCR amplified using a nested PCR protocol (section 2.2.7.3.1) and primer pairs are detailed in Table 2.3.

3.3 Results

3.3.1 Discovery of Kidney-specific kinase deficient transcript

The mouse WNK1 gene (mWNK1) is large, spanning >120 kb, with a coding region showing 86% identity with human WNK1 (hWNK1). mWNK1 produces large transcripts (>10 kb) with cDNA encoded by 28 exons (Figure 3.1a), having a predicted 2377 amino acid protein. Northern blot hybridisation with exons 6 to 9 revealed widespread distribution of these large transcripts (Figure 3.2a) with high expression seen in testis > heart, lung, kidney, placenta > skeletal muscle, brain, and low-level expression elsewhere. Additional Northern blots show placental transcripts are of similar size to the major widely found isoform. In kidney, a smaller, more abundant mWNK1 transcript is seen, differing in size by at least 1.5 to 2 kb (Figure 3.2a). A 3'-polyadenylation (poly-A) site *A1* (Figure 3.1) is positioned approximately 800 bp downstream of the ORF. To assess whether the use of an alternative poly-A

site could account for this size difference, cDNA sequence encoding a second poly-A site approximately 2400 bp downstream of the ORF was isolated (Figure 3.1, *A2*). Northern blot hybridisation with cDNA between these alternative poly-A sites, revealed a similar expression profile to that described above (Figure 3.2b). Both transcripts in kidney were detected implying most WNK1 transcripts terminate at the second 3'-poly-A site (Figure 3.1, *A2*) and thus differential polyA site use is not the mechanism behind the generation of the different WNK1 isoforms seen in kidney by Northern blot. Having excluded this possibility, a probe to exon 1, overlapping the ORF (Figure 3.1), was designed within the 5' region of WNK1. Northern blot hybridisation probing for exon 1 revealed a similar expression profile for the large mWNK1 transcript but strikingly the smaller kidney-specific transcript was completely undetected, indicating it lacks exon 1 (Figure 3.2c).

To investigate whether this kidney-specific isoform lacked further 5' exons, nested PCR was used to produce separate probes against exons 2, 3, 4, 5, and 6 of mWNK1 (Figure 3.1), ensuring amplification of mWNK1 cDNA only (confirmed by sequencing) across the highly conserved kinase domain region. Northern blot analysis of kidney and testis RNA, showed that probes to exons 2, 3, and 4 only detect the large mWNK1 transcript, and not the smaller kidney-specific isoform (Figure 3.2d). In contrast, probes to exons 5 and 6 detect both mWNK1 transcripts. Thus, the smaller mWNK1 transcript in kidney lacks exons 1 to 4. Screening submitted expressed sequence tag (EST) databases suggested an alternative exon preceding exon 5 in kidney, positioned between exons 4 and 5 in the genomic sequence and therefore termed exon 4A. Conclusively, Northern blot hybridisation probing for this exon only detects the smaller mWNK1 transcript (Figure 3.2d), confirming inclusion of exon 4A in the kidney-specific isoform (Figure 3.1b).

3.3.2 Spatial distribution of WNK1 Expression

3.3.2.1 Distribution of Total WNK1 (WNK1-T) Expression in Kidney

ISH to exons 6 to 9 allowed detailed study of WNK1-T expression in mouse kidney. Figure 3.3 reveals clear WNK1 expression above background in distal nephron extending from early DCT (DCT1) into CNT and at lower level into CCD (lower

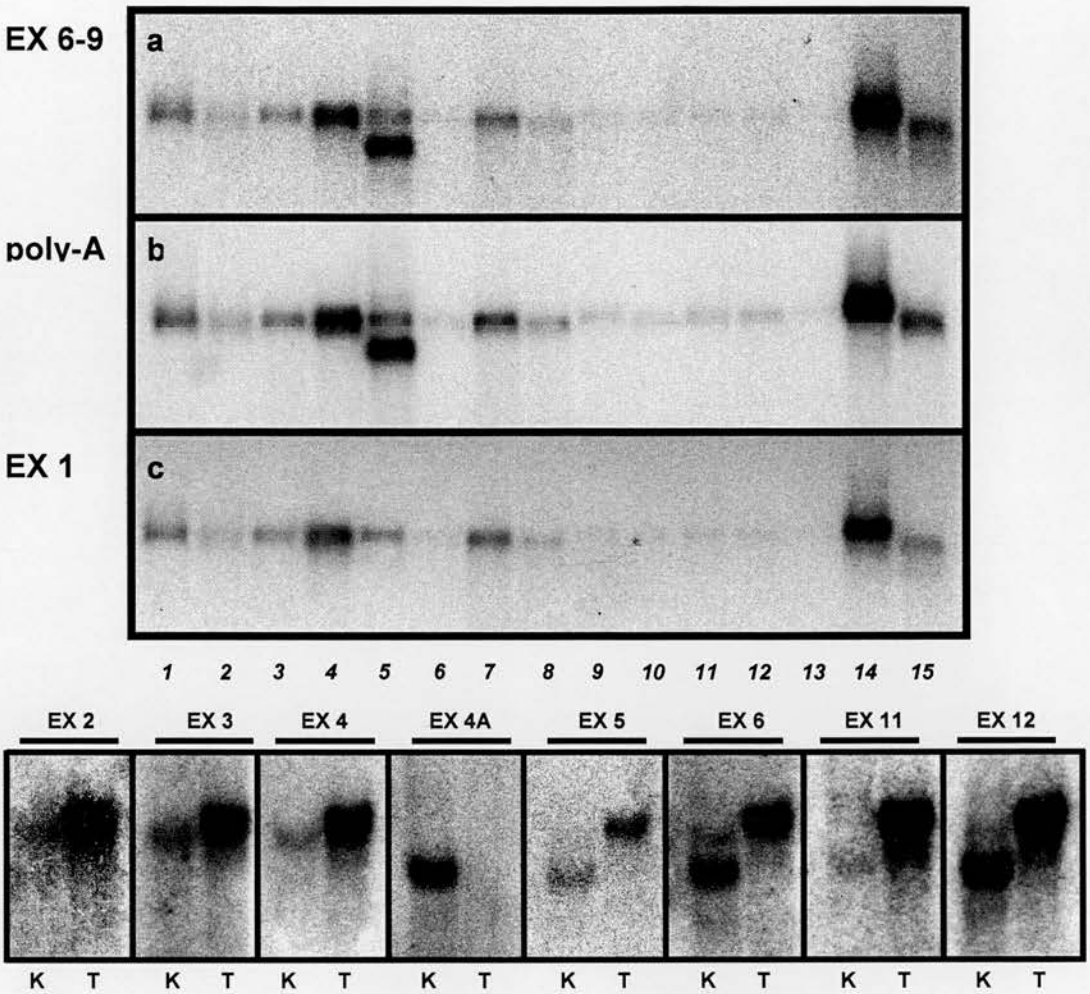

Figure 3.2: Northern analysis of WNK1 expression. Hybridisation with a probe incorporating exons 6-9 (a) detects widespread expression of large transcripts, approximately 10.2 kb in size. In addition, smaller and more prominent transcripts are detected in kidney (*lane 5*). This expression profile is also observed in (b) when hybridising with the poly-A probe (refers to sequence located between the two 3'-polyadenylation signals *A1* and *A2*). (c) Probing with exon 1 fails to detect the smaller kidney-specific transcripts. (d) Northern analysis reveals differential expression of individual exons in WNK1 isoforms in kidney (K) and testis (T). Hybridisation with probes against exons 2, 3, 4, 5 and 6 detect the large WNK1 isoform, strongly in testis but weakly in kidney. The smaller and more abundant kidney-specific isoform is only detected by probes to exons 5 and 6. A probe to an alternative exon, 4A, detects the smaller kidney-specific isoform only. Hybridisation with a probe to exon 11 detects the large WNK1 isoform in testis but signal is low for either isoform in kidney. In contrast, hybridisation with exon 12 readily detects both the kidney-specific isoform and the large WNK1 testis isoform. WNK1 expression was studied in (a, b, and c) across a range of mouse tissues. *Lane 1*, brain; *lane 2*, forebrain; *lane 3*, skeletal muscle; *lane 4*, heart; *lane 5*, kidney; *lane 6*, liver; *lane 7*, lung; *lane 8*, spleen; *lane 9*, stomach; *lane 10*, duodenum; *lane 11*, jejunum; *lane 12*, ileum; *lane 13*, colon; *lane 14*, testis; *lane15*, placenta (E16.5).

expression level in medullary rays; Figure 3.3). Strong expression in DCT continues adjacent to glomeruli and is seen looping close to their vascular pole (Figure 3.3 right panels) the site of the *macula densa*. Additionally, lower expression, approaching but above sense background levels, is distributed more extensively. This appears to have a different origin from the higher expression seen in DCT (i.e. different WNK1 transcripts; see below). Figure 3.4 illustrates the nephron anatomy and structures involved in the expression patterns described.

3.3.2.2 Distribution of WNK1-L and WNK1-S Expression in Kidney

To investigate the renal distribution of the two WNK1 isoforms, adult kidney sections were hybridised with probes to exons 1, 4A, and 6 to 9 (Figure 3.5, top left panel) allowing detection of the long, short, and both isoforms, respectively. Probing with exon 1 detects widespread signal at a low level (Figure 3.5a), whereas with exon 4A, only strong punctate signal in cortex is detected (Figure 3.5c). The expression pattern seen with exons 6 to 9 is thus a combination of that seen with exons 1 and 4A (Figure 3.5e).

Thus, the majority of WNK1-T expression is due to WNK1-S and limited to renal cortex (Figure 3.5(c)). Analysis of dipped slides reveals high levels of WNK1-S in distal tubules dropping off sharply distally from CNT-CCT-CCD (Figure 3.6(c)) and proximally dropping 10-fold at the TAL:DCT junction (Figure 3.6(a-b)) with expression (including the *macula densa*) falling off in late TAL. Hence WNK1-S has only a limited weak extension into medullary rays. Serial sections show strong WNK1-T cortical (labyrinth) expression (attributable to WNK1-S) overlapping NCC expression in DCT but also extending beyond the NCC overlap, representing particularly extension into CNT (Figure 3.7).

3.3.2.3 Distribution of WNK1-L and WNK1-S Expression in Development

These probes were also hybridised to embryo tissue slices (E16.5), to examine developmental mWNK1 expression. Probing with exons 6 to 9 revealed a wide mWNK1 distribution, with high expression in tissues such as placenta, nasal

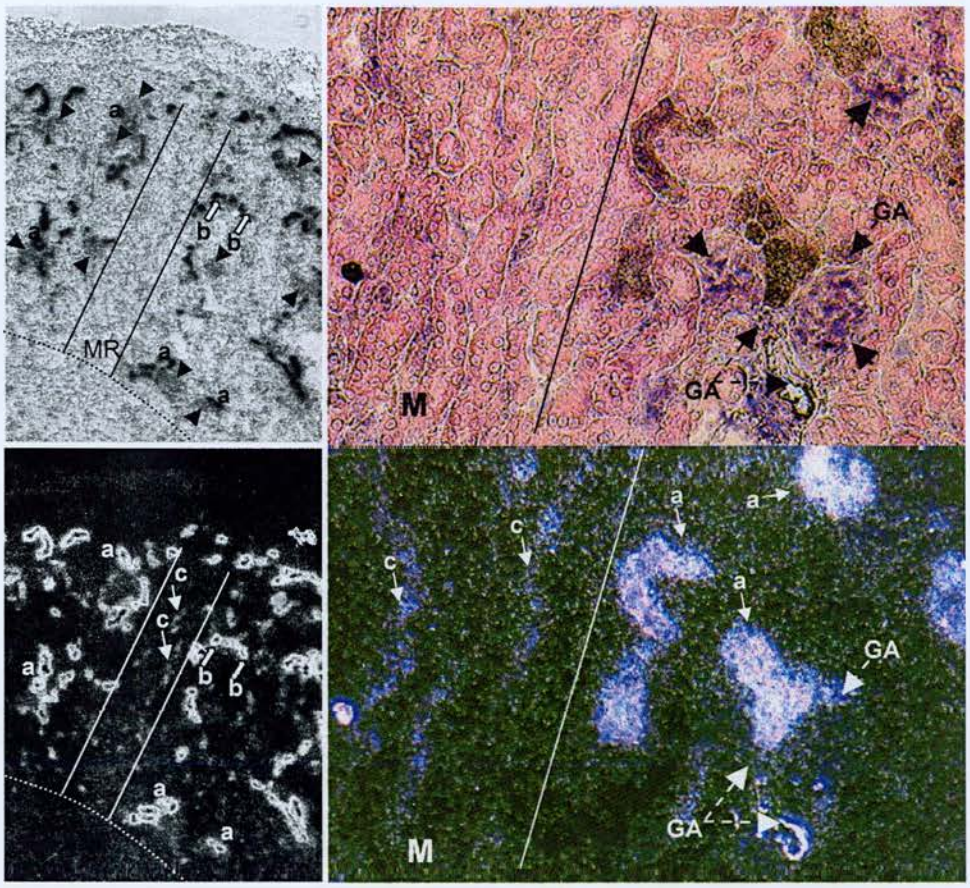

Figure 3.3: ISH of WNK1 in mouse kidney. ISH study using probe to WNK1 exons 6-9, panels show images of emulsion dipped slides (Eosin/Cresyl Violet counterstain) captured at x40 (left) and x200 magnification. View of renal cortex with a medullary ray (MR) demarcated between the parallel lines and cortical labyrinth lateral to them. Below dashed line is outer medulla. Bright field on top (black = strong expression), corresponding dark field view on bottom (white = expression whilst very highest expression (showing black on bright field) obscures light – hence appearance of strongest expressing tubules as black-holes with ring outlines on darkfield view (bottom left). Short black arrows indicate glomeruli, a = examples of DCT largely adjacent to glomeruli, b = example of CNT in mid-cortical labyrinth arcades (adjacent to radial vessels), c = CCD in medullary rays. GA = glomerular arteriole. *Left panels*: Study with long exposure (5 weeks) demonstrating wide range of expression level. Note regional expression at 3 levels: (i)widespread low level (low level white seen in darkfield), (ii)higher in CCD (faint but distinct tubular outline seen on dark field, pale grey on bright field) and (iii) highest in DCT and CNT (darker grey/black on bright field and bright ring with black hole centre when silver grains confluent). *Right panels*, (3 week exposure) note proximity of strongly expressing DCTs to glomerulus and its vascular pole (between arterioles) and stronger expression than in CCD. See Figure 3.4 for detailed illustration of nephron anatomy.

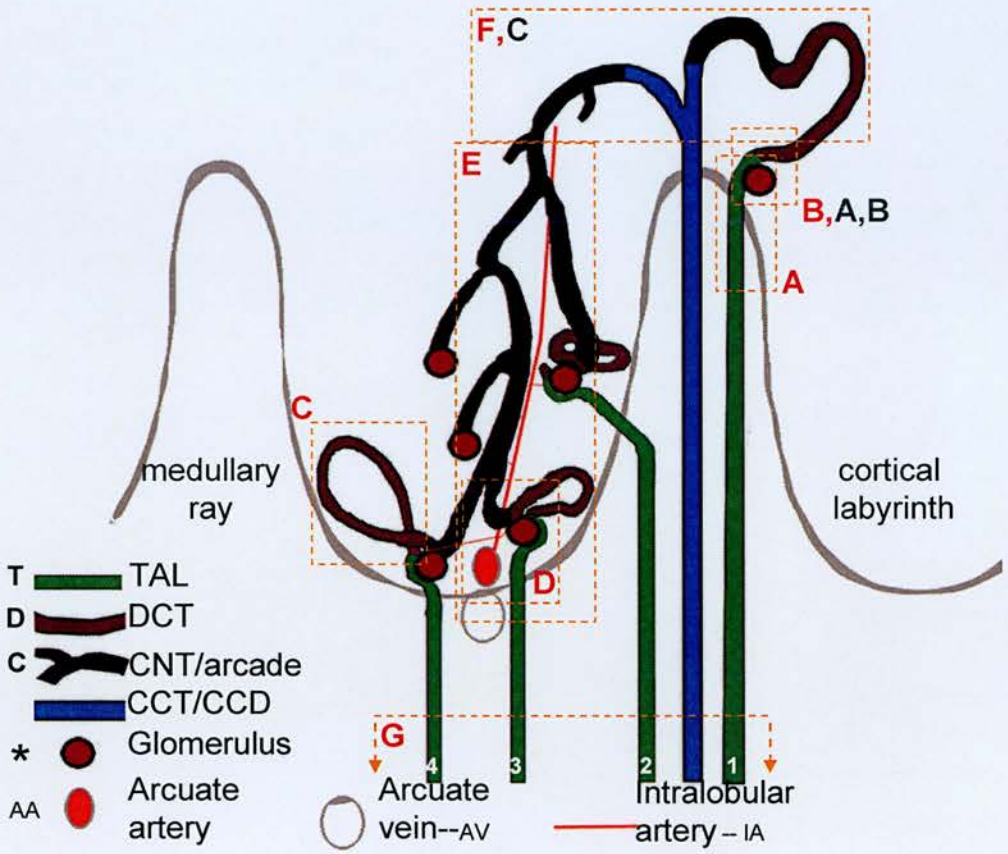

Figure 3.4: Nephron structure. Several distal nephrons draining into one CCD are shown. Distal nephron begins in the renal medulla in TAL (numbered), which ascends into cortical medullary rays and enters the cortical labyrinth contacting its glomerulus (specialized *macula densa* cells at contact point) then shortly beyond this enters DCT, CNT and finally initial/cortical collecting tubule (ICT/CCT) which re-enters medullary rays as CCD and re-descends into medulla. Nephrons of superficial glomeruli (e.g. TAL1) typically have a simple structure, with a short usually unbranched CNT. In contrast in most species, nephrons of mid-cortical (e.g. TAL2) and some juxtamedullary glomeruli (TAL3+4) commonly drain through well developed branched arcades of CNT. A considerably higher proportion of nephrons form arcades in mouse than human. Arcades are arranged around vascular axes with CNT being close to arcuate and especially intralobular vessels. The ***dashed boxes*** and lettering delimit regional views relevant to Figure 3.6. (***grey letters***) and Figure 4.3 (***red letters***).

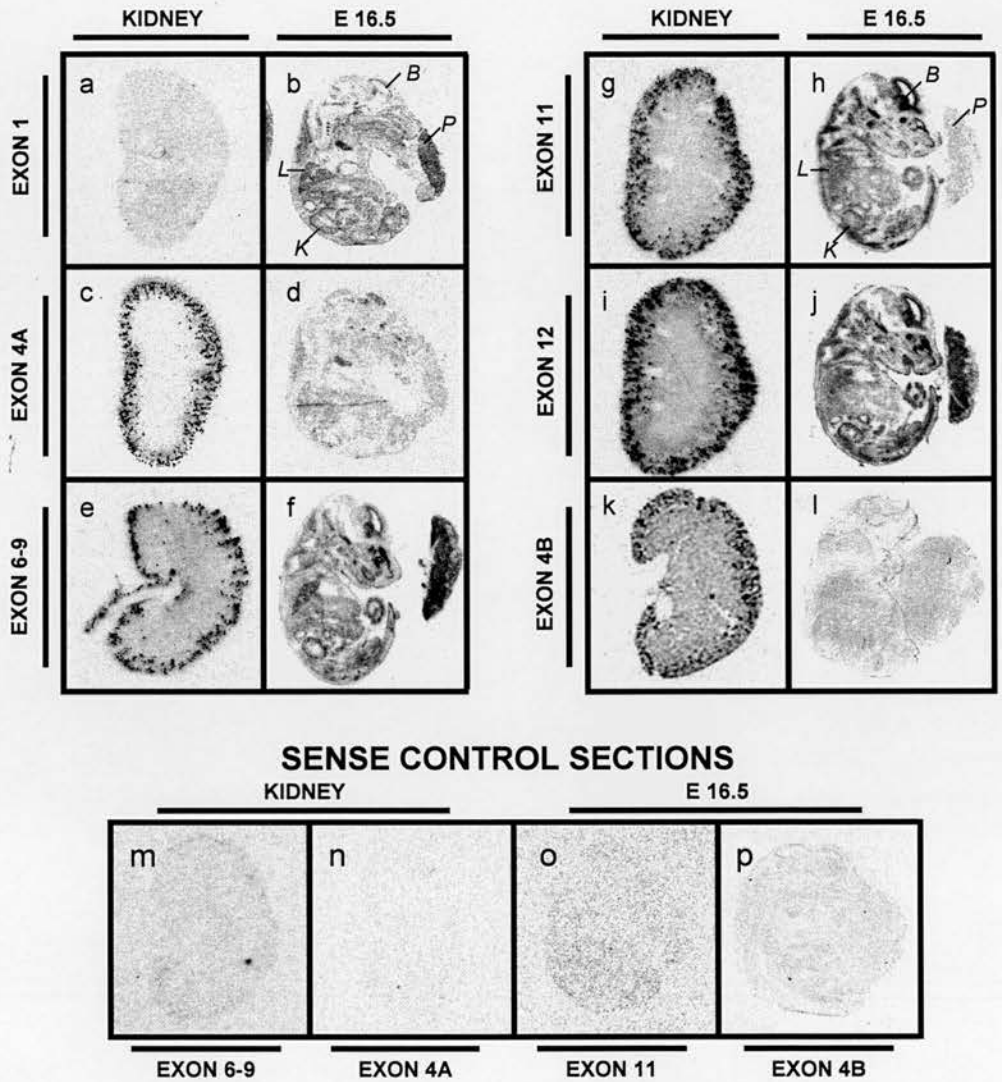

Figure 3.5: Analysis of WNK1 expression by ISH of mouse adult kidney and fetal sections (E16.5). Cryostat sections were subjected to ISH analysis using a range of probes against WNK1 (section 3.2.2.). *Left columns of top panels* show local distribution within the kidney (a, c, e, g, i and k). *Right columns of top panels* show corresponding developmental expression patterns (b, d, f, h, j and l). *Bottom panel* shows sense controls for both kidney (m and n) and fetal (o and p) sections. Exposure times for detection of ISH signal were as follows: *exon 1*, (a and b) 1 day; *exon 4A*, (c) 1 day, (d) 4 days, (n) 1 week; *exon 6-9*, (e and f) 1 day, (m) 3 days; *exon 11*, (g, h, and o) 3 days; *exon 12*, (i and j) 3 days; *exon 4B*, (k, l, and p), 2.5 weeks. *Key: B = brain; K = kidney; L = lung; P = placenta.*

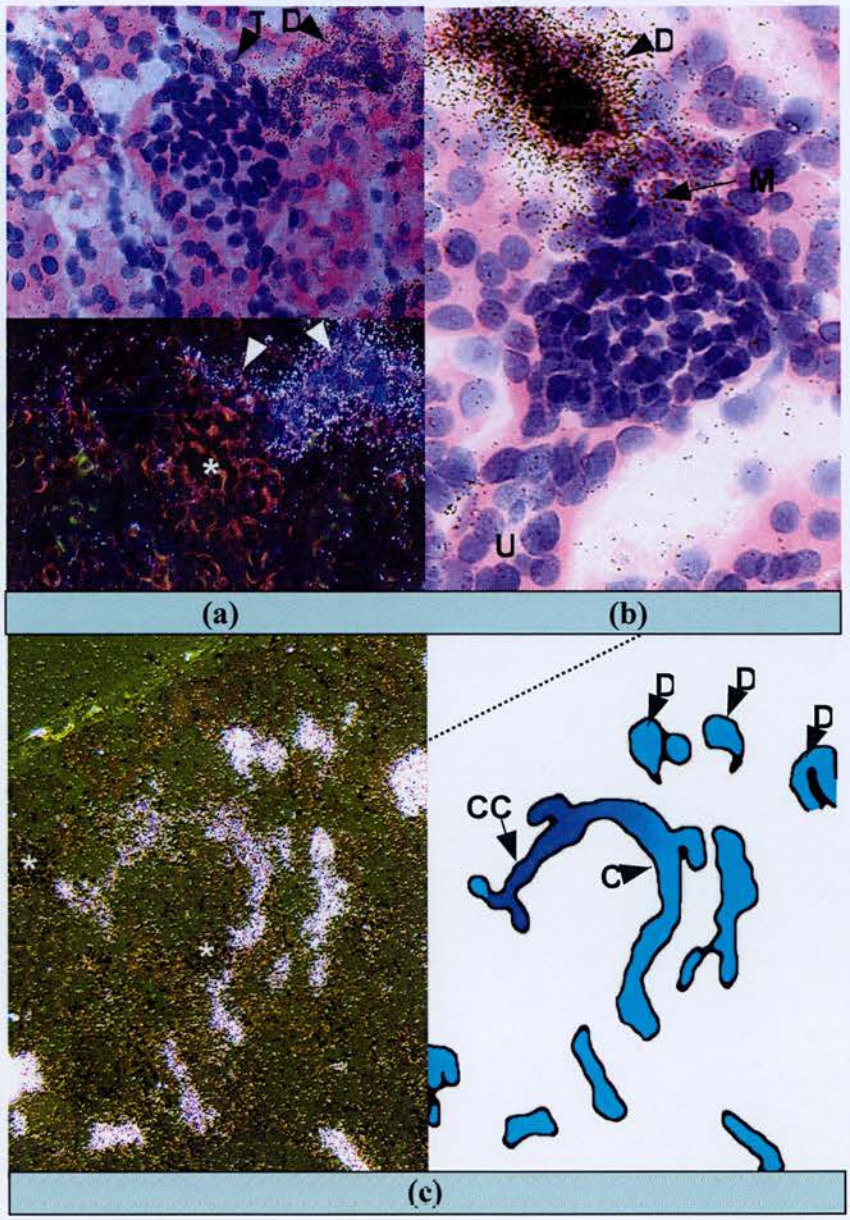

Figure 3.6: WNK1-S gene expression in mouse kidney. ISH studies: in bright field view in 5(a, top) and 5(b); blue dark-field in 5(a, lower) and dark-field in 5(c). Note WNK1-S gene expression is present in late TAL (T) including at the macula densa (MD) but rises to much higher levels in DCT (D) and CNT(C) reducing somewhat by CCT. (d) Strong WNK1-S cortical (labyrinth) expression is seen beyond NCC overlap (DCT), representing particularly extension into CNT, (NCC being DCT-restricted). *- glomerulus; dashed line – position of renal capsule; U, proximal tubule emerging from urinary pole of glomerulus (see also Figure 3.4 grey labeled boxes).

epithelium, lung, intestine, regions of the brain and developing renal cortex (Figure 3.5f). As expected, the expression patterns, revealed by probing with exons 1 and 4A, were components of that seen for exons 6 to 9, with exon 1 widely expressed, particularly in placenta, lung, kidney, intestine, thymus, and forebrain (Figure 3.5b),

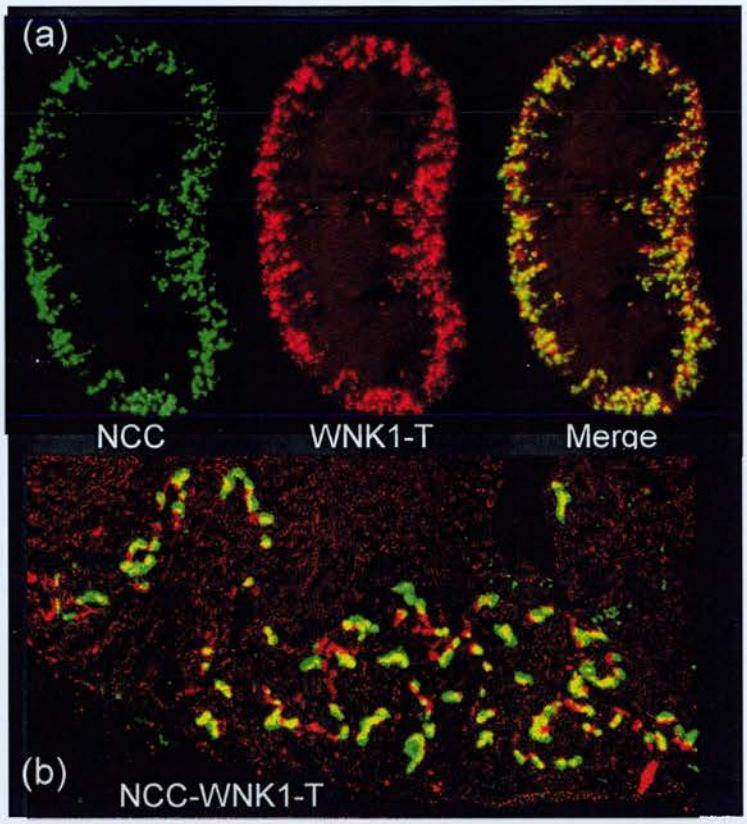

Figure 3.7: WNK1 expression overlaps NCC in DCT. ISH for the genes indicated in mouse kidney. (a)Two-colour dark-field views for paired serial saggital sections, merging showing co-localisation (yellow shift). (b)Two-colour merge views of panel (a; merge) at higher magnification. WNK1-T expression in distal nephron overlaps NCC in DCT but extends beyond this segment representing particularly extension into CNT. NCC (expressed only in DCT).

whereas exon 4A revealed much lower expression, with high signal detected in restricted regions such as nasal epithelium, forebrain, thymus and kidney (Figure 3.5d). Sense control sections showed no specific hybridisation (Figure 3.5).

3.3.3 Evidence of WNK1 alternative splicing

3.3.3.1 Alternative Splicing of Exons 11 and 12

EST sequences suggest that alternative splicing of mWNK1, primarily concerning exons 11 and 12, takes place in some tissues (Figure 3.1). To investigate this, kidney and testis RNA was subjected to Northern blot analysis with probes specific for each of these exons. Exon 11 hybridisation studies detect the large mWNK1 isoform in testis, but signal is greatly diminished for either isoform in kidney (Figure 3.2d), suggesting that exon 11 is usually spliced out in both kidney mWNK1 transcript

classes. In contrast, hybridisation with a probe to exon 12 shows strong signal for mWNK1 in testis and for the smaller kidney-specific transcript. The large mWNK1 transcript in kidney is also detected at a lower level (Figure 3.2d). To investigate tissue-specific and developmental variations in these splicing events, adult mouse kidney and fetal (E 16.5) sections were subjected to ISH analysis. The expression patterns seen when probing adult kidney sections with either exon 11 or 12 are similar to that described above for exons 6 to 9, showing low-level, widespread expression throughout the kidney, overlaid with strong punctate cortical expression (Figure 3.5, g and i). However, developmental expression studies using these probes indicate that although many fetal tissues express both exons similarly, there is striking tissue-specific splicing in some developing organs. For example, transcripts containing exon 11 are abundant in some neural tissues but are rare or absent in placenta (Figure 3.5, h and j). Sense control sections showed no specific hybridisation (Figure 3.5).

RT-PCR studies across exons 11 and 12 confirm these splicing events (Figure 3.8a). Amplification in kidney, by means of primers spanning the exon 7/8 splice site down to the exon 15/16 splice site shows two major bands, corresponding in size to PCR products having either exon 11, or both exons 11 and 12 spliced out (Figure 3.8b). Additional RT-PCR studies that use alternative primers spanning this region also show major bands, similarly representative of these splice variants.

3.3.3.2 Alternative Splicing of Exon 4B

EST sequences also suggest that in addition to exons 4 and 4A, a third exon positioned between exon 4A and 5 in the mouse genomic sequence and therefore termed 4B, may precede exon 5 in some mWNK1 transcripts (Accession No. AK052468). The EST evidence suggests that unlike the kidney-specific transcripts described above containing exon 4A, which lack all known upstream exons, transcripts containing 4B splice directly from exon 4 to exon 4B to exon 5. ISH analysis probing with exon 4B shows a similar pattern to that seen previously in kidney, with high cortical expression overlaying a low widespread distribution (Figure 3.5k). However, splicing events producing transcripts containing exon 4B

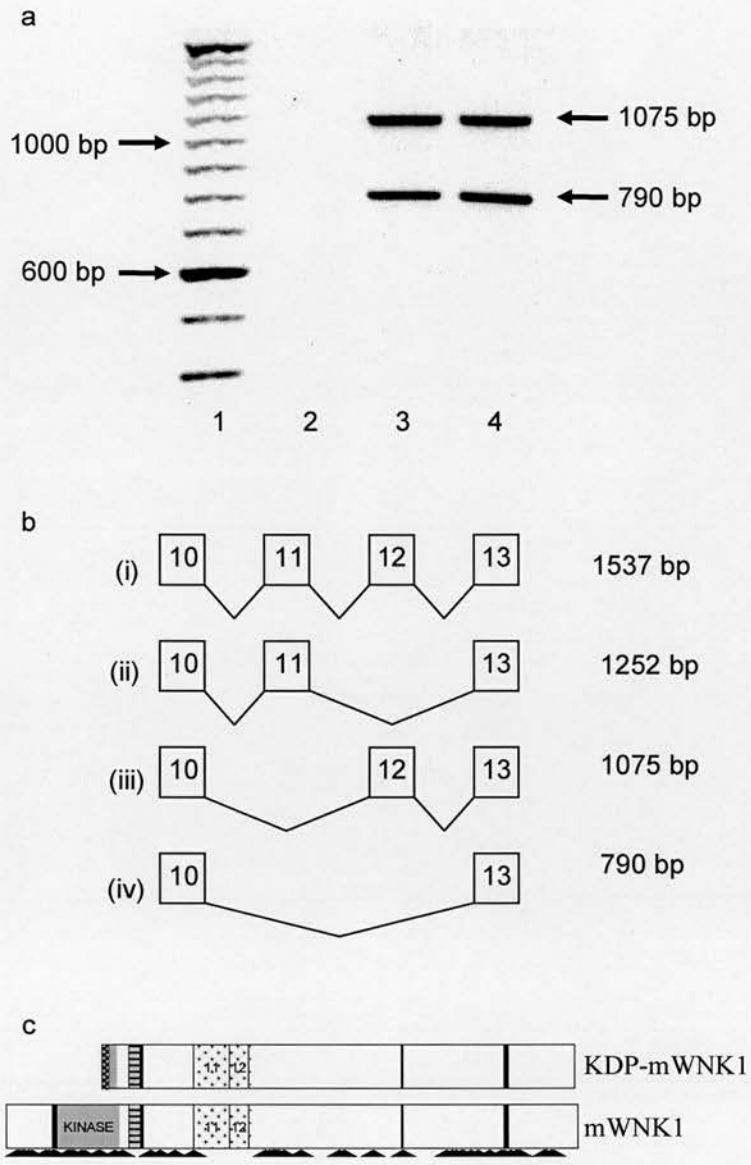

Figure 3.8: Detection of WNK1 alternative splicing. (a) Ethidium bromide-stained agarose gel, showing RT-PCR-amplified fragments in duplicate. These products were amplified with mWNK1 primer pair P7 and P8, spanning a region from the exon 7/8 splice site down to the exon 15/16 splice site (lanes 3 and 4). A negative control is seen in lane 2. Lane 1 shows a 100 bp DNA ladder. (b) Schematic depiction of WNK1 alternative splicing involving exons 11 and 12. The major products seen correspond to (iii) and (iv). (c) Schematic representation of the major predicted WNK1-derived proteins. mWNK1 is 2377 amino acids in length and is particularly serine-, glutamine- and proline-rich, having 26 PXXP sites potentially recognised by SH3 domains. Black bars denote four putative coiled coil domains, and a conserved WNK autoinhibitory domain is represented by horizontal stripes (identified in rWNK1 by Xu *et al.*[152]). Black arrowheads indicate the positions of predicted potential phosphorylation sites; intriguingly none of which overlap with the region encoded by exons 11 and 12. Exon 11 encodes a leucine zipper (LXXLL) motif. WNK1-S has a truncated N-terminus, lacking one coiled coil domain and deleting a major portion of the kinase domain. This region is substituted with a highly cysteine-rich stretch of thirty amino acids.

appear to be rare, judged by the lower ISH signal (requiring exposures several-fold longer for clear detection). Furthermore, signal detected on fetal sections was low and widespread, lacking the striking tissue-specific differences in expression levels seen with probes to other exons (Figure 3.5l), and was only marginally higher than that seen for sense controls (Figure 3.5p).

3.3.3.3 Evidence of Further Novel mWNK1 Transcripts

As described above, Northern blot studies examining expression of exon 11 detect very weak signal for the transcripts of both long and short WNK1 isoforms in kidney, despite their high expression in testis. In contrast, ISH studies suggest that exon 11 is expressed at levels comparable with exon 12 in kidney. This discrepancy led to further Northern blot analysis looking for evidence of further novel mWNK1 transcripts in kidney containing exon 11. These studies revealed at least two novel mWNK1 transcripts in kidney and testis, evidently several kb smaller than the two isoforms described above (Figure 3.9). Intriguingly, transcripts of similar size were detected in additional northern analysis of exon 4A expression in both tissues (Figure 3.9).

3.4 Discussion

This study details WNK1 gene expression in mouse, reporting a broad distribution across a range of tissues. Several WNK1 transcript classes are demonstrated, showing tissue-, developmental-, and nephron-segment–specific expression. Importantly, in kidney, the most prominent transcripts are smaller than elsewhere, having the first four exons replaced by an alternative 5'-exon (exon 4A)[157], thereby deleting the kinase domain. This phenomenon of a shorter predominant kidney WNK1 isoform (WNK1-S) has been reported in previous studies[148], appears to be conserved between species, and was previously attributed to alternative 3'-polyadenylation (shown here to be incorrect)[18;137;148;151]. Unlike WNK1-L which has a low-level widespread renal distribution, WNK1-S expression is largely confined to the distal nephron, with expression highest in DCT and CNT, dropping sharply both distally in CCD and proximally in cortical TAL (cTAL), with weak expression detected in *macula densa*. We were the first to report the difference between these

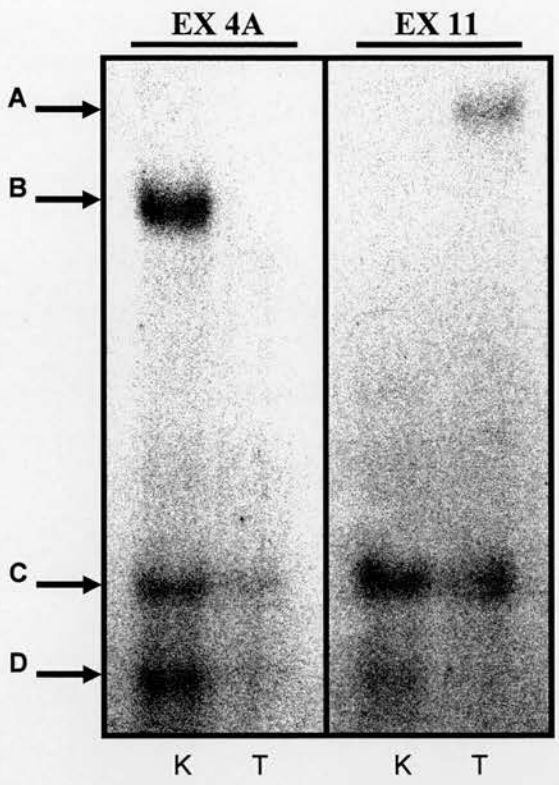

Figure 3.9: Detection of smaller WNK1 transcripts in kidney and testis by Northern blot. Probing with exon 4A detects the kidney-specific WNK1 transcript (B), but also reveals two additional transcripts several kb smaller (C and D) in both kidney (K) and testis (T). These transcripts are also seen when probing with exon 11, which also detects the large WNK1 transcript (A) as expected.

WNK1 isoforms showing unique and detailed renal distributions and including the sequence of novel 5'exons and the predicted amino acid sequence for WNK1-S[109]. Shortly after our report an independent study supported our findings[24] (Chapter 9).

Alternative splicing of exons 11 and 12 is prominent; with transcripts containing exon 11 abundant in neural tissues and testis, but predominantly absent in placenta. In kidney, we show that exon 12 is usually included in WNK1-S, whereas exon 11 is largely absent in both WNK1-L and WNK1-S. Alternative splicing of these exons has also been reported for hWNK1[137]. Furthermore, the published rat WNK1 sequence (Accession No. NM_053794) corresponds to the splice variant lacking both

exons. Further studies indicate the production of substantial levels of novel smaller alternatively spliced transcripts from the WNK1 gene, with Northern blot analysis implicating the inclusion of both exons 11 and 4A. These smaller transcripts are seen in kidney but also in testis, a tissue in which exon 4A expression was previously unsuspected because testis lacks obvious expression of the much larger 'kidney-specific' 4A transcript. Preliminary investigations suggest that these transcripts differ from this largely kidney-specific 4A transcript, described above, being much smaller in size. However, RT-PCR in testis easily amplifies a product from exon 4A to exon 11, suggesting these smaller transcripts contain this region.

This study was the first to assess WNK1 expression in development by means of ISH analysis, demonstrating that WNK1 is widely expressed in the mouse embryo (E 16.5), in both epithelial tissues (e.g., developing renal cortex, intestine, lung, nasal epithelia, and placenta) and in nonepithelial tissues (e.g., regions of the CNS). Again, there are tissue specific differences in the pattern of transcripts expressed in developing organs, with WNK1-L showing high widespread but non-uniform expression and WNK1-S showing high expression only in restricted sites. The importance of WNK1 in development is emphasised by a study reporting homozygote WNK1 deficient mice are embryonic lethal with embryos failing to survive past day 13 of gestation[165].

It would have been reasonable to have supposed WNK1, a kinase, probably regulates ion transport through the activity of its kinase domain. However, the major WNK1 transcript in kidney lacks this functional entity as a result of the replacement of exons 1 to 4 with exon 4A (Figure 3.8c). Additionally, a coiled coil motif predicted just N-terminal to the kinase domain is lost, possibly disrupting interactions with molecular targets. This implies that the remainder of the WNK1 protein makes an important functional contribution to the WNK1 regulatory pathway. Exons 11 and 12 are of key interest because, splicing of this region is conserved between species, is clearly tissue-specific, and would produce a repertoire of proteins likely to be co-expressed in the same tissues and cells (Figure 3.5). Intriguingly, although WNK1 contains numerous potential phosphorylation sites (~66), no such site occurs within the

exon11-12 region, implying that signalling through protein kinase pathways acting on WNK1 is not affected by such splicing events. Clearly, experimental studies are required to fully investigate these possibilities.

Also of interest is the addition of thirty amino acids to the N-terminus of kinase-deficient WNK1-S, contributed by exon 4A. This exon may have no major functional effect other than deleting the kinase domain. However, this sequence is strikingly cysteine rich. Within a cluster of six likely very reactive cysteine residues, at least three have a high predictive index for forming either disulphide bonds or bonds with other molecules (e.g., metal-containing moieties). Moreover, the N-terminal positioning of this cysteine cluster may promote this region as a potential point of anchorage to other structures. Furthermore, the novel small bands seen by Northern blot clearly indicate the production of WNK1 transcripts lacking several kilobases compared with the kidney-specific 4A band. Therefore, it is very likely that these may add to the repertoire of variation in WNK1 protein structure having profound effects on WNK1 function.

The transcriptional modifications described above would greatly influence the potential complement of proteins produced from the WNK1 gene and may be the manifestations of different functional aspects of the WNK1 gene that have been conserved in evolution. Kinase-deficient WNK1-S proteins may act to inhibit other WNK1 proteins with "active" kinase domains, via interactions through the remaining coiled-coil motifs (Figure 3.8c). This is supported by the recent report of a WNK1 autoinhibitory domain, positioned between residues 515-569 in the rat sequence, which is conserved between species and also within the WNK family (Figure 3.5c). Preliminary evidence was also reported for WNK1 tetramer formation via the coiled-coil motif C-terminal to the autoinhibitory domain (Figure 3.8c)[152].

This work provides a number of insights into the cause of Gordon syndrome. WNK1 expression is examined in some detail, further elucidating kidney-specific and distal-nephron-specific WNK1 transcripts. The findings described imply the use of alternative promoters, one initiating transcription in exon 1 and the second giving

rise to transcripts having exon 4A in place of exons 1-4. It is therefore reasonable to suggest that *cis* elements within intron 1 (>34 kb in mouse) affect the second promoter regulating such 4A transcripts. Dominant negative regulation could arise from intronic deletions causing Gordon syndrome leading to abnormally high expression of kinase-deficient WNK1-S transcripts in kidney, in turn causing excessive inhibition of "normal" WNK1 function. Alternatively, the intron 1 deletions could interrupt splicing enhancer or silencer sequences, thereby disrupting the normal complement of alternatively spliced WNK1 transcripts. A similar effect is seen in Marfan syndrome, another autosomal dominant disorder affecting connective tissue, where a superficially "silent" intronic mutation actually results in exon skipping[71]. In Ataxia-telangiectasia, an intronic deletion in the ATM gene results in aberrant inclusion of a cryptic exon[110].

The pathway disrupted in Gordon syndrome involving WNK1 is regarded as different from other signalling pathways known to regulate BP. The findings presented here reveal the central importance of the transcriptional control of this gene in generating a complement of kidney-specific, WNK1-derived proteins. The correct balance within this complement of proteins must mediate the effects on ion transport that constitute this novel BP regulatory pathway. Clearly the regulation of alternative promoter use and splicing is likely to participate in the control of BP by WNK1-derived proteins.

Chapter 4 WNK4 mRNA distribution in mouse.

4.1 Introduction

In a number of *in vitro* studies, WNK4 has been proposed to regulate many renal electrolyte transporters (Table 1.3). The renal localisation of these electrolyte transporters ranges from proximal tubule, for example CFEX[52], to the more distal nephron segments, for example NCC in DCT[149;161], ROMK in DCT2-CD[56], and NKCC1 in outer medullary collecting duct (OMCD)[52]. Moreover some putative interacting transporters are located in the apical plasma membrane, for example NCC, others in the basolateral membrane, for example NKCC1, while WNK4 interaction with Claudins is expected to be localised in lateral tight junctions[53;159]. In order to assess the potential *in vivo* significance of specific molecular interactions identified *in vitro*, it is essential to establish which tissues and cells types show WNK4 gene expression *in vivo*. Within kidney, which shows the highest WNK4 expression, it is important to establish the nephron segment expression of WNK4, as the molecular make-up of the nephron varies greatly from segment to segment. For example, although the basolateral Na^+/K^+-ATPase pump is expressed by all cells throughout the distal nephron, the machinery responsible for apical Na^+ transport varies from segment to segment; NKCC2 in TAL, NCC in DCT, ENaC in CNT and CD. So depending on where WNK4 (and similarly WNK1) is expressed, the complement of potential interacting candidates and the pathways in which they participate may vary. Having determined WNK1 gene expression in mouse (described in Chapter 3), the next logical step was to similarly investigate WNK4 gene expression and distribution in this model species. Bioinformatic evidence from sequence databases and the distribution of ESTs suggest transcriptional diversity of WNK4. Accordingly, additional studies were undertaken to assess the possibility of WNK4 alternative splicing.

4.2 Materials and Methods

Initially no mouse WNK4 cDNA sequence was available, so one was "stitched" together in April 2002 from a "contig" constructed in house with high quality C57BL/6 mouse sequence (from ESTs, cDNAs, and high quality mouse genome trace sequence giving ≥3-fold coverage for all but 108bp (2-fold) of the 4144bp stitched cDNA). The junctions between the 19 exons were determined by use of

genomic sequence and reference to the equivalent human WNK4 gene structure. In January 2003 a 3718bp cDNA submitted by the Lifton group (AY187027) was released, having 100% identity to the in house sequence which extended 74bp and 352bp 5' and 3' of the AY187027 sequence, respectively. By sequence comparison and BLAST alignment it became apparent there was evidence suggestive of transcript heterogeneity and alternative splicing that could be assessed by examining expression of exons 1, 10, 12-13 and 14-15. Accordingly, in addition to the main investigation of WNK4 gene expression utilising a probe sequence spanning exons 6-9, additional probes to these regions were utilised in assessing for variant WNK4 transcript expression. For primer sequences, used in the generation of ISH probes for analysis of WNK4 gene expression see Table 2.3.

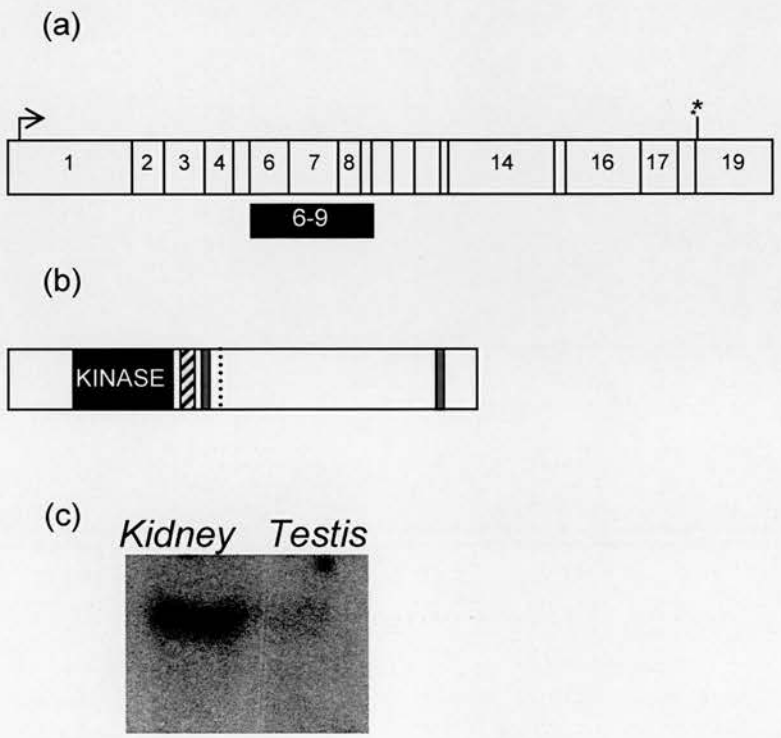

Figure 4.1: Mouse WNK4. (a) Schematic representation of WNK4 cDNA structure showing exon composition and standard probe position. The cDNA structure of WNK4 is illustrated with vertical bars representing exon:exon boundaries. Numbers within rectangles refer to exon numbers. Black box specifies the standard WNK4 cDNA region (exons 6 to 9) targeted in hybridisation studies. (b) Schematic representation of the predicted WNK4 protein showing the kinase domain (black box), coiled coil domains (grey boxes), and the familial autoinhibitory domain (checked box; originally identified in rWNK1, be subsequently found in all WNK kinases including WNK4[147]). Three out of four of the mutations in WNK4 that are associated with Gordon syndrome are clustered in a conserved acidic region (depicted by a dashed line) just distal to the first coiled coil domain. (c) Northern blot analysis of WNK4 expression. Hybridisation with a probe incorporating exons 6 to 9 detects WNK4 in mouse kidney.

4.3 Results

4.3.1 WNK4 expression in adult mouse kidney

Mouse WNK4 (mWNK4) is encoded by 19 exons contained within 17kb of genomic DNA on chromosome 11, producing a 4139 bp mRNA transcript (Figure 4.1(a)). The predicted 1222 amino acid mWNK4 protein (Figure 4.1(b)) shows 86% identity to human WNK4 (hWNK4) but is shorter than the human orthlog by 21 amino acids. Preliminary Northern hybridisation analysis with exons 6 to 9 detected mWNK4 in kidney as expected (Figure 4.1(c)). Longer exposure of this blot suggested weak expression of a smaller WNK4 transcript in kidney and also even weaker expression of full-length WNK4 in testis. These bands were extremely faint and very difficult to detect on scanned images, and are therefore not shown.

4.3.2 Spatial distribution of WNK4 in mouse adult kidney

To investigate the renal distribution of WNK4, adult mouse kidney sections were hybridised with exons 6 to 9. WNK4 gene expression is illustrated in Figures 4.2 and 4.3 with an overview of expression shown in Figure 4.2 and key expression details in Figure 4.3. The nephron anatomy and structures involved (and their abbreviations) in superficial and deep distal nephrons are illustrated in Figure 3.4. Although WNK4 is expressed at lower levels than WNK1 (3-4 fold longer exposures for WNK4 than for WNK1(-S or –T; Chapter 3), WNK4 has a broader distribution than WNK1 in kidney with strong expression seen in both renal cortex and medulla. WNK4 gene expression is strongest in distal tubule structures (DCT/CNT), similar to WNK1-S, but extends beyond distal tubule, at somewhat reduced levels, more proximally into TAL including *macula densa* and medullary TAL (mTAL; Figure 4.3(a), (b), (d), (g)) and more distally at quite low expression levels (compared to DCT) in CD (Figure 4.4(f)). Thus, substantial WNK4 expression extends into medullary rays and outer (but not inner) medulla (Figures 4.2(a), 4.3(g)) involving much too high a proportion of tubules to be due to outer medullary CD (OMCD) alone (γENaC vs. WNK4 -Figure 4.3(g)) rather resembling the density of mTAL tubules (shown by NKCC2 – Figure 4.3(g)).

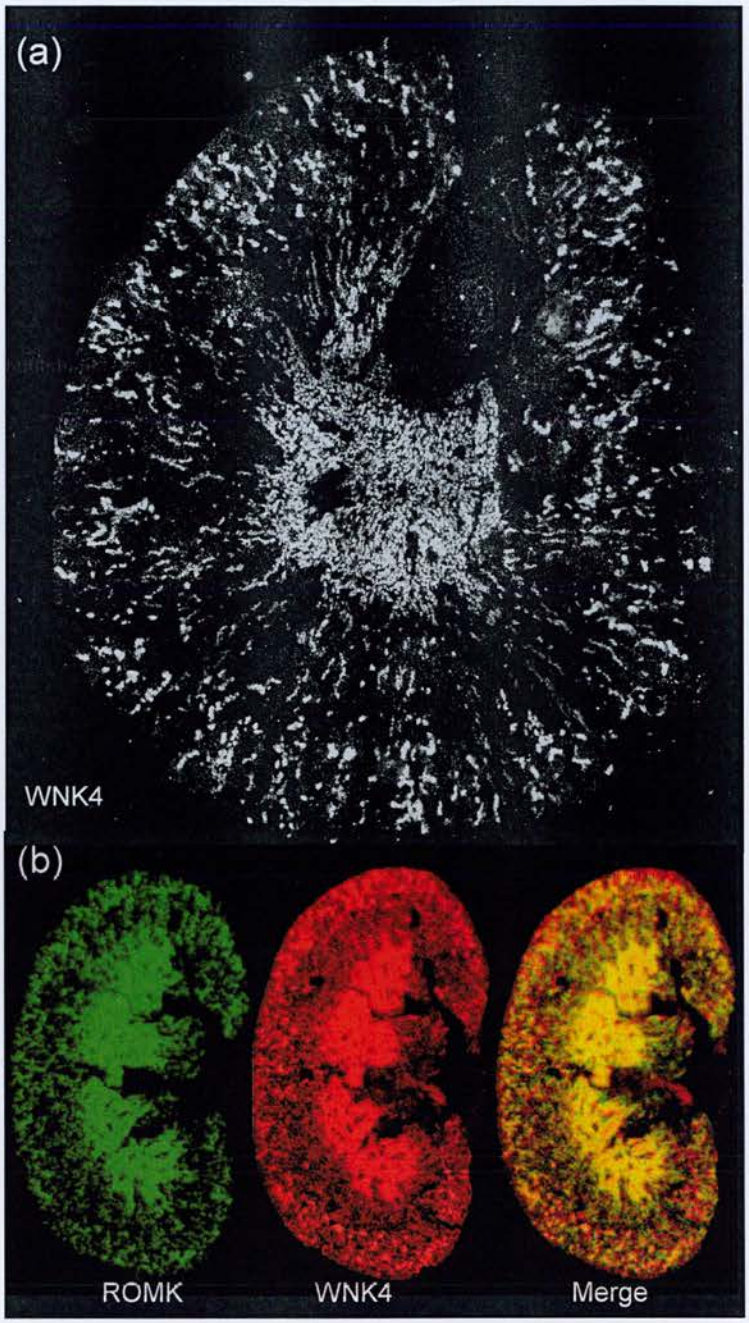

Figure 4.2: ISH analysis of WNK4 gene expression in kidney. (a)Serial transverse section (dark-field view). (b)Two-colour dark-field views for paired serial saggital sections, merging showing co-localisation (yellow shift). Note that WNK4 expression coincides with WNK1-S in the cortex, but unlike WNK1-S, major WNK4 expression extends substantially into medullary rays and outer medulla where it has a similar distribution pattern to that of ROMK.

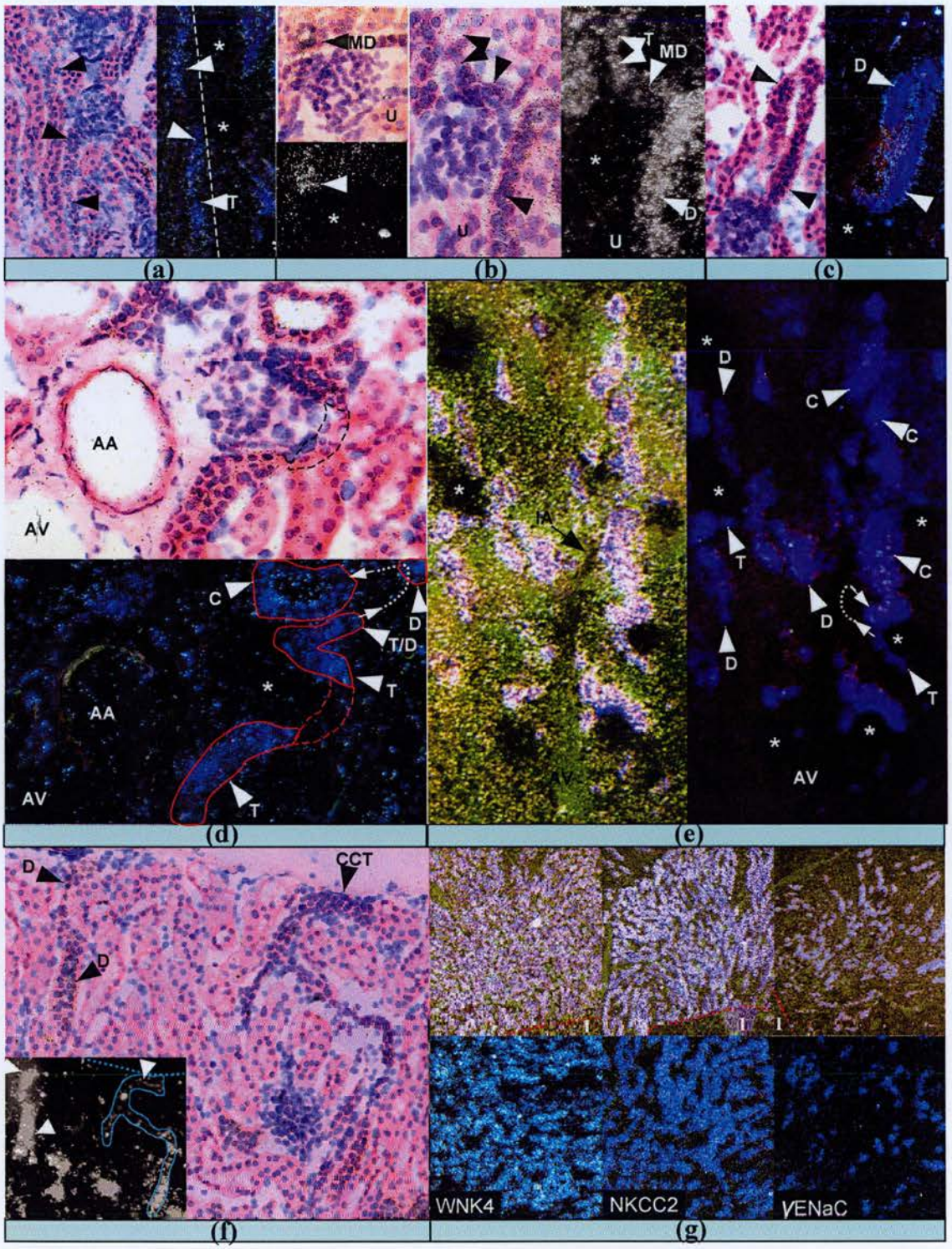

Figure 4.3: WNK4 gene expression in specific nephron segments. ISH studies in bright field, dark-field and blue dark-field (dark-field under blue light to limit tissue stain visibility). Throughout the panels (4.4 a-g) similar regions of view are illustrated in Figure 3.4 (red labeled (a-g) boxes). Simple label abbreviations are used as in Figure 3.4 or below. (a) WNK4 expression in TAL (T) in medullary ray, crossing boundary (dashed line) to contact glomeruli (•) in cortical labyrinth. (b) Substantial expression in segment of *macula densa* (MD), and higher still in DCT (D), also seen in (c). U = proximal tubule emerging from urinary

dashed outline) fall outside the plane of section. (e) Extensive WNK4 expression throughout a well developed deep cortical arcade. Vascular axis (arcuate artery (AA) and vein (AV) and intralobular artery (IA) and associated glomeruli are seen in left panel. Note extensive DCT loops adjacent to glomerulus marked (·) in left panel. Dashed arrow = connections of DCT convolutions (out of section plane). (f) Superficial cortex with loops of DCT and ICT/CCT passing near renal capsule. Whilst both segments have WNK4 expression, note level is strikingly higher in DCT. Dashed line = renal capsule. (g) Views of ISH studies for the genes indicated in inner stripe of renal outer medulla (a segment with TAL and collecting duct (OMCD) as largest tubules – upper panels x50 dark-field, lower x100 blue dark-field. Note the relative density of WNK4 positive tubules is hugely different and greater than that for γENaC (γ-subunit of ENaC: an OMCD marker), but similar to NKCC2 (Na^+K^+Cl cotransporter type2: a TAL marker). Dashed red line = boundary of outer and inner medulla (I).

4.3.3 WNK4 Splicing

To investigate potential splicing of WNK4 adult kidney sections were hybridised with exons 1, 10, 12 to 13 and 14 to 15. Our standard probe against exons 6 to 9 of WNK4 was used in this study as a positive control. No differences were seen in WNK4 spatial distribution (Figure 4.4). Sense control sections showed no specific hybridisation.

4.3.4 WNK4 expression outside kidney

Clues from the literature, the distribution of WNK1 expression (Chapter 3), as well as evidence from our Northern hybridization analysis (section 4.3.1) and fetal ISH (section 4.3.5), highlighted a number of tissues, including testis and brain, as possible sites of WNK4 expression outside the kidney. Adult mouse brain and testis were hybridized with a probe against exons 6 to 9 of WNK4. When brain tissue was harvested for these studies, the pituitary gland was placed on top of the brain prior to freezing at -80°C. This allows easy sectioning of this small tissue. Highest WNK4 expression was detected in the pituitary gland, with lower expression seen in the dentate gyrus and the cerebellum (Figure 4.5(a)). High WNK4 expression was also detected in the epithelia of testis and epididymis; seen clearly over the lower level uniform hybridization elsewhere (Figure 4.5(b)). ISH analysis of other tissues including lung, liver, and heart did not clearly detect WNK4 expression.

4.3.5 WNK4 expression in mouse development

Fetal tissue sections (E16.5) were also hybridised with the WNK4 exon 6-9 probe to examine WNK4 expression in development. This revealed a limited mWNK4 distribution (Figure 4.6), with highest expression seen in colon and tongue and

weaker punctate expression seen in kidney. Sense control sections showed no specific hybridisation.

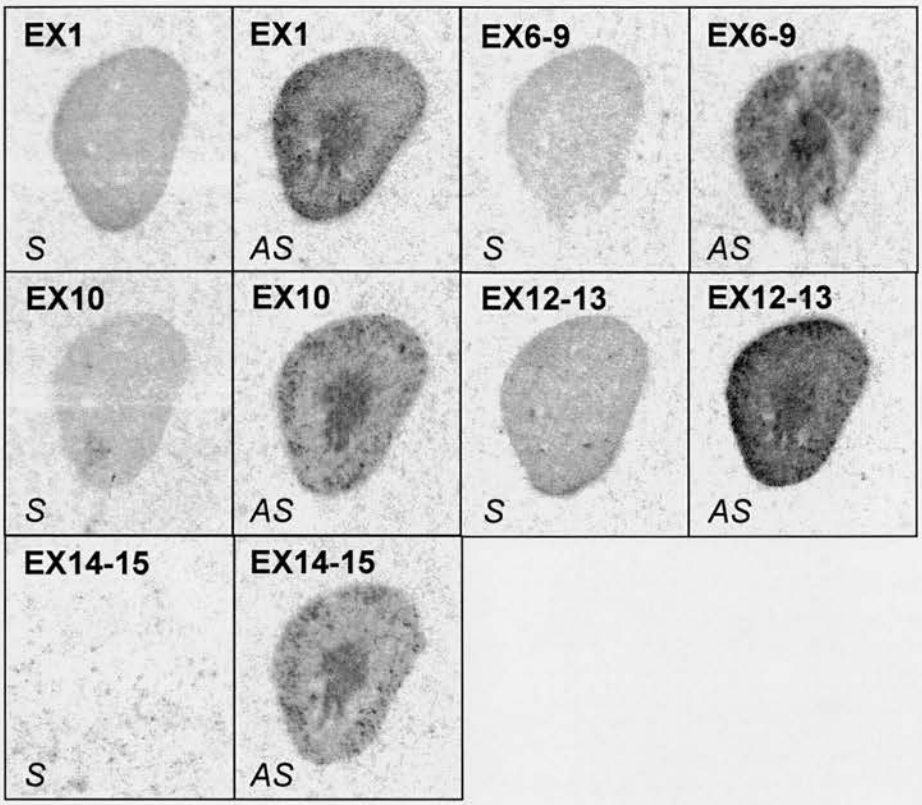

Figure 4.4: ISH analysis of potential WNK4 splicing. Hybridisation of adult mouse kidney sections with probes designed against exons 1, 10, 12 to 13 and 14 to 15 showed no differences in distribution pattern compared to kidney sections hybridised with a probe against exon 6 to 9 used as standard throughout our localisation studies. Hybridisations with sense probes are shown in the left panel, and antisense hybridisations are shown in the right panel.

4.4 Discussion

Using a probe against the WNK4 region just distal to the kinase domain we detected WNK4 expression in kidney by Northern blot. The detection of a very faint smaller band in kidney with longer exposure suggests the possibility of alternative splicing or alternative 3'-polyadenylation of WNK4. Renal localisation studies by ISH show strong WNK4 expression in distal nephron segments, important in long-term electrolyte balance[16;47;82] with strongest WNK4 expression in distal tubule (DCT, CNT) extending at substantially lower level into CD. WNK4 expression extends to TAL including *macula densa* and represents stable expression at a substantial level. This has not been recognised before and may indicate different WNK4 isoforms or

post-translational modifications affect WNK4 in TAL[148]. These seem particularly common in transport pathways e.g. NKCC2 in TAL.

In vitro, WNK4 can interact directly or indirectly via other kinases (e.g. OSR1, SPAK, other WNKs), to regulate proteins of key importance in TAL-DCT transport, including NCC[149;161], ROMK[56] and, it appears, NKCC2[97;139]. The prospect WNK4 may regulate transport in TAL-DCT (including *macula densa*) is intriguing, as upregulated NaCl reabsorption here would be expected to drive hyperkalaemia, acidosis and low-renin hypertension: all features of Gordon syndrome and manifesting the inverse of Gitelman's and Bartter salt-wasting syndromes of DCT and TAL, respectively. NCC overactivity accounts particularly well for Gordon syndrome, including the thiazide hyper-responsiveness and hypercalcuria features of WNK4 Gordon syndrome families; their normomagnesemia, however, appears anomalous[87]. Interestingly, normagnesemia would be expected with upregulated NaCl transport in TAL (normagnesemia in Bartter's) which, in *macula densa*, would promote low-renin hypertension with augmented afferent arteriolar resistance.

Gordon syndrome features were lacking in transgenic mice expressing human Gordon syndrome mutant WNK4 protein in TAL and DCT (at heterogeneous levels)[160]. Expression was transgenic cDNA-driven rather than genomic, altering distribution and curtailing native potential for transcriptional diversity. These studies report ROMK localisation appears unaltered by co-localised Gordon syndrome mutant WNK4 protein[160]. However, the basis for absence of Gordon syndrome features in these mice remains uncertain as this was not the goal of this work.

Lifton and colleagues report renal WNK4 expression in DCT and CCD seen by immunohistochemistry but could not detect WNK4 elsewhere in kidney[148]. Clearly this reported expression profile apparently restricted entirely to cortex conflicts with the strong medullary expression seen here by ISH. This immunohistochemistry study utilises a WNK4 antibody directed against the peptide, MGQMRRPPGRNLRR (residues 657-670 of WNK4), encoded within exon 10 of human WNK4[148]. One possible explanation for the discrepancy in WNK4 distribution profiles between the

two techniques is that there is transcriptional or post-translational heterogeneity, for example through splicing or post-translational processing which removes or modifies the epitope recognised by this particular antisera.

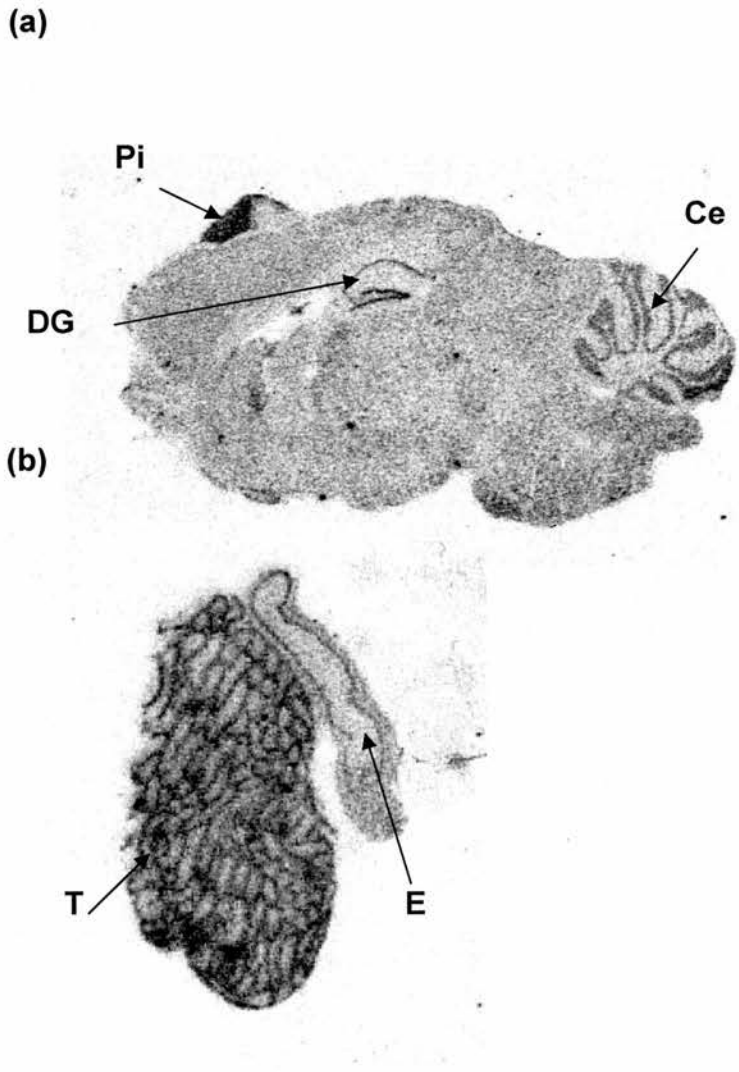

Figure 4.5: Extra-renal WNK4 expression. Adult mouse brain (a) and testis (b) were hybridized with a probe against exons 6 to 9 of WNK4. (a) WNK4 expression is seen in the pituitary gland (frozen on top of brain when dissected for ease of sectioning), dentate gyrus and cerebellum. (b) High WNK4 expression is seen in the epithelia of testis and epididymis, over lower level uniform expression.
Ce, cerebellum, DG, dentate gyrus; E, epididymis; Pi, pituitary; T, testis

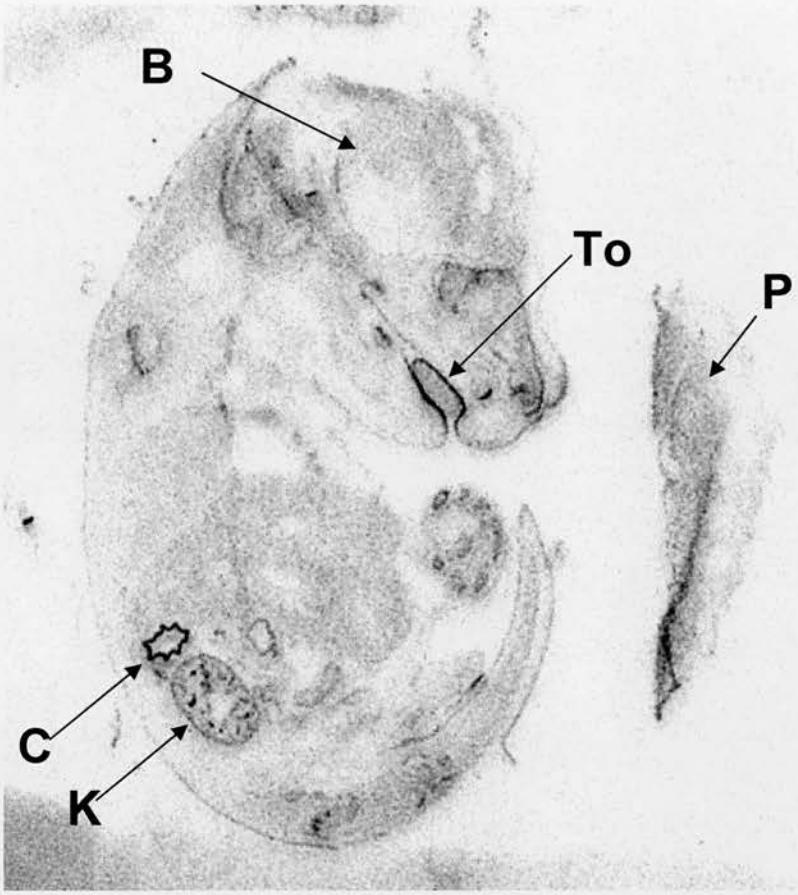

Figure 4.6: WNK4 expression in mouse development. Mouse foetal sections (E16.5) were hybridized with a probe against exons 6 to 9 of WNK4. Highest expression is detected in colon and tongue, with lower level punctate expression in kidney.
B, brain; C, colon; K, kidney; P, placenta; To, tongue

The potential existence of alternative WNK4 isoforms was previously highlighted by additional bands on the WNK4 immunoblot in the original Lifton study reporting WNK gene mutations in Gordon syndrome and also by the weaker small WNK4 band suggested by our Northern hybridisation analysis (data not shown). At the time of this study the WNK4 gene was not fully annotated in the NCBI database. However, EST evidence suggests the possible splicing of exons 12 to 13 and 14 to 15. Exon 10 is also of interest as this is the exon encoding the epitope for the antibody used in immunohistochemistry studies. The possibility that WNK4 may be transcriptionally regulated to produce a kinase-deficient isoform similar to WNK1-S, also highlighted exon 1 for investigation. Using individual ISH probes specific for exons 1, 10, 12 to 13, and 14 to 15, we examined the specific distribution of these WNK4 exons, but failed to find any evidence of their differential expression in

kidney. In conjunction with the absence of any RT-PCR evidence of splicing during ISH probe production, this suggests that alternative splicing of these exons in WNK4 is either too rare to detect or simply does not occur in kidney. It is possible such transcriptional diversity may be clearly present in other organs expressing WNK4. Another possibility for the discrepancy between our findings and immunohistochemistry evidence is that a portion of the WNK4 protein (including the epitope against which the Lifton antibody was raised) is not exposed in certain situations. For example in certain nephron segments, binding of WNK4 with a potential interacting partner may shield the epitope and prevent antibody binding. Indeed, as WNK4 may localise in tight junctional complexes[148] in some nephron segments this may limit the accessibility of WNK4 epitopes in immunohistochemistry. Having employed probes against five different regions of WNK4 and detected a similar distribution in each case, it is likely that the distribution reported here is accurate. At times the principal mechanisms proposed for the action of the WNK pathway have focused on WNK gene expression in CD. It is clear from CD-specific knockout of αENaC[117], where mice have only minor perturbation of electrolyte handling and normal BP, that CD might not be so pivotal to these matters as previously thought. Our findings suggest the vast majority of both WNK1 and WNK4 expression lies more proximally than CD and consequently it seems quite possible these more proximal segments play the key role in the WNK pathway regulation of electrolyte handling and BP.

Longer exposure also detected WNK4 expression by Northern hybridisation at a much lower level in testis, suggesting that although WNK4 was originally thought to be restricted to kidney, it seems to be expressed in other tissues although at lower levels. Moreover, additional ISH studies demonstrating WNK4 expression in the epithelia of testis and epididymis, and foetal colon suggest that WNK4 may play a role in the regulation of electrolyte transport in epithelial tissues beyond the kidney. Indeed, a study by Kahle *et al.* demonstrating discreet WNK4 expression in several non-renal epithelia by immunohistochemistry supports such a theory[52]. The precise role of WNK4 in non-epithelial tissues such as brain (including the pituitary gland) has yet to be determined.

Chapter 5 Antibody Development to WNK1 and WNK4.

5.1 Introduction

Antibodies specific for mouse WNK1 or WNK4 were not available at the commencement of this study. Initial reports of WNK expression utilised antibodies raised against human WNK1 and WNK4[148]. The distribution patterns reported in this study, based on immunohistochemistry on mouse kidney using these antibodies, differ from our findings based on ISH studies using multiple probes against the same genes (Chapters 3 and 4). Notably WNK4 expression was not detected outside the cortex, conflicting with our studies repeatedly showing strong medullary WNK4 expression (Chapter 4). Interestingly, western blot analysis using this WNK4 antibody detected two bands (supplementary information). However, the reason for this remains obscure and the identity or significance of the second band was not discussed[148].

Moreover, antibodies capable of differentiating between the different isoforms of WNK1 from any species were not available. Not only is the WNK1 antibody used by Wilson *et al.* unable to differentiate between WNK1-L and WNK1-S, but this antibody is directed against an epitope encoded by exon 12 which is subject to alternative splicing in many tissues. For example, no WNK1 protein expression was detected in heart[148] despite strong evidence of WNK1 expression in this tissue from Northern hybridisation studies.

The determination of mouse WNK1 and WNK4 cDNA sequences, and the identification of cDNA sequence unique to each WNK1 isoform, (exons 1-4 of WNK1-L and exon 4a of WNK1-S; Chapter 3) made the prospect of raising specific anti-WNK antisera possible.

5.2 Materials and Methods

5.2.1 Peptide selection

Eurogentec, a commercial company with headquarters near Seraing, Belgium (near Leige University), specialising in peptide antibodies, was chosen for production. The initial and most important step of peptide antibody production is peptide selection. Two peptides for each isoform (where possible) were selected to boost our chances

of success and avoid the inherent risk of obtaining antibodies that recognise the peptide used for production but not the protein from which the sequence has been derived. The amino acid sequences of WNK1-L, WNK1-S and WNK4, predicted from the cDNA sequence, were inspected to choose suitable regions to use in peptide-carrier conjugates for antisera generation (Table 5.1). Great care was taken to avoid homologous regions (particularly the kinase domain, and familial autoinhibitory domain), regions subject to alternative splicing (e.g. exons 11 and 12 of WNK1), hydrophobic sequences and also regions with a strongly predicted secondary structure (unlikely to be exposed in native protein). Amino acid sequences favouring flexibility, lack of secondary structure, and predicted as likely to be surface-exposed were of key interest given the high predicted antigenicity of these combined characteristics (albeit within a still inexact science). Peptides were chosen for WNK1 which would differentiate between WNK1-L and WNK1-S, or detect both (WNK1-T). Peptide selection for WNK1-S was difficult because only a 30 amino acid stretch of unique sequence exists at the N-terminus, encoded by exon 4a. This region is also extremely cysteine-rich, which can be problematic for peptide antibody production. Use of peptides with internal cysteines is largely precluded as cysteine residues are often used to conjugate the peptide to the carrier protein. Only one peptide sequence unique to WNK1-S was predicted to be suitably antigenic (Table 5.1).

Table 5.1: Peptides selected for antibody production.

Target	Peptide	Coding Exon	KLH Coupling
WNK1-T	GRHEGRTTKRHYRKS	Exon 14	C-terminus
WNK1-L	RRHTMDKDSRGAA	Exon 1	C-terminus
WNK1-S	MDFMKKDFC	Exon 4A	C-terminus
WNK4	PDPPDSAGPTRSPP	Exon 1	C-terminus
WNK4	RASKGVTFAGDIGRM	Exon 18	N-terminus

5.2.2 Conjugation and immunisation

The selected peptides were covalently coupled to a carrier protein, keyhole limpet hemacyanin (KLH; from the mollusc *Megathura crenulata*), a standard carrier protein favoured for raising polyclonal antisera to peptide-carrier conjugates, where

KLH assists in enhancing the antigenicity of these short peptides. Two specific pathogen free (SPF)-rabbits were immunised with conjugated peptide, inoculated initially in Freund's complete adjuvant and boosting monthly in Freund's incomplete adjuvant over a three month period (involving four injections, and four bleedings). The immunisation protocol chosen was the Eurogentec Double X program whereby two SPF-rabbits are immunised with both conjugated peptides, derived from the same protein. This cost-effective program, on which there were additional savings at the time of arrangement, corresponds to two normal complete peptide antibody production programs, but reduces the number of rabbits required from four to two. In this way antibodies against both peptides are produced in each rabbit. Antibodies can be separated following production according to antigen-specificity by affinity purification for each peptide separately.

5.2.3 ELISA testing

Eurogentec provided an ELISA antisera testing service against both components of the conjugate inoculated: the delivered free peptides and the carrier protein (KLH). The ELISA results indicated detection of both peptide antigens at >1/100 to 1/1000 dilution by both rabbit antisera for WNK1 (WNK1-Rabbit 1, WNK1-R1; WNK1-Rabbit 2, WNK1-R2) and also WNK4 (WNK4-Rabbit 3, WNK1-R3; WNK4-Rabbit 4, WNK4-R4). However, the ELISA results for WNK1-S antisera (WNK1S-Rabbit 5, WNK1-R5) were negative, suggesting that this antibody production program was less successful.

The antisera were further tested by western blotting and immunohistochemistry according to the methods outlined in Chapter 2.

5.3 Results

5.3.1 Western blotting

The antisera generated were tested for the ability to detect WNK1 or WNK4 in kidney lysate protein on western blots. The predicted WNK4 and especially WNK1 proteins are very large, ranging from 1,222 amino acids (WNK4) to 2,377 amino acids (full-length WNK1). We expected to detect a ~250kDa band for WNK1-L, a

~207kDa band for WNK1-S and a ~132kDa band for WNK4. Alternative splicing of exon 11, exon 12 or both exons 11 and 12 would reduce WNK1 (both isoforms) by ~16kDa (154 amino acids), ~10kDa (95 amino acids) or ~26kDa (249 amino acids) respectively. These estimates do not consider any post-translational modifications which may occur.

WNK4 has been reported to localise to tight junction complexes in some kidney tubule cells[148]. It has also been suggested that WNK1 may be present in a large protein complex in the cell[94]. For this reason individual strips cut from a western blot with alternate lanes of both soluble and insoluble mouse kidney protein were processed with four antisera (WNK1-R1/R2 and WNK4-R3/R4). Soluble and insoluble protein fractions were prepared from kidney homogenate as described in section 2.2.8.1. Briefly, following centrifugation in lysis buffer soluble protein was retained in the supernatant wheras insoluble protein precipitated in a pellet, which was then resuspended for separation by SDS-PAGE.

As WNK1 and WNK4 are very large proteins, great care was taken to ensure both adequate separation and Western blot transfer of kidney lysate proteins. Protein integrity was confirmed by staining SDS polyacrylamide gels with coomassie blue. Adequate protein transfer was confirmed by reversibly staining membranes with Ponceau red. Preliminary studies encountered a number of problems including high background on the membranes. This may be because the antisera were not affinity-purified. Further dilution of the secondary antibody (from 1:1000 to 1:10,000) reduced (but did not eliminate) background in most cases. Blocking with 5%Milk/1xTBS/0.1%Tween was standard, but variations using different blocking agents were tried when attempting to optimise immunodetection and reduce background.

5.3.1.1 WNK4 Immunodetection by WNK4-R3

WNK4-R3 antiserum was tested over a range of blocking conditions (varying concentrations of milk/BSA and TBS). Ultimately, 5% BSA /1xTBS/0.1%TWEEN seemed the best blocking solution, while still allowing detection of two potential

WNK4 bands: WNK4a and WNK4b (Figure 5.1). The WNK4a band, although occasionally faint, was detected in the insoluble fraction at a 1:1000 dilution of WNK4-R3. This band was bigger than expected (~180kDa), and appeared "fuzzy". This may be due to related post-translational modifications of WNK4 producing a series of bands varying slightly in size and larger than the unmodified protein. WNK4b, a smaller more distinct, band (~100kDa) was detected in the soluble fraction. The relevance of this smaller band is also difficult to assess but it may be due to post-translational cleavage of WNK4.

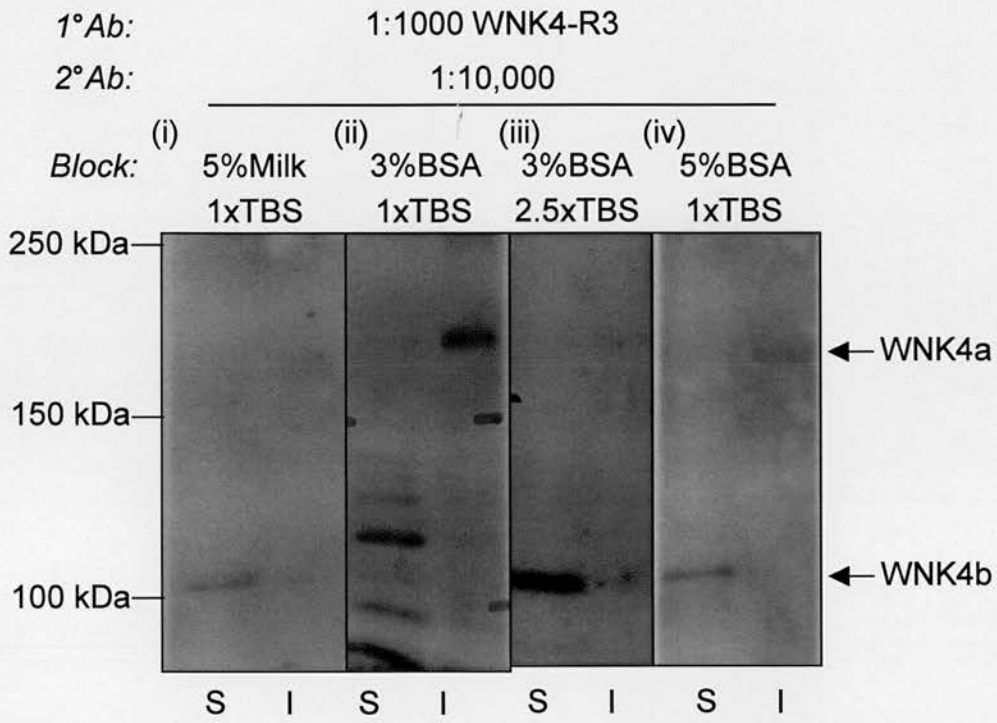

Figure 5.1: WNK4 immunodetection by Western blot with WNK4-R3. Strips from a Western blot are shown, containing alternate lanes of soluble (S) and insoluble (I) kidney protein lysate. WNK4-R3 antiserum detects two bands across a range of antibody dilutions and blocking conditions: a faint and "fuzzy" band (~180kDa), termed WNK4a, in the insoluble fraction; and a smaller, more distinct band (~100kDa), termed WNK4b, in the soluble fraction. 5% BSA was a potent blocking agent allowing detection of both WNK4a and WNK4b with little or no background or unspecific binding.

5.3.1.2 WNK4 Immunodetection by WNK4-R4

WNK4-R4 antiserum was also tested across a range of conditions. A similar band to that detected by WNK4-R3 (WNK4a) was seen in both fractions (faint but strongest in insoluble fraction) by WNK4-R4 (1:1000) blocking with

5%Milk/1xTBS/0.1%Tween (Figure 5.2). Detection was enhanced by reducing the antiserum dilution (1:500). On varying the degree of blocking treatment very little difference was observed between 5% and 7.5%Milk in the blocking solution. Increasing the blocking solution further to 10%Milk began to reduce the detection signal. The second smaller band detected by WNK4-R3, WNK4b, was not detected by WNK4-R4 under any of the conditions tried.

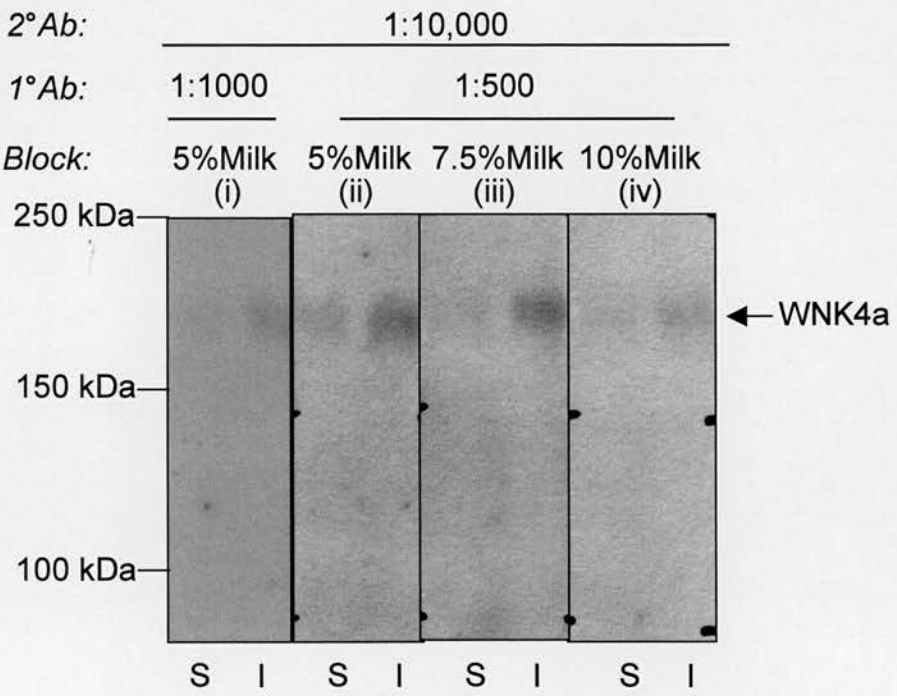

Figure 5.2: WNK4 immunodetection by Western blot with WNK4-R4. Strips from a Western blot are shown, containing alternate lanes of soluble (S) and insoluble (I) kidney protein lysate. WNK4-R4 antiserum detects a similar band to that detected previously, WNK4a, in both fractions. Reducing the antisera dilution (1:500) enhanced detection in blocking solutions containing either 5%Milk or 7.5%Milk. The second smaller band detected by WNK4-R3, WNK4b, was not detected by WNK4-R4.

Differences between the two WNK4 antisera suggest that they are raised against distinct inoculated epitopes. The WNK4 epitope against which WNK4-R3 is raised may only be exposed in the insoluble fraction but also in a protein of smaller size, possibly a cleaved fragment of WNK4, in the soluble fraction. The WNK4 epitope against which WNK4-R4 is raised is apparently exposed in both protein fractions, but is not present in this potential smaller WNK4 variant.

5.3.1.3 WNK1 Immunodetection

Antisera raised against WNK1 were also tested across a range of conditions but showed less promising results. A very faint band (WNK1a), which was larger than expected (280kDa; possibly due to post-translational modifications), was detected for WNK1 in both fractions by WNK1-R1 (1:1000; Figure 5.3). Due to its size this band likely represents WNK1-L, although it is impossible to determine whether or not alternative splicing of exon 11 and/or 12 has occurred. Detection was enhanced slightly by reducing the antisera dilution (1:500) and increasing the secondary antibody. An additional smaller band (WNK1b; ~140 kDa) was occasionally detected for WNK1 in both fractions (usually stronger in the soluble fraction). This WNK1b band is much smaller than would be expected for WNK1-S, and its nature and relevance remain uncertain. It is possible that this WNK1b band may be related to the small novel WNK1 bands seen by Northern hybridisation (section 3.3.3.3).

No bands of appropriate size were detected by WNK1-R2 antiserum under any of the conditions tried. However, it is still possible that this antiserum would detect native WNK1 protein by a different technique such as immunohistochemistry.

5.3.1.4 Future work

Despite difficulties with this western analysis potential bands for WNK1 and WNK4 were detected. It is noteworthy that bands detected by antisera raised against WNK1 were not detected by antisera raised against WNK4 and *vice versa*. WNK1-S antisera were not tested by western blotting, as this antibody production program lagged behind that of WNK1 and WNK4. Future work could include western analysis of this antisera. A limited amount of free peptide was supplied by Eurogentec. A logical next step could involve pre-absorption of antisera with antigen. In addition, immunoblots could be repeated with pre-immune antisera. These techniques would confirm specific antigen:antisera interaction and identify any non-specific binding. In the case of multiple bands, it would also allow resolution of which immunised peptide contains the epitope detected in which protein band. It may also be worthwhile to test antisera derived from earlier bleeds in case a superior but transient anti-WNK immune response was evident.

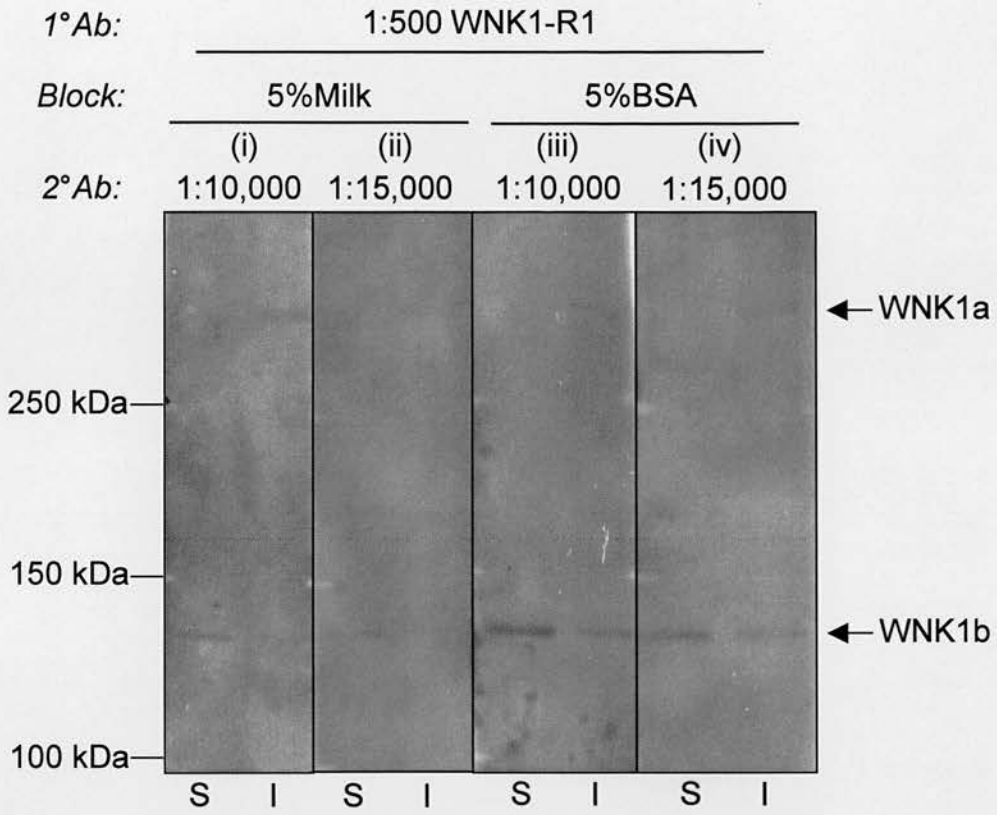

Figure 5.3: WNK1 immunodetection by Western blot with WNK1-R1. Strips from a Western blot are shown, containing alternate lanes of soluble (S) and insoluble (I) kidney protein lysate. WNK1-R1 antiserum detects two bands across a range of antibody dilutions and blocking conditions: a very faint band (~280kDa), termed WNK1a in the insoluble fraction; and a smaller band (~140 kDa), termed WNK1b in both fractions (usually stronger in the soluble fraction).

5.3.1.5 Immunodetection of recombinant WNK4

Shortly after this western analysis we contacted Dr. Dario Alessi and colleagues (University of Dundee) who have generated recombinant WNK4 protein. Using our antisera raised against WNK4 (WNK4-R3 and WNK4-R4) in parallel with their own antibodies, they were able to demonstrate detection of recombinant WNK4 protein (FLAG-tagged) by both WNK4-R3 (most potent) and WNK4-R4 (Figure 5.4). In a similar study, however, they were unable to detect endogenous WNK4 protein from tissue lysates. This suggests that endogenous WNK4 may be modified in some way or may exist in a protein complex, and so is not in a form capable of interacting with these antibodies.

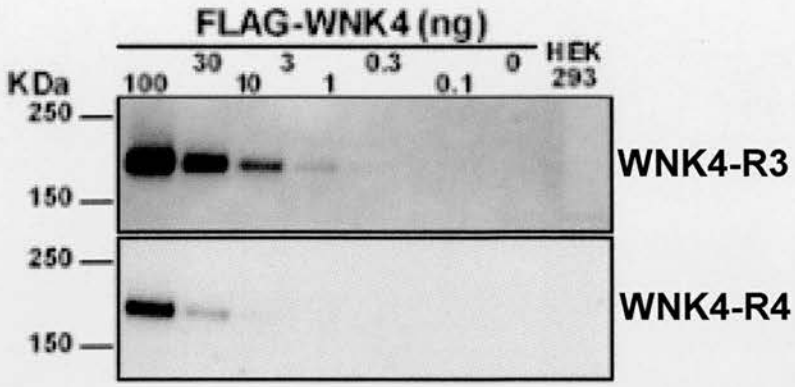

Figure 5.4: Immunodetection of recombinant FLAG-tagged WNK4. Both WNK4 antisera (1:500; in 5%BSA/1xTBS/0.1%Tween) recognised purified FLAG-tagged recombinant WNK4 protein at levels as low as 1ng by western blot.

5.3.2 Immunohistochemistry

The antisera were also tested for the ability to detect WNK1 or WNK4 in their native state by immunohistochemistry. mRNA localisation studies by *ISH* provided strong clues as to the expected distribution of WNK1 and WNK4 protein (Chapters 3 and 4).

5.3.2.1 WNK antisera testing by immunohistochemistry

An initial round of immunohistochemistry on adult mouse paraffin-embedded kidney sections was carried out using a series of dilutions (1:500, 1:1000, 1:1500) of the antisera: WNK1-R1, WNK1-R2, WNK4-R3 and WNK1S-R5. All sections underwent a process of antigen retrieval in sodium citrate buffer and the DAB detection system was used. A negative control was included, whereby the primary antibody was rabbit IgG (I-1000, *Vector*). No specific antibody:antigen binding was detected in this immunohistochemistry for any of the antisera in comparison to the negative control.

Following this initial negative immunohistochemistry result, we decided to select just one antiserum (WNK1-R1) and process it through a series of different conditions. Immunohistochemistry was carried out using lower dilutions of WNK1-R1 on both frozen and paraffin-embedded adult mouse kidney sections. Evidence from Northern blots suggest that WNK1 is strongly expressed in testis and so additional paraffin

embedded testis (and ovary) sections were included to determine any tissue-specific problems. Paraffin sections underwent antigen retrieval in either sodium citrate buffer or glycine/EDTA buffer. An alternative detection system (APAAP) was also tried instead of DAB. No specific antibody:antigen binding was detected for WNK1-R1 antisera in any of the tissues tested, frozen or paraffin-embedded, in comparison to negative controls.

5.3.2.2 Positive control for analysis by immunohistochemistry

After these negative immunohistochemistry studies it became important to have a positive control and steps were taken to work up a commercially available antibody to mouse ROMK *(APC-001, Alomone Labs)* and an antibody to mouse NCC *(gift from Jan Loffing)* for use as such a positive control in further studies in kidney.

Immunohistochemistry was carried out on paraffin-embedded sections of adult mouse kidney using serial dilutions (1:25, 1:50, 1:100, and 1:200) of the anti-ROMK antibody. Sections underwent a process of antigen retrieval in sodium citrate buffer and the DAB detection system was used. No specific antibody:antigen binding was detected in comparison to a negative control.

A second round of immunohistochemistry was carried out using an antibody raised against NCC. Both paraffin embedded (+/- undergoing sodium citrate buffer antigen retrieval) and frozen adult mouse kidney sections were processed. DAB detection revealed specific staining for NCC in distal nephron segments, following antigen retrieval on paraffin embedded sections. Staining was predominantly apical, as expected, in tubules typical of DCT in morphology and cortical distribution[72;108]. Negative controls showed no specific antibody:antigen binding.

5.3.2.3 Future immunohistochemistry studies

Unfortunately due to a shortage of time, further immunohistochemical work was not possible. Ideally, future analysis of WNK antisera should be carried out alongside both positive and negative controls. The anti-ROMK and particularly anti-NCC antibodies used in this study seemed good candidates to act as a positive control.

They are both expressed at substantial levels in kidney with distinct distribution patterns. The anti-ROMK antibody has been reported to work in immunohistochemistry studies on kidney[93] in the past. It is unclear why this antibody did not work in our studies. Perhaps further variation of conditions such as tissue fixation, antigen retrieval, blocking, antibody dilution, and detection may yield positive results for this antibody in the future. Further work including the anti-NCC antibody as a positive control would facilitate assessment of the WNK antisera using a protocol demonstrated to work in kidney, so that firm conclusions could be drawn about the effectiveness of these antisera in immunohistochemical detection of WNK proteins in mouse tissues.

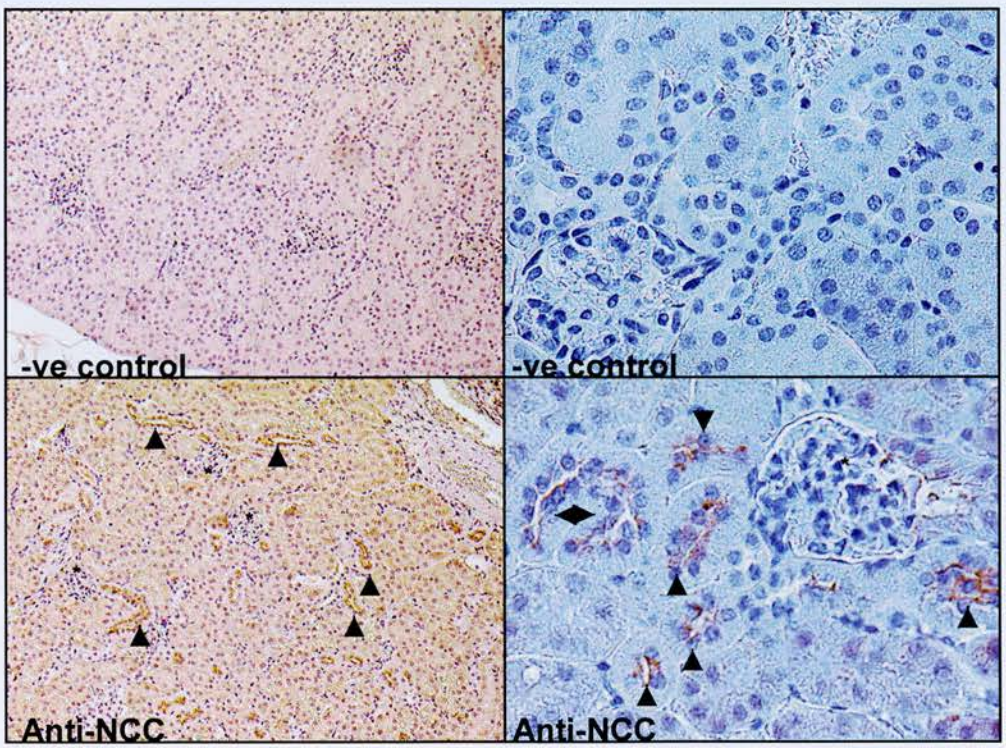

Figure 5.5: Detection of NCC by immunohistochemistry. Images of paraffin embedded mouse kidney sections (magnification: left, x10; right x40) counterstained with hematoxylin. Anti-NCC antibody (1:500) detects NCC in DCT (arrowheads) looping close to glomeruli (*). Negative controls show no specific signal.

5.4 Discussion

At present there is a lack of commercially available high quality anti-WNK antibodies. In particular, there are no antibodies capable of differentiating between the WNK1 isoforms. The original study reporting the distribution of WNK1

expression employed an antibody raised to an exon which is often subject to alternative splicing[148]. Most *in vitro* WNK studies currently rely on commercial antibodies raised to incorporated protein tags (e.g. FLAG). However, such antibodies are not useful when investigating *in vivo* expression of native protein.

We have attempted to raise antisera to mouse WNK1 (long, short, and total) and WNK4. Western analysis detected potential bands for both proteins in mouse kidney. A potential band, larger in size than expected, was detected for WNK1. Limited western blot analysis described in other studies, however, report a band of similar size[137]. Thus, it is possible that this size difference is due to post-translational modifications of WNK1, such as glycosylation or phosphorylation, which would not be unexpected given the sheer size of this protein. Anti-WNK4 antisera also detected a larger band than expected, and the "fuzzy" appearance of this band suggests post-translational modifications.

Although not striking, these results are promising, particularly as others in the WNK field have been unable to detect native protein in tissue lysates, despite readily detecting recombinant protein *in vitro*. Perhaps WNKs are sequestered in multiprotein complexes as suggested in some studies, possibly even in tight junctions, which shield the targeted epitopes from antibody binding. Bands that were inappropriately smaller in size were also detected for both WNK1 and WNK4. These smaller bands suggest the possibility of a post-translational cleavage event. In fact, smaller bands were detected for WNK1 by Northern hybridisation (Figure 3.9). Many kinases are subject to such post-translational cleavage events, with subsequent trafficking of the cleaved fragment elsewhere in the cell[32]. Such a cleaved WNK fragment may play regulatory role within the WNK pathway.

The success of our immunohistochemistry studies with the anti-NCC antibody facilitates further assessment of these WNK antisera in conjunction with this strong positive control. If successful this would greatly broaden the possibilities for future work on this pathway, and could potentially resolve the discrepancy between the protein distributions reported by Lifton and colleagues and our *ISH* localisation

studies reported in Chapters 3 and 4. Clearly, further work is required to determine the potential applications of these anti-WNK antisera.

Chapter 6 Dietary Electrolyte Driven Responses in the Renal WNK Kinase Pathway *in Vivo*.

6.1 Introduction

The role of WNK1 and WNK4 in the control of electrolyte balance and BP first became apparent with their mutation being associated with Gordon syndrome[148], a disorder featuring a NaCl/K^+ and H^+ imbalance. Patients are hyper-responsive to thiazide diuretics, further implicating a renal[42;112] electrolyte handling defect as the basis of this disease. Mutations in either WNK1 or WNK4 cause a broadly similar phenotype (hypertension and hyperkalaemia despite a normal GFR) suggesting that WNK1 and WNK4 function in a common pathway. Unlike most monogenic disorders affecting BP, which feature reciprocal Na^+ and K^+ (and/or H^+) imbalances and share a relationship to the aldosterone pathway (Table 1.1 and Figure 1.6), Gordon syndrome features concurrent NaCl and K^+ (and/or H^+) retention[13;42;148]. This unusual characteristic indicates the existence of a novel "WNK pathway" functioning in normal physiology to enable independent balance of K^+ and Na^+ (and ECF volume) by the kidney, ultimately regulating electrolyte balance and maintaining BP within the normal range. The BP-regulatory role of this WNK pathway is conserved in evolution as WNK1+/- mice are hypotensive[165].

Expression studies[109;148] (including those described in Chapters 3 and 4 of this thesis) demonstrate that components of the WNK pathway, most notably WNK1-S and WNK4, co-localise with a number of important electrolyte transporters in nephron segments which have major influence on long-term NaCl reabsorption, BP, K^+ and acid-base balance[47;82]; processes all disrupted in Gordon syndrome. Early functional studies suggest that, at least *in vitro*, WNK1 and WNK4 may regulate a number of these renal electrolyte transporters (Table 1.3). Most intriguingly, *Xenopus* oocyte studies suggest a WNK signalling pathway where WNK4 restrains two major effectors of kidney electrolyte transport: K^+ secretion via ROMK[56] and NaCl reabsorption via NCC[149;163], reducing their cell surface expression. Evidence also suggests that WNK1-L can in turn suppress this WNK4-mediated inhibition[161;162], providing further support for the theory that WNK1 and WNK4 participate in a common pathway. However, at the time of our studies described in this chapter, there were no reports of a functional role for kinase-deficient WNK1-S, the predominant

WNK1 isoform in kidney, nor was there any information on how the WNK pathway may be regulated *in vivo* in mammalian kidney.

Based on findings from this *Xenopus* oocyte work, the WNK molecular switch theory was proposed (section 1.5.1)[10;56]. This hypothesis suggests that regulation of renal electrolyte transport by the WNK pathway plays a key role in normal physiology, powerfully contributing to the renal response to fluctuations in blood volume and K^+ load. This WNK molecular switch would generate a response matching each of these stimuli that may complement aldosterone which is similarly induced by the very different stimuli of hypovolemia or K^+ load. To begin to test this hypothesis, we chose to focus on one side of this molecular switch, principally examining the response of the WNK pathway to dietary K^+ flux. In order to progress from the valuable insights of these *Xenopus* oocyte studies, we adopted a more relevant model, the mouse, which allowed us to investigate the physiological role of the WNK pathway *in vivo*, in an epithelial, renal, mammalian system. It is well established that the full renal response to maintain normal BP or to compensate for altered dietary electrolyte intake involves a substantial component that is slow to fully develop (taking many hours/days), persistent and accompanied by significant changes in nephron ultrastructure and gene expression[16;44]. Based on this we tracked the *in vivo* gene expression responses of the WNK pathway to chronic challenges altering renal electrolyte handling in mice, driven through variations in dietary electrolyte intake and aldosterone level.

6.2 Materials and Methods

6.2.1 Animal Treatments

The K^+-diet study involved adult male C57BL/6J mice, housed in pairs in mouse metabolic cages. Following three days of acclimatisation, groups (n=6) of mice commenced specific diets as outlined in Table 6.1. Batch-analysis confirmed diets were well matched for Na^+ (0.28±0.05%: all diets) and Cl^- content (0.7±0.12%: NK and LK). Mice took the specified diets for 10 days, with daily monitoring of bodyweight, food and water intake and 24hr urine collections for volume and electrolyte composition. Measurement of K^+, Na^+ and Cl^- in urine collections

allowed changes in electrolyte balance in response to the altered dietary intake to be monitored. Electrolytes were expressed as a ratio of creatinine or Na^+-excretion (Cl/Cre, K/Cre, K/Na). Collections over a 24hour period and normalisation to creatinine standardises measurements, making these observations much more robust against inaccuracies of incomplete collections.

Table 6.1: Experimental groups in the dietary K^+ study.

Group	Treatment Description	K^+ Composition
LK	Low potassium	(0.006%)K^+ diet
NK	Normal potassium	(0.33%)K^+ diet
HK	High potassium	(3.3%)K^+, (4.4%)Cl^- diet

The aldosterone study[†] involved adult male C57BL/6J mice, housed in pairs in normal cages. Groups of mice (n=6) were given normal (0.3%) Na^+ diet and had subcutaneous MP implanted delivering treatments as outlined in Table 6.2.

Table 6.2: Experimental groups in the aldosterone study.

Group	Treatment Description	MP Infusion	Delivery Rate
Adx	Bilateral adrenalectomy*	Saline only	-
Ctrl	Control	Saline only	-
Aldo150	High Aldosterone	Aldosterone	150 µg/kg/d

**0.9% saline drinking water*

The Na^+-diet experiment[‡] involved adult male C57BL/6J mice, housed in pairs in mouse metabolic cages. Animals were allowed one week to acclimatise, following which they commenced specific Na^+-dietary treatments (as outlined in Table 6.3) lasting 7 days.

6.3 Results

6.3.1 Effects of Chronic Variation in Dietary K^+ *in Vivo*.

Mice were given group treatments varying dietary K^+-intake for 10 days (LK/NK/HK; Table 6.1).

[†] Dr. Elaine Marshall provided resources for this study.
[‡] Wei Xue provided resources for this study.

Table 6.3: Experimental Groups in Na^+ Study.

Group	Treatment Description	Na^+ Composition
LNa	Low sodium	0.03% Na^+ Diet
NNa	Normal sodium	0.3% Na^+ Diet
HNa	High sodium	3% Na^+ Diet

6.3.1.1 Bodyweight, Food Intake and Fluid Balance

The LK group showed borderline lower weight becoming significant vs. HK (but not NK) at the end of the experiment (25.6±0.6g versus 27.3±0.6g, respectively; $p=0.03$) but mice appeared healthy throughout (Table 6.4 and Figure 6.1(a-c)). Both HK and LK groups developed a higher fluid intake and urinary output compared to the NK group (HK vs. NK significant at conclusion: >3.4-fold higher intake ($p<0.05$) and >4.9-fold higher output ($p<0.01$)).

6.3.1.2 Urinary Electrolytes

Mice were allowed a period of three days (days 1-3) to acclimatise to metabolic cages. Following this, during the initial 3 days of active treatment with specific diets (days 4-6) K/Cre and Cl/Cre rose 6.8-fold and 4.9-fold respectively with HK, remained unchanged with NK and K/Cre showed a dramatic 24.4-fold decrease with LK. After day 5-6 group K/Cre ratios did not significantly change indicating re-establishment of appropriate electrolyte balance. The HK and LK groups demonstrated a >17-fold increase and a >14-fold decrease respectively in K/Na by day 6 (Figure 6.1(d-f)).

6.3.1.3 Plasma Measurements

As expected, HK induced a small but significant increase in plasma K^+ within the normal range (HK vs. NK: 4.85±0.2 mmol/L versus 4.1±0.2 mmol/L respectively, $p=0.03$). Plasma aldosterone was elevated with HK (1879 ±387pmol/L versus NK, 793 ±207pmol/L), but was unchanged with LK (834 ±297pmol/L; Table 6.4). Plasma renin activity (PRA) and corticosterone did not change significantly across the treatment groups (Table 6.4).

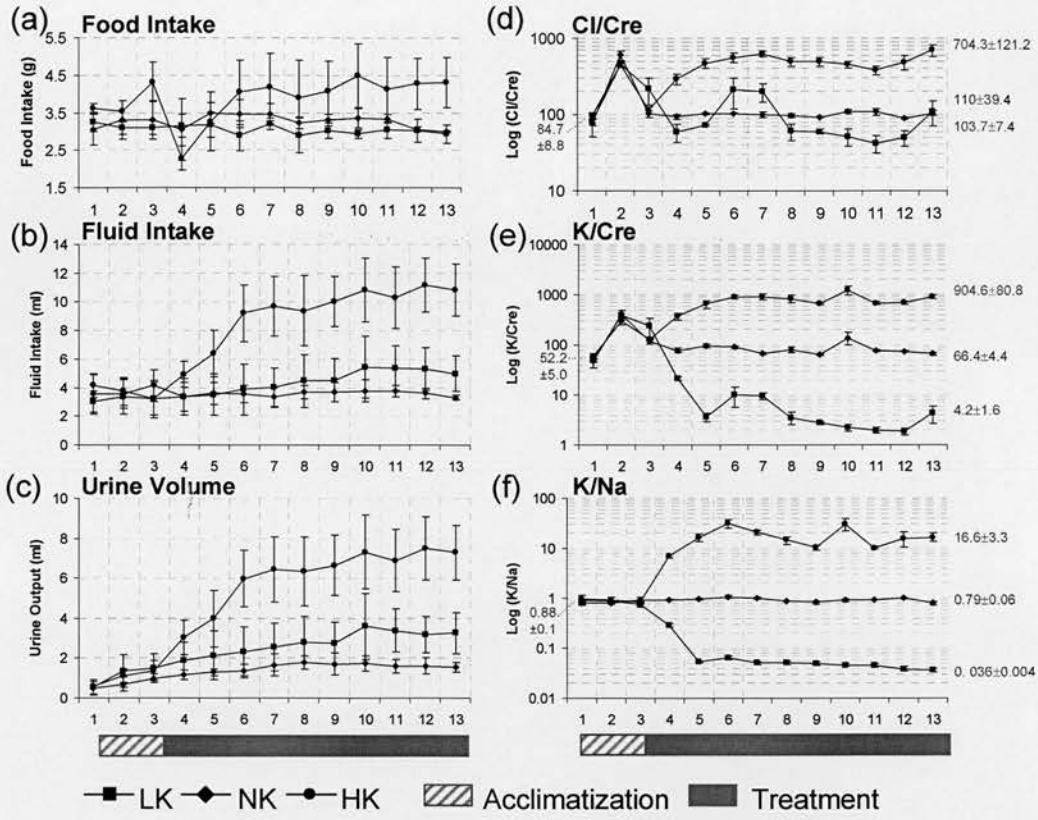

Figure 6.1: Effect of dietary K^+ intake on metabolic measurements. Mice were treated with LK/NK/HK diets (as outlined in Table 6.1) for 10 days, and daily measurements of (a) food intake, (b) fluid intake and (c) urine output were recorded. Urinary electrolyte excretion was measured daily , reflected changes in dietary electrolyte intake and was expressed as a ratio of creatinine or Na^+-excretion (Cl/Cre, K/Cre, K/Na: d-f) A transient decrease in food intake was observed in the HK group on day 4 immediately following the introduction of treatment diet.

6.3.1.4 WNK expression responses to dietary K^+ challenge

Specific real-time PCR assays were used to detect WNK expression responses to dietary K^+ intake (Figure 6.2). This real-time PCR analysis indicated that both renal WNK1-S and WNK4 expression is regulated by increasing dietary K^+ intake. Specifically WNK1-S was downregulated by 20±9.3% with LK (p=0.04) and upregulated by 30±10.4% with HK (p=0.01, a 50±10.2% rise from LK to HK), as was total WNK1 (WNK1-T: 24±7% increase, P=0.0009) compared to NK (Figure 6.3(a)). WNK4 was upregulated with HK (48±24.2%, p=0.01) but unchanged with LK.

Table 6.4: Metabolic measurements in K^+ Study.

	Low K(LK)	Normal K(NK)	High K(HK)
Initial Bodyweight(g)	29.7±0.7	28.8±0.5	29.8±0.6
Final Bodyweight(g)	25.6±0.5	26.9±0.3	27.3±0.6
Plasma K^+(mM)^A	4.13±0.22	4.08±0.22	4.85±0.2
Plasma Na^+(mM)^B	145.4±0.4	146±0.6	144.3±0.7
Plasma Cl^-(mM)^C	114.4± 1.54	112±1	114.5±1.05
Plasma Creatinine(μM)^D	13.8±2.24	14.4±1.21	12.5±1.44
Aldosterone(pmol/L)	834.2±297.2	793±206.8	1878.7±387.1
PRA(ng/ml/h)	4.38±1.12	4.45±0.83	5.71±0.34
Corticosterone(nmol/L)	345.8±48.8	342±58.2	300±42.6

Plasma concentrations of Na^+, K^+, Cl^- and creatinine were measured on commercial clinical chemistry analysers and remained within the normal range for all groups. Normal plasma ranges for: $^AK^+$, 3.0-8.3mmol/L[91], but carefully taken having a narrower range probably nearer 3.8-6.8mmol/[133;146;168]; $^BNa^+$, 139-157mmol/L; $^CCl^-$, 104-119mmol/L[17]; ^{D}Creatinine, 5-67micromol/L[91]. Values are means±SE.

In regions with clear WNK1-S expression (Figure 6.3(b)) ISH analysis showed upregulation in cortex by HK (vs. NK: 2.1±0.6-fold, (p=0.003) [1-3.3; 95% confidence interval]). WNK1-S distribution remained cortical without striking change. Over kidney regions with clear WNK4 expression there was a 2.3±0.6-fold [1.1-3.5] upregulation in expression with HK (p=0.02) (Figure 6.3(c)), whilst the apparent possible increase in WNK4 with LK (82±51.3% vs. NK) did not reach significance.

6.3.2 WNK expression response to aldosterone challenge

As aldosterone plays a key role in K^+ secretion we also examined the effect of fluctuations in aldosterone level on WNK expression. In this experiment, groups of mice were given treatments (Table6.2) involving excess aldosterone via MP (Aldo; 150μg aldosterone/kg/day[50]) or adrenalectomised (Adx; supplemented with 0.9% saline drinking water) to abolish aldosterone production. Real-time PCR showed that WNK1-S expression rose significantly across the Adx-aldo excess range (43±7.6%,

p=0.0002). Specifically, aldo treatment induced a 32±6.7% [18.9-45.2] WNK1-S upregulation (p=0.0002) without affecting WNK1-L or WNK4 expression (Figure 6.4). Adx had no significant effect on WNK expression compared to the control group.

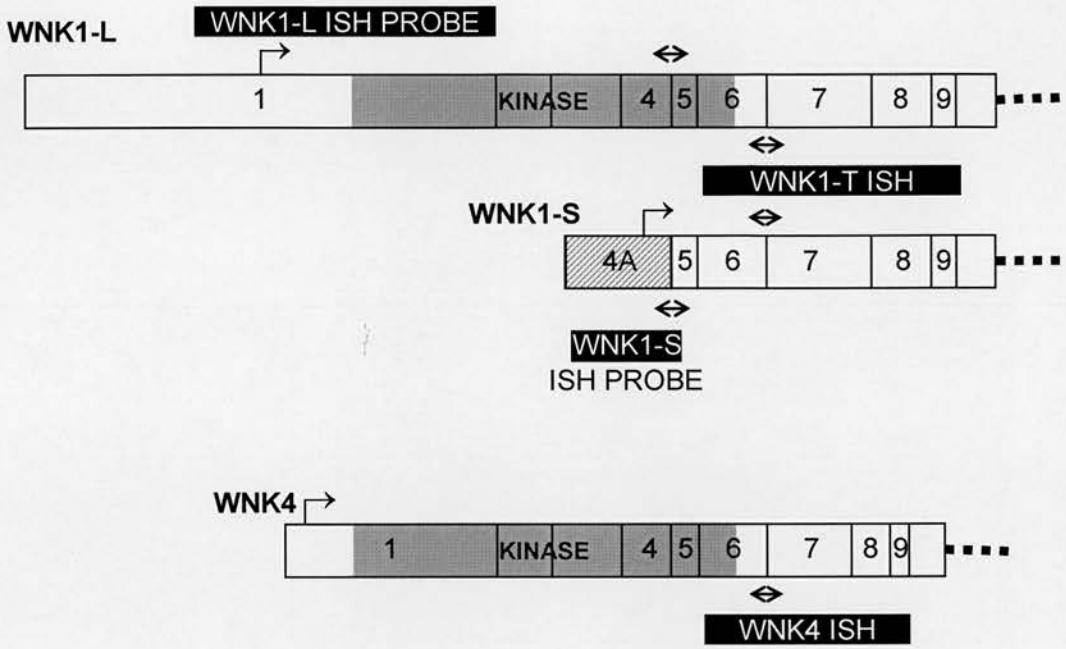

Figure 6.2: Schematic representation of WNK cDNA structure showing 5'-exon composition and probe positions. The cDNA structures of the 5'-regions of kinase-intact WNK1-L (containing exons 1-4), kinase-deficient WNK1-S (containing exon 4a in place of exons 1-4) and WNK4 are illustrated with vertical bars representing exon:exon boundaries. Numbers within rectangles refer to exon numbers. Black boxes specify the cDNA region probed by ISH. Double-headed arrows indicate the exon:exon boundary crossed by probes used in real-time PCR studies. Horizontal dashed lines indicate further exons not included in this illustration.

6.3.3 WNK expression response to dietary Na^+ challenge

To test whether varied dietary Na^+ induces similar WNK expression changes, mice were fed diets with a specific Na^+ content (LNa/NNa/HNa; Table 6.3) for 6 days. WNK1-S showed a just significant downregulation, by 39±16% of control levels, between HNa and LNa (p=0.049, $ANOVA_{LSD}$; Figure 6.5). No other significant changes in WNK expression were observed across the treatment groups.

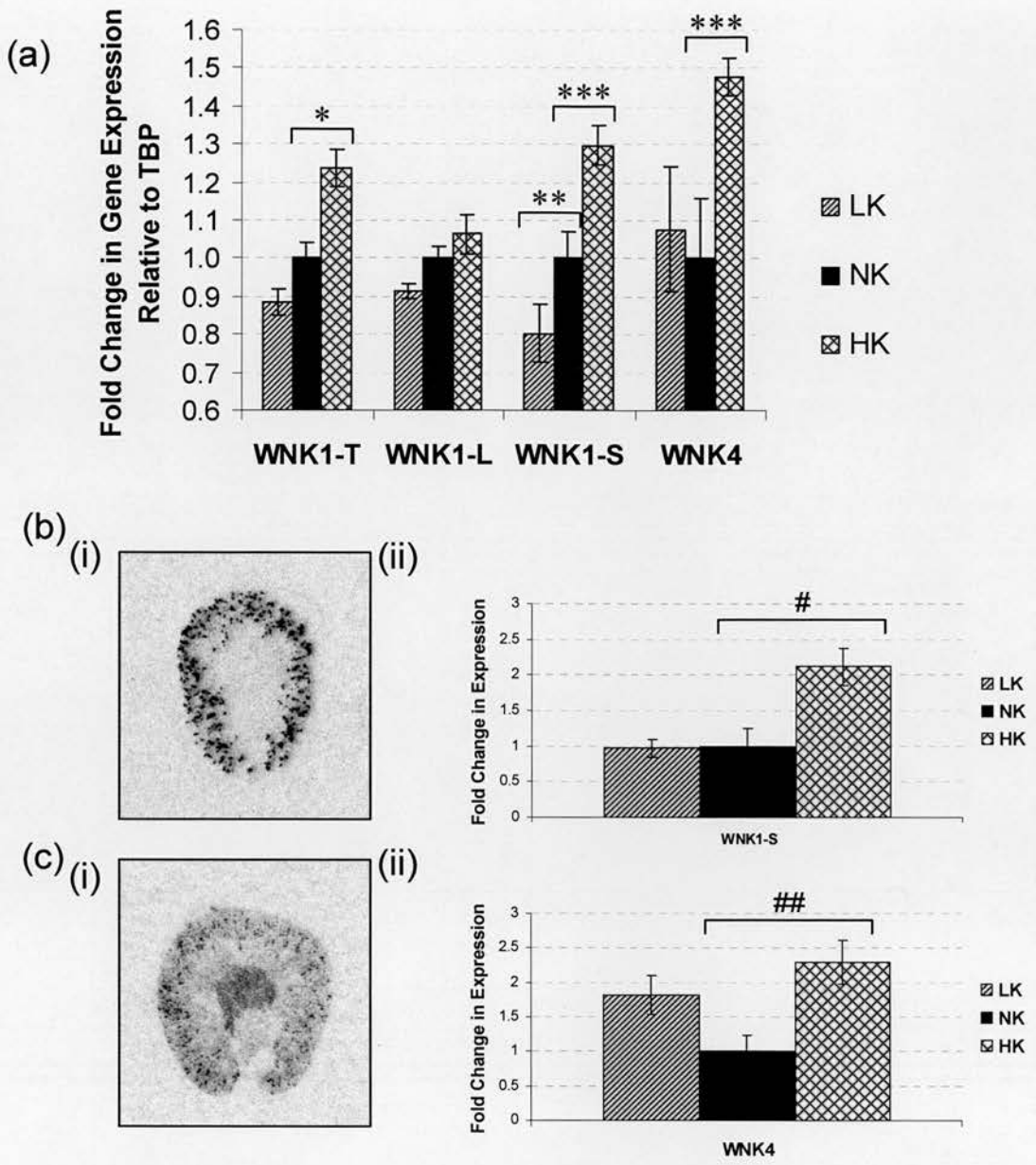

Figure 6.3: WNK expression in response to varied K^+ intake. (a) Real-time PCR results from renal RNA from groups of mice (n=6) with variations in dietary K^+. WNK1-S expression is significantly downregulated with LK whilst WNK1-S and WNK4 are upregulated with HK. No significant changes were observed in WNK1-L expression across the experimental groups. (b-c) ISH analysis of WNK1-S (n=6) and WNK4 (n=6 for LK and HK groups and n=4 for NK group owing to some sections being unsuitable for full analysis) in kidney did not detect any major shifts in distribution and level of WNK expression with varied dietary K^+ at the regional level. (i) Representative sections and (ii) densitometric analysis from ISH studies. WNK1-S (b) and WNK4 (c) have different expression profiles with WNK1-S expression restricted to the cortex, and WNK4 restricted to cortex and outer medulla. WNK1-S and WNK4 expression are both upregulated with HK.
*p=0.009; **p=0.04; ***p=0.01; $^{\#}$p=0.003; $^{\#\#}$p=0.02.

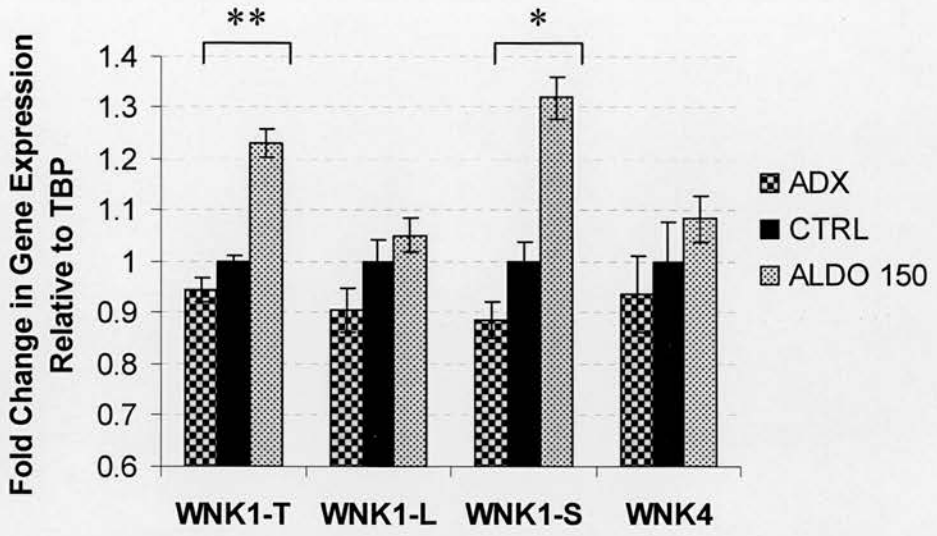

Figure 6.4: WNK expression in response to variations in aldosterone. Mice were given (n=6) subcutaneous (Alzet®) MP treatments for 6 days as outlined in Table 6.2. PRA and aldosterone measurements allowed confirmation of adequacy of treatments. WNK1-S expression was upregulated by chronic aldosterone treatment (150µg/kg/day, 6 days) but was unchanged in the absence of aldosterone following Adx. No changes in WNK1-L or WNK4 were observed across the experimental groups.
*p=0.0002; **p=0.02.

6.4 Discussion

This study is one of the first to investigate the WNK pathway *in vivo* in a physiologically relevant system, the mouse. It is well established that relevant aspects of human physiology and their disorders are very well modelled in mice particularly mechanisms of electrolyte handling and the extent to which abnormalities in such mechanisms affect long-term BP control[16;82;121]. For example, where transgenic models of human distal nephron disorders have been created, the disease phenotypes have been largely faithfully reproduced e.g. Liddle's syndrome[115] and Bartter syndrome[76;132].

Up to now, *Xenopus* oocyte studies have provided invaluable evidence of WNK pathway regulation of important mediators of distal nephron electrolyte transport (Table1.3). These key studies led to the proposal that the WNK pathway plays a fundamental role in normal physiology, determining the renal response to fluctuations in blood volume and K^+ load, essentially forming a molecular switch. In the current study we have attempted to investigate one side of this WNK molecular

switch *in vivo* by challenging mice with varied dietary K^+ intake and examining the renal WNK gene expression response.

We found notable changes in renal expression of WNK genes with varied dietary K^+ intake, indicating that the WNK pathway responds *in vivo* to this physiological determinant of electrolyte balance and BP. WNK1-S expression changes correlate with K^+-intake, stressing the importance of this isoform, and segments strongly expressing it (DCT and CNT), in K^+ homeostasis. High K^+-intake also increased WNK4 expression. These coordinated WNK expression changes seem functionally significant as merely heterozygous changes in WNK1 or WNK4 cause substantial BP and electrolyte abnormalities[13;42;148;165].

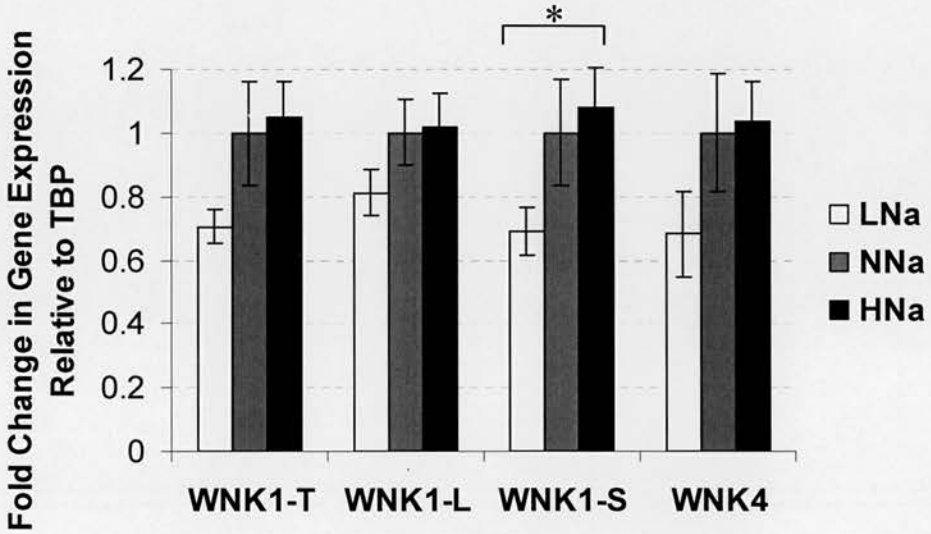

Figure 6.5: WNK expression in response to varied Na^+ intake. Mice were treated with LNa/NNa/HNa diets for 7 days as outlined in Table 6.3. WNK1-S showed a just significant downregulation (by $ANOVA_{LSD}$) between high and low Na^+ diet. No other significant changes in WNK expression were observed across the treatment groups.
*p=0.049 ($ANOVA_{LSD}$)

The theory that both aldosterone-dependent and independent mechanisms are involved in K^+-secretion[47;82], made examination of effects of fluctuations in circulating aldosterone levels of potential interest. In a preliminary investigation of this, we looked at renal WNK gene expression using resources from another study† where animals had very low aldosterone (due to Adx), normal aldosterone (control group) or high aldosterone (11.2-fold elevation versus controls via MP infusion). Our

findings indicate that aldosterone does not regulate WNK1-L or WNK4 expression but may play some role in WNK1-S regulation. However, aldosterone seems unlikely to be the sole regulator of WNK1-S expression. Indeed, lack of effect of Adx (loss of aldosterone) suggests decreased WNK1-S expression with LK was aldosterone-independent and indeed plasma aldosterone in the LK and NK groups were not significantly different. Furthermore, the observed WNK1-S expression changes do not correlate with plasma aldosterone. Thus similar changes in WNK1-S expression accompany very different aldosterone elevations, 2.3-fold (with HK) and 11.2-fold (with aldosterone infusion). This evidence suggests aldosterone-independent regulation of WNK1-S expression.

This is supported by Gordon syndrome physiology where plasma aldosterone is often in the normal range[30] and a phenotype of combined hypertension and hyperkalaemia (indicative of *both* NaCl *and* K^+ retention) could not be produced by a mutation solely in the aldosterone pathway which classically regulates Na^+ and K^+ balance in a reciprocal manner[14]. The nephron *must* switch via a different mechanism to a mode uncoupling Na^+-reabsorption and K^+-secretion[56]. It may be that on a HK diet the animals become more responsive to aldosterone: such increased aldosterone-responsiveness has been reported in mice with Liddle's syndrome[22]. So, although aldosterone levels are much lower with HK treatment compared to treatment where aldosterone is given in excess, similar upregulation of WNK1-S occurs. Clearly further studies may fully clarify the relative importance of aldosterone in WNK expression regulation.

We also took a preliminary look at the opposite side of the WNK molecular switch. As sodium balance is key in determining ECF volume and influencing BP WNK gene expression responses across a wide range (100-fold) of chronic dietary Na^+ intake[‡] were studied. With variations in dietary Na^+, a trend to lower WNK1-S expression as dietary Na^+ reduced just reached significance when comparing high and low Na^+ groups. It is intriguing that this might represent a response of the WNK pathway to subtle reductions in ECF volume as dietary Na^+ falls. Clearly, to examine this side of the switch properly would require more extensive experiments to look

more directly at this regulation and involve studies where volume status is accurately controlled.

How do these results expand understanding of this novel WNK pathway? The pathology of Gordon syndrome highlights the importance of DCT (where WNK1-S is strongly expressed) in electrolyte balance and BP control, as patients are usually hyper-responsive to thiazide diuretics[13;42;119]. *Xenopus* oocyte work suggests WNK4 may inhibit NCC in DCT and WNK1-L prevents this inhibition[149;161]. This work provides some of the first clues as to the role *in vivo* of WNK1-S, the predominant WNK1 isoform in kidney.

WNK1-S is kinase deficient, but retains domains (e.g. coiled-coils) likely involved in multimeric/tetrameric WNK1 assembly[151;152]. Intriguingly, strongest WNK1-S and WNK4 expression co-localise in DCT-CNT, where they may contribute to the same mechanism regulating K^+ homeostasis. Consequently, we propose in DCT-CNT, WNK1-S could bind and counterbalance WNK1-L effects, especially shielding WNK4 from inhibition. Alternatively, WNK1-S could shield WNK4 from any form of inhibitory kinase (not just WNK1-L), interacting directly with a WNK-binding site on WNK4 or on an inhibitory kinase. Thus, an increase in WNK1-S or WNK4 (as in our *in vivo* study) would downregulate NCC-mediated NaCl reabsorption in DCT, increasing distal Na^+ delivery. This directly stimulates K^+-loss, as Na^+ is reabsorbed distally to DCT1 via ENaC, in exchange for K^+[82]. This putative pathway is illustrated in Figure 6.6. This phenomenon accompanies thiazide diuretic treatment driving a similar increase in K^+-secretion[82]. Finally, downregulation of WNK1-S on chronically reducing dietary Na^+ suggests this distal delivery of Na^+ is restrained when there is a need to conserve body sodium and ECF volume.

We propose that the alleged molecular switch[56] suggested to explain Gordon syndrome is based on the distal delivery of Na^+ (Figure 6.6). This hypothesis is also supported by careful ultrastructural studies[57] showing that on a HK diet early CNT develops extensive hypertrophy and increased Na^+/K^+-ATPase[57]. Similar CNT changes occur with NCC-/- Gitelman's mice or high dose thiazide diuretics where

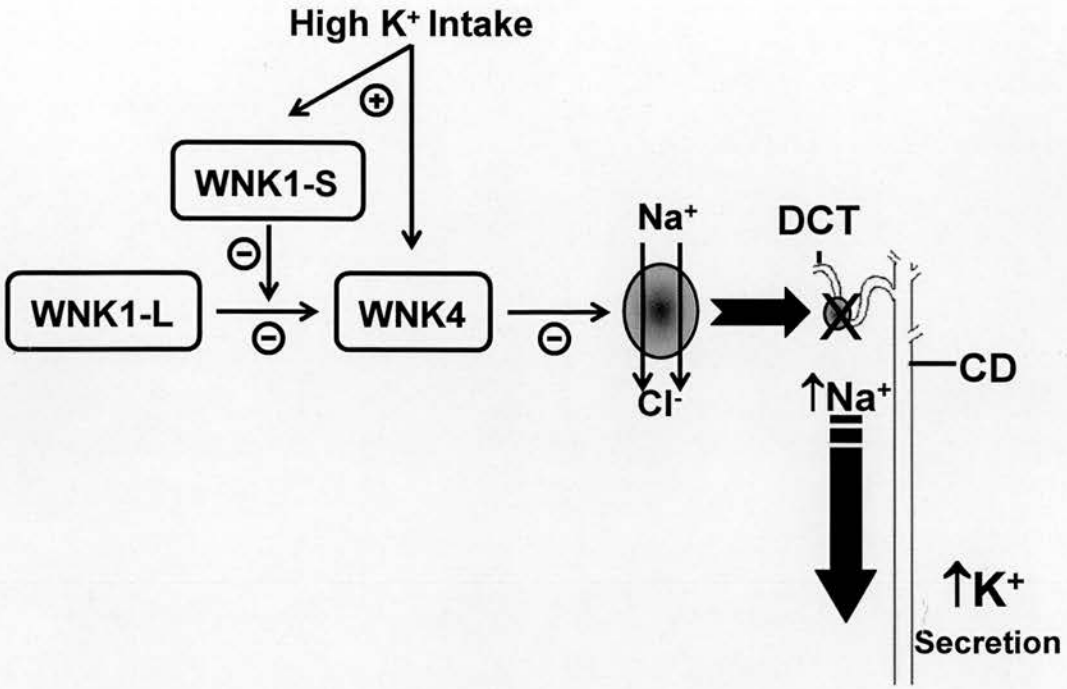

Figure 6.6: Schematic depiction of potential WNK pathway in distal nephron. The WNK pathway is suggested to regulate the extent of NaCl reabsorption in (early) DCT in the manner of the alleged molecular switch[56] proposed in explaining Gordon syndrome. A high K^+ intake switches to lower Na^+ reabsorption via NCC in DCT so distal Na^+ delivery rises allowing K^+ to be cleared. In Gordon syndrome, however, the switch appears to be jammed in the opposite direction. Excessive reabsorption of Na^+ occurring in DCT, due to loss of inhibition of NCC by the WNK pathway, would lead to a reduction in distal Na^+ delivery. Consequently, K^+ could not be cleared efficiently, leading to both hypertension and hyperkalaemia.

reduced DCT reabsorption directs NaCl distally predisposing to hypokalaemia. In Gordon syndrome the switch appears jammed in the opposite direction, inappropriately engaging a response these studies suggest is normal when body K^+ or Na^+ (and so ECF volume) are falling and require conservation. Excessive Na^+-reabsorption in DCT (diminished inhibition of NCC) reduces distal Na^+ delivery and K^+-secretion, causing hypertension *and* hyperkalaemia (Figure 6.6).

Chapter 7 Distribution and Regulation of ROMK Gene Expression in Mouse.

7.1 Introduction

The kidney plays a dominant role in long-term regulation of both BP and K^+ balance, features that are simultaneously disrupted in Gordon syndrome. The renal mechanisms achieving such regulation of K^+ balance are far from fully understood, take many minutes/hours to fully develop, are powerful in restoring K^+ balance, and sophisticated in usually achieving this with minimal effect on other electrolytes or fluid balance. Whilst in health this results in the regulation of K^+ and ECF volume/BP seemingly little influenced by one another, it is revealing that when key elements in such homeostatic control are disrupted (e.g. mutations of the aldosterone-ENaC or the WNK kinase pathways or the renal epithelial K^+ channel ROMK, see below) there are usually linked disorders in K^+, BP and indeed also acid-base regulation (Table 1.1 and Figure 1.6). This clearly shows these largely seemingly unconnected renal homeostatic processes are in fact interwoven. In this regard the channel ROMK is of key importance being both important in K^+ handling and in its various forms at the intersection of these key pathways.

Dietary K^+ intake plays a key role in modulating K^+ secretion: an increase in K^+ intake stimulates, whereas a low K^+ intake inhibits K^+ secretion[70;82;83]. Remarkably, during K^+ depletion, the CD switches from a largely K^+ secreting segment to a site of K^+ reabsorption. In severe K^+ restriction several attendant processes assist in renal function with minimal K^+, including the induction and recycling of NH_4^+, an ion which can substitute for K^+ to maintain key transport of NaCl by NKCC2 and Na^+/K^+-ATPase. The colonic isoform of the H^+/K^+-ATPase pump (cHKA) in OMCD may play an important role in this K^+ scavenging switch when renal function is run in a K^+ conserving state as it is reportedly upregulated in K^+-deficiency[4;28;61;62;103;105]. Increased cHKA could facilitate increased K^+ reabsorption and/or proton secretion (facilitating NH_4^+ excretion) in the OMCD depending on the extent of K^+ recycling.

In a normal or high K^+ state, K^+ secretion is mediated by a two step process: entry through the basolateral Na^+/K^+-ATPase pump of principal cells, and secretion into the lumen along an electrochemical gradient via apical K^+ channels. Patch-clamp studies identified "epithelial K^+ channels" apparently capable of such apical K^+

secretion in distal nephron. Many years later a cDNA was identified encoding a member of the ATP-sensitive inward rectifying K^+ channel family, with apical expression in distal nephron seeming to fulfil such a function, the ROMK channel[47]. This epithelial K^+ channel is reported to mediate net K^+ secretion in CNT and CCD and also apical K^+ recycling in TAL[3;47]. Loss-of-function mutations in the human ROMK gene (KCNJ1) cause Bartter syndrome[1;127], featuring hypokalaemic metabolic alkalosis and renal salt wasting, consistent with the crucial role of ROMK in facilitating NaCl reabsorption through NKCC2 (despite a low luminal K^+ concentration) in the TAL. A ROMK-/- mouse has been generated[73], confirming that ROMK forms the 30 pS (low conductance) K^+ recycling/secretory channel in the TAL and CD[76] and is also required for expression of the 70 pS (medium conductance) K^+ recycling channel in the TAL[75].

The ROMK gene contains several exons producing alternatively spliced transcripts[8;9;11;12;48;60;124;164;167], with ROMK1-3 being the major kidney isoforms. Rat ROMK1 and ROMK2 are similar to the corresponding human isoforms, however a rat homolog of the third human ROMK isoform has not been identified[47]. At the time of these studies the exon-intron structure and alternative isoforms of the mouse ROMK gene were less well defined. Alternative splicing of ROMK generates proteins that differ in the amino acid sequence and length of their NH_2 termini, but are identical to each other over the remainder of the peptide. Some studies of differential expression of ROMK isoforms along the nephron from TAL to OMCD in rat[12;65] have been widely reported to show ROMK2 and 3 expressed in TAL and DCT, while principal cells in CCD express ROMK1 and 2. The OMCD cells only express ROMK1.

ROMK expression and function is intricately regulated by a wide variety of factors, including intracellular pH[19;29;88;156] and ATP[48;90;118], with increasing intracellular pH and ADP activating the channel. A number of studies have also examined ROMK gene expression in response to dietary K^+ intake, but the findings have been somewhat inconsistent. Nonetheless, the overview has been that ROMK is upregulated with high K^+ intake and downregulated with low K^+ intake[47]. The

regulation of individual ROMK isoforms by dietary K^+ intake remains largely unexplored, particularly in mouse, due at least in part to the lack of isoform-specific antibodies.

Despite huge advances in our understanding of K^+ homeostasis, a number of issues remain unresolved. For example, although ROMK is regarded as the main exit portal for K^+ in the kidney, (type II) Bartter syndrome patients, with inactivating ROMK mutations, and ROMK-/- mice are hypokalaemic and have a high rate of urinary K^+ excretion. Thus, the precise pathways employed by the kidney to manage K^+ balance require further investigation. As ROMK was reported as a target of the WNK pathway, the purpose of the present study was to examine the effects of fluctuations in dietary K^+ intake on mouse ROMK gene expression in the kidney, so extending the study of these mechanisms driven by chronic K^+ diet beyond WNK1 and WNK4 (Chapter 6) to examine this key channel, ROMK, and its conserved isoforms. We found striking differences in mouse ROMK isoform distributions in keeping with the literature available from studies in human and rat. However, we also found striking differential regulation of these isoforms by high or low dietary K^+ intake. Changes in ROMK isoform expression with K^+ depletion were paralleled by changes in cHKA allowing the potential to facilitate H^+ and NH_4^+ excretion and acid-base homeostasis in K^+ deficiency. These findings may have important implications for our understanding of the role of ROMK isoforms in K^+, H^+, and acid-base balance.

7.2 Materials and Methods

This study utilised resources outlined in Chapter 6. Primers, probes and real-time PCR assays are outlined in Tables 2.1-2.3.

7.3 Results

7.3.1 ROMK isoform distribution in mouse kidney

ROMK expression is reportedly regulated in parallel with K^+-intake. However, real-time PCR, detecting all ROMK isoforms, indicated no significant change across K^+-diet groups, (8.5±8.3%, p=NS, Figure 7.1). Accordingly, we investigated individual isoform expression using exon-specific ISH probes for major ROMK isoforms

(Figure 7.2), ROMK1, 2, and 3 on adult mouse kidney (Figure 7.3). Serial sections were probed for ROMK isoforms and NKCC2 or γENaC (TAL and CD markers respectively). It is strikingly clear in medulla, ROMK1 is expressed in OMCD, (like γENaC, Figure 7.3 (*lower panels*)) with limited cortical (CCD) extension, whilst γENaC expression spans late DCT-OMCD, being strongest in cortex[78]. In contrast, ROMK2 expression overlaps that of NKCC2 in TAL and also γENaC in cortex (including CCD) (Figure 7.3 (*upper panels*)). No clear expression of ROMK3 was detected.

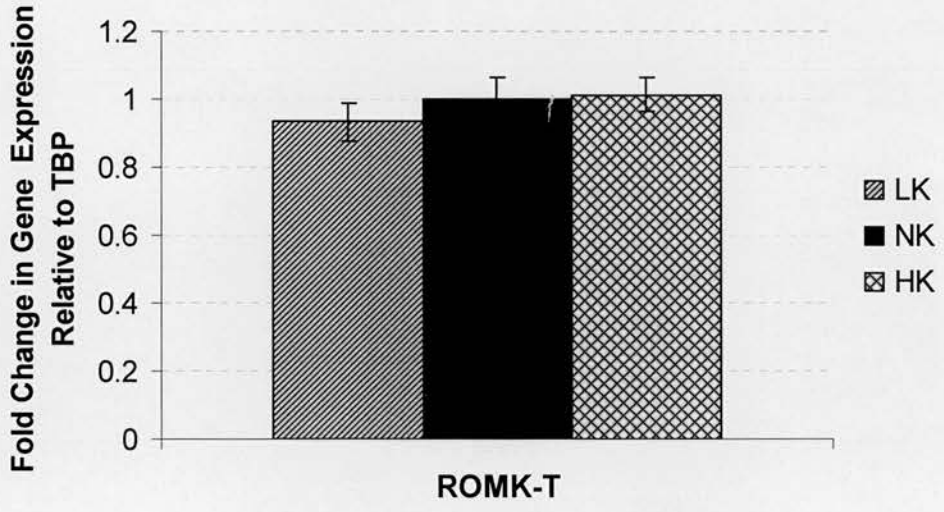

Figure 7.1: ROMK expression in response to varied K^+ intake. No significant changes were observed in ROMK-T expression (representing combined expression of all isoforms) using real-time PCR.

7.3.2 Expression of ROMK isoforms in response to changes in K^+-intake

Real-time PCR revealed upregulation of ROMK2 with HK by 47±17.6% (vs. NK, p=0.008) but unchanged with LK. In contrast, ROMK1 was unchanged with HK but strongly increased, 2.6±0.3-fold [2-3.2], with LK (vs. NK, p=0.0002). ISH studies showed with LK ROMK1 extended further into CCD Figure 7.4(d) and image analysis revealed a 2.2±0.3-fold [1.7-2.7] increase in renal ROMK1 expression (LK vs. NK, p=0.0001; Figure 7.4(b)) but no significant differences with HK. In contrast, HK induced a 76±33% [12-141] increase in ROMK2 expression (vs. NK, p=0.01; Figure 7.4(c)) with no significant change on LK. Thus, the shift in ROMK2/ROMK1

expression revealed by these studies was 3.8-fold and reciprocal as K^+-intake varied (Figure 7.4(a-d)).

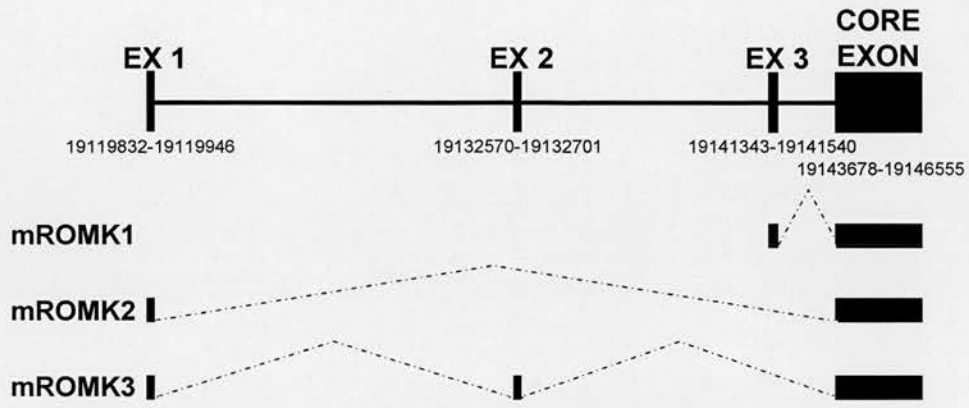

Figure 7.2: Schematic depiction of ROMK isoforms in mouse. The human and rat ROMK genes produce alternatively spliced transcripts all sharing a core exon. The most predominant isoforms in kidney are hROMK1-3(NM_000220, NM_153764 and NM_153765 respectively)[124]. In rat similarly rROMK1-3 isoforms are identified with rROMK1-2 being homologues of hROMK1-2 respectively, but rROMK3 (AF081367) having no homology to hROMK3. The exon-intron structure and alternative isoforms of mouse ROMK gene is less well defined. For the purpose of these studies we identified mouse homologs of hROMK1 (exon 3), hROMK2 (exon 1) and rROMK3 (132bp, 86% homology and appropriately positioned within the mouse ROMK gene locus to be a homolog of the unique alternate 5' exon (termed exon 2 above) in rROMK3). There was no clearly identifiable mouse homolog of hROMK3. Base-pair positions given in this figure refer to the mouse genome on contig NT_039472.3 which spans the ROMK locus (chromosome 9 at 33.359-32.386Mb build 33.1).

7.3.3 Expression of cHKA in response to changes in K^+-intake

Consistent with reports of upregulation of non-gastric H^+/K^+-ATPase in K^+-deficient states, cHKA expression was increased 4.1±0.7-fold [2.7-5.5] by LK (vs. NK: p=0.0002; Figure 7.5(a)). ISH analysis clearly showed upregulated medullary expression with LK, but usual analysis was impaired by high background. Normalising for this allowed an estimate of at least 2.0±0.2-fold [1.6-2.45] (p=0.001) increased medullary cHKA expression (LK vs. NK: Figure 7.5(b)), however the limitations because of high background mean this is likely to be an underestimate.

7.4 Discussion

As part of our K^+ study (outlined in Chapter 6) we looked at the expression of ROMK and cHKA, genes known to play key roles in renal K^+ handling, using isoform-specific real-time PCR assays and ISH. Very few tools reliably

differentiating isoforms of these genes are currently available especially when quantifying changes and examining distribution. Moreover, this study allows investigation of changes within kidney regions not easily accessible to micropuncture techniques (e.g. OMCD, deep distal nephron arcades/CNT), and avoids dangers of unequal RNA degradation, a concern associated with microdissection. Unfortunately, there are no good, well validated, cell-line models for several nephron segments, including OMCD and CNT. Thus, this study provided a unique opportunity to examine the distribution and gene expression responses of ROMK and cHKA to substantial variation in dietary K^+ intake.

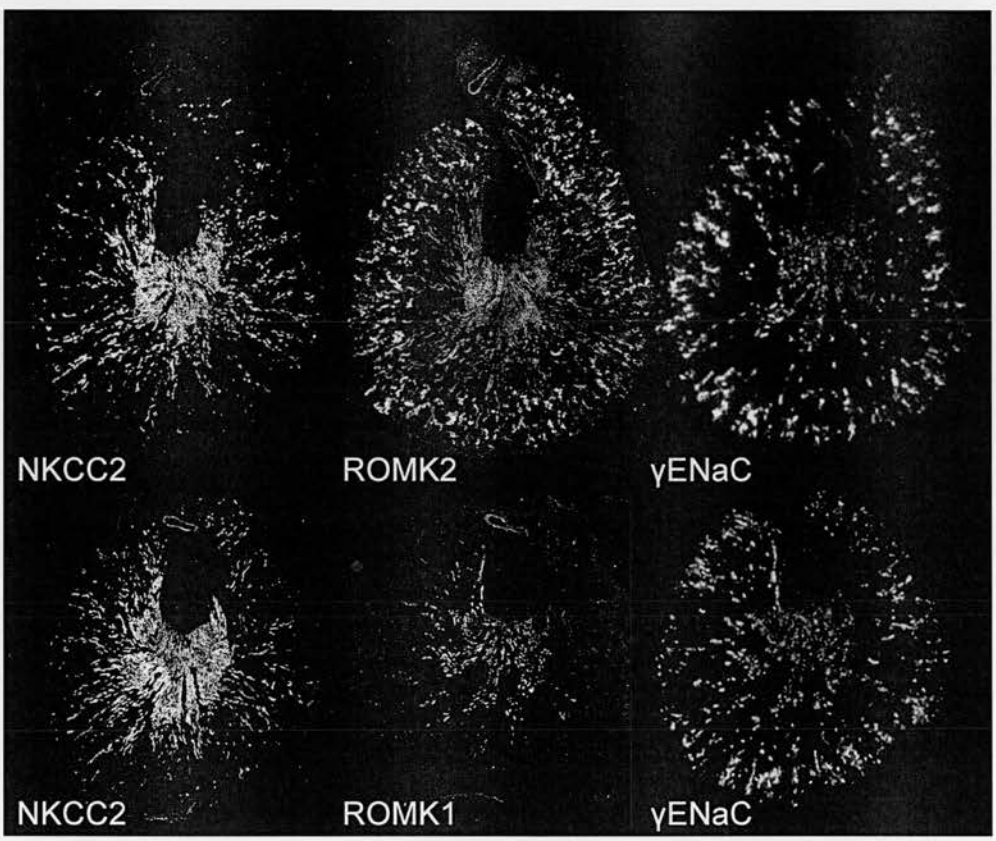

Figure 7.3: Distribution of gene expression for ROMK1 and ROMK2 in mouse. Top and bottom panels each show dark-field ISH studies for the genes indicated on 3 serial transverse kidney sections. The expression pattern of NKCC2 and γENaC in the sections flanking ROMK isoforms allows the distribution of TAL (NKCC2) and late DCT-CD (to inner stripe/inner medulla junction: γENaC) to be compared. ROMK1 clearly has CD expression matching γENaC but only weakly extending to cortex. ROMK2 matches NKCC2 but has greater spread of cortical expression than NKCC2 and γENaC combined as it is expressed in early DCT as well.

Contrary to reports that ROMK expression is regulated in parallel with K^+-intake, we were unable to detect any significant change in total ROMK expression across the treatment groups. Studies reporting changes in ROMK expression generally involve dissection of cortical and medullary regions, or even individual nephron segment dissection. Here we used a real-time PCR assay directed against a conserved ROMK region and examined ROMK expression at the whole kidney level. Alternatively, the discrepancy may be due to differences in experimental design, for example differences in precise dietary K^+ content or in the duration of treatment or possibly the animal model, with most previously reported studies having involved rats.

To investigate the contributions of individual isoforms we identified the mouse homologs of the major ROMK isoforms in kidney and examined their expression. By ISH we identified differential distributions for mouse ROMK1 and ROMK2 in keeping with the distributions described for the corresponding rat homologs. We found ROMK1 expression in OMCD with limited cortical (CCD) extension and ROMK2 expression in TAL and also in CCD. No clear expression of ROMK3 was detected. Although the transcript region probed by ISH for ROMK2 (exon1; Figure 7.2) is also present in ROMK3, we also used a real-time PCR assay specific for ROMK2 (transcripts with exon 1-core exon splicing) which detected abundant ROMK2, whilst a ROMK3-specific probe (exon 2) was unable to detect ROMK3 expression in mouse kidney by ISH. Intriguingly, a remarkable pattern of differential regulation of this key gene in K^+ balance emerged as we found that K^+-restriction increases ROMK1 but not ROMK2 transcripts and that conversely high K^+ diet increases ROMK2 but not ROMK1 transcripts. These changes were substantial and were determined by *both* real-time PCR and ISH. When merely examining total ROMK expression these key expression changes are not evident as the striking reciprocal variations in the expression level of these two conserved ROMK isoforms will tend to cancel one another out in terms of their contributions to total ROMK expression. Whilst other as yet unreported mouse ROMK isoforms may be contributing to ROMK-T, ROMK1 and ROMK2 are the major conserved isoforms recognised and we did not detect mouse ROMK3 expression.

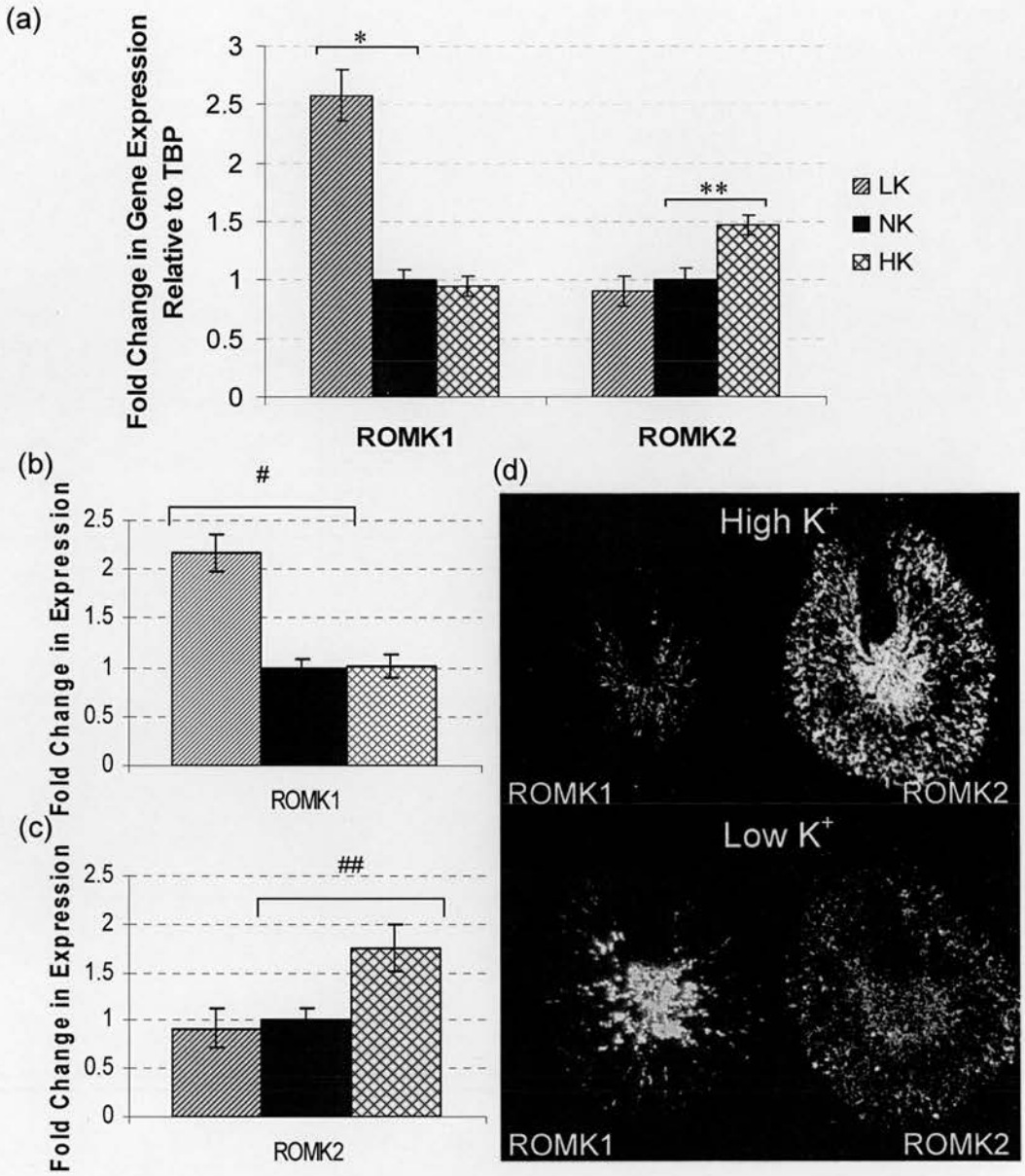

Figure 7.4: ROMK1 and ROMK2 expression in response to varied K^+ intake. ROMK1 and 2 regulation by K^+ diet examined by (a) isoform-specific real-time PCR assays distinguishing ROMK1 and ROMK2 and (b and c) ISH (n=6). There is a striking reciprocal regulation of these isoforms, with ROMK1 upregulation by low K^+ and ROMK2 upregulation by high K^+. (d)Dark-field ISH studies for ROMK1 and 2 gene expression illustrating this differential regulation and greater extent of ROMK1 expression in renal cortex with chronic low K^+ diet. *p=0.0002; **p=0.008; #p=0.0001; ##p=0.01.

Our findings identify that ROMK2 expression fits with an important role in conventionally described regulation of K^+-secretion: it is upregulated with HK and strongly expressed where electrogenic (ENaC) Na^+ transport is greatest (DCT2-CNT-ICT-CCD). The importance of ROMK2/ENaC co-expression in DCT2-CNT-

ICT is reflected in Na^+-K^+ balance not being significantly affected, even on altered diets, by knock-out of αENaC in CD[117]. In contrast, ROMK1 (20 additional N-terminal amino-acids and driven by a distinct promoter) is upregulated with LK, and expressed in OMCD-deeper CCD (Figure 7.4): segments normally regarded as having limited electrogenic Na^+-reabsorption which, going distally, are increasingly concerned with H^+-secretion and K^+-reabsorption rather than playing any significant role in regulation of Na^+ balance. Interestingly, one study[104] in rat reports, as we have found in mouse, that LK increased ROMK1 in medulla. The ROMK1 changes reported here would be missed looking at ROMK-T in cortex, or indeed in CCD with higher ROMK2 expression changing reciprocally. Increased ROMK1 in long-term K^+-deficiency could assist in acid-base balance through apical K^+-recycling and electroneutral H^+ secretion (Figure 7.6) when a "lumen-positive" charge gradient impedes alternative electrogenic routes (e.g. H^+-ATPase). LK diet induces a gastric-to-colonic H^+/K^+-ATPase isoform switch with upregulation of the latter (Figure 7.6) reported in principal cells of OMCD (as well as intercalated cells) with lesser changes in CCD[25]. LK diet thus appears to coordinate ROMK and H^+/K^+-ATPase isoform switching. To understand the potential significance of this co-regulation it is useful to consider the cytoplasmic face of active H^+/K^+-ATPase, where the pH and ADP/ATP ratio will rise with increasing H^+/K^+-ATPase activity; both these changes are well known activators of adjacent ROMK, perhaps especially if coupled to an ABC protein (e.g. CFTR)[47;74]. Such coupling may ensure ROMK1 K^+-secretion is effectively gated to occur when the H^+/K^+-ATPase pump is active. So ROMK1 thereby provides K^+ efflux, in effect recycling K^+ for H^+/K^+-ATPase to use in an efficient coupling induced when tubular K^+ will be deficient and the need for H^+ secretion continues, particularly facilitating excretion of NH_4^+, production of which is also induced in K^+ deficiency.

It could be argued that an increase in ROMK1 expression on LK diet as we have found may not necessarily imply a higher activity of the luminal K conductance in the OMCD. ROMK channels are believed to be tetrameric (possibly forming homo and/or heterotetramers)[47]. It is possible that a change in the ratio ROMK1/ROMKX could result in a conductance with modified activity and regulation. However,

ROMK1 is the only ROMK isoform expressed in OMCD and the upregulation reported here by both real-time PCR and ISH is substantial and sustained over a long period. We think it is unlikely that such gene expression regulation would not have important implications on a functional level, especially when there is some indication these changes could be conserved in evolution[104].

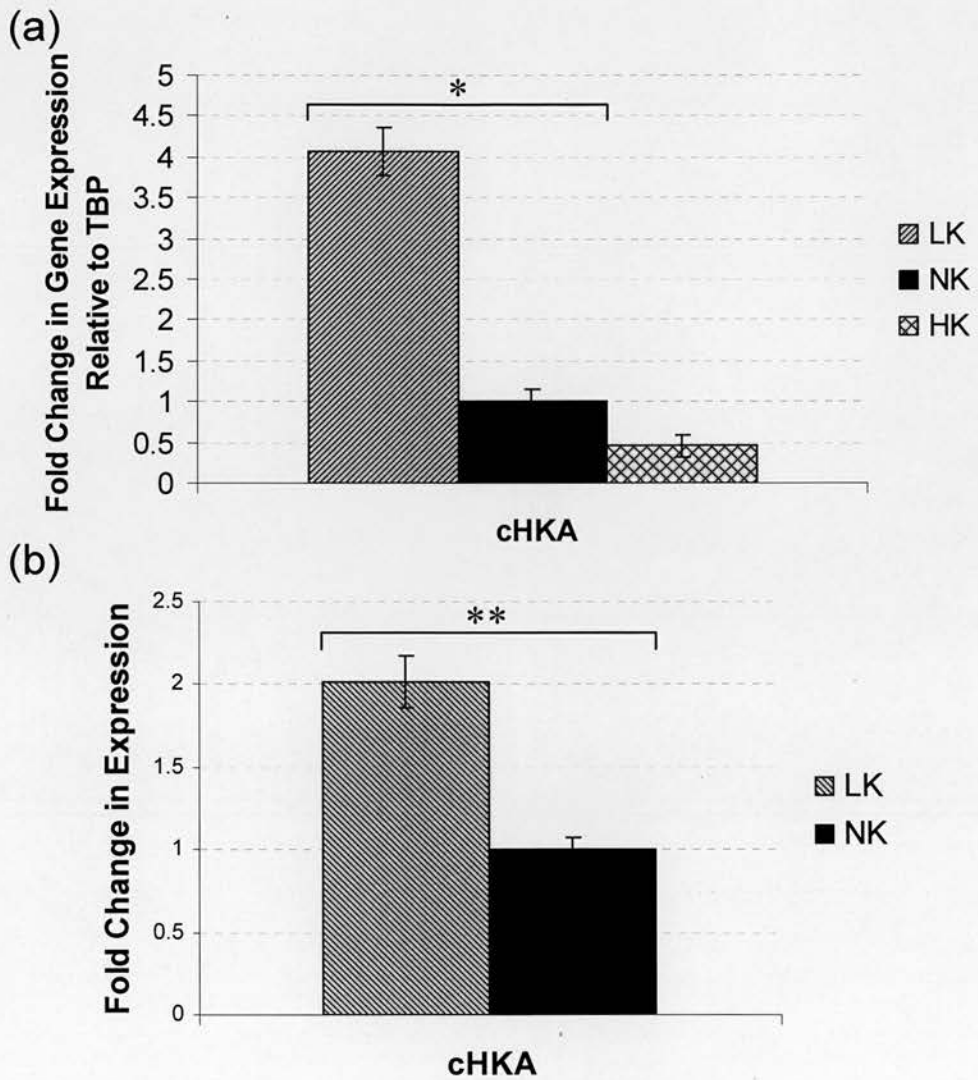

Figure 7.5: cHKA expression in response to varied K^+ intake. cHKA reabsorbs K^+ from renal tubular filtrate in exchange for H^+. A striking, upregulation of cHKA was observed by real-time PCR (4.1±0.7-fold [2.7-5.5]; n=6) and (b) by ISH (2.0±0.2-fold [1.6-2.45]; **n=4**) on LK (vs. NK) diet. Background levels were high in this ISH study, meaning expression was difficult to visualise and so images are not shown. Also as a consequence of high background, values quoted are a conservative estimate and may underestimate true expression changes. *p=0.0002; **p=0.001.

Control of ROMK1 channel numbers and their apical trafficking represent two separate levels of regulation. When co-expressed with active H^+/K^+-ATPase the regulated withdrawal of ROMK1 from the apical membrane would increase K^+-reabsorption but may diminish H^+-secretion. There has been great progress in understanding ROMK trafficking[47]. With no ROMK isoform-specific antibodies or knockouts, *in vivo* studies in CD, which have favoured CCD, usually reflect segment-specific ROMK (i.e. CD which expresses ROMK2 and ROMK1). OMCD is a relative "blind-spot" being difficult to study *in vivo* and without good OMCD cell-lines. The pathways regulating ROMK export-retrieval in OMCD may involve:- protein kinase A-export[79;89;158] (e.g. vasopressin-driven); tyrosine kinase-import[69;96;144] (e.g. driven via free radicals or medullary tonicity-EphA2) and ROMK1-specific effects via a PKC site at Serine-4[68]. These signalling pathways may thereby have important influence on K^+ conservation and acid-base balance through effects on ROMK1 conductance in K^+ deficiency. Thus, for example, it is well known vasopressin is required for efficient conservation of K^+ and lack of vasopressin leads, for several reasons, to a K^+-wasting state.

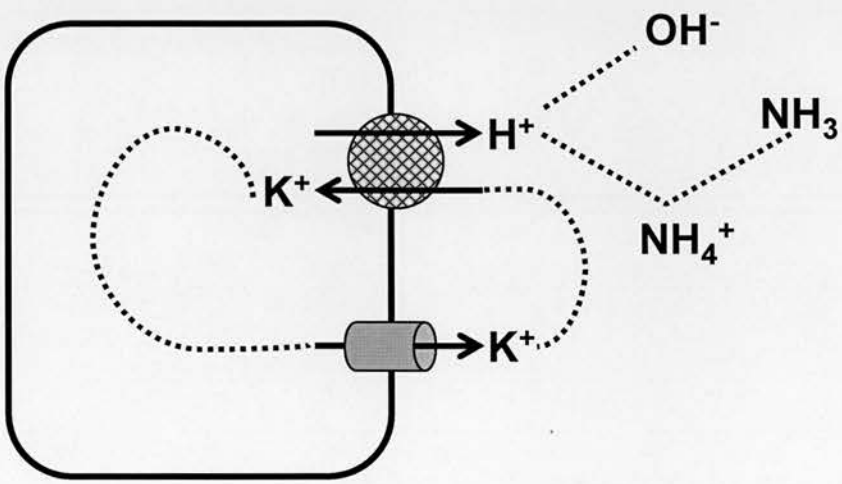

Figure 7.6: Schematic depiction of potential ROMK1 function. An upregulation of ROMK1 in a K^+-deficient environment as observed in this study could facilitate apical K^+ recycling to allow the efficient electroneutral secretion of H^+ ions via the H^+/K^+-ATPase pump.

This work uncovers features suggesting the ROMK gene is precisely regulated in an isoform- and nephron segment-specific manner. This could have important

implications for aspects of our understanding of K^+ regulation and the role of ROMK isoforms. The changes shown are substantial, chronically sustained over many days and will be missed by tools not discriminating between ROMK isoforms. Whilst one assessment concludes knockout of neither H^+/K^+-ATPase (colonic or gastric) significantly impairs renal K^+ conservation (although $cHKA^{-/-}$ mice are hypokalaemic) no assessment has examined the role of cHKA in K^+/acid-base balance across the water loaded-dehydration spectrum nor in the maladaptive perpetuation of alkalosis often seen in hypokalaemia. Clearly these findings merit further investigation and may couple to the necessary changes in H^+-secretion required when NH_3/NH_4^+ production is upregulated in hypokalaemia[134].

Chapter 8 Differentiating the roles of dietary K^+ intake and aldosterone.

8.1 Introduction

In health chronic K^+ balance is tightly regulated and remains within normal limits due to appropriate adjustment in renal handling so average K^+ loss is matched to intake. K^+ intake and circulating aldosterone play major roles in renal K^+ handling and K^+ balance. These two factors are not mutually exclusive as part of the response to K^+ load is mediated by changes in plasma aldosterone. Increased aldosterone secretion from the adrenal gland stimulates both basolateral Na^+/K^+-ATPase and apical Na^+ channels, promoting K^+ secretion[111]. This occurs mainly through augmentation of the electrochemical driving force for K^+ exit across the apical membrane. However, aldosterone-independent mechanisms are also involved in K^+ secretion. Hyperkalaemia reduces fluid and Na^+ reabsorption, thereby increasing distal fluid and Na^+ delivery and promoting K^+ secretion in the CNT and CCD[15;40]. As described in Chapter 7, K^+ loading also increases K^+ secretion through induction of ROMK. More recent evidence suggests a potential role for the maxi-K^+ (BK) channel which mediates flow-dependent K^+ secretion in CCD[150] and is activated by high dietary K^+[101], but this remains to be clarified.

The studies described in chapters 6 and 7 of this thesis, show regulation of expression within the WNK pathway and of ROMK isoforms in response to chronic changes in dietary K^+ intake. However, as aldosterone action is inextricably linked to K^+ homeostasis, it is difficult to assess if the changes seen in these studies are a direct effect of dietary K^+ intake, or if they are, even partially, indirect effects occurring through stimulation of aldosterone secretion. To resolve this issue we designed a study to attempt to differentiate between these two modes of regulation. In this study we measured the direct effects of dietary K^+ on gene expression by challenging mice with varied dietary K^+ intake while maintaining plasma aldosterone constant. We also measured aldosterone induced gene expression changes by varying aldosterone in mice maintained on the same normal K^+ dietary intake.

8.2 Materials and Methods

8.2.1 Animal Treatment

Groups of adult male C57BL/6J mice (n=5-7) were segregated into groups, housed in mouse metabolic cages and fed a normal K^+ diet. Following two days acclimatization, bilateral Adx operations were performed on all mice under general anaesthesia (day 0). Alzet® Mini-Osmotic Pumps (MP (Model 2004); preloaded with aldosterone (at various doses) and dexamethasone (sufficient to deliver 50µg/kg/d) were implanted subcutaneously to facilitate corticosteroid replacement. Groups were given specific K^+ diets in combination with corticosteroid replacement as outlined in Table 8.1. Treatments lasted 2 weeks, commencing from the day of surgery, with regular monitoring of food and water intake and bodyweight. 24hr urine collections were made on the final two days of treatment to allow volume and electrolyte composition measurements.

Table 8.1: Experimental groups in the dietary K^+ and aldosterone study.

Group	Description	MP Infusion*	Delivery rate	Diet
CTRL	Control	Dexamethasone Aldosterone	50 µg/kg/d 15 µg/kg/d	Normal (0.4%)K^+
LK	Low K^+	Dexamethasone Aldosterone	50 µg/kg/d 15 µg/kg/d	Low (0.009%)K^+
HK	High K^+	Dexamethasone Aldosterone	50 µg/kg/d 15 µg/kg/d	High KCl (3.8%)K^+
LA	Low Aldo	Dexamethasone	50 µg/kg/d	Normal (0.4%)K^+
HA	High Aldo	Dexamethasone Aldosterone	50 µg/kg/d 150 µg/kg/d	Normal (0.4%)K^+

*Vehicle: DMSO:Polyethylene Glycol (1:1)

8.3 Results

Mice were adrenalectomised and given group-specific treatments for 2 weeks, either varying dietary K^+-intake (LK/CTRL/HK) while holding plasma aldosterone constant via MP infusion (15 µg/kg/d), or the opposite, varying plasma aldosterone (0, 15, or 150 µg/kg/d) and holding dietary K^+-intake constant (normal K^+). All mice

were given dexamethasone infusions (50 μg/kg/d) via MP to replace glucocorticoid following Adx (Table 8.1).

8.3.1 Bodyweight, Food Intake and Fluid Balance

There was no significant difference in bodyweight between the groups throughout the experiment (Table 8.2). In the initial stages of treatment (day 0-2), a dip in food and water intake was observed immediately following Adx and MP implant surgery (Figure 8.1(a) and (b)). The animals recovered quickly and there was no significant difference in food intake across the treatment groups, throughout the experiment.

Table 8.2: Metabolic measurements in K^+/Aldo Study.

	CTRL	Low K	High K	Low Aldo	High Aldo
Initial Bodyweight (g)	25.6±0.7	26.0±1.1	24.7±1.0	25.5±0.6	25.9±0.6
Final Bodyweight (g)	26.0±0.6	25.1±1.0	24.9±0.8	24.8±0.4	25.0±0.6
Plasma K^+ (mM)	3.6±0.2	3.0±0.1	3.9±0.1	5.8±0.6	2.8±0.3
Plasma Na^+ (mM)	147.0±0.5	147.7±1.5	147.4±3.0	138.8±0.8	148.0±2.5
Plasma Cl^- (mM)	110.6± 1.2	105.2±1.4	111.8±1.8	111.0±2.5	104.8±1.4
Plasma Creatinine (μM)	22.0±1.3	22.7±1.5	19.0±0.7	24.3±1.4	22.0±0.8
Aldosterone (pmol/L)	1147.2±193.8	1366.7±366.8	1476.4±171.7	86.1±22.2	12469.7±2698.6
Renin Activity (ng/ml/h)	3.3±0.6	6.1±1.1	4.7±1.3	9.3±3.9	2.7±0.8
Corticosterone (nmol/L)	39.4±6.3	45.3±9.7	36.7±16.9	41.3±8.8	20.7±2.9

During the experiment, the LK group developed a higher fluid intake (Figure 8.1(b)) compared to the CTRL group, reaching significance on day 5 ($p<0.05$; $ANOVA_{LSD}$) and remaining significantly higher until day 13 ($p<0.04$; $ANOVA_{LSD}$), with fluid intake slightly lower in all groups on day 14. The HA group also developed a higher

fluid intake (Figure 8.1(b)) compared to the CTRL group, reaching significance on day 5 ($p<0.003$), remaining consistently higher for the rest of the experiment. The HK group also showed a modest trend towards higher fluid intake but this only reached significance compared to the CTRL group on day 4 ($p<0.05$; $ANOVA_{LSD}$), day 5 ($p<0.05$; $ANOVA_{LSD}$), and day 9 ($p<0.05$). Fluid intake in the LA group was not significantly different from the CTRL group throughout the experiment.

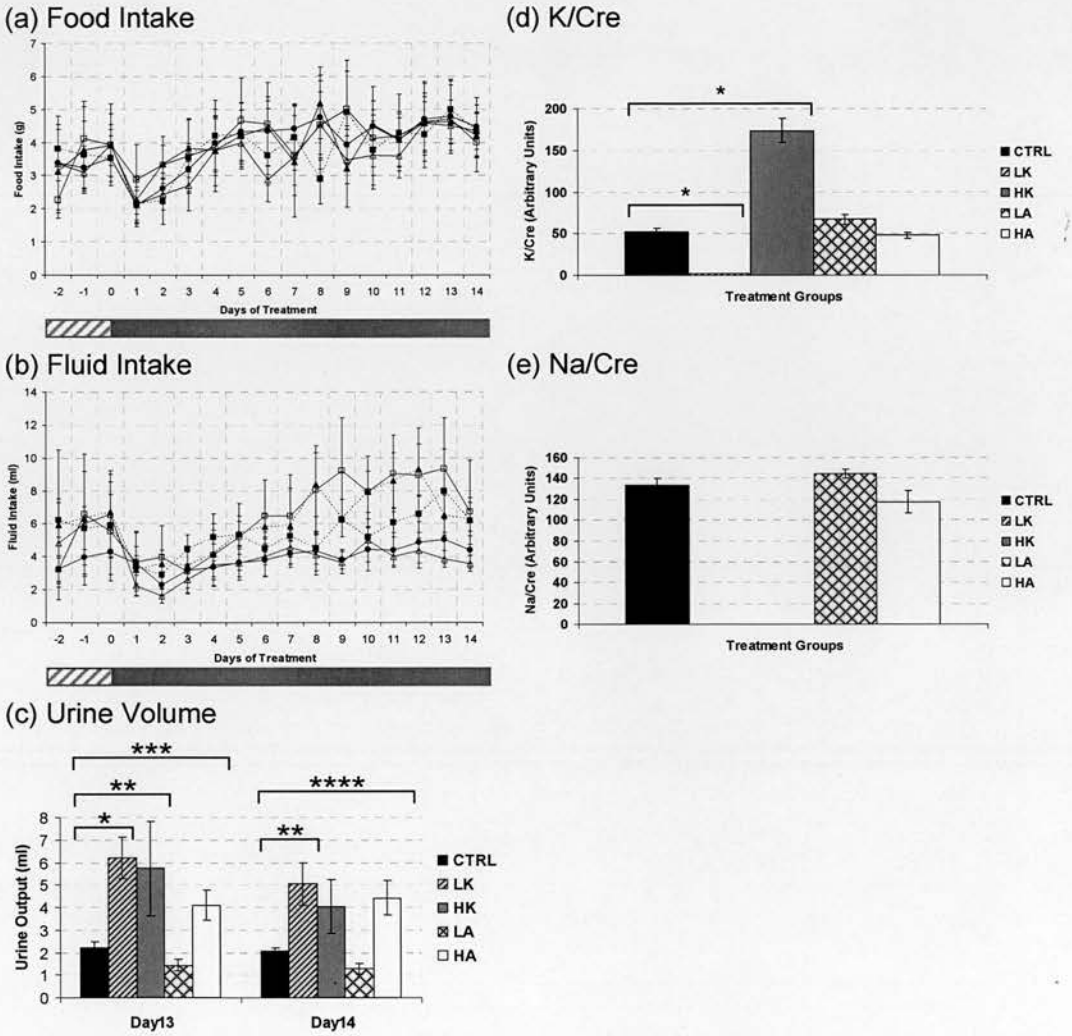

Figure 8.1: Effect of combined dietary K^+ intake and aldosterone challenge on metabolic measurements. Mice were treated (as outlined in Table 8.1) for 14 days, and daily measurements of (a) food and (b) fluid intake. Urine output over 24hrs (c) was recorded on the final two days of treatment. Urinary electrolyte excretion was measured over the final two days of treatment. The mean values were taken and expressed as a ratio of creatinine excretion (K/Cre, Na/Cre: d-e).

Urine collections (24hr) were made on the last two days of treatment (day 13 and 14). Volume measurements (Figure 8.1(c)) revealed increased urine output in the HA group on both days (HA vs. CTRL: 4.1±0.7 ml vs. 2.2±0.3 ml respectively, $p<0.005$ on day 13; 4.4±0.8 ml vs. 2.1±0.2 ml respectively, $p<0.002$ on day 14), consistent with a high fluid intake. Similarly, the LK group also had increased urine output compared to the CTRL group on both days, but this barely reached significance (6.2±0.9 ml, $p<0.03$ ($ANOVA_{LSD}$) and 5.1±0.9 ml, $p<0.05$ on days 13 and 14, respectively). There was also a significant increase in urine output with HK on day 13 (5.7±2.1 ml, $p<0.05$), but there was no significant difference compared to the CTRL group on day 14. Urine output in the LA group was not significantly different from the CTRL group.

8.3.2 Urinary Electrolytes

Urine K^+ and Na^+ concentrations were measured in samples collected on the final two days of treatment (Figure 8.1(d-e)). The mean measurements over the two days were taken and expressed as a ratio over creatinine. K/Cre was significantly lower in the LK group (96.1±0.37% decrease, $p<0.0002$) and significantly higher in the HK group (3.3±0.35-fold increase, $p<0.0002$) compared to the CTRL group. There were no differences in K/Cre or Na/Cre in the LA or HA groups compared to the CTRL group. Unfortunately, Na/Cre measurements were unavailable for the LK and HK groups[†].

8.3.3 Plasma Measurements

LA induced a significant increase in plasma K^+ (LA vs. CTRL: 5.8±0.6 mmol/L vs. 3.6±0.2 mmol/L respectively, $p<0.002$), accompanied by a decrease in plasma Na^+ (LA vs. CTRL: 138.8±0.8 mmol/L vs. 147±0.5 mmol/L respectively, $p<0.009$; Table 8.2). HA induced a significant decrease in plasma Cl^- (HA vs. CTRL: 104.8±1.4 vs. 110.6±1.2 respectively, $p<0.04$). The LK group also showed a significant but small

[†] Certain electrolyte measurements are unavailable as they were beyond the accurate range of the assaying technique. Some of these samples may be diluted and re-assayed. However, time constraints toward the end of the PhD limited this option.

decrease in plasma Cl^- (105.2±1.4, $p<0.02$) compared to the CTRL group, but was still within the normal range. There were no significant changes in plasma creatinine.

As expected following infusion treatments, plasma aldosterone was significantly elevated in the HA group (12,469±2698.6 pmol/L, $p<0.0002$) and reduced (although not significantly; 86.1±22.2 pmol/L) in the LA group compared to the CTRL group (1147.2±193.8 pmol/L). There was no significant difference in plasma renin activity, plasma renin concentration, or plasma corticosterone compared to the CTRL group. Very low level plasma corticosterone (<104 nmol/L) was detected in all groups despite Adx.

8.3.4 WNK Pathway Expression

Real-time PCR analysis indicated WNK1-S expression was downregulated by 33±10.7% [11.6-53.6] with LA ($p=0.03$; $ANOVA_{LSD}$), as was WNK1-T expression (20±8.9% [2.7-37.5] decrease, $p=0.05$; $ANOVA_{LSD}$) compared to the CTRL group (Figure 8.2). WNK1-S expression also showed a trend towards downregulation by 27±11% [5.7-48.9] with LK compared to HK, however this change did not reach significance. WNK4 was upregulated by 34±9% [16.5-52.1] ($p=0.04$; $ANOVA_{LSD}$) across the dietary K^+ spectrum. A downward trend in WNK4 expression was also seen with LA compared to the CTRL group, but this small change did not reach significance. HA had no significant effect on WNK expression in this study and WNK1-L expression was unchanged across all treatment groups.

8.3.5 ROMK and cHKA Expression

ROMK-T expression was unchanged across the treatment groups. ROMK2 expression was downregulated by 28±8.5% [11.7-44.9] with LK ($p<0.05$; $ANOVA_{LSD}$) compared to the CTRL group (Figure 8.3(a)), but was unchanged with HK. In contrast, real-time PCR showed a 2.4±0.3-fold upregulation in ROMK1 expression by LK ($p<0.0002$) compared to the CTRL group (2.6±0.4-fold upregulation compared to HK, $p<0.0002$). ROMK1 expression was also upregulated by 26.7±12.6% [1.9-51.3] with LA ($p<0.04$) compared to the CTRL group.

cHKA expression (Figure 8.3(b)) was upregulated by 97±32.4% [33.6-160.7] as dietary K^+ content decreased from HK to LK ($p<0.003$). Similarly cHKA expression was upregulated by 62.6±23.7% [16-109.1] as aldosterone level decreased from HA to LA ($p<0.09$).

8.4 Discussion

In order to achieve K^+ balance secretion must equal intake even when intake increases several fold. This balance between urinary excretion and dietary intake underscores the importance of the kidneys in maintaining K^+ homeostasis. An increase in dietary K^+ intake promotes aldosterone secretion. However, both aldosterone-dependent and -independent pathways contribute to stimulation of K^+ secretion to balance the greater K^+ intake. This *in vivo* study was designed to differentiate between the effects of dietary K^+ and aldosterone on the expression of the WNK pathway, and a number of genes likely linked to it. Mice were given treatments either varying dietary K^+-intake while holding plasma aldosterone constant (via Adx and MP infusion), or the opposite, varying plasma aldosterone while holding dietary K^+-intake constant.

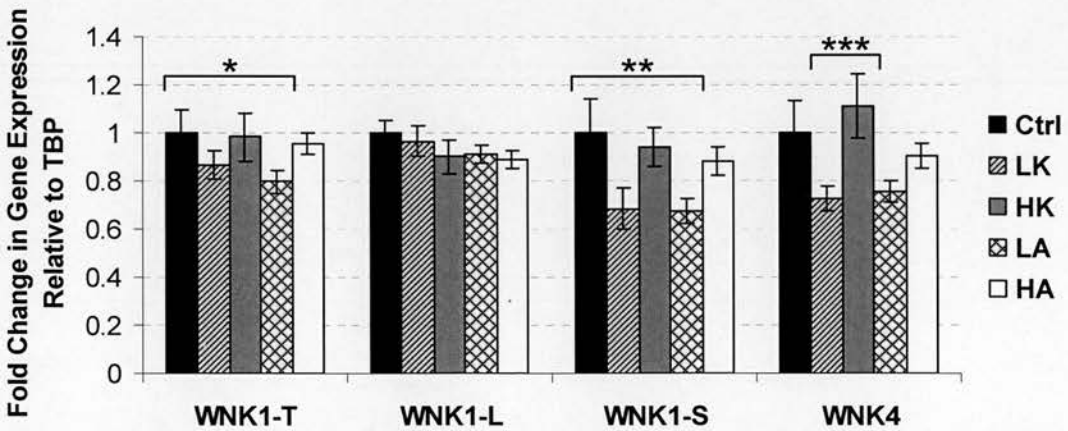

Figure 8.2: WNK expression in response to varied K^+ intake and aldosterone challenge. Real-time PCR reveals WNK1-S and WNK1-T expression are significantly downregulated with LA compared to CTRL. WNK4 expression changes significantly across the dietary K^+ spectrum. Downregulation of WNK1-S with LK (vs. HK) and WNK4 with LA (vs. CTRL) were also suggested, but these changes did not reach significance. No significant changes were observed in WNK1-L expression across the experimental groups.
*$p<0.05$ ($ANOVA_{LSD}$), **$p<0.03$ ($ANOVA_{LSD}$), ***$p<0.04$ ($ANOVA_{LSD}$)

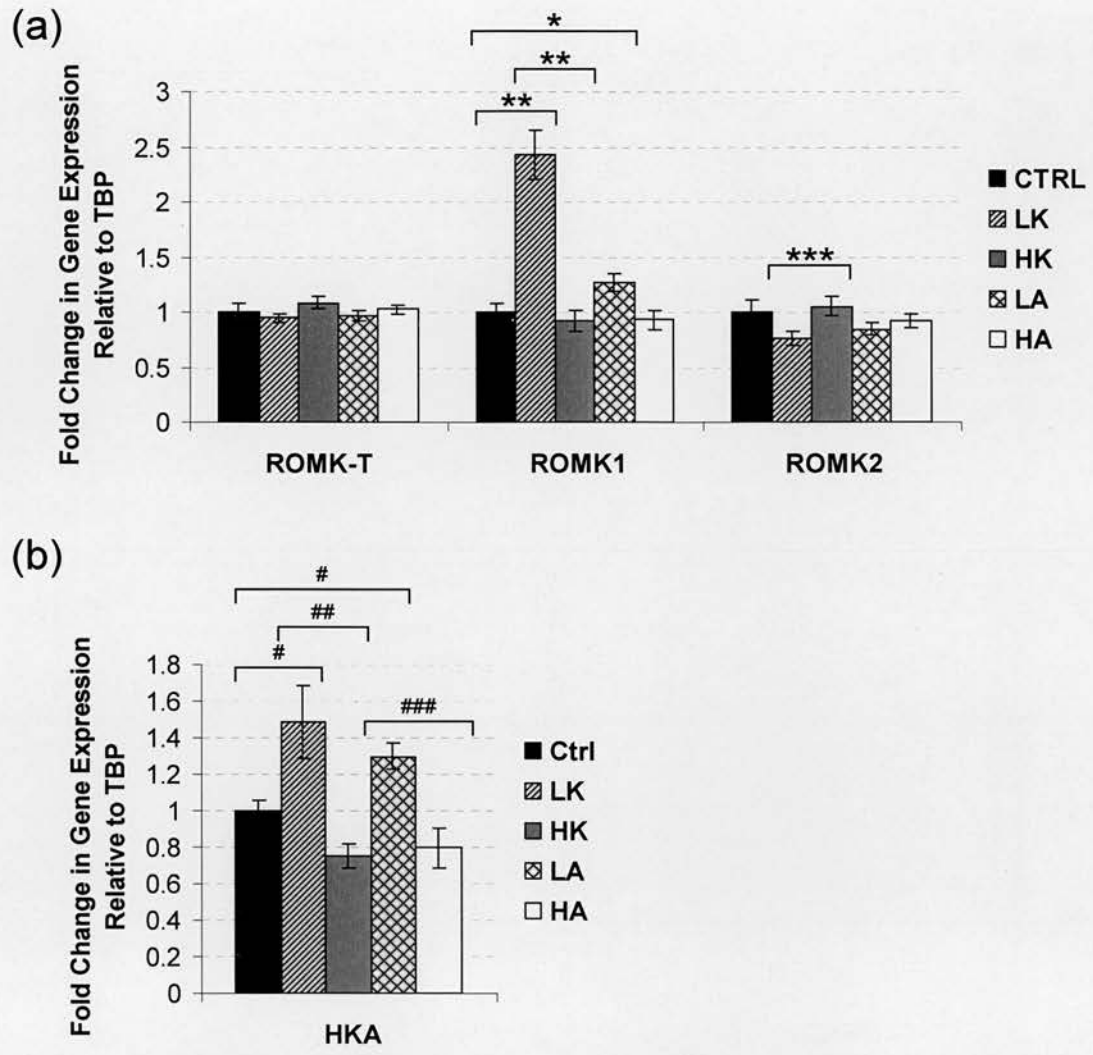

Figure 8.3: ROMK and cHKA expression in response to varied K^+ intake and aldosterone challenge. (a) ROMK1 was strikingly upregulated with LK and modestly upregulated with LA. ROMK2 expression was downregulated with LK compared to CTRL but was unchanged with HK. Aldosterone had no effect on ROMK2 expression. No significant changes were observed in ROMK-T expression across the experimental groups. (b) Upregulation of cHKA was observed with both LK and LA.
*p<0.04 and **p<0.0002, ***p<0.05 ($ANOVA_{LSD}$)
#p<0.02, ##p<0.003, ###p<0.09

Real-time PCR analysis of WNK expression reveals similar findings to our previous study (Chapter 6). However, in this study expression in the control group has shifted, so that basal expression is now closer to that seen previously with high K^+. This may be an effect of extended duration of treatment (four days longer), anaesthetic, Adx, or dexamethasone treatment. In fact a recent *in vitro* study[106] demonstrates increased WNK1-S expression with dexamethasone treatment. Nonetheless, if the overall

expression profile across the full dietary K^+ range, from LK-CTRL-HK, is considered, the changes seen are compatible, with WNK1-S and WNK4 expression increasing from LK to HK. This WNK1-S change, however, does not reach significance. A similar trend in WNK1-S expression is seen from low to high aldosterone. Again, the CTRL group seems to set a higher baseline in this study with a significant decrease in WNK1-S expression seen in the LA group, whereas in the previous study WNK1-S increased from control to high aldosterone.

Supporting our findings in the previous study (Chapter 7), ROMK1 was strikingly upregulated with LK. ROMK2 expression was downregulated with LK compared to the CTRL group but was unchanged with HK. This result differs slightly from the previous study where ROMK2 expression was upregulated with high K^+ compared to normal K^+, but unchanged with low K^+. Again, the basal expression level set by the control group is higher. However, the same reciprocal trend is present, with ROMK2 expression rising from LK to HK, while ROMK1 expression rises from HK to LK. cHKA expression was also upregulated with LK. This is consistent with our findings in Chapter 8 and together with ROMK1 upregulation supports our theory that these two genes may function side-by-side to promote H^+ and NH_4^+ secretion, while conserving K^+ in K^+-deficient states.

Modest upregulation in ROMK1 expression was seen with LA. ROMK1 is most abundant in OMCD, with expression barely reaching the cortex on a normal K^+ diet. A study by Wald *et al.*[140] examining ROMK expression but not differentiating between isoforms, reported that Adx decreased ROMK mRNA abundance in cortex but increased transcript abundance in the medulla. K^+-deficiency combined with Adx in the same study reduced ROMK mRNA to control levels, suggesting that the hyperkalaemia associated with Adx was the cause for the increased ROMK expression in medulla. This upregulation of medullary ROMK could be due at least in part to increased ROMK1 in OMCD, particularly since no change in ROMK2 expression was observed with LA in the present study. Aldosterone administration by MP to adrenal intact rats has been shown to increase ROMK2 expression in whole kidney[8], however we saw no change in ROMK2 expression with HA in this study.

This may be due to differences in study design (e.g. Adx with dexamethasone (50 μg/kg/day) and aldosterone infusion (150μg/kg/day) versus adrenal intact plus aldosterone infusion (20 μg/kg/day)), technique (real-time PCR versus competitive PCR) or this may be a species issue (mouse versus rat). Upregulation of cHKA was also observed with LA, supporting the theory that cHKA and ROMK1 expression may be coupled.

Clearly there are discrepancies between these findings and the changes observed in the studies described in Chapters 6 and 7. As suggested above, these discrepancies may be due to differences in experimental protocol. In an attempt to understand the variation between the two studies, and also to try to discriminate the roles of dietary K^+ intake and aldosterone, linear regression analysis was performed, allowing case-wise examination of continuous variables in individual mice (or cages). Analysis across all the genes examined in this study and also those described in Chapters 6 and 7, consistently revealed that K^+ was the most significant regulator of gene expression (Table 8.3). Urinary K/Cre was the better indicator of K^+ regulation, with K^+ intake also an important index.

Table 8.3: Regression analysis of gene expression.

	Study	K^+ Intake	Urinary K/Cre	Aldosterone
WNK1-S	Dietary K^+	+ 75% (p<0.0004)	+ 75% (p<0.0004)	+ 30% (p=0.266; NS)
	K^+/Aldo	+ 15% (p=0.433; NS) *[+ 33% (p=0.119; NS, minus CTRL]*	+ 27% (p=0.134; NS) *[+ 51% (p<0.02), minus CTRL]*	+ 4.4% (p=0.812; NS) *[+ 16.2% (p=0.448; NS), minus CTRL]*
WNK4	Dietary K^+	+ 53% (p<0.03)	+ 56% (p<0.02)	+ 25% (p=0.346; NS)
	K^+/Aldo	+ 31% (p=0.088; NS)	+ 47% (p<0.05)	+ 3.2% (p=0.863; NS)
ROMK1	Dietary K^+	- 51% (p<0.03)	- 54% (p<0.02)	- 37% (p=0.159; NS)
	K^+/Aldo	- 34% (p=0.065; NS)	- 54% (p<0.002)	- 17% (p=0.35; NS)
ROMK2	Dietary K^+	+ 66% (p<0.003)	+ 69% (p<0.002)	+ 53% (p<0.04)
	K^+/Aldo	+ 27% (p=0.143; NS)	+ 41% (p<0.02)	- 6% (p=0.731; NS)
cHKA	Dietary K^+	- 61% (p<0.008)	- 64% (p<0.005)	- 42% (p=0.109; NS)
	K^+/Aldo	- 38% (p<0.04)	-46% (p<0.009)	- 27% (p=0.145; NS)

(NS, non-significant)

ROMK1 and HKA expression negatively correlated with K^+ and were not associated with aldosterone level in either study (Table 8.3). ROMK2 expression also correlated with K^+ in the original dietary K^+ study, but aldosterone also had a significant effect. The K^+ effect was weaker but still significant in the more recent study, whereas the correlation with aldosterone disappeared. WNK4 expression was not significantly affected by aldosterone level but correlated with K^+ across both studies. WNK1-S expression strongly correlated with K^+ in the original study but this effect was not clearly apparent in the study described in this chapter. As suggested earlier, we wondered if the CTRL group was causing this discrepancy, so regression analysis was repeated without this group. This revealed a significant correlation between WNK1-S expression and K^+.

This analysis indicates very little aldosterone regulation of the genes under investigation in these experiments. In fact the only gene showing a significant correlation with aldosterone is ROMK2 in the original dietary K^+ study. This effect is not unexpected as ROMK2 is an effector of aldosterone signalling albeit indirectly via ENaC regulation. However, this aldosterone effect was not seen in the K^+/aldosterone study, possibly a consequence of the aldosterone dose given or perhaps dexamethasone treatment. Thus, although further work is required to fully discriminate between dietary K^+ and aldosterone regulation, the evidence presented here strongly suggests that K^+ plays a more dominant role.

Chapter 9 Discussion.

In 2001, mutations in WNK1 and WNK4 were linked to Gordon syndrome[148], implicating these novel ser/thr kinases in the regulation of electrolyte balance and BP. As mutations in WNK1 and WNK4 cause a broadly similar phenotype (hypertension and hyperkalaemia with normal glomerular filtration), it seemed likely that these novel proteins function in a common WNK pathway. Beyond this, nothing was known of the function of WNK1 or WNK4 when the studies of this thesis began, with only limited information reported regarding their expression in human and rat[137;148;151]. The fundamental objective of this PhD was to contribute to our understanding of how WNK1 and WNK4 might function to regulate electrolyte balance and BP.

9.1 The predominant WNK1 isoform in kidney is not a kinase.

From an early stage, it was of great interest to us how intronic deletions in WNK1, a widely expressed gene, could cause an autosomal dominant disease, with a pathology seemingly targeting the kidney[43;92]. Identification and detailed expression analysis of the nature of an alternative, abundant short WNK1 transcript in kidney showed that rather than merely being a polyA-tail variant as originally suggested[18;137;148;151], this transcript is truncated at the 5'-end. In fact this predominant short kidney-specific WNK1 transcript (WNK1-S) actually completely lacks a kinase domain. Two months after our report describing WNK1-S expression[109], another independent study confirmed our findings, reporting an alternative promoter and an enhancer element upstream of the novel 5'-exon[24]. We and others have also identified additional WNK1 transcripts arising from a combination of alternative promoter usage[24] and splicing[24;109;137;148].

9.1.1 Impact of WNK1-S Discovery

The breakthrough that WNK1 gene transcription in kidney differed from elsewhere, and in kidney this WNK1 kinase gene was actually overwhelmingly expressing a kinase-deficient product, demanded a revision of ideas as to how mutations of this gene might cause autosomal dominant disease. At this time much of the research on WNK1 was directed towards defining upstream kinases and downstream targets for

this novel kinase[138;152;155]. The discovery of WNK1-S shifted the focus of WNK1 research and highlighted the possibility that the role of WNK1 at least in kidney may involve features beyond a simple kinase cascade. Studies exploring the physiological role of WNK1-S are still at the embryonic stage; however a specific disruption in the expression of this isoform in kidney may be the mechanism behind the seemingly kidney-restricted phenotype of Gordon syndrome despite the broad expression profile of WNK1. The original study linking WNK1 to Gordon syndrome reported increased WNK1 expression in patient leucocytes[148]. As the nature of WNK1-S was not known at this point, the technique used to quantify WNK1 expression did not differentiate between WNK1 isoforms. So it is currently unknown whether one or both isoforms are involved in this upregulation. Furthermore, WNK1 expression in leucocytes may not be representative of WNK1 expression in kidney, particularly as WNK1-S may not be expressed in leucocytes. Indeed, Northern blot analysis of leucocyte RNA revealed very little expression of either WNK1 isoform in the original study[148].

9.2 WNK Localisation

9.2.1 WNK1-L and WNK1-S have different distributions in kidney.

These studies also uncovered strikingly different renal distributions for WNK1-S and WNK1-L. Low level widespread expression of WNK1-L is seen throughout the kidney, whereas WNK1-S expression is highest in DCT-CNT (Figure 9.1). Thus, not only are these isoforms structurally and functionally distinct, but they are also differentially distributed. These studies localise WNK1-S to adjacent nephron segments known to play important roles in the regulation of electrolyte balance and BP (section 1.1.4), the very processes so clearly disrupted when WNK1 is mutated in Gordon syndrome. Thus, this further suggests that WNK1-S may be the key isoform affected by WNK1 mutations causing a $NaCl/K^+$ and H^+ imbalance and driving hypertension. Moreover, antibodies capable of differentiating between the different isoforms of WNK1 are not available, so the techniques employed in these studies are particularly informative. Indeed the antibody used in the original report describing WNK1 distribution in kidney[148] is directed against an epitope encoded by exon 12 which will limit detected WNK1 protein to a subset, as exon 12 is subject to

alternative splicing in many tissues (including kidney) in all species examined[109;137;148;151]. Also, contrary to our findings this study reports WNK1 expression in CCD and MCD (medullary collecting duct), segments of the nephron where we see very little WNK1 expression compared to DCT-CNT by ISH with multiple probes directed against different regions of WNK1.

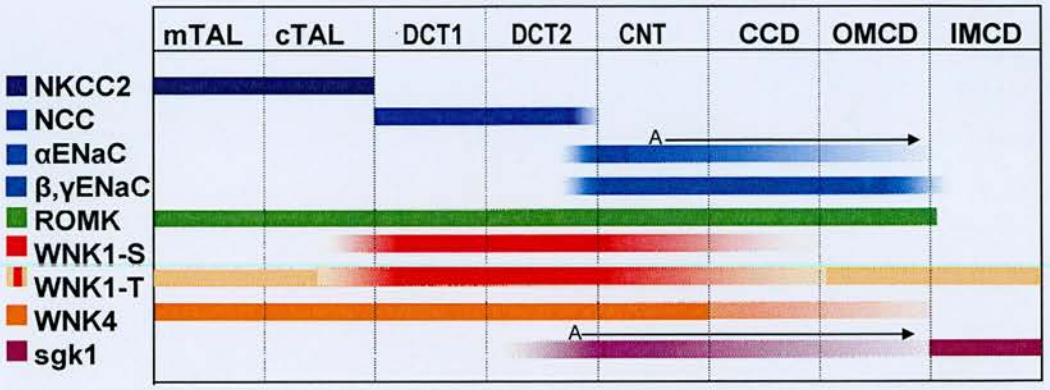

Figure 9.1: Distribution of gene expression of key genes involved in Na^+ and K^+ balance in distal nephron. For αENaC/SGK expression, arrows represent regulated expression by rising aldosterone (A).

9.2.2 Novel domains of WNK4 expression in TAL

Detailed localization studies, undertaken as part of this thesis, show that WNK4 is highly expressed in DCT-CNT, consistent with earlier findings[148], and supporting the possibility that WNK4 may interact with transporters such as NCC and ROMK in these nephron segments. However, contrary to reports by Wilson *et al.*, we found much lower WNK4 expression in CCD, with very limited detectable expression extending into OMCD (Figure 9.1). A substantial novel domain of WNK4 expression was also identified in TAL (including *macula densa*). This finding questions the physiological relevance of *in vitro* WNK4 interactions with transporters found exclusively in this nephron segment.

9.2.3 Impact of WNK localisation on functional evidence

Reports of *in vitro* interactions between WNK4 and/or WNK1 and a number of renal electrolyte transporters have been flooding into the literature implying a surprising diversity of possible regulatory roles of these genes in electrolyte balance (Table 1.3). In particular, WNK4 interactions with transporters expressed in nephron

segments ranging from proximal tubule (e.g. CFEX[52]) to more distal segments (e.g. NCC in DCT[149;161], ROMK in DCT2-CD[56], and NKCC1 in OMCD[52]) have been reported *in vitro,* as have effects on tight junction Claudin proteins, thereby also indicating the potential of affecting distal nephron paracellular transport[53;159]. However, the potential *in vivo* significance of these *in vitro* findings can only be extrapolated if WNK4 co-localises along the nephron with the transporter in question.

The discovery of substantial, previously unrecognized, WNK4 expression in TAL and *macula densa* may have a major impact on WNK4 research which is currently focused on more distal nephron segments (DCT-CD). This domain of WNK4 expression was missed by immunohistochemistry in the original study describing WNK4 expression in kidney[148]. The reason for this remains to be clarified but possibilities include shortcomings of the antisera perhaps because WNK4 protein in TAL has different properties to WNK4 in other nephron segments. The prospect WNK4 may regulate transport in TAL-DCT (including *macula densa*) is intriguing, as upregulated NaCl reabsorption here would be expected to drive hyperkalaemia, acidosis and low-renin hypertension: all features of Gordon syndrome.

9.2.3.1 Possible WNK4:ROMK interaction in TAL

WNK4 expressed in TAL may interact with ROMK which is also highly expressed in this segment, and interestingly ROMK here facilitates NaCl reabsorption (via NKCC2) and facilitates K^+ reabsorption (via lumen positive charge driving paracellular K^+ absorption), so overactivity here may resemble the Gordon's phenotype. A WNK4:ROMK interaction has been reported previously *in vitro*[56] but has only been considered in the context of the CCD, where ROMK acts simply to allow K^+ secretion and so inhibition of ROMK would result in K^+ retention. ROMK inhibition in TAL would prevent K^+ recycling in this nephron segment, potentially blocking NaCl reabsorption via NKCC2, resulting in increased distal Na^+ delivery. However, transgenic mice expressing a *human* Gordon syndrome mutant WNK4 (D564A) protein in TAL and DCT (at heterogeneous levels)[160] did not have a Gordon syndrome phenotype and ROMK localization appeared unaltered by co-

localised mutant WNK4. The basis for absence of Gordon syndrome features remains uncertain, but mutant WNK4 expression was transgenic cDNA-driven (via the promoter of the *human* CLCNkb chloride channel gene) rather than genomic, altering distribution (WNK4 localised to cytoplasm and not tight junctions in distal tubules and to apical membranes in TAL) and curtailing native potential for transcriptional diversity[160]. Thus this transgenic expression may have differed significantly from equivalent native expression with WNK4 Gordon syndrome mutations and this remains a likely explanation for the lack of phenotype in these mice about which no further reports have been published.

9.2.3.2 Regulation of cation-chloride cotransport by WNK:SPAK complex.

WNK4 is reported to interact *in vitro* with SPAK[35;113;114;139], another ser/thr kinase structurally related to WNKs and widely expressed in transporting epithelia. This kinase binds to several cation-chloride transporters, and is thought to be a scaffolding protein involved in MAPK signalling (WNK kinases are distant homologs of MAP kinases). This WNK4:SPAK complex regulates the activity of NKCC1 and KCC2 in *Xenopus* oocytes[35;36;113]. Our studies highlight that expression of important elements of the WNK pathway co-localise with two other key members of this cotransport family of key importance in NaCl reabsorption and BP control: NKCC2 (TAL) and NCC (DCT), targets for loop and thiazide diuretics, respectively. Moreover increasing activity of either will limit K^+ excretion (by lowering distal Na^+ delivery) whilst a decrease in their activity will promote diuresis, lower BP, and predispose to hypokalaemia (as is the case with use of these diuretics).

A report, by Vitari *et al.*, showed that WNK1 associates with SPAK, and that *both* WNK1 and WNK4 phosphorylate and activate SPAK/OSR1, leading to phosphorylation of NKCC1[139]. This is consistent with reports that both WNK1 and WNK4 contain putative SPAK binding motifs consisting of the consensus: R/K-F-x-V/I[20]. Moriguchi *et al.* also show evidence that WNK1 interacts with SPAK (in HEK293 cells) and report direct WNK1 phosphorylation of SPAK/OSR1. Additional evidence suggests that low Cl^- hypotonic stress increases WNK1 kinase activity, activating SPAK/OSR1 and inducing phosphorylation of NCC, indicating that a

WNK1:SPAK/OSR1 complex may mediate the hypotonic stress signalling pathway to NCC and possibly other cation-chloride-coupled transporters to regulate electrolyte balance[97]. NKCC2 is also subject to regulation by SPAK[97]. Thus, in addition to NKCC1 regulation, a WNK1/WNK4:SPAK complex may regulate NCC and NKCC2 in kidney.

9.2.3.2.1 WNK3 and SPAK

Furthermore, WNK3, a related member of the WNK kinase family, has recently been cloned[49] and shown to regulate a number of electrolyte transporters[23;54;66;116] including NKCC2 and NCC. Kinase-active WNK3 activates, while kinase-inactive WNK3 inhibits, NKCC2 and NCC in *Xenopus* oocytes (Figure 9.2), by altering their surface expression[116]. WNK3 is structurally related to WNK1 and WNK4, sharing homology across the kinase domain, autoinhibitory domain, an acidic region (site of WNK4 Gordon syndrome mutations), and coiled coil regions[49]. Unlike WNK1-S and WNK4, WNK3 is reportedly present in all nephron segments, with highest expression in the proximal convoluted tubule and TAL, and lower levels of expression in the DCT and CD[116]. Both WNK4 and WNK3 can regulate NCC, and so it is tempting to speculate that WNK4 may also regulate NKCC2 (Figure 9.2). The relative abundance of WNK3 compared to WNK4 and whether or not they are co-expressed in the same cells is currently unknown. Certainly, initial studies suggest levels of WNK3 expression are very low, detectable by RT-PCR but not Northern hybridisation[49].

9.2.3.3 WNK1 phosphorylates WNK4 relieving NCC inhibition.

Due to the recent discovery of WNK1-S and possibly the lack of an antibody specific to this isoform, the majority of WNK1 functional studies reported to date have focused on WNK1-L. WNK1-L was reported to suppress WNK4-mediated inhibition of NCC, thereby restoring cotransporter activity[161], and was shown to physically associate with WNK4 via their homologous N-terminal kinase domains. WNK4 has to be phosphorylated to suppress its inhibition of NCC and WNK1-L is capable of this WNK4 inhibition possibly facilitated by WNK1 tetramer formation[162]. The

kinase-deficient kidney-specific isoform, WNK1-S, would not be expected to inhibit WNK4 as kinase activity is required.

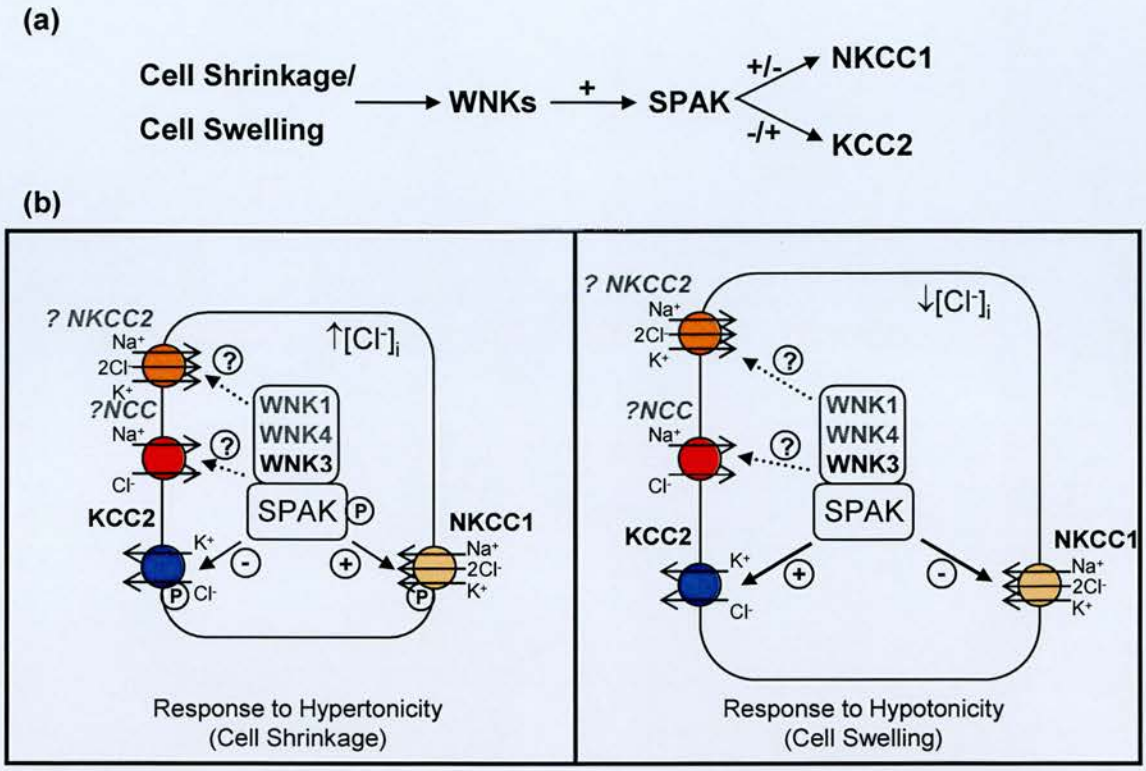

Figure 9.2: WNK kinases interact with SPAK. (a)Schematic depiction of the causal chain in WNK:SPAK interaction. (b)In response to cell shrinkage (hypertonic stress) WNK3 has been shown to interact with and activate SPAK, which phosphorylates both NKCC1 and KCC2, leading to their activation and deactivation, respectively. Cell swelling induces the opposite effect with deactivation of NKCC1 and activation of KCC2. WNK1 and WNK4 have also been shown to interact with SPAK but the effect of this interaction is not yet fully understood. We speculate that if may involve NCC and/or NKCC2, which have also been shown to interact with SPAK.

9.2.3.4 WNK1-L scaffold facilitates ENaC Regulation by SGK.

Two recent papers by Xu *et al.* report that WNK1-L positively regulates ENaC through SGK1[153;154]. ENaC β and γ subunits are subject to C-terminal PY motif ubiquitination which then leads to retrieval of the ubiquitin tagged ENaC channels from the cell surface. In kidney this is mediated by the ubiquitin ligase Nedd4-2 and this process is involved in regulation of cell surface ENaC channel density. Indeed when the β or γENaC C-terminal PY motifs are mutated this leads to impaired retrieval, increased ENaC conductance and the hypertensive disorder Liddle's syndrome (Table 1.1 and Figure 1.6).

It is known that phosphorylation of the ubiquitin E3 ligase Nedd4-2 by SGK1 reduces the interaction between Nedd4-2 and its substrates including ENaC, thus increasing ENaC surface expression and consequently increasing Na^+ current. Na^+ transport via ENaC is regulated by insulin and mineralocorticoid hormones. Xu *et al.* show that WNK1 interacts with SGK1 (not necessarily directly) and promotes SGK1 activation through increased phosphorylation of its activation loop (although WNK1 itself does not phosphorylate SGK1). They demonstrate that SGK1 activation by WNK1 (not requiring WNK1 kinase activity) involves the kinases PI-3-kinase and Akt. Expression of endogenous WNK1 is necessary for SGK1 activation by IGF-1. WNK1 Thr58 has been shown to be an IGF-1-stimulated site of Akt phosphorylation (Figure 9.3). Xu *et al.* report that the N-terminus of WNK1, when phosphorylated on Thr58, is capable of activating SGK1 and ENaC, independently of WNK1 catalytic activity. The authors propose that WNK1 and PDK1 (believed to phosphorylate SGK1 within the activation loop) cooperate to activate SGK1 and that WNK1 may form a scaffold to assemble a protein complex required for efficient SGK1 activation. They hypothesise that phosphorylation of WNK1 on Thr58 may create a binding site for such proteins or induce a conformational change in SGK1 that is permissive for its activation. However, the relevance of these findings in kidney is unclear, particularly as WNK1-L is not expressed at very high levels in any nephron segment. Whilst these reports suggest a role and potential mechanism for WNK1-L in the regulation of distal nephron electrogenic Na^+ transport, they are largely derived from *in vitro* studies, often in non-epithelial cells (e.g. *Xenopus* oocytes). Moreover, their relation to the pathogenesis of Gordon syndrome remains unclear as activation of ENaC leads to hypertension with hypokalaemia rather than hyperkalaemia.

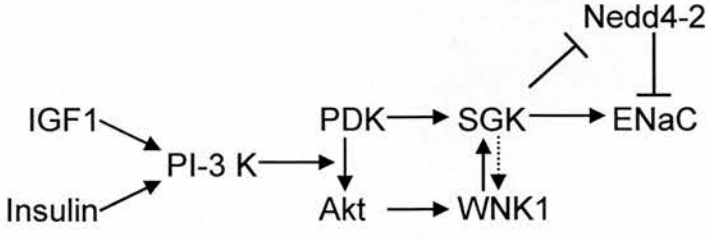

Figure 9.3: Proposed role of WNK1 in the regulation of SGK and ENaC.

9.3 Regulation of the WNK pathway *in vivo*.

Based on these *in vitro* findings that WNK1 and WNK4 can affect the activity of key Na^+ and K^+ transporters (especially ROMK and NCC) it was proposed this WNK pathway worked as an *in vivo* molecular switch[10;55;56], eliciting coordinated effects on key ion transport pathways, to maintain homeostasis during physiological perturbation. In the kidney, such a WNK molecular switch was proposed to react to stimuli such as hypovolemia and hyperkalaemia, generating a response that may complement aldosterone which is induced in these two very different states. To begin to test this hypothesis, we focused on one side of this putative molecular switch, principally examining the response of the WNK pathway to dietary K^+ flux, but we also examined the effect of allied variations in dietary Na^+ and aldosterone. At the time of these studies, there were no published reports of WNK pathway regulation *in vivo*, nor were there any functional roles described for WNK1-S, the predominant WNK1 isoform in kidney.

We found significant transcriptional regulation of elements of the WNK pathway, specifically upregulation of WNK1-S and WNK4 with high K^+ intake. A preliminary look at the alleged volume side of the WNK molecular switch, examining WNK expression in response to a wide (100-fold) range of chronic dietary NaCl intakes, revealed a just significant trend to lower WNK1-S expression as dietary Na^+ reduced across the high to low spectrum. These coordinated WNK expression changes seem functionally significant as merely heterozygous changes in WNK1 or WNK4 cause substantial BP and electrolyte abnormalities[13;42;148;165].

A preliminary investigation of the contribution of aldosterone to the changes seen in WNK1-S expression across the dietary K^+ spectrum suggested that aldosterone may play a role in the regulation of WNK1-S expression in the HK group. In an experiment designed to discriminate the roles of dietary K^+ intake and circulating aldosterone, linear regression analysis revealed strong correlations between K^+ and gene expression. In contrast correlations with aldosterone were much weaker, failing to reach significance in most cases. Aldosterone signalling upregulated ENaC activity, thereby increasing the lumen negative charge in DCT2-CD, and also

upregulated Na^+/K^+-ATPase activity. Both of these effects enhance the electrochemical driving force for K^+ secretion via ROMK2. Intriguingly, ROMK2 expression correlated closely with circulating aldosterone level. Overall, however, aldosterone had little or no effect on WNK pathway, ROMK1 or cHKA expression in this analysis.

A recent study by Náray-Fejes-Tóth and colleagues explored the hormonal regulation of WNK1 expression in a mouse CCD cell-line (M1 cells) stably expressing MR[106]. They concluded that aldosterone treatment at physiological concentrations increased the expression of WNK1-S but not WNK1-L. WNK1-S expression was also upregulated with dexamethasone treatment. Stable overexpression of WNK1-S caused a significant increase in transepithelial Na^+ transport via ENaC. The authors propose that WNK1-S regulates the subcellular localisation but not the expression of ENaC. However, as discussed previously, this WNK1 effect alone would promote Na^+ reabsorption but also reciprocal K^+ secretion rather than the K^+ retention characteristic of Gordon syndrome.

9.3.1 WNK pathway molecular switch based on distal Na^+ delivery.

Findings from our *in vivo* studies led us to propose a model whereby K^+ loading (such as with chronic high K^+ diet) increased WNK1-S/WNK4 which inhibited NCC and so enhanced distal Na^+ delivery facilitating enhanced K^+-excretion. Thus, an increased K^+ load evoked a WNK pathway response appropriately increasing K^+ excretion. This model is based on hierarchical inhibitory regulation (triple negative) down the regulatory chain WNK1-S-WNK1-L-WNK4-NCC, translating a rising K^+ balance into a regulation of the site of NaCl reabsorption (Figure 6.6). Such hierarchical inhibitory regulation is not unusual in kinase cascades and can facilitate powerful amplification of physiological stimuli, and indeed often seems to generate a decisive switch-like response[32]. In addition, such a hierarchy can also facilitate cross-talk between dominant stimuli (such as K^+ balance here) and modifier stimuli acting lower down the hierarchy – it is thus intriguing that *in vivo* the WNK pathway may have these attributes. Moreover, this hypothesis was recently supported by another independent study by Subramanya *et al.*, showing (exactly as in Figure 6.6) that there

seems to be a WNK1-S-WNK1-L-WNK4-NCC inhibitory hierarchy as studies in *Xenopus* oocytes report WNK1-S downregulates NCC activity indirectly through the suppression of WNK1-L, relieving the inhibition of WNK4. WNK1-S and WNK1-L reportedly interact in a protein complex (a heteromultimer, most likely a heterotetramer) with WNK1-S capable of inhibiting WNK1-L kinase activity *in vitro* via multiple inhibitory sequences[131]. Additional support for WNK1-S inhibition of WNK1-L is provided by a very recently published study showing firstly that WNK1-L inhibits ROMK1 in *Xenopus* occytes and secondly that WNK1-S antagonises this WNK1-L-mediated inhibition. This study also examined the effect of dietary K^+ intake on WNK1-S expression in rat, reporting increasing WNK1-S expression with increasing K^+, consistent with our findings (and the model in Figure 6.6)[63].

9.3.2 ROMK1 and cHKA coupling in K^+, NH_4^+, and acid-base balance.

Studies described in this thesis also uncover novel features of ROMK isoform expression, including striking reciprocal regulation of ROMK1 and ROMK2 in response to dietary K^+ intake. This is the first report of ROMK isoform expression in mouse and could have important implications for aspects of our understanding of K^+ regulation and role of ROMK isoforms. In particular, upregulation of ROMK1 in K^+ deficiency co-ordinates with changes in cHKA in a way which would allow fine regulation of K^+ and acid-base balance. Renal NH_4^+ production and excretion forms a major component of renal acid-base homeostasis, particularly in response to hypokalaemia[134], and occurs via a highly regulated pathway, whereby NH_4^+ is delivered to multiple nephron sites where it substitutes for K^+ ions and this facilitates undisturbed homeostasis despite relative K^+ deficiency. NH_4^+ is produced via the metabolism of glutamine in the proximal tubular cells, secreted into the tubular fluid via $Na^+/H^+(NH_4^+)$ exchange[129], and reabsorbed via NKCC2 $(Na^+/K^+(NH_4^+)/2Cl^-)$[41] and K^+/NH_4^+ antiport[5;6] in TAL, where it accumulates in the medullary interstitium and is finally secreted into the CNT-CD[33].

For years, the mechanism of NH_4^+ secretion along the CD was thought to occur through active H^+ secretion in parallel with the non-ionic diffusion of NH_3 down its

concentration gradient[33]. Moreover the low permeability of CD epithelia to NH_4^+ minimizes back diffusion of NH_4^+, promoting excretion in the urine. More recent studies suggest that NH_4^+ transport across the basolateral membrane of MCD cells may also occur by active transport of NH_4^+ via the $Na^+/K^+(NH_4^+)$-ATPase[143]. This may be particularly relevant in hypokalaemic states when reduced medullary interstitial K^+ concentration augments Na^+/NH_4^+ exchange rather than Na^+/K^+ exchange[141;142]. Furthermore, it has recently been proposed that NH_4^+ transport across the apical membrane may occur actively in exchange for K^+ via cHKA[104]. This suggests that cHKA upregulation in K^+ deficiency may occur to facilitate acid-base balance, rather than primarily conserve K^+. Thus, parallel upregulation of ROMK1 with cHKA in OMCD, as we have seen in our studies, would allow recycling of reabsorbed K^+ back into the lumen via ROMK1, thus enabling H^+ secretion via cHKA (Figure 7.6). This seems a particularly efficient coupling as either increased pH or ADP/ATP ratio on the cytoplasmic face of active H^+/K^+-ATPase would activate adjacent ROMK[47] and both are likely to be present in the vicinity of active H^+/K^+-ATPase pumps, but not otherwise, ensuring negligible ROMK1 K^+-secretion in excess of requirement for H^+/K^+-ATPase.

9.4 Integrated role of WNK molecular switch in renal physiology.

Based on our findings we have proposed that the WNK molecular switch is based on distal delivery of Na^+ to the aldosterone-sensitive nephron. Such a switch likely plays a fundamental role in electrolyte balance, potentially explaining a long-standing paradox in renal physiology. Aldosterone secretion from the adrenal glomerulosa is stimulated in two very different physiological situations: (1) hyperkalaemia, in which potassium is a direct stimulus for aldosterone secretion; and (2) hypovolemia, in response to the activation of the renin-angiotensin system and angiotensin II action. How the kidney differentiates between these two states to induce maximal K^+ secretion in the first scenario, but maximal NaCl reabsorption in the second, in response to the same aldosterone stimulus, is not very well understood, but clearly the same aldosterone response pathway cannot deliver this sophisticated differential response alone and a second independent or cross-talking response seems possible.

9.4.1 Aldosterone as the sole regulator of renal electrolyte balance.

Aldosterone is firmly established as a powerful regulator of electrolyte balance. However, it seems that the circulatory aldosterone level is not the *sole* factor controlling the balance between Na^+ reabsorption and K^+ secretion in the distal nephron. For example, during volume depletion, aldosterone secretion functions to re-establish euvolemia by stimulating Na^+ reabsorption in the principal cells of the CNT and CD. This occurs through enhanced electrogenic Na^+ transport apically via ENaC and basolaterally via Na/K-ATPase in exchange for K^+ secretion. This simple mechanism is particularly effective in restoring fluid balance. However, as the sole response to volume depletion, it would be disadvantageous as it would merely replace the hypovolemic condition with potentially fatal hypokalaemia. Therefore the kidney must have another mechanism to facilitate the uncoupling of Na^+ reabsorption and K^+ secretion in appropriate situations.

9.4.2 Two-compartment model of electrolyte homeostasis.

The WNK pathway seems well positioned to achieve this, primarily working in a compartment proximal to, but complementing the aldosterone pathway. Effectively, the WNK and aldosterone pathways would form a two-compartment model for the regulation of electrolyte balance (Figure 9.4). According to our findings, hyperkalaemia would induce increased inhibition of Na^+ reabsorption in the upper compartment via WNKs, driving Na distally. Aldosterone, secreted in response to elevated K^+, will stimulate Na reabsorption in the lower compartment in exchange for K^+ secretion. From our limited studies directed towards the volume side of the switch we can attempt to predict what might happen in a high volume state. In this scenario, increased inhibition by WNKs in the upper compartment will similarly drive distal Na^+ delivery (so increasing Na^+ and volume balance will elicit an appropriate response to augment NaCl excretion). However suppression of aldosterone secretion in response to hypervolemia results in Na^+ excretion in the urine as Na^+ reabsorption in the aldosterone-responsive DCT2-CD is downregulated. Such a mechanism would re-establish euvolemia without disrupting K^+ balance.

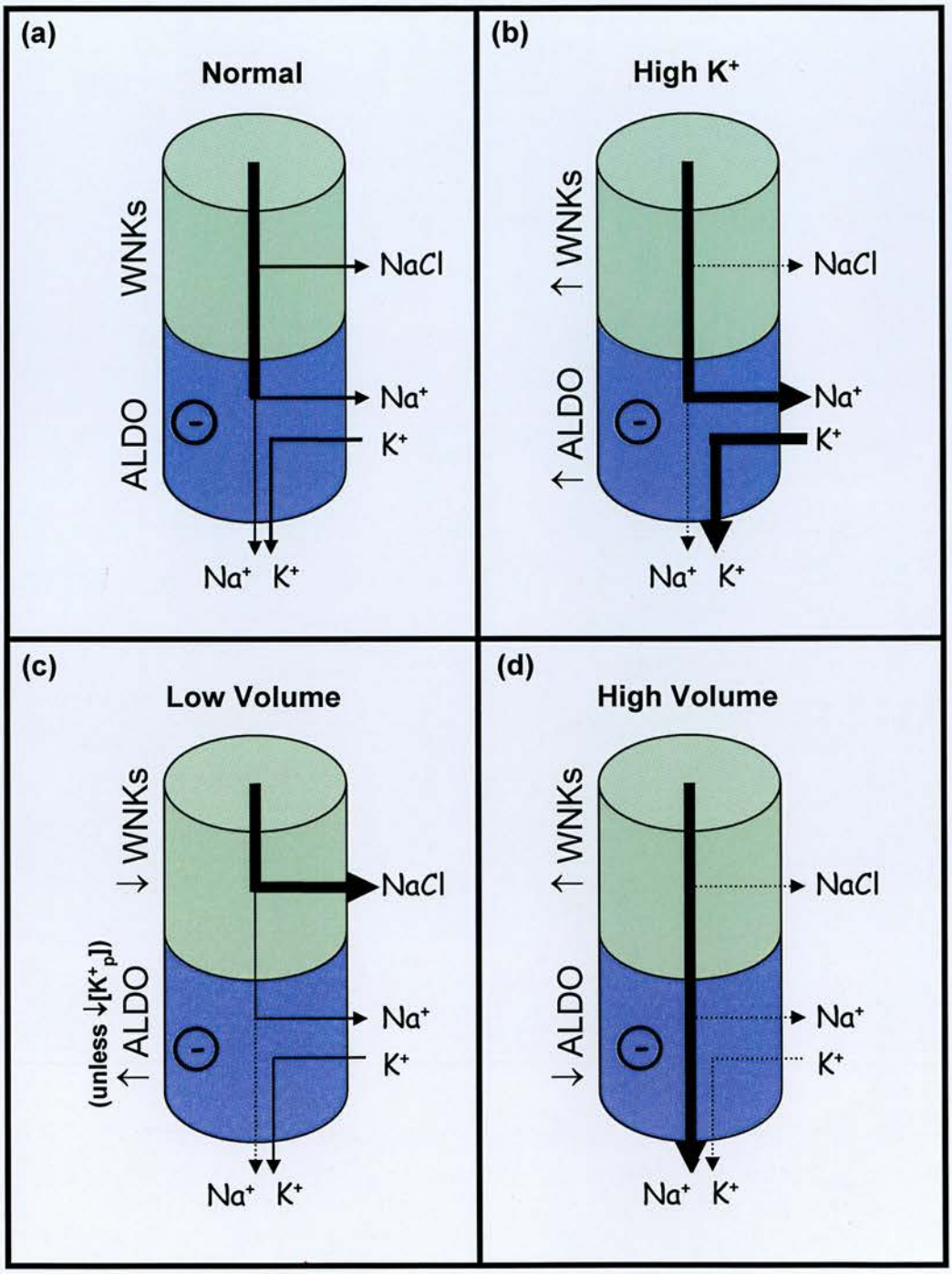

Figure 9.4: Two compartment model of electrolyte balance in distal nephron. Coordinated regulation of electrolyte balance via WNKs in an upper compartment and aldosterone in a lower compartment allows appropriate Na^+ reabsorption and K^+ secretion (a)under normal conditions and in the setting of (b)high plasma K^+ (c)low volume and (d) high volume. Regulation of electrolyte balance in response to K^+ deficiency is shown in Figure 9.5.

Potentially, in K^+ deficient states, a third compartment operating distal to this aldosterone-sensitive region, would be induced, in which the coupled activity of ROMK1 and cHKA would facilitate acid-base balance (Figure 9.5).

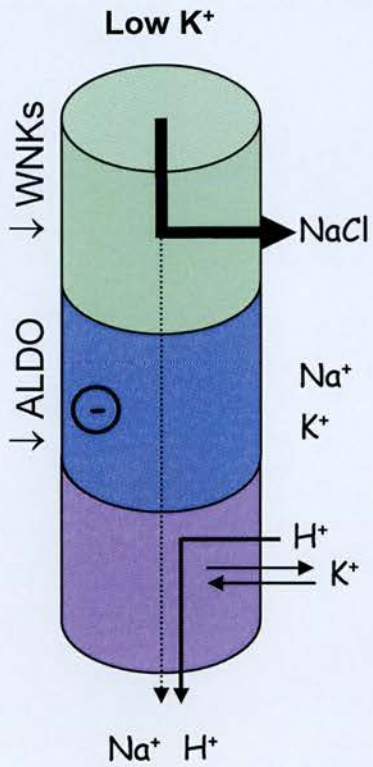

Figure 9.5: Three compartment model of electrolyte balance in K^+ deficiency. The coupled induction of ROMK1 and cHKA in K^+ deficiency suggests that a third compartment operating further distally, but working in concert with the two upper compartments, is involved in K^+ conservation and acid-base balance.

A loss of regulation via the WNK pathway, such as occurs in Gordon syndrome, would result in unrestrained NaCl reabsorption in the upper compartment. Consequently hypervolemic suppression of Ang II (and so relatively low aldosterone) and reduced distal Na^+ delivery would dissipate the electrochemical driving force for K^+ secretion in the aldosterone-sensitive lower compartment, resulting in hypervolemia, hypertension and hyperkalaemia: Gordon syndrome's cardinal features.

Supporting a key role for NCC in BP regulation, Majid and Navar[81] identify NCC as the major renal Na^+ entry pathway in the distal nephron mediating arterial pressure-

induced changes in sodium excretion. Also, Wang *et al.*[145] highlight decreased NCC activity as an important mechanism to restore natriuresis, despite the continuous presence of a high concentration of aldosterone in aldosterone-induced hypertension.

9.5 WNK1 and WNK4 Gordon syndrome phenotypes.

Although mutations in either WNK1 or WNK4 cause Gordon syndrome, the precise clinical phenotypes caused by the individual mutations may not be identical. This possibility is supported by current evidence indicating that WNK1 and WNK4 have different nephron segment expression profiles and may regulate different electrolyte transporters (at least *in vitro*). Moreover, only WNK4 has been reported to affect paracellular electrolyte transport[53;159]. Indeed, even though only limited kindreds have been reported since the association of WNK1 and WNK4 with Gordon syndrome, a number of variables distinguishing the WNK1 and WNK4 phenotypes have been documented.

Phenotypic analysis of a large French pedigree with the WNK1 deletion[2] highlighted notable differences compared to the clinical features resulting from the WNK4 (Q565E) mutation. The French WNK1 family had normal urine Ca^{2+} excretion, compared to hypercalcuria (and low plasma Ca^{2+}) described in the Israeli WNK4 family[87]. Furthermore hypertension, when present, was much less severe than in the Israeli family and did not develop until the fourth decade. Resolution of hypertension during pregnancy has also been associated with the WNK4 (Q565E) mutation[86]. WNK1 and WNK4 are also expressed in extrarenal tissues, notably in tissues with extensive epithelial systems[18;52]. It remains to be seen if any of these tissues prove to be sites of minor phenotypic effects, previously unrecognised in Gordon syndrome. Indeed WNK1-/- mice are embryonic lethal by mid-gestation highlighting the systemic importance of WNK1[165]. In addition, Gordon syndrome is a dominant disorder, with individuals bearing a Gordon syndrome mutation in one copy of WNK1 or WNK4 suffering from the disease. More dramatic, perhaps lethal, phenotypic effects could be anticipated in an individual homozygous for such a mutation. Studies in Chapters 3 and 4 reveal extensive expression of WNK1 and WNK4 before birth and show specific WNK1 splicing. Clearly it seems likely there

are important indeed vital functional roles for these WNK genes in non-renal tissues as well. If a clinical feature in a more accessible tissue is discovered, it may facilitate the development of a simple, direct, non-invasive test for the diagnosis of Gordon syndrome, as is already the case in Liddle syndrome diagnosis[7].

9.6 Concluding remarks

The elucidation of the respective physiological roles of WNK1 and WNK4 is in its infancy, and the various factors involved in the different pathophysiological features of Gordon syndrome remain to be more clearly defined. Further investigation of this pathway *in vivo* in different physiological settings, and the development of transgenic models, will no doubt identify new branches of the WNK pathway as well as verify existing *in vitro* models. Undoubtedly this is a pathway of major systemic importance, and has potent effects through its actions in kidney. Unravelling the mechanisms of the WNK pathway within kidney has the potential to advance our understanding of the integrated physiology regulating electrolyte balance and BP, and may even yield insights into the mechanisms involved in essential hypertension[107;135;166].

References

1. Mutations in the gene encoding the inwardly-rectifying renal potassium channel, ROMK, cause the antenatal variant of Bartter syndrome: evidence for genetic heterogeneity. International Collaborative Study Group for Bartter-like Syndromes. Hum Mol Genet 1997; 6(1):17-26.

2. Achard JM, Warnock DG, Disse-Nicodeme S, Fiquet-Kempf B, Corvol P, Fournier A, Jeunemaitre X. Familial hyperkalemic hypertension: phenotypic analysis in a large family with the WNK1 deletion mutation. Am J Med 2003; 114(6):495-498.

3. Aguilar-Bryan L, Clement JP, Gonzalez G, Kunjilwar K, Babenko A, Bryan J. Toward understanding the assembly and structure of KATP channels. Physiol Rev 1998; 78(1):227-245.

4. Ahn KY, Park KY, Kim KK, Kone BC. Chronic hypokalemia enhances expression of the H(+)-K(+)-ATPase alpha 2-subunit gene in renal medulla. Am J Physiol 1996; 271(2 Pt 2):F314-F321.

5. Amlal H, Paillard M, Bichara M. NH4+ transport pathways in cells of medullary thick ascending limb of rat kidney. NH4+ conductance and K+/NH4+(H+) antiport. J Biol Chem 1994; 269(35):21962-21971.

6. Attmane-Elakeb A, Boulanger H, Vernimmen C, Bichara M. Apical location and inhibition by arginine vasopressin of K+/H+ antiport of the medullary thick ascending limb of rat kidney. J Biol Chem 1997; 272(41):25668-25677.

7. Baker E, Jeunemaitre X, Portal AJ, Grimbert P, Markandu N, Persu A, Corvol P, MacGregor G. Abnormalities of nasal potential difference measurement in Liddle's syndrome. J Clin Invest 1998; 102(1):10-14.

8. Beesley AH, Hornby D, White SJ. Regulation of distal nephron K+ channels (ROMK) mRNA expression by aldosterone in rat kidney. J Physiol 1998; 509 (Pt 3):629-634.

9. Beesley AH, Ortega B, White SJ. Splicing of a retained intron within ROMK K+ channel RNA generates a novel set of isoforms in rat kidney. Am J Physiol 1999; 276(3 Pt 1):C585-C592.

10. Bindels RJ. A molecular switch controlling renal sodium and potassium excretion. Nat Genet 2003; 35(4):302-303.

11. Bock JH, Shuck ME, Benjamin CW, Chee M, Bienkowski MJ, Slightom JL. Nucleotide sequence analysis of the human KCNJ1 potassium channel locus. Gene 1997; 188(1):9-16.

12. Boim MA, Ho K, Shuck ME, Bienkowski MJ, Block JH, Slightom JL, Yang Y, Brenner BM, Hebert SC. ROMK inwardly rectifying ATP-sensitive K+

channel. II. Cloning and distribution of alternative forms. Am J Physiol 1995; 268(6 Pt 2):F1132-F1140.

13. Bonny O, Rossier BC. Disturbances of Na/K balance: pseudohypoaldosteronism revisited. J Am Soc Nephrol 2002; 13(9):2399-2414.

14. Booth RE, Johnson JP, Stockand JD. Aldosterone. Adv Physiol Educ 2002; 26(1-4):8-20.

15. Brandis M, Keyes J, Windhager EE. Potassium-induced inhibition of proximal tubular fluid reabsorption in rats. Am J Physiol 1972; 222(2):421-427.

16. Brown RW, Mullins JJ, Webb DJ. Mechanisms and Molecular Pathways in Hypertension. In: Chien KR, editor. The Molecular Basis of Cardiovascular Disease, A Companion to Braunwald's Heart Disease. Philadelphia: Elsevier/Mosby, 2004: 566-649.

17. Canadian Council on Animal Care. Clinical Biochemistry Reference Values, Appendix V in Guide to the Care and Use of Experimental Animals. 15-350 Albert St.,Ottawa, Ontario, Canada, K1R 1B1.1(2nd).1999. 1[2nd]. 2005. 1999.
Ref Type: Electronic Citation

18. Choate KA, Kahle KT, Wilson FH, Nelson-Williams C, Lifton RP. WNK1, a kinase mutated in inherited hypertension with hyperkalemia, localizes to diverse Cl- -transporting epithelia. Proc Natl Acad Sci U S A 2003; 100(2):663-668.

19. Choe H, Zhou H, Palmer LG, Sackin H. A conserved cytoplasmic region of ROMK modulates pH sensitivity, conductance, and gating. Am J Physiol 1997; 273(4 Pt 2):F516-F529.

20. Cope G, Golbang A, O'shaughnessy KM. WNK kinases and the control of blood pressure. Pharmacol Ther 2005; 106(2):221-231.

21. Critchley HO, Osei J, Henderson TA, Boswell L, Sales KJ, Jabbour HN, Hirani N. Hypoxia-inducible factor-1alpha expression in human endometrium and its regulation by prostaglandin E-series prostanoid receptor 2 (EP2). Endocrinology 2006; 147(2):744-753.

22. Dahlmann A, Pradervand S, Hummler E, Rossier BC, Frindt G, Palmer LG. Mineralocorticoid regulation of epithelial Na+ channels is maintained in a mouse model of Liddle's syndrome. Am J Physiol Renal Physiol 2003; 285(2):F310-F318.

23. de Los HP, Kahle KT, Rinehart J, Bobadilla NA, Vazquez N, San Cristobal P, Mount DB, Lifton RP, Hebert SC, Gamba G. WNK3 bypasses the tonicity

requirement for K-Cl cotransporter activation via a phosphatase-dependent pathway. Proc Natl Acad Sci U S A 2006; 103(6):1976-1981.

24. Delaloy C, Lu J, Houot AM, Disse-Nicodeme S, Gasc JM, Corvol P, Jeunemaitre X. Multiple promoters in the WNK1 gene: one controls expression of a kidney-specific kinase-defective isoform. Mol Cell Biol 2003; 23(24):9208-9221.

25. Dherbecourt O, Cheval L, Bloch-Faure M, Meneton P, Doucet A. Molecular identification of Sch28080-sensitive K-ATPase activities in the mouse kidney. Pflugers Arch 2005; .

26. Disse-Nicodeme S, Achard JM, Desitter I, Houot AM, Fournier A, Corvol P, Jeunemaitre X. A new locus on chromosome 12p13.3 for pseudohypoaldosteronism type II, an autosomal dominant form of hypertension. Am J Hum Genet 2000; 67(2):302-310.

27. Disse-Nicodeme S, Desitter I, Fiquet-Kempf B, Houot AM, Stern N, Delahousse M, Potier J, Ader JL, Jeunemaitre X. Genetic heterogeneity of familial hyperkalaemic hypertension. J Hypertens 2001; 19(11):1957-1964.

28. DuBose TD, Jr., Codina J, Burges A, Pressley TA. Regulation of H(+)-K(+)-ATPase expression in kidney. Am J Physiol 1995; 269(4 Pt 2):F500-F507.

29. Fakler B, Schultz JH, Yang J, Schulte U, Brandle U, Zenner HP, Jan LY, Ruppersberg JP. Identification of a titratable lysine residue that determines sensitivity of kidney potassium channels (ROMK) to intracellular pH. EMBO J 1996; 15(16):4093-4099.

30. Farfel Z, Iaina A, Levi J, Gafni J. Proximal renal tubular acidosis: association with familial normaldosteronemic hyperpotassemia and hypertension. Arch Intern Med 1978; 138(12):1837-1840.

31. Farfel Z, Mayan H, Yaacov Y, Mouallem M, Shaharabany M, Pauzner R, Kerem E, Wilschanski M. WNK4 regulates Na transport in airways. Eur J Clin Invest 2005; 35(6):410-415.

32. Ferrell JE, Jr. Self-perpetuating states in signal transduction: positive feedback, double-negative feedback and bistability. Curr Opin Cell Biol 2002; 14(2):140-148.

33. Flessner MF, Wall SM, Knepper MA. Permeabilities of rat collecting duct segments to NH3 and NH4+. Am J Physiol 1991; 260(2 Pt 2):F264-F272.

34. Fu Y, Subramanya A, Rozansky D, Cohen DM. WNK kinases influence TRPV4 channel function and localization. Am J Physiol Renal Physiol 2006.

35. Gagnon KB, England R, Delpire E. Volume sensitivity of cation-chloride cotransporters is modulated by the interaction of two kinases: SPAK and WNK4. Am J Physiol Cell Physiol 2005.

36. Gagnon KB, England R, Delpire E. Characterization of SPAK and OSR1, regulatory kinases of the Na-K-2Cl cotransporter. Mol Cell Biol 2006; 26(2):689-698.

37. Gamba G. Role of WNK kinases in regulating tubular salt and potassium transport and in the development of hypertension. Am J Physiol Renal Physiol 2005; 288(2):F245-F252.

38. Geller DS, Farhi A, Pinkerton N, Fradley M, Moritz M, Spitzer A, Meinke G, Tsai FT, Sigler PB, Lifton RP. Activating mineralocorticoid receptor mutation in hypertension exacerbated by pregnancy. Science 2000; 289(5476):119-123.

39. Geller DS, Rodriguez-Soriano J, Vallo BA, Schifter S, Bayer M, Chang SS, Lifton RP. Mutations in the mineralocorticoid receptor gene cause autosomal dominant pseudohypoaldosteronism type I. Nat Genet 1998; 19(3):279-281.

40. Giebisch G. Renal potassium transport: mechanisms and regulation. Am J Physiol 1998; 274(5 Pt 2):F817-F833.

41. Good DW. Active absorption of NH4+ by rat medullary thick ascending limb: inhibition by potassium. Am J Physiol 1988; 255(1 Pt 2):F78-F87.

42. Gordon RD. Syndrome of hypertension and hyperkalemia with normal glomerular filtration rate. Hypertension 1986; 8(2):93-102.

43. Gordon RD, Klemm SA, Tunny TJ, Stowasser M. Gordon's syndrome: A sodium-volume-dependent form of hypertension with a genetic basis. In: Laragh JH, Brenner BM, editors. Hypertension: Pathophysiology, Diagnosis, and Management. New York: Raven Press, 1995: 2111-2123.

44. Guyton AC. Blood pressure control--special role of the kidneys and body fluids. Science 1991; 252(5014):1813-1816.

45. Guyton AC, Coleman TG, Cowley AV, Jr., Scheel KW, Manning RD, Jr., Norman RA, Jr. Arterial pressure regulation. Overriding dominance of the kidneys in long-term regulation and in hypertension. Am J Med 1972; 52(5):584-594.

46. Hansson JH, Nelson-Williams C, Suzuki H, Schild L, Shimkets R, Lu Y, Canessa C, Iwasaki T, Rossier B, Lifton RP. Hypertension caused by a truncated epithelial sodium channel gamma subunit: genetic heterogeneity of Liddle syndrome. Nat Genet 1995; 11(1):76-82.

47. Hebert SC, Desir G, Giebisch G, Wang W. Molecular diversity and regulation of renal potassium channels. Physiol Rev 2005; 85(1):319-371.

48. Ho K, Nichols CG, Lederer WJ, Lytton J, Vassilev PM, Kanazirska MV, Hebert SC. Cloning and expression of an inwardly rectifying ATP-regulated potassium channel. Nature 1993; 362(6415):31-38.

49. Holden S, Cox J, Raymond FL. Cloning, genomic organization, alternative splicing and expression analysis of the human gene WNK3 (PRKWNK3). Gene 2004; 335:109-119.

50. Hou J, Speirs HJ, Seckl JR, Brown RW. Sgk1 gene expression in kidney and its regulation by aldosterone: spatio-temporal heterogeneity and quantitative analysis. J Am Soc Nephrol 2002; 13(5):1190-1198.

51. Jiang ZY, Zhou QL, Holik J, Patel S, Leszyk J, Coleman K, Chouinard M, Czech MP. Identification of WNK1 as a substrate of Akt/protein kinase B and a negative regulator of insulin-stimulated mitogenesis in 3T3-L1 cells. J Biol Chem 2005; 280(22):21622-21628.

52. Kahle KT, Gimenez I, Hassan H, Wilson FH, Wong RD, Forbush B, Aronson PS, Lifton RP. WNK4 regulates apical and basolateral Cl- flux in extrarenal epithelia. Proc Natl Acad Sci U S A 2004; 101(7):2064-2069.

53. Kahle KT, Macgregor GG, Wilson FH, Van Hoek AN, Brown D, Ardito T, Kashgarian M, Giebisch G, Hebert SC, Boulpaep EL, Lifton RP. Paracellular Cl- permeability is regulated by WNK4 kinase: insight into normal physiology and hypertension. Proc Natl Acad Sci U S A 2004; 101(41):14877-14882.

54. Kahle KT, Rinehart J, de Los HP, Louvi A, Meade P, Vazquez N, Hebert SC, Gamba G, Gimenez I, Lifton RP. WNK3 modulates transport of Cl- in and out of cells: implications for control of cell volume and neuronal excitability. Proc Natl Acad Sci U S A 2005; 102(46):16783-16788.

55. Kahle KT, Wilson FH, Lalioti M, Toka H, Qin H, Lifton RP. WNK kinases: molecular regulators of integrated epithelial ion transport. Curr Opin Nephrol Hypertens 2004; 13(5):557-562.

56. Kahle KT, Wilson FH, Leng Q, Lalioti MD, O'Connell AD, Dong K, Rapson AK, Macgregor GG, Giebisch G, Hebert SC, Lifton RP. WNK4 regulates the balance between renal NaCl reabsorption and K+ secretion. Nat Genet 2003; 35(4):372-376.

57. Kaissling B. Structural aspects of adaptive changes in renal electrolyte excretion. Am J Physiol 1982; 243(3):F211-F226.

58. Kamide K, Takiuchi S, Tanaka C, Miwa Y, Yoshii M, Horio T, Mannami T, Kokubo Y, Tomoike H, Kawano Y, Miyata T. Three novel missense mutations of WNK4, a kinase mutated in inherited hypertension, in Japanese hypertensives: implication of clinical phenotypes. Am J Hypertens 2004; 17(5 Pt 1):446-449.

59. Kokubo Y, Kamide K, Inamoto N, Tanaka C, Banno M, Takiuchi S, Kawano Y, Tomoike H, Miyata T. Identification of 108 SNPs in TSC, WNK1, and

WNK4 and their association with hypertension in a Japanese general population. J Hum Genet 2004; 49(9):507-515.

60. Kondo C, Isomoto S, Matsumoto S, Yamada M, Horio Y, Yamashita S, Takemura-Kameda K, Matsuzawa Y, Kurachi Y. Cloning and functional expression of a novel isoform of ROMK inwardly rectifying ATP-dependent K+ channel, ROMK6 (Kir1.1f). FEBS Lett 1996; 399(1-2):122-126.

61. Kone BC, Higham SC. A novel N-terminal splice variant of the rat H+-K+-ATPase alpha2 subunit. Cloning, functional expression, and renal adaptive response to chronic hypokalemia. J Biol Chem 1998; 273(5):2543-2552.

62. Kraut JA, Hiura J, Besancon M, Smolka A, Sachs G, Scott D. Effect of hypokalemia on the abundance of HK alpha 1 and HK alpha 2 protein in the rat kidney. Am J Physiol 1997; 272(6 Pt 2):F744-F750.

63. Lazrak A, Liu Z, Huang CL. Antagonistic regulation of ROMK by long and kidney-specific WNK1 isoforms. Proc Natl Acad Sci U S A 2006; 103(5):1615-1620.

64. Lee BH, Min X, Heise CJ, Xu BE, Chen S, Shu H, Luby-Phelps K, Goldsmith EJ, Cobb MH. WNK1 phosphorylates synaptotagmin 2 and modulates its membrane binding. Mol Cell 2004; 15(5):741-751.

65. Lee WS, Hebert SC. ROMK inwardly rectifying ATP-sensitive K+ channel. I. Expression in rat distal nephron segments. Am J Physiol 1995; 268(6 Pt 2):F1124-F1131.

66. Leng Q, Kahle KT, Rinehart J, Macgregor GG, Wilson FH, Canessa CM, Lifton RP, Hebert SC. WNK3, a kinase related to genes mutated in hereditary hypertension with hyperkalaemia, regulates the K+ channel ROMK1 (Kir1.1). J Physiol 2006; 571(Pt 2):275-286.

67. Lifton RP, Gharavi AG, Geller DS. Molecular mechanisms of human hypertension. Cell 2001; 104(4):545-556.

68. Lin D, Sterling H, Lerea KM, Giebisch G, Wang WH. Protein kinase C (PKC)-induced phosphorylation of ROMK1 is essential for the surface expression of ROMK1 channels. J Biol Chem 2002; 277(46):44278-44284.

69. Lin DH, Sterling H, Lerea KM, Welling P, Jin L, Giebisch G, Wang WH. K depletion increases protein tyrosine kinase-mediated phosphorylation of ROMK. Am J Physiol Renal Physiol 2002; 283(4):F671-F677.

70. Linas SL, Peterson LN, Anderson RJ, Aisenbrey GA, Simon FR, Berl T. Mechanism of renal potassium conservation in the rat. Kidney Int 1979; 15(6):601-611.

71. Liu W, Qian C, Francke U. Silent mutation induces exon skipping of fibrillin-1 gene in Marfan syndrome. Nat Genet 1997; 16(4):328-329.

72. Loffing J, Vallon V, Loffing-Cueni D, Aregger F, Richter K, Pietri L, Bloch-Faure M, Hoenderop JG, Shull GE, Meneton P, Kaissling B. Altered renal distal tubule structure and renal Na(+) and Ca(2+) handling in a mouse model for Gitelman's syndrome. J Am Soc Nephrol 2004; 15(9):2276-2288.

73. Lorenz JN, Baird NR, Judd LM, Noonan WT, Andringa A, Doetschman T, Manning PA, Liu LH, Miller ML, Shull GE. Impaired renal NaCl absorption in mice lacking the ROMK potassium channel, a model for type II Bartter's syndrome. J Biol Chem 2002; 277(40):37871-37880.

74. Lu M, Leng Q, Egan ME, Caplan MJ, Boulpaep EL, Giebisch GH, Hebert SC. CFTR is required for PKA-regulated ATP sensitivity of Kir1.1 potassium channels in mouse kidney. J Clin Invest 2006; 116(3):797-807.

75. Lu M, Wang T, Yan Q, Wang W, Giebisch G, Hebert SC. ROMK is required for expression of the 70-pS K channel in the thick ascending limb. Am J Physiol Renal Physiol 2004; 286(3):F490-F495.

76. Lu M, Wang T, Yan Q, Yang X, Dong K, Knepper MA, Wang W, Giebisch G, Shull GE, Hebert SC. Absence of small conductance K+ channel (SK) activity in apical membranes of thick ascending limb and cortical collecting duct in ROMK (Bartter's) knockout mice. J Biol Chem 2002; 277(40):37881-37887.

77. Luft FC. Mendelian Forms of Human Hypertension and Mechanisms of Disease. Clin Med Res 2003; 1(4):291-300.

78. MacDonald P, MacKenzie S, Ramage LE, Seckl JR, Brown RW. Corticosteroid regulation of amiloride-sensitive sodium-channel subunit mRNA expression in mouse kidney. J Endocrinol 2000; 165(1):25-37.

79. Macgregor GG, Xu JZ, McNicholas CM, Giebisch G, Hebert SC. Partially active channels produced by PKA site mutation of the cloned renal K+ channel, ROMK2 (kir1.2). Am J Physiol 1998; 275(3 Pt 2):F415-F422.

80. MacPhee IA, Antoni FA, Mason DW. Spontaneous recovery of rats from experimental allergic encephalomyelitis is dependent on regulation of the immune system by endogenous adrenal corticosteroids. J Exp Med 1989; 169(2):431-445.

81. Majid DS, Navar LG. Blockade of distal nephron sodium transport attenuates pressure natriuresis in dogs. Hypertension 1994; 23(6 Pt 2):1040-1045.

82. Malnic G, Bailey MA, Giebisch G. Control of Renal Potassium Excretion. In: Brenner BM, Levine SA, editors. Brenner and Rector's The Kidney. Philadelphia: Saunders, 2004: 453-497.

83. Malnic G, Klose RM, Giebisch G. Micropuncture study of distal tubular potassium and sodium transport in rat nephron. Am J Physiol 1966; 211(3):529-547.

84. Manning G, Whyte DB, Martinez R, Hunter T, Sudarsanam S. The protein kinase complement of the human genome. Science 2002; 298(5600):1912-1934.

85. Mansfield TA, Simon DB, Farfel Z, Bia M, Tucci JR, Lebel M, Gutkin M, Vialettes B, Christofilis MA, Kauppinen-Makelin R, Mayan H, Risch N, Lifton RP. Multilocus linkage of familial hyperkalaemia and hypertension, pseudohypoaldosteronism type II, to chromosomes 1q31-42 and 17p11-q21. Nat Genet 1997; 16(2):202-205.

86. Mayan H, Mouallem M, Shaharabany M, Pauzner R, Farfel Z. Resolution of hypertension during pregnancy in familial hyperkalemia and hypertension with the WNK4 Q565E mutation. Am J Obstet Gynecol 2005; 192(2):598-603.

87. Mayan H, Munter G, Shaharabany M, Mouallem M, Pauzner R, Holtzman EJ, Farfel Z. Hypercalciuria in familial hyperkalemia and hypertension accompanies hyperkalemia and precedes hypertension: description of a large family with the Q565E WNK4 mutation. J Clin Endocrinol Metab 2004; 89(8):4025-4030.

88. McNicholas CM, Macgregor GG, Islas LD, Yang Y, Hebert SC, Giebisch G. pH-dependent modulation of the cloned renal K+ channel, ROMK. Am J Physiol 1998; 275(6 Pt 2):F972-F981.

89. McNicholas CM, Wang W, Ho K, Hebert SC, Giebisch G. Regulation of ROMK1 K+ channel activity involves phosphorylation processes. Proc Natl Acad Sci U S A 1994; 91(17):8077-8081.

90. McNicholas CM, Yang Y, Giebisch G, Hebert SC. Molecular site for nucleotide binding on an ATP-sensitive renal K+ channel (ROMK2). Am J Physiol 1996; 271(2 Pt 2):F275-F285.

91. Meneton P, Ichikawa I, Inagami T, Schnermann J. Renal physiology of the mouse. Am J Physiol Renal Physiol 2000; 278(3):F339-F351.

92. Meneton P, Oh YS, Warnock DG. Genetic renal tubular disorders of renal ion channels and transporters. Semin Nephrol 2001; 21(2):81-93.

93. Mennitt PA, Frindt G, Silver RB, Palmer LG. Potassium restriction downregulates ROMK expression in rat kidney. Am J Physiol Renal Physiol 2000; 278(6):F916-F924.

94. Min X, Lee BH, Cobb MH, Goldsmith EJ. Crystal structure of the kinase domain of WNK1, a kinase that causes a hereditary form of hypertension. Structure (Camb) 2004; 12(7):1303-1311.

95. Moe OW, Baum M, Berry CA, Rector FC, Jr. Renal Transport of Glucose, Amino Acids, Sodium, Chloride and Water. In: Brenner BM, editor. Brenner & Rector's The kidney. Saunders, 2004: 413-452.

96. Moral Z, Dong K, Wei Y, Sterling H, Deng H, Ali S, Gu R, Huang XY, Hebert SC, Giebisch G, Wang WH. Regulation of ROMK1 channels by protein-tyrosine kinase and -tyrosine phosphatase. J Biol Chem 2001; 276(10):7156-7163.

97. Moriguchi T, Urushiyama S, Hisamoto N, Iemura S, Uchida S, Natsume T, Matsumoto K, Shibuya H. WNK1 regulates phosphorylation of cation-chloride-coupled cotransporters via the STE20-related kinases, SPAK and OSR1. J Biol Chem 2005; 280(52):42685-42693.

98. Mosterd A, D'Agostino RB, Silbershatz H, Sytkowski PA, Kannel WB, Grobbee DE, Levy D. Trends in the prevalence of hypertension, antihypertensive therapy, and left ventricular hypertrophy from 1950 to 1989. N Engl J Med 1999; 340(16):1221-1227.

99. Mune T, Rogerson FM, Nikkila H, Agarwal AK, White PC. Human hypertension caused by mutations in the kidney isozyme of 11 beta-hydroxysteroid dehydrogenase. Nat Genet 1995; 10(4):394-399.

100. Murakami-Kojima M, Nakamichi N, Yamashino T, Mizuno T. The APRR3 component of the clock-associated APRR1/TOC1 quintet is phosphorylated by a novel protein kinase belonging to the WNK family, the gene for which is also transcribed rhythmically in Arabidopsis thaliana. Plant Cell Physiol 2002; 43(6):675-683.

101. Najjar F, Zhou H, Morimoto T, Bruns JB, Li HS, Liu W, Kleyman TR, Satlin LM. Dietary K+ regulates apical membrane expression of maxi-K channels in rabbit cortical collecting duct. Am J Physiol Renal Physiol 2005; 289(4):F922-F932.

102. Nakamichi N, Murakami-Kojima M, Sato E, Kishi Y, Yamashino T, Mizuno T. Compilation and characterization of a novel WNK family of protein kinases in Arabiodpsis thaliana with reference to circadian rhythms. Biosci Biotechnol Biochem 2002; 66(11):2429-2436.

103. Nakamura S, Amlal H, Galla JH, Soleimani M. Colonic H+-K+-ATPase is induced and mediates increased. Kidney Int 1998; 54(4):1233-1239.

104. Nakamura S, Amlal H, Galla JH, Soleimani M. NH4+ secretion in inner medullary collecting duct in potassium deprivation: role of colonic H+-K+-ATPase. Kidney Int 1999; 56(6):2160-2167.

105. Nakamura S, Wang Z, Galla JH, Soleimani M. K+ depletion increases. Am J Physiol 1998; 274(4 Pt 2):F687-F692.

106. Naray-Fejes-Toth A, Snyder PM, Fejes-Toth G. The kidney-specific WNK1 isoform is induced by aldosterone and stimulates epithelial sodium channel-mediated Na+ transport. Proc Natl Acad Sci U S A 2004; 101(50):17434-17439.

107. Newhouse SJ, Wallace C, Dobson R, Mein C, Pembroke J, Farrall M, Clayton D, Brown M, Samani N, Dominiczak A, Connell JM, Webster J, Lathrop GM, Caulfield M, Munroe PB. Haplotypes of the WNK1 gene associate with blood pressure variation in a severely hypertensive population from the British Genetics of Hypertension study. Hum Mol Genet 2005; 14(13):1805-1814.

108. Nijenhuis T, Hoenderop JG, Loffing J, van der Kemp AW, van Os CH, Bindels RJ. Thiazide-induced hypocalciuria is accompanied by a decreased expression of Ca2+ transport proteins in kidney. Kidney Int 2003; 64(2):555-564.

109. O'Reilly M, Marshall E, Speirs HJ, Brown RW. WNK1, a gene within a novel blood pressure control pathway, tissue-specifically generates radically different isoforms with and without a kinase domain. J Am Soc Nephrol 2003; 14(10):2447-2456.

110. Pagani F, Buratti E, Stuani C, Bendix R, Dork T, Baralle FE. A new type of mutation causes a splicing defect in ATM. Nat Genet 2002; 30(4):426-429.

111. Palmer LG, Antonian L, Frindt G. Regulation of apical K and Na channels and Na/K pumps in rat cortical collecting tubule by dietary K. J Gen Physiol 1994; 104(4):693-710.

112. Paver WK, Pauline GJ. Hypertension and hyperpotassaemia without renal disease in a young male. Med J Aust 1964; 35:305-306.

113. Piechotta K, Garbarini N, England R, Delpire E. Characterization of the interaction of the stress kinase SPAK with the Na+-K+-2Cl- cotransporter in the nervous system: evidence for a scaffolding role of the kinase. J Biol Chem 2003; 278(52):52848-52856.

114. Piechotta K, Lu J, Delpire E. Cation chloride cotransporters interact with the stress-related kinases Ste20-related proline-alanine-rich kinase (SPAK) and oxidative stress response 1 (OSR1). J Biol Chem 2002; 277(52):50812-50819.

115. Pradervand S, Wang Q, Burnier M, Beermann F, Horisberger JD, Hummler E, Rossier BC. A mouse model for Liddle's syndrome. J Am Soc Nephrol 1999; 10(12):2527-2533.

116. Rinehart J, Kahle KT, de Los HP, Vazquez N, Meade P, Wilson FH, Hebert SC, Gimenez I, Gamba G, Lifton RP. WNK3 kinase is a positive regulator of NKCC2 and NCC, renal cation-Cl- cotransporters required for normal blood pressure homeostasis. Proc Natl Acad Sci U S A 2005; 102(46):16777-16782.

117. Rubera I, Loffing J, Palmer LG, Frindt G, Fowler-Jaeger N, Sauter D, Carroll T, McMahon A, Hummler E, Rossier BC. Collecting duct-specific gene

inactivation of alphaENaC in the mouse kidney does not impair sodium and potassium balance. J Clin Invest 2003; 112(4):554-565.

118. Ruknudin A, Schulze DH, Sullivan SK, Lederer WJ, Welling PA. Novel subunit composition of a renal epithelial KATP channel. J Biol Chem 1998; 273(23):14165-14171.

119. Schambelan M, Sebastian A, Rector FC, Jr. Mineralocorticoid-resistant renal hyperkalemia without salt wasting (type II pseudohypoaldosteronism): role of increased renal chloride reabsorption. Kidney Int 1981; 19(5):716-727.

120. Schneeberger EE, Lynch RD. The tight junction: a multifunctional complex. Am J Physiol Cell Physiol 2004; 286(6):C1213-C1228.

121. Schnermann J. Sodium transport deficiency and sodium balance in gene-targeted mice. Acta Physiol Scand 2001; 173(1):59-66.

122. Schuster VL, Stokes JB. Chloride transport by the cortical and outer medullary collecting duct. Am J Physiol 1987; 253(2 Pt 2):F203-F212.

123. Shimkets RA, Warnock DG, Bositis CM, Nelson-Williams C, Hansson JH, Schambelan M, Gill JR, Jr., Ulick S, Milora RV, Findling JW, . Liddle's syndrome: heritable human hypertension caused by mutations in the beta subunit of the epithelial sodium channel. Cell 1994; 79(3):407-414.

124. Shuck ME, Bock JH, Benjamin CW, Tsai TD, Lee KS, Slightom JL, Bienkowski MJ. Cloning and characterization of multiple forms of the human kidney ROM-K potassium channel. J Biol Chem 1994; 269(39):24261-24270.

125. Simon DB, Bindra RS, Mansfield TA, Nelson-Williams C, Mendonca E, Stone R, Schurman S, Nayir A, Alpay H, Bakkaloglu A, Rodriguez-Soriano J, Morales JM, Sanjad SA, Taylor CM, Pilz D, Brem A, Trachtman H, Griswold W, Richard GA, John E, Lifton RP. Mutations in the chloride channel gene, CLCNKB, cause Bartter's syndrome type III. Nat Genet 1997; 17(2):171-178.

126. Simon DB, Karet FE, Hamdan JM, DiPietro A, Sanjad SA, Lifton RP. Bartter's syndrome, hypokalaemic alkalosis with hypercalciuria, is caused by mutations in the Na-K-2Cl cotransporter NKCC2. Nat Genet 1996; 13(2):183-188.

127. Simon DB, Karet FE, Rodriguez-Soriano J, Hamdan JH, DiPietro A, Trachtman H, Sanjad SA, Lifton RP. Genetic heterogeneity of Bartter's syndrome revealed by mutations in the K+ channel, ROMK. Nat Genet 1996; 14(2):152-156.

128. Simon DB, Nelson-Williams C, Bia MJ, Ellison D, Karet FE, Molina AM, Vaara I, Iwata F, Cushner HM, Koolen M, Gainza FJ, Gitleman HJ, Lifton RP. Gitelman's variant of Bartter's syndrome, inherited hypokalaemic

alkalosis, is caused by mutations in the thiazide-sensitive Na-Cl cotransporter. Nat Genet 1996; 12(1):24-30.

129. Soleimani M, Singh G. Physiologic and molecular aspects of the Na+/H+ exchangers in health and disease processes. J Investig Med 1995; 43(5):419-430.

130. Spring KR. Routes and mechanism of fluid transport by epithelia. Annu Rev Physiol 1998; 60:105-119.

131. Subramanya AR, Yang CL, Zhu X, Ellison DH. Dominant-Negative Regulation of WNK1 by its Kidney-Specific Kinase-Defective Isoform. Am J Physiol Renal Physiol 2005.

132. Takahashi N, Chernavvsky DR, Gomez RA, Igarashi P, Gitelman HJ, Smithies O. Uncompensated polyuria in a mouse model of Bartter's syndrome. Proc Natl Acad Sci U S A 2000; 97(10):5434-5439.

133. Takaya J, Matsusaka T, Katori H, Tamura M, Miyazaki Y, Homma T, Ichikawa I. In situ demonstration of angiotensin-dependent and independent pathways for hyperaldosteronism during chronic extracellular fluid volume depletion. Mol Endocrinol 2001; 15(12):2229-2235.

134. Tannen RL. Relationship of renal ammonia production and potassium homeostasis. Kidney Int 1977; 11(6):453-465.

135. Tobin MD, Raleigh SM, Newhouse S, Braund P, Bodycote C, Ogleby J, Cross D, Gracey J, Hayes S, Smith T, Ridge C, Caulfield M, Sheehan NA, Munroe PB, Burton PR, Samani NJ. Association of WNK1 gene polymorphisms and haplotypes with ambulatory blood pressure in the general population. Circulation 2005; 112(22):3423-3429.

136. Van Itallie CM, Anderson JM. The molecular physiology of tight junction pores. Physiology (Bethesda) 2004; 19:331-338.

137. Verissimo F, Jordan P. WNK kinases, a novel protein kinase subfamily in multi-cellular organisms. Oncogene 2001; 20(39):5562-5569.

138. Vitari AC, Deak M, Collins BJ, Morrice N, Prescott AR, Phelan A, Humphreys S, Alessi DR. WNK1, the kinase mutated in an inherited high-blood-pressure syndrome, is a novel PKB (protein kinase B)/Akt substrate. Biochem J 2004; 378(Pt 1):257-268.

139. Vitari AC, Deak M, Morrice NA, Alessi DR. The WNK1 and WNK4 protein kinases that are mutated in Gordon's hypertension syndrome phosphorylate and activate SPAK and OSR1 protein kinases. Biochem J 2005; 391(Pt 1):17-24.

140. Wald H, Garty H, Palmer LG, Popovtzer MM. Differential regulation of ROMK expression in kidney cortex and medulla by aldosterone and potassium. Am J Physiol 1998; 275(2 Pt 2):F239-F245.

141. Wall SM, Davis BS, Hassell KA, Mehta P, Park SJ. In rat tIMCD, NH4+ uptake by Na+-K+-ATPase is critical to net acid secretion during chronic hypokalemia. Am J Physiol 1999; 277(6 Pt 2):F866-F874.

142. Wall SM, Fischer MP, Kim GH, Nguyen BM, Hassell KA. In rat inner medullary collecting duct, NH uptake by the Na,K-ATPase is increased during hypokalemia. Am J Physiol Renal Physiol 2002; 282(1):F91-102.

143. Wall SM, Koger LM. NH+4 transport mediated by Na(+)-K(+)-ATPase in rat inner medullary collecting duct. Am J Physiol 1994; 267(4 Pt 2):F660-F670.

144. Wang WH, Lin DH, Sterling H. Regulation of ROMK channels by protein tyrosine kinase and tyrosine phosphatase. Trends Cardiovasc Med 2002; 12(3):138-142.

145. Wang XY, Masilamani S, Nielsen J, Kwon TH, Brooks HL, Nielsen S, Knepper MA. The renal thiazide-sensitive Na-Cl cotransporter as mediator of the aldosterone-escape phenomenon. J Clin Invest 2001; 108(2):215-222.

146. Wang Z, Wang T, Petrovic S, Tuo B, Riederer B, Barone S, Lorenz JN, Seidler U, Aronson PS, Soleimani M. Renal and intestinal transport defects in Slc26a6-null mice. Am J Physiol Cell Physiol 2005; 288(4):C957-C965.

147. Wang Z, Yang CL, Ellison DH. Comparison of WNK4 and WNK1 kinase and inhibiting activities. Biochem Biophys Res Commun 2004; 317(3):939-944.

148. Wilson FH, Disse-Nicodeme S, Choate KA, Ishikawa K, Nelson-Williams C, Desitter I, Gunel M, Milford DV, Lipkin GW, Achard JM, Feely MP, Dussol B, Berland Y, Unwin RJ, Mayan H, Simon DB, Farfel Z, Jeunemaitre X, Lifton RP. Human hypertension caused by mutations in WNK kinases. Science 2001; 293(5532):1107-1112.

149. Wilson FH, Kahle KT, Sabath E, Lalioti MD, Rapson AK, Hoover RS, Hebert SC, Gamba G, Lifton RP. Molecular pathogenesis of inherited hypertension with hyperkalemia: the Na-Cl cotransporter is inhibited by wild-type but not mutant WNK4. Proc Natl Acad Sci U S A 2003; 100(2):680-684.

150. Woda CB, Bragin A, Kleyman TR, Satlin LM. Flow-dependent K+ secretion in the cortical collecting duct is mediated by a maxi-K channel. Am J Physiol Renal Physiol 2001; 280(5):F786-F793.

151. Xu B, English JM, Wilsbacher JL, Stippec S, Goldsmith EJ, Cobb MH. WNK1, a novel mammalian serine/threonine protein kinase lacking the catalytic lysine in subdomain II. J Biol Chem 2000; 275(22):16795-16801.

152. Xu BE, Min X, Stippec S, Lee BH, Goldsmith EJ, Cobb MH. Regulation of WNK1 by an autoinhibitory domain and autophosphorylation. J Biol Chem 2002; 277(50):48456-48462.

153. Xu BE, Stippec S, Chu PY, Lazrak A, Li XJ, Lee BH, English JM, Ortega B, Huang CL, Cobb MH. WNK1 activates SGK1 to regulate the epithelial sodium channel. Proc Natl Acad Sci U S A 2005; 102(29):10315-10320.

154. Xu BE, Stippec S, Lazrak A, Huang CL, Cobb MH. WNK1 activates SGK1 by a phosphatidylinositol 3-kinase-dependent and non-catalytic mechanism. J Biol Chem 2005; 280(40):34218-34223.

155. Xu BE, Stippec S, Lenertz L, Lee BH, Zhang W, Lee YK, Cobb MH. WNK1 activates ERK5 by an MEKK2/3-dependent mechanism. J Biol Chem 2004; 279(9):7826-7831.

156. Xu H, Yang Z, Cui N, Giwa LR, Abdulkadir L, Patel M, Sharma P, Shan G, Shen W, Jiang C. Molecular determinants for the distinct pH sensitivity of Kir1.1 and Kir4.1 channels. Am J Physiol Cell Physiol 2000; 279(5):C1464-C1471.

157. Xu Q, Modrek B, Lee C. Genome-wide detection of tissue-specific alternative splicing in the human transcriptome. Nucleic Acids Res 2002; 30(17):3754-3766.

158. Xu ZC, Yang Y, Hebert SC. Phosphorylation of the ATP-sensitive, inwardly rectifying K+ channel, ROMK, by cyclic AMP-dependent protein kinase. J Biol Chem 1996; 271(16):9313-9319.

159. Yamauchi K, Rai T, Kobayashi K, Sohara E, Suzuki T, Itoh T, Suda S, Hayama A, Sasaki S, Uchida S. Disease-causing mutant WNK4 increases paracellular chloride permeability and phosphorylates claudins. Proc Natl Acad Sci U S A 2004; 101(13):4690-4694.

160. Yamauchi K, Yang SS, Ohta A, Sohara E, Rai T, Sasaki S, Uchida S. Apical localization of renal K channel was not altered in mutant WNK4 transgenic mice. Biochem Biophys Res Commun 2005; 332(3):750-755.

161. Yang CL, Angell J, Mitchell R, Ellison DH. WNK kinases regulate thiazide-sensitive Na-Cl cotransport. J Clin Invest 2003; 111(7):1039-1045.

162. Yang CL, Zhu X, Wang Z, Subramanya AR, Ellison DH. Mechanisms of WNK1 and WNK4 interaction in the regulation of thiazide-sensitive NaCl cotransport. J Clin Invest 2005; 115(5):1379-1387.

163. Yang SS, Yamauchi K, Rai T, Hiyama A, Sohara E, Suzuki T, Itoh T, Suda S, Sasaki S, Uchida S. Regulation of apical localization of the thiazide-sensitive NaCl cotransporter by WNK4 in polarized epithelial cells. Biochem Biophys Res Commun 2005; 330(2):410-414.

164. Yano H, Philipson LH, Kugler JL, Tokuyama Y, Davis EM, Le Beau MM, Nelson DJ, Bell GI, Takeda J. Alternative splicing of human inwardly rectifying K+ channel ROMK1 mRNA. Mol Pharmacol 1994; 45(5):854-860.

165. Zambrowicz BP, Abuin A, Ramirez-Solis R, Richter LJ, Piggott J, BeltrandelRio H, Buxton EC, Edwards J, Finch RA, Friddle CJ, Gupta A, Hansen G, Hu Y, Huang W, Jaing C, Key BW, Jr., Kipp P, Kohlhauff B, Ma ZQ, Markesich D, Payne R, Potter DG, Qian N, Shaw J, Schrick J, Shi ZZ, Sparks MJ, Van S, I, Vogel P, Walke W, Xu N, Zhu Q, Person C, Sands AT. Wnk1 kinase deficiency lowers blood pressure in mice: a gene-trap screen to identify potential targets for therapeutic intervention. Proc Natl Acad Sci U S A 2003; 100(24):14109-14114.

166. Zhang H, Staessen JA. Association of blood pressure with genetic variation in WNK kinases in a white European population. Circulation 2005; 112(22):3371-3372.

167. Zhou H, Tate SS, Palmer LG. Primary structure and functional properties of an epithelial K channel. Am J Physiol 1994; 266(3 Pt 1):C809-C824.

168. Zhou X, Hansson GK. Effect of sex and age on serum biochemical reference ranges in C57BL/6J mice. Comp Med 2004; 54(2):176-178.

169. Zimdahl H, Kreitler T, Gosele C, Ganten D, Hubner N. Conserved synteny in rat and mouse for a blood pressure QTL on human chromosome 17. Hypertension 2002; 39(6):1050-1052.

J Am Soc Nephrol 14: 2447–2456, 2003

WNK1, a Gene within a Novel Blood Pressure Control Pathway, Tissue-Specifically Generates Radically Different Isoforms with and without a Kinase Domain

MICHELLE O'REILLY,* ELAINE MARSHALL,* HELEN J.L. SPEIRS,* and ROGER W. BROWN*

**Molecular Endocrinology, University of Edinburgh, Edinburgh, Scotland.*

Abstract. WNK1 is a member of a novel serine/threonine kinase family, With-No-K, (lysine). Intronic deletions in the encoding gene cause Gordon syndrome, an autosomal dominant, hypertensive, hyperkalemic disorder particularly responsive to thiazide diuretics, a first-line treatment in essential hypertension. To elucidate the novel WNK1 BP control pathway active in distal nephron, WNK1 expression in mouse was studied. It was found that WNK1 is highly expressed in testis > heart, lung, kidney, placenta > skeletal muscle, brain, and widely at low levels. Several WNK1 transcript classes are demonstrated, showing tissue-, developmental-, and nephron-segment–specific expression. Importantly, in kidney, the most prominent transcripts are smaller than elsewhere, having the first four exons replaced by an alternative 5'-exon, deleting the kinase domain, and showing strong distal nephron expression, whereas larger transcripts show low-level widespread distribution. Alternative splicing of exons 11 and 12 is prominent—for example, transcripts containing exon 11 are abundant in neural tissues, testis, and secondary renal transcripts but are predominantly absent in placenta. The transcriptional diversity generated by these events would produce proteins greatly differing in both structure and function. These findings help further define and clarify the role of WNK1 and the thiazide-responsive pathway relevant to essential hypertension in which it participates.

Gordon syndrome (also known as pseudohypoaldosteronism type 2, PHA 2; Online Mendelian Inheritance in Man 145260) is a familial form of hypertension with an autosomal dominant mode of inheritance (1). Patients have suppressed plasma renin activity and present with symptoms of severe hypertension (attributed to increased renal Na^+ reabsorption), hyperkalemia (despite normal glomerular filtration), and metabolic acidosis as a result of reduced renal K^+ and H^+ excretion, respectively (2). These features are chloride dependent and are particularly well ameliorated by administration of thiazide diuretics (2–4). In common with other chloride transport–related disorders affecting BP, such as Bartter syndrome (5,6), it seemed possible that the etiology lay in a direct mutation in a chloride channel subunit or transporter (7).

However, mutations in human *WNK1* and *WNK4* genes have recently been associated with Gordon syndrome (8). The encoded proteins of these genes are described as members of a novel family of serine/threonine kinases known as WNK (*With No K*, lysine) because of the atypical positioning of a conserved lysine residue within the catalytic domain (9). How they relate to ion transport abnormalities is of key importance as this seems to represent a novel BP regulatory pathway (10–12). Moreover, intriguingly, cases attributed to WNK1 mutations in this autosomal dominant disorder are due to intronic deletions and are not recognized as directly affecting WNK1 coding sequence (8).

It is of great interest how such WNK1 mutations, in a widely expressed gene, cause an autosomal dominant disease, with a mechanism seemingly explicable by a distal nephron–limited ion transport defect (2,13). One possibility sees the intronic region involved in transcriptional regulation, and some preliminary evidence maintains this as a reasonable explanation. Alternatively, this apparently "silent" mutation may alter the complement of spliced products transcribed from the gene. Such silent mutations have been shown to cause dominant diseases by altering splicing, *e.g.*, in the fibrillin-1 gene, causing Marfan syndrome (14). Thus, evidence relating to promoter use and alternative splicing of WNK1, especially relating to kidney, is of interest.

The study presented here describes, in some detail, several isoforms produced from the *WNK1* gene, some of which show strikingly different tissue-specific distributions, including one showing abundant expression in kidney that is seen at low level, if at all, in other tissues. Such modifications, generating this transcriptional diversity, also produce predicted proteins of very different structure and proposed function. The findings reported thus help elucidate not only probable mechanisms by which the WNK1 intronic deletions cause disease, but also further clarify the novel WNK1 BP control pathway.

Received May 29, 2003. Accepted July 5, 2003.
Correspondence to Dr. Roger W. Brown, Molecular Medicine Centre, Western General Hospital, Edinburgh, EH4 2XU, United Kingdom. Phone: 0044-131-651-1024/1037; Fax: 0044-131-651-1085; E-mail: Roger.Brown@ed.ac.uk
1046-6673/1410-2447
Journal of the American Society of Nephrology
Copyright © 2003 by the American Society of Nephrology
DOI: 10.1097/01.ASN.0000089830.97681.3B

Copyright © American Society of Nephrology. Unauthorized reproduction of this article is prohibited.

Materials and Methods

Northern Blot Analysis

Total RNA was extracted in TRIzol Reagent (Invitrogen, Inchinnan, UK) and separated (15 μg/lane) by denaturing (formamide/formaldehyde) agarose electrophoresis (0.8%), and blotted onto Hybond-N^+ membrane (Amersham Biosciences, Little Chalfont, UK). Blots were hybridized with PCR-amplified mouse WNK1 (mWNK1) DNA fragments, radiolabeled with ^{32}P-dCTP (Rediprime II Random Prime Labeling System, Amersham Biosciences, UK), at 65°C overnight in hybridization buffer (0.5 M Na_2PO_4·NaH_2PO_4 pH 7.2/7% SDS with 100 μg/ml denatured salmon sperm and 20 μg/ml yeast tRNA). Washes were at 65°C with 50 mM Na_2PO_4·NaH_2PO_4 pH 7.2/1% SDS. Blots were exposed to Kodak x-ray film (BioMax MS-1; Sigma, Poole, UK) at −70°C. cDNA templates for Northern blot probe production were PCR amplified with primers as detailed in Table 1 and Figures 1 and 2.

RT-PCR

Promega Reverse Transcription System (random primed) (Promega, Southampton, UK) generated PCR templates (5 μl, diluted 1:20), used in standard PCR reactions, denaturing at 95°C for 3 min, then incubating on ice, and adding 15 pmol each primer, 250 μmol dNTP, and 2 U *Taq* DNA Polymerase (Promega) to a final volume of 50 μl in 1× PCR buffer. The PCR program used was as follows: 3 min at 95°C, then 35 to 40 cycles of 60 s at 95°C, 60 s at 60°C, 120 s at 72°C, and finally 10 min at 72°C. For negative controls, template was replaced with water. Products were visualized by agarose gel electrophoresis and purified with QIAquick PCR Purification Kit (Qiagen, Crawley, UK).

Production of Single-Stranded RNA Probes

RNA probes for *in situ* hybridization (ISH) analysis, produced as described previously (15) to specific regions of mWNK1, used a nested PCR method with primers, including 5' extensions containing phage polymerase consensus sites, with sense and antisense primer pairs incorporating T3 (TCTAGATTAACCCTCACTAAAGGGA) and T7 (GGATCCTAATACGACTCACTATAGGG) sites, respectively. The PCR program used was as follows: 5 cycles of 45 s at 95°C, 45 s at 55°C, 120 s at 72°C, followed by 30 cycles of 45 s at 95°C, 45 s at 69°C, and 120 s at 72°C, and finally 10 min at 72°C. The required DNA-dependent RNA phage polymerase (T3-sense, T7-antisense) was then used on these purified PCR products to produce single-stranded ^{35}S-UTP–labeled RNA probes of the corresponding inserts for ISH, as described elsewhere (15).

Table 1. Primer sequences

Primer	Sequence (5′-3′)[a]	Orientation	Position[b]
P1	CTTGTCAGTGCTGAGTGGGAGTC	Sense	1
P2	CAGATTTTGTTAACTTTCGATCCTGCAATTC	Antisense	938
P3	GTTGTGAGCTGTGTGTGAAAGATAAGG	Sense	8439
P4	CAGACCTCACTCAGAATGACTAAACC	Antisense	9313
P5	GTATCCGACAAAACAAAGATGAAAGATATTCC	Sense	1523
P6	CTGTATTCCCTGCTGCTGAGGATG	Antisense	2382
P7	CTAGTATATCTGTGTTGTCTGATGGAACC	Sense	2084
P8	GTCATTGTTCACCATAATTGTTGCTATCTC	Antisense	3633
P9	AGAAACTACTAGTAGCAAAATCCCTGTC	Sense	Figure 1c
P10	GCTTCACTCCCTCATTTATACAATCC	Antisense	Figure 1c
P11	CCAAGGCAGTGGGAATGTCCAATG	Sense	773
P12	CGTTTTCTCTTAATTAAGGACACCCTATC	Antisense	1853
P13	GTCGCTTTCTCAAATTTGACATCGAAATC	Sense	799
P14	CTTTGATAGCTTTAGCCATGGTCTTGTG	Antisense	1825
P15	GCAGGATCGAAAGTTAACAAAATCTGAAAG	Sense	903
P16	ACGTCTTAAGTGTTCCAGATGTCATTAG	Antisense	1081
P17	GAAAATCAAAGTTTTAAGAAGCTGGTGTC	Sense	1104
P18	TCTTGGCAAAAGAAGCCCGCTTTAGAG	Antisense	1291
P19	ACCCCAGAGTTTATGGCTCCTGAG	Sense	1303
P20	CACTCCACTGGTCACTCGAC	Antisense	1464
P21	GTGGAGTGAAGCCAGCCAGTTTTG	Sense	1457
P22	GAATATCTTTCATCTTTGTTTTGTCGGATAC	Antisense	1553
P23	GACCTTTTGAACCATGCCTTTTTCCAG	Sense	1587
P24	CTCAACCATTTCTTGAGCAACATCTTCTG	Antisense	1773
P25	TCTAGATTAACCCTCACTAAAGGGACTTCCAGTTTCCCAGACAG	Sense	2497
P26	GGATCCTAATACGACTCACTATAGGGTACAAAACATCTCCAGAGG	Antisense	2956
P27	TCTAGATTAACCCTCACTAAAGGGAGCTTCCCATCTCGACTG	Sense	2960
P28	GGATCCTAATACGACTCACTATAGGGCTCCAGAACTGCTTGCTG	Antisense	3243

[a] Primer sequences are based on mouse WNK1 sequence (accession no. AY309076).
[b] Primer position refers to the position of the most 5′ base according to the orientation of the primer.

Copyright © American Society of Nephrology. Unauthorized reproduction of this article is prohibited.

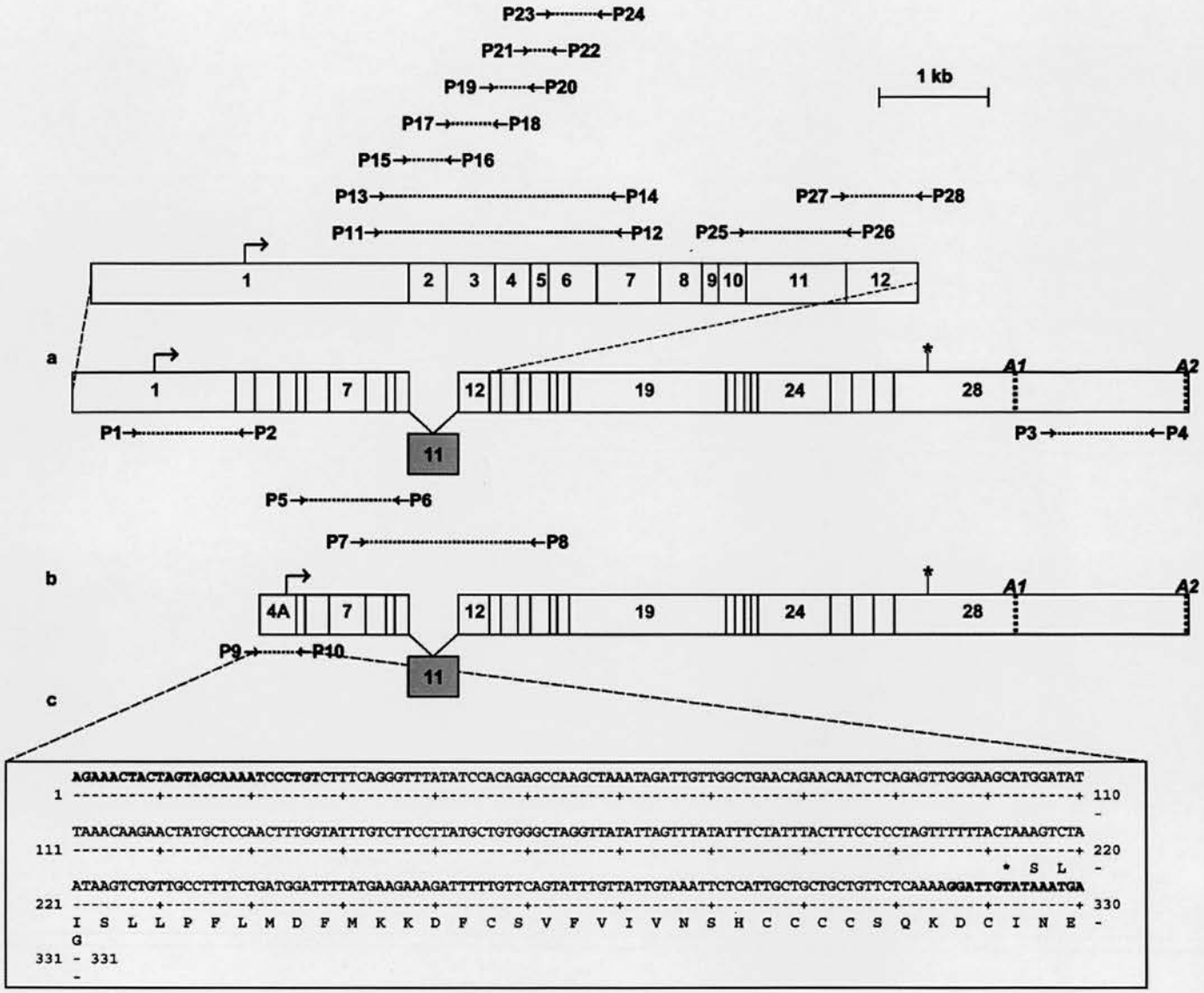

Figure 1. Schematic representation of WNK1 cDNA structure showing primer positions. (a and b) cDNA structure of WNK1 and kidney-specific WNK1 containing exon 4A, respectively, with vertical bars representing splice junctions and dashed vertical bars indicating 3' polyadenylation sites *A1* and *A2*. Numbers within rectangles refer to exon numbers. Primers are represented by arrows and are numbered P1 to P28. Additional primer details are given in Table 1. Horizontal dashed lines specify the cDNA region amplified by PCR with the corresponding primer pairs. (c) cDNA sequence of exon 4A (accession no. AY319934). The predicted amino acid sequence also shown would continue in frame across the splice site to exon 5.

ISH Analysis

ISH, as described previously (15,16), used cryostat sections (10 μm) cut from adult mouse kidney and mouse embryo samples (gestation day 16.5) mounted on silane-coated glass microscopic slides. Slides were fixed in 4% paraformaldehyde, incubated with prehybridization buffer at 50°C, hybridized with denatured ^{35}S-UTP–labeled RNA probes (at a final concentration of approximately 10×10^6 cpm/ml in hybridization buffer at 50°C for approximately 16 h), followed by washes in 2× SSC, treatment with RNase A, and further washes to a maximum stringency of 0.1× SSC at 60°C. After ethanol series dehydration, slides were exposed to Kodak x-ray film (BioMax MR-1; Sigma). Slides were then emulsion dipped and exposed in a light-tight box for 3 to 5 wk before being developed.

Results

The mouse *WNK1* gene (mWNK1) is large, spanning >100 kb, with a coding region showing 86% identity with human *WNK1* (hWNK1). mWNK1 produces large transcripts (>10 kb) with cDNA encoded by 28 exons (Figure 1a), having a predicted 2377 amino acid protein. Northern blot hybridization with exons 6 to 9 revealed widespread distribution of these large transcripts (Figure 2a) with high expression seen in testis > heart, lung, kidney, placenta > skeletal muscle, brain, and low-level expression elsewhere. Additional Northern blots show placental transcripts are of similar size to the major widely found isoform. In kidney, a smaller, more abundant

Copyright © American Society of Nephrology. Unauthorized reproduction of this article is prohibited.

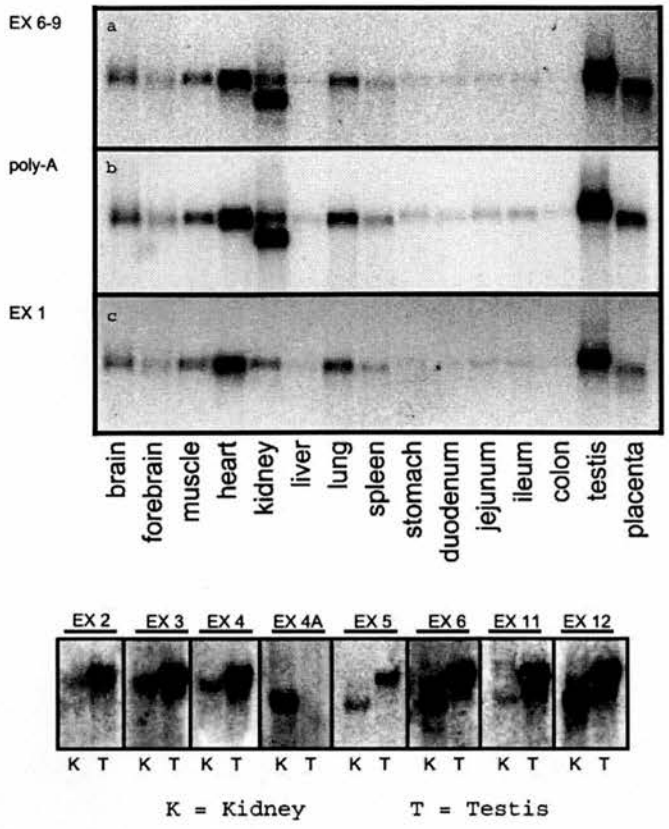

Figure 2. Northern blot analysis of WNK1 expression. Hybridization with a probe incorporating exons 6 to 9 (a) detects widespread expression of large transcripts approximately 10.2 kb in size. In addition, smaller and more prominent transcripts are detected in kidney. This expression profile is also observed in (b) when hybridizing with the poly-A probe (refers to sequence located between the two 3' polyadenylation signals *A1* and *A2*). (c) Probing with exon 1 fails to detect the smaller kidney-specific transcripts. (d) Northern blot analysis reveals differential expression of individual exons in WNK1 isoforms in kidney (K) and testis (T). Hybridization with probes against exons 2, 3, 4, 5, and 6 detect the large WNK1 isoform, strongly in testis but weakly in kidney. The smaller and more abundant kidney-specific isoform is only detected by probes to exons 5 and 6. A probe to an alternative exon, 4A, detects the smaller kidney-specific isoform only. Hybridization with a probe to exon 11 detects the large WNK1 isoform in testis but signal is low for either isoform in kidney. In contrast, hybridization with exon 12 readily detects both the kidney-specific isoform and the large WNK1 testis isoform. WNK1 expression was studied across a range of adult mouse tissues and in placenta (E16.5). Probe templates were PCR amplified with the following primer pairs: exons 6 to 9, P5/P6 (860 bp); poly-A, P3/P4 (875 bp); exon 1, P1/P2 (928 bp); exon 2, P15/P16 (180 bp); exon 3, P17/P18 (187 bp); exon 4, P19/P20 (161 bp); exon 4A, P9/P10 (340 bp); exon 5, P21/P22 (96 bp); exon 6, P23/P24 (212 bp); exon 11, P25/P26 (462 bp); and exon 12, P27/P28 (278 bp). For primer positions and sequences, refer to Figure 1 and Table 1, respectively.

mWNK1 transcript is seen differing by at least 1.5 to 2 kb (Figure 2a). A 3'-polyadenylation (poly-A) site *A1* (Figure 1) is positioned approximately 800 bp downstream of the open reading frame (ORF). To assess whether the use of an alternative poly-A site could account for this size difference, we isolated cDNA sequence encoding a second poly-A site approximately 2400 bp downstream of the ORF (Figure 1, *A2*). Northern blot hybridization with cDNA between these poly-A sites revealed a similar expression profile to that described above (Figure 2b). Both transcripts in kidney were detected implying most WNK1 transcripts terminate at the second 3' poly-A site (Figure 1, *A2*). Having excluded this possibility, an exon 1 probe, overlapping the ORF (Figure 1), was designed against the 5' region. Northern blot hybridization with exon 1 revealed a similar expression profile for the large mWNK1 transcript, but the smaller kidney-specific transcript remained completely undetected, indicating it lacks exon 1 (Figure 2c).

To investigate whether this kidney-specific isoform lacked further 5' exons, nested PCR was used to produce probes against exons 2, 3, 4, 5, and 6 (Figure 1), ensuring amplification of mWNK1 cDNA only (confirmed by sequencing) across this highly conserved kinase domain region. Northern blot analysis of kidney and testis RNA showed probes to exons 2, 3, and 4 only detect the large mWNK1 transcript and not the smaller kidney-specific isoform (Figure 2d). In contrast, exon 5 and 6 probes detect both mWNK1 transcripts. Thus, the smaller mWNK1 transcript in kidney lacks exons 1 to 4. Screening submitted expressed sequence tag (EST) databases suggested an alternative exon preceding exon 5 in kidney, positioned between exons 4 and 5 in the genomic sequence and therefore termed exon 4A. Northern blot hybridization with this exon only detects the smaller mWNK1 transcript (Figure 2d), confirming inclusion of exon 4A in the kidney-specific isoform (Figure 1b).

ISH to exons 6 to 9 allowed detailed study of mWNK1 expression in mouse kidney. Figure 3 reveals clear WNK1 expression above background in distal nephron extending from early distal convoluted tubule (DCT) into connecting tubule and at lower level into cortical collecting duct (lower expression in medullary rays; Figure 3). Strong expression in DCT continues adjacent to glomeruli and is seen looping close to their vascular pole (Figure 3 right panels) the site of the macula densa. Additionally, lower expression, above background, is distributed more extensively. This appears to have a different origin from the higher expression seen in DCT (*i.e.,* different WNK1 transcripts; see below).

To investigate the distribution of the two kidney isoforms, adult kidney sections were hybridized with exons 1, 4A, and 6 to 9 (Figure 4, top left panel). Probing with exon 1 detects widespread signal at a low level (Figure 4a), whereas with exon 4A, only strong punctate signal in cortex is detected (Figure 4c). The expression pattern seen with exons 6 to 9 is thus a combination of that seen with exons 1 and 4A (Figure 4e). These probes were also hybridized to embryo tissue slices (E16.5) to examine developmental mWNK1 expression. Probing with exons 6 to 9 revealed a wide mWNK1 distribution, with high expression in tissues—for example, placenta, nasal epithelium, lung, intestine, regions of the brain, and developing renal cortex (Figure 4f). As expected, the expression patterns revealed by probing with exons 1 and 4A were subtypes of that seen for exons 6 to 9,

Copyright © American Society of Nephrology. Unauthorized reproduction of this article is prohibited.

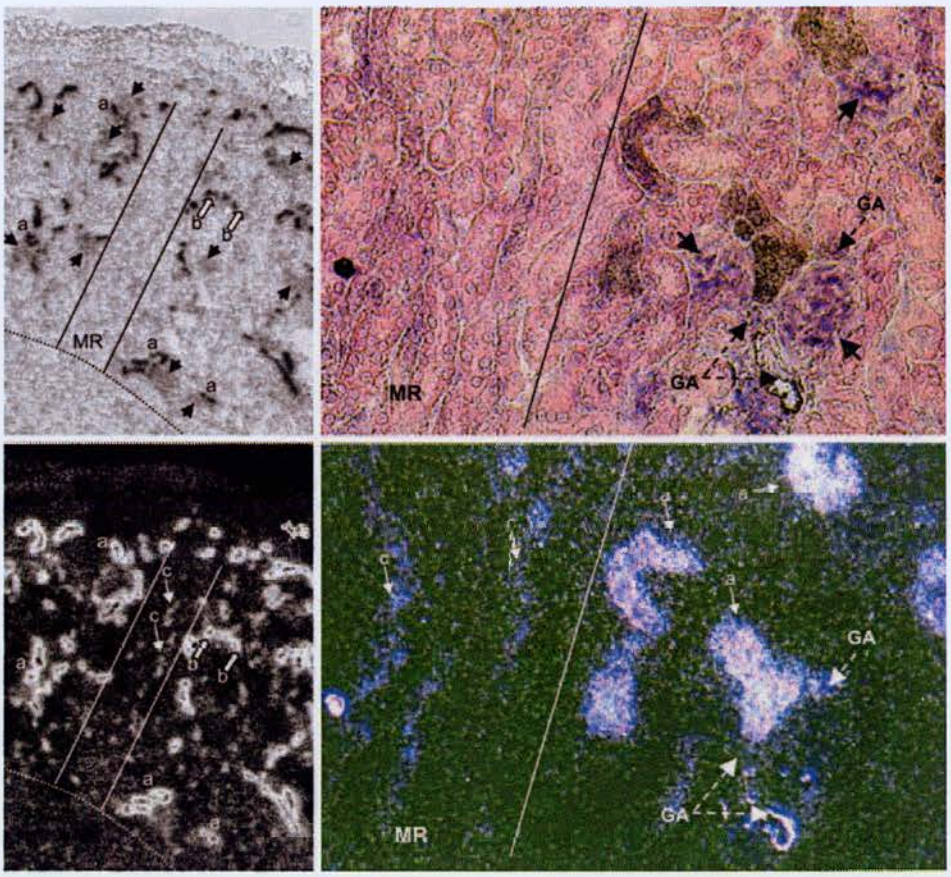

Figure 3. In situ hybridization (ISH) of WNK1 in mouse kidney. The ISH study used a probe to WNK1 exons 6 to 9. Images are of emulsion-dipped slides (eosin/cresyl violet counterstain; original magnification: left, ×40; right, ×200). View of renal cortex with a medullary ray (MR) demarcated between the parallel lines and cortical labyrinth lateral to them. Below the dashed line is the outer medulla. Bright field on top (black, strong expression), corresponding dark field view on bottom (white, expression). The very highest expression—showing black on bright field—obscures light, and hence the strongest expressing tubules appear as black holes with ring outlines on dark field view (bottom left). Short black arrows indicate glomeruli; a, examples of distal convoluted tubules (DCT) largely adjacent to glomeruli; b, example of connecting tubules (CNT) in midcortical labyrinth arcades (adjacent to radial vessels); c, cortical collecting duct (CCD) in medullary rays; and GA, glomerular arteriole. (left) Study with long exposure (5 wk) demonstrating wide range of expression level. Note regional expression at 3 levels: (*1*) widespread low level (low level white seen in darkfield), (*2*) higher in CCD (faint but distinct tubular outline seen on dark field, pale gray on bright field); and (*3*) highest in DCT and CNT (darker gray-black on bright field and bright ring with black hole center when silver grains confluent). (right) Three-week exposure: note the proximity of strongly expressing DCT to glomerulus and its vascular pole (between arterioles) and stronger expression than in collecting duct.

with exon 1 widely expressed, particularly in placenta, lung, kidney, intestine, thymus, and forebrain (Figure 4b), whereas exon 4A revealed much lower expression, with high signal detected in restricted regions (*e.g.*, nasal epithelium, forebrain, thymus, and kidney; Figure 4d). Sense control sections showed no specific hybridization (Figure 4).

EST sequences suggest that alternative splicing of mWNK1, primarily concerning exons 11 and 12, takes place in some tissues (Figure 1). To investigate this, we subjected kidney and testis RNA to Northern blot analysis with probes specific for each exon. Hybridization with exon 11 detects the large mWNK1 isoform in testis, but signal is greatly diminished for either isoform in kidney (Figure 2d), suggesting exon 11 is usually spliced out in both kidney mWNK1 transcript classes. In contrast, hybridization with exon 12 shows strong signal for mWNK1 in testis and for the smaller kidney-specific transcript. The large mWNK1 transcript in kidney is also detected at a lower level (Figure 2d). To investigate tissue-specific and developmental variations in these splicing events, we subjected adult mouse kidney and fetal (E16.5) sections to ISH analysis. The expression patterns seen when probing adult kidney sections with either exon are similar to that described above for exons 6 to 9, showing low-level, widespread expression throughout the kidney, overlaid with strong punctate cortical expression (Figure 4, g and i). However, developmental expression studies that use these probes indicate that although many fetal tissues express both exons similarly, striking tissue-specific splicing occurs in some developing organs. For example, transcripts containing exon 11 are abundant in some neural tissues but are rare or absent in placenta (Figure 4, h and j). Sense-control sections showed no specific hybridization (Figure 4).

Copyright © American Society of Nephrology. Unauthorized reproduction of this article is prohibited.

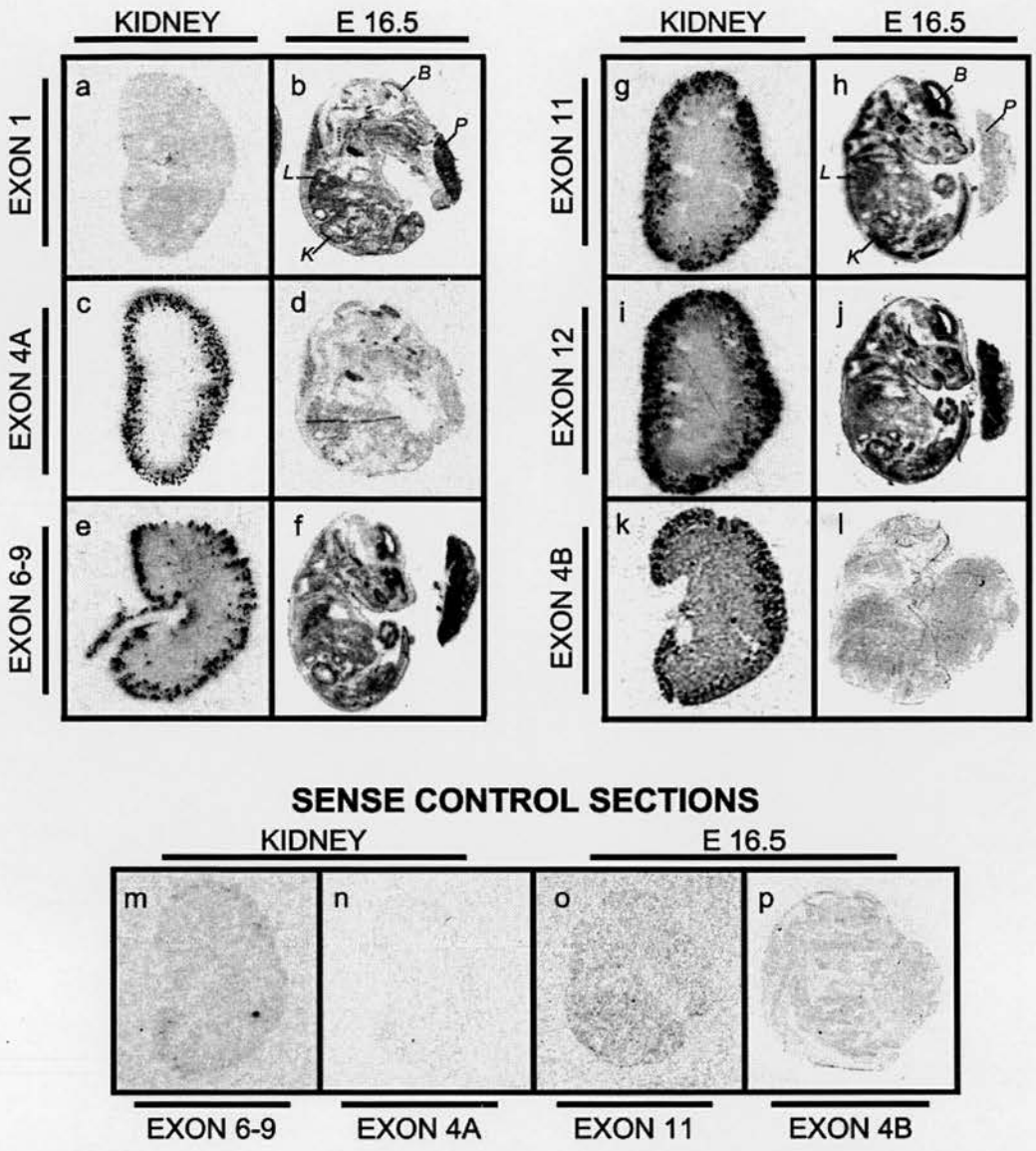

Figure 4. Analysis of WNK1 expression by *in situ* hybridization (ISH) of mouse adult kidney and fetal sections (E16.5). Cryostat sections were subjected to ISH analysis; a range of probes against WNK1 were used. Left columns of top panels show local distribution within the kidney (a, c, e, g, i, and k). Right columns of top panels show corresponding developmental expression patterns (b, d, f, h, j, and l). Bottom panel shows sense controls for both kidney (m and n) and fetal (o and p) sections. Probes were constructed against exon 1 (434 bp), exon 4A (280 bp), exons 6 to 9 (552 bp), exon 11 (460 bp), exon 12 (283 bp), and exon 4B (108 bp). Exposure times for detection of ISH signal were as follows: exon 1, (a and b) 1 d; exon 4A, (c) 1 d, (d) 4 d, (n) 1 wk; exon 6 to 9, (e and f) 1 d, (m) 3 d; exon 11, (g, h, and o) 3 d; exon 12, (i and j) 3 d; exon 4B, (k, l, and p), 2.5 wk. For details of probe lengths and production, see Materials and Methods. B indicates brain; K, kidney; L, lung; and P, placenta.

Reverse transcriptase–PCR (RT-PCR) studies across exons 11 and 12 confirm these splicing events (Figure 5a). Amplification in kidney by means of primers spanning the exon 7/8 splice site down to the exon 15/16 splice site shows two major bands, corresponding in size to PCR products having either exon 11, or both exons 11 and 12 spliced out (Figure 5b). Additional RT-PCR studies that use alternative primers spanning this region also show major bands, similarly representative of these splice variants. However, it is difficult to interpret the importance of additional large weak products occasionally amplified by RT-PCR.

EST sequences also suggest that in addition to exons 4 and 4A, a third exon positioned between exons 4A and 5 in the mouse genomic sequence and therefore termed 4B, may precede exon 5 in some mWNK1 transcripts (accession no. AK052468). The EST evidence suggests that unlike the kidney-specific transcripts described above containing exon 4A, which lack all known upstream exons, transcripts containing 4B splice directly from exon 4 to 4B to 5. ISH analysis probing with exon 4B shows a similar pattern to that seen previously in kidney, with high cortical expression overlaying a low widespread distribution (Figure 4k). How-

Copyright © American Society of Nephrology. Unauthorized reproduction of this article is prohibited.

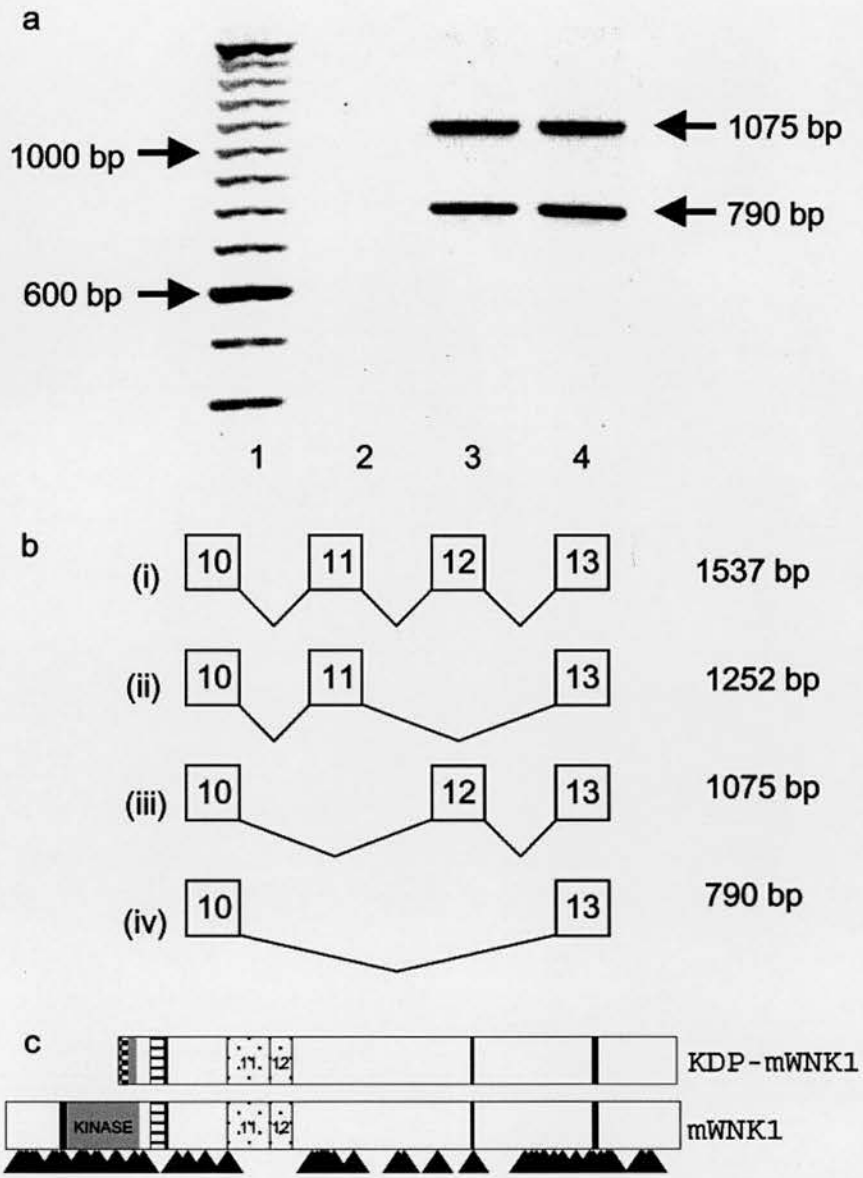

Figure 5. Detection of WNK1 alternative splicing. (a) Ethidium bromide–stained agarose gel, showing reverse transcriptase–PCR–amplified fragments in duplicate. These products were amplified with mWNK1 primer pair P7 and P8, which span a region from the exon 7/8 splice site down to the exon 15/16 splice site (lanes 3 and 4). A negative control is seen in lane 2. Lane 1 shows a 100-bp DNA ladder. (b) Schematic depiction of WNK1 alternative splicing involving exons 11 and 12. The major products seen correspond to (b) (iii) and (b) (iv). (c) Schematic representation of the major predicted WNK1-derived proteins. mWNK1 is 2377 amino acids in length and is particularly rich in serine, glutamine, and proline, having 26 PXXP sites potentially recognized by SH3 domains. Black bars denote four putative coiled coil domains, and a conserved WNK autoinhibitory domain is represented by horizontal stripes. Black arrowheads indicate the positions of all potential phosphorylation sites; intriguingly none of which overlap with the region encoded by exons 11 and 12. Exon 11 encodes a leucine zipper (LXXLL) motif. Kinase-deficient (KDP) WNK1 has a truncated N-terminus, lacking one coiled coil domain and deleting a major portion of the kinase domain. This region is substituted with a highly cysteine-rich stretch of 30 amino acids.

ever, splicing events producing transcripts containing exon 4B appear to be rare, judged by the lower ISH signal (requiring severalfold longer for clear detection). Furthermore, signal detected on fetal sections was low and widespread, lacking the striking tissue-specific differences in expression levels seen with probes to other exons (Figure 4l), and was only marginally higher than that seen for sense controls (Figure 4p).

As described above, Northern blot studies examining exon 11 expression detect very weak signal for both isoforms in kidney, despite high expression in testis. In contrast, ISH studies suggest exon 11 is expressed at levels comparable with exon 12 in kidney. This discrepancy led to further Northern blot analysis looking for evidence of further novel mWNK1 kidney transcripts containing exon 11. These studies revealed at least two novel mWNK1 transcripts in kidney and testis,

Copyright © American Society of Nephrology. Unauthorized reproduction of this article is prohibited.

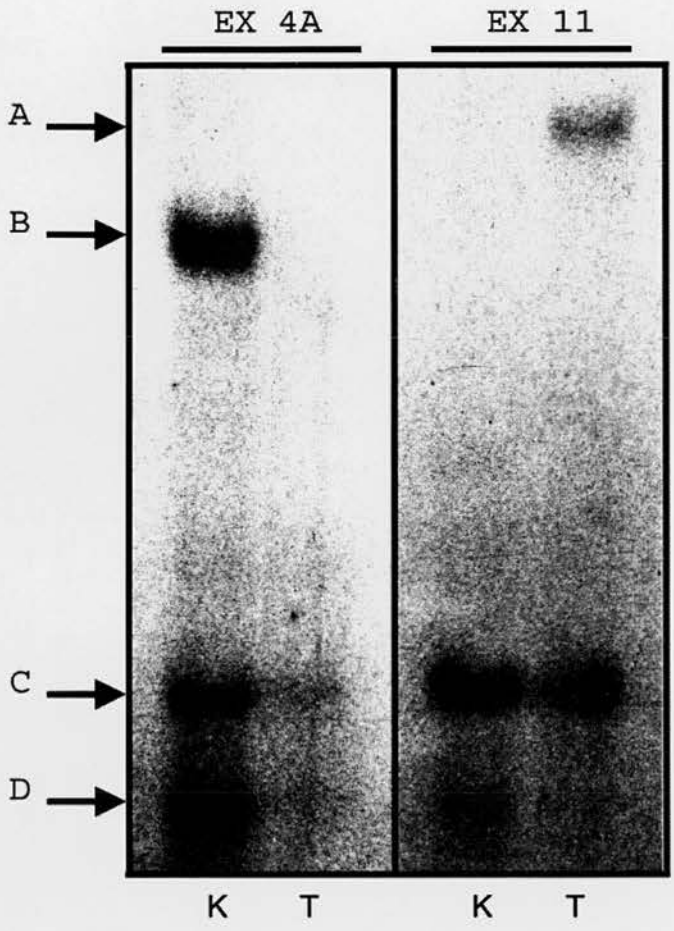

Figure 6. Detection of smaller WNK1 transcripts in kidney and testis by Northern blot (short exposure). Probes to exon 4A detect the kidney-specific WNK1 transcript (B), but also reveal two additional transcripts several kilobases smaller (C and D) in both kidney (K) and testis (T). These transcripts are also seen when probing with exon 11, which also detects the large WNK1 transcript (A) as expected.

evidently several kilobases smaller than the two isoforms described above (Figure 6). Intriguingly, transcripts of similar size were detected in additional Northern blot analysis of exon 4A expression in both tissues (Figure 6).

Discussion

In this study, we show multiple WNK1 mRNA species are expressed in both adult mouse and during development, with some showing striking tissue-specific expression differences. Large transcripts—greater than 10 kb in size—were seen by Northern blot in virtually all tissues examined, with expression highest in testis > heart, lung, kidney, placenta > skeletal muscle, brain. Transcripts detected in testis appeared larger than transcripts common to most other tissues, attributed to the inclusion of exon 11 (462 bp). The major transcripts seen in kidney, however, were smaller than elsewhere. This phenomenon has been reported in previous studies (8) and appears to be conserved between species. We have demonstrated that the difference between these transcripts is not the result of the use of an alternative 3' polyadenylation site, as previously suggested (8,9,17,18). Instead, we show that the first four exons in the smaller, more prominent kidney transcripts are replaced by an alternative exon, exon 4A (19). The sequence of this novel exon and the resulting predicted amino acid sequence are presented for the first time (Figure 1c). ISH analysis revealed strong punctate expression of these smaller transcripts restricted to cortex, localizing to distal nephron, whereas the large transcripts showed uniform low-level expression throughout the kidney. These expression patterns are combined in that seen for exons 6 to 9, found in both transcript classes. In addition to exons 4 and 4A, another novel exon, exon 4B, was found to precede exon 5 in some WNK1 kidney transcripts; however, weak ISH signal suggests that this is a rare splicing event.

Use of exon-specific primers identified two relatively abundant, alternatively spliced mWNK1 mRNAs in kidney, corresponding in size to transcripts lacking either exon 11 or both exon 11 and 12. Alternative splicing of these exons has also been reported for hWNK1 (17). Furthermore, the published rat WNK1 sequence (accession no. NM_053794) corresponds to the splice variant lacking both exons. Exon-specific ISH detected expression in kidney, with probes to both exons showing a similar pattern to that described above for exons 6 to 9. In contrast, Northern blot analysis showed that although exon 12 is usually included in the small abundant kidney isoform, exon 11 is largely absent in both kidney isoforms. Further studies indicate the production of substantial levels of novel smaller alternatively spliced transcripts from the *WNK1* gene, with Northern blot analysis implicating the inclusion of both exons 11 and 4A. These smaller transcripts are seen in kidney but also in testis, a tissue in which exon 4A expression was previously unsuspected because testis lacks obvious expression of the much larger "kidney-specific" 4A transcript. Preliminary investigations suggest that these transcripts differ from this largely kidney-specific 4A transcript, described above, being much smaller in size. However, RT-PCR in testis easily amplifies a product from exon 4A to exon 11, suggesting these smaller transcripts contain this region.

This study was the first to assess WNK1 expression in development by means of ISH analysis, demonstrating that WNK1 is widely expressed in the mouse embryo (E16.5), in both epithelial tissues (*e.g.*, developing renal cortex, intestine, lung, nasal epithelia, and placenta) and in nonepithelial tissues (*e.g.*, regions of the CNS). Again, there are tissue-specific differences in the pattern of transcripts expressed in developing organs, with transcripts containing exon 1 showing high widespread but nonuniform expression and exon 4A–containing transcripts showing high expression only in restricted sites. Exon-specific ISH also showed striking tissue-specific differences in expression of exons 11 and 12—for example, transcripts containing exon 11 are abundant in some neural tissues but are very low or absent in placenta.

It is appropriate to suggest that WNK1 regulates ion transport through the kinase domain. However, the major WNK1 transcript in kidney lacks this functional entity as a result of the replacement of exons 1 to 4 with exon 4A (Figure 5c). Additionally, a coiled coil motif predicted just N-terminal to the

Copyright © American Society of Nephrology. Unauthorized reproduction of this article is prohibited.

kinase domain is lost, possibly disrupting interactions with molecular targets. This implies that the remainder of the WNK1 protein must contribute functionally to the WNK1 regulatory pathway. Exons 11 and 12 are of key interest because splicing of this region is conserved between species, is clearly tissue specific, and would produce a repertoire of proteins likely to be coexpressed in the same tissues and probably the same cells (Figure 4). The predicted amino acid sequence encoded by these exons is proline rich (approximately 15%), and analysis suggests a potential transmembrane span flanked by a flexible conformation. This region also shows homology to a number of extracellular matrix proteins (*e.g.*, mucins, glycosaminoglycans, and sialoproteins). Clearly, this is of interest in the context of proteins that may play a role in tight junction regulation. Conversely, when this stretch of amino acids is removed, these features disappear. The resulting juxtaposed sequence is predicted to form an exposed loop region with homology to proteins that tend to bind ligands and/or act as transcription factors. Intriguingly, although WNK1 contains numerous potential phosphorylation sites, no such site occurs within the exon 11 to 12 region, implying that signaling through protein kinase pathways acting on WNK1 is not affected by such splicing events. Clearly, experimental studies are required to fully investigate these possibilities.

Also of interest is the addition of thirty amino acids to the N-terminus of kinase-deficient (KDP) WNK1, contributed by exon 4A. This exon may have no major functional effect other than deleting the kinase domain. However, this sequence is strikingly cysteine rich. Within a cluster of six likely very reactive cysteine residues, at least three have a high predictive index for forming either disulfide bonds or bonds with other molecules (*e.g.*, metal-containing moieties). Moreover, the N-terminal positioning of this cysteine cluster may promote this region as a potential point of anchorage to other structures. Furthermore, the novel small bands seen by Northern blot clearly indicate the production of WNK1 transcripts lacking several kilobases compared with the kidney-specific 4A band. Therefore, it is very likely that additional changes in WNK1 protein structure exist that have profound effects on WNK1 function.

The transcriptional modifications described above would greatly influence the potential complement of proteins produced from the *WNK1* gene and may have evolved to regulate WNK1 function. KDP-WNK1 proteins may act to inhibit other WNK1 proteins, having "active" kinase domains, via interactions through the remaining coiled-coil motifs (Figure 5c). This is supported by the recent report of a WNK1 autoinhibitory domain, positioned between residues 515 to 569 in the rat sequence, which is conserved between species and also within the WNK family (Figure 5c). Preliminary evidence was also reported for WNK1 tetramer formation via the coiled-coil motif C-terminal to the autoinhibitory domain (Figure 5c) (20).

This work provides a number of insights into the cause of Gordon syndrome. We have examined WNK1 expression in some detail, further elucidating kidney-specific and distal-nephron–specific WNK1 transcripts. Our findings imply the use of alternative promoters, one initiating transcription in exon 1 and the second giving rise to transcripts having exon 4A in place of exons 1 to 4. It is therefore reasonable to suggest that *cis* elements within intron 1 affect the second promoter regulating such 4A transcripts. Dominant negative regulation would imply that intronic deletions causing Gordon syndrome lead to abnormally high expression of KDP-WNK1 transcripts in kidney, in turn causing excessive inhibition of "normal" WNK1 function. Alternatively, the intron 1 deletions could interrupt splicing enhancer or silencer sequences, thereby affecting the inclusion or exclusion of exons and disrupting the complement of alternatively spliced WNK1 transcripts. A similar effect is seen in Marfan syndrome, another autosomal dominant disorder affecting connective tissue, where a silent mutation results in exon skipping (14). In ataxia-telangiectasia, an intronic deletion in the *ATM* gene results in aberrant inclusion of a cryptic exon (21).

The pathway disrupted in Gordon syndrome involving WNK1 is regarded as different from other signaling pathways known to regulate BP. The findings presented here reveal the central importance of the transcriptional control of this gene in generating a complement of kidney-specific, WNK1-derived proteins. The correct balance within this complement of proteins must mediate the effects on ion transport that constitute this novel BP regulatory pathway. Clearly the regulation of alternative promoter use and splicing is likely to participate in the control of BP by WNK1-derived proteins.

Acknowledgments

We thank Susan K. Coan for her technical assistance, and we thank the Wellcome Trust (grant 065616; PhD Studentship to MOR) and the British Heart Foundation (grant PG2001075) for their support.

References

1. Gordon RD: Syndrome of hypertension and hyperkalemia with normal glomerular filtration rate. *Hypertension* 8: 93–102, 1986
2. Gordon RD, Klemm SA, Tunny TJ, Stowasser M: Gordon's syndrome: A sodium-volume–dependent form of hypertension with a genetic basis. In: *Hypertension: Pathophysiology, Diagnosis, and Management*, 2nd Ed., edited by Laragh JH, Brenner BM, New York, Raven Press, 1995, pp 2111–2123
3. Schambelan M, Sebastian A, Rector FC Jr: Mineralocorticoid-resistant renal hyperkalemia without salt wasting (type II pseudohypoaldosteronism): Role of increased renal chloride reabsorption. *Kidney Int* 19: 716–727, 1981
4. Bonny O, Rossier BC: Disturbances of Na/K balance: Pseudohypoaldosteronism revisited. *J Am Soc Nephrol* 13: 2399–2414, 2002
5. Estevez R, Boettger T, Stein V, Birkenhager R, Otto E, Hildebrandt F, Jentsch TJ: Barttin is a Cl^- channel beta-subunit crucial for renal Cl^- reabsorption and inner ear K^+ secretion [Comment]. *Nature* 414: 558–561, 2001
6. Lifton RP, Gharavi AG, Geller DS: Molecular mechanisms of human hypertension. *Cell* 104: 545–556, 2001
7. Hubner CA, Jentsch TJ: Ion channel diseases. *Hum Mol Genet* 11: 2435–2445, 2002
8. Wilson FH, Disse-Nicodeme S, Choate KA, Ishikawa K, Nelson-Williams C, Desitter I, Gunel M, Milford DV, Lipkin GW, Achard JM, Feely MP, Dussol B, Berland Y, Unwin RJ, Mayan H, Simon DB, Farfel Z, Jeunemaitre X, Lifton RP: Human

Copyright © American Society of Nephrology. Unauthorized reproduction of this article is prohibited.

hypertension caused by mutations in WNK kinases. *Science* 293: 1107–1112, 2001
9. Xu B, English JM, Wilsbacher JL, Stippec S, Goldsmith EJ, Cobb MH: WNK1, a novel mammalian serine/threonine protein kinase lacking the catalytic lysine in subdomain II. *J Biol Chem* 275: 16795–16801, 2000
10. Yang CL, Angell J, Mitchell R, Ellison DH: WNK kinases regulate thiazide-sensitive Na-Cl cotransport. *J Clin Invest* 111: 1039–1045, 2003
11. Rossier BC: Negative regulators of sodium transport in the kidney: Key factors in understanding salt-sensitive hypertension? *J Clin Invest* 111: 947–950, 2003
12. Wilson FH, Kahle KT, Sabath E, Lalioti MD, Rapson AK, Hoover RS, Hebert SC, Gamba G, Lifton RP: Molecular pathogenesis of inherited hypertension with hyperkalemia: The Na-Cl cotransporter is inhibited by wild-type but not mutant WNK4. *Proc Natl Acad Sci U S A* 100: 680–684, 2003
13. Meneton P, Oh YS, Warnock DG: Genetic renal tubular disorders of renal ion channels and transporters. *Semin Nephrol* 21: 81–93, 2001
14. Liu W, Qian C, Francke U: Silent mutation induces exon skipping of fibrillin-1 gene in Marfan syndrome. *Nat Genet* 16: 328–329, 1997
15. MacDonald P, MacKenzie S, Ramage LE, Seckl JR, Brown RW: Corticosteroid regulation of amiloride-sensitive sodium-channel subunit mRNA expression in mouse kidney. *J Endocrinol* 165: 25–37, 2000
16. Brown RW, Chapman KE, Kotelevtsev Y, Yau JL, Lindsay RS, Brett L, Leckie C, Murad P, Lyons V, Mullins JJ, Edwards CR, Seckl JR: Cloning and production of antisera to human placental 11 beta- hydroxysteroid dehydrogenase type 2. *Biochem J* 313[Pt 3]: 1007–1017, 1996
17. Verissimo F, Jordan P: WNK kinases, a novel protein kinase subfamily in multi-cellular organisms. *Oncogene* 20: 5562–5569, 2001
18. Choate KA, Kahle KT, Wilson FH, Nelson-Williams C, Lifton RP: WNK1, a kinase mutated in inherited hypertension with hyperkalemia, localizes to diverse Cl^--transporting epithelia. *Proc Natl Acad Sci U S A* 100: 663–668, 2003
19. Xu Q, Modrek B, Lee C: Genome-wide detection of tissue-specific alternative splicing in the human transcriptome. *Nucleic Acids Res* 30: 3754–3766, 2002
20. Xu BE, Min X, Stippec S, Lee BH, Goldsmith EJ, Cobb MH: Regulation of WNK1 by an autoinhibitory domain and autophosphorylation. *J Biol Chem* 277: 48456–48462, 2002
21. Pagani F, Buratti E, Stuani C, Bendix R, Dork T, Baralle FE: A new type of mutation causes a splicing defect in ATM. *Nat Genet* 30: 426–429, 2002

Copyright © American Society of Nephrology. Unauthorized reproduction of this article is prohibited.

JASN Express. Published on August 9, 2006 as doi: 10.1681/ASN.2005111197

Basic Science Articles

Dietary Electrolyte–Driven Responses in the Renal WNK Kinase Pathway *In Vivo*

Michelle O'Reilly,* Elaine Marshall,* Thomas MacGillivray,† Manish Mittal,* Wei Xue,* Chris J. Kenyon,* and Roger W. Brown*

**Endocrinology, Centre for Cardiovascular Science, Queen's Medical Research Institute, and †Wellcome Trust Clinical Research Facility, Western General Hospital, Edinburgh, United Kingdom*

WNK1 and WNK4 are unusual serine/threonine kinases with atypical positioning of the catalytic active-site lysine (WNK: With-No-K[lysine]). Mutations in these WNK kinase genes can cause familial hyperkalemic hypertension (FHHt), an autosomal dominant, hypertensive, hyperkalemic disorder, implicating this novel WNK pathway in normal regulation of BP and electrolyte balance. Full-length (WNK1-L) and short (WNK1-S) kinase-deficient WNK1 isoforms previously have been identified. Importantly, WNK1-S is overwhelmingly predominant in kidney. Recent *Xenopus* oocyte studies implicate WNK4 in inhibition of both thiazide-sensitive co-transporter–mediated Na^+ reabsorption and K^+ secretion *via* renal outer medullary K^+ channel and now suggest that WNK4 is inhibited by WNK1-L, itself inhibited by WNK1-S. This study examined WNK pathway gene expression in mouse kidney and its regulation *in vivo*. Expression of WNK1-S and WNK4 is strongest in distal tubule, dropping sharply in collecting duct and with WNK4 also expressed in thick ascending limb and the macula densa. These nephron segments that express WNK1-S and WNK4 mRNA have major influence on long-term NaCl reabsorption, BP, K^+, and acid-base balance, processes that all are disrupted in FHHt. *In vivo*, this novel WNK pathway responds with significant upregulation of WNK1-S and WNK4 with high K^+ intake and reduction in WNK1-S on chronic lowering of K^+ or Na^+ intake. A two-compartment distal nephron model explains these *in vivo* findings and the pathophysiology of FHHt well, with WNK and classic aldosterone pathways responding to drivers from K^+ balance, extracellular volume, and aldosterone and cross-talk through distal Na^+ delivery regulating electrolyte balance and BP.

J Am Soc Nephrol 17: 2402–2413, 2006. doi: 10.1681/ASN.2005111197

The role of WNK1 and WNK4 in control of electrolyte balance and BP first became apparent with their mutation being associated with familial hyperkalemic hypertension (FHHt; also known as Gordon syndrome and pseudohypoaldosteronism type 2), a human autosomal dominant disorder that features hypertension, hyperkalemia, and acidosis that usually are hyperresponsive to thiazide diuretics (1,2). FHHt can be caused by intronic deletions in WNK1 or missense mutations in WNK4 (3). Mutations in either cause a broadly similar phenotype, suggesting that WNK1 and WNK4 function in a common pathway. Unlike most monogenic disorders that affect BP, which feature reciprocal Na^+ and K^+ (and/or H^+) imbalances and share a relationship to the aldosterone pathway (4), FHHt features concurrent NaCl and K^+(and/or H^+) retention (1,3,5). This unusual characteristic indicates the existence of a novel "WNK pathway" functioning in normal physiology, which may allow the "independent of aldosterone" regulation of K and Na balance (and extracellular volume) by the kidney, ultimately also maintaining BP within the normal range. The BP-regulatory role of this WNK pathway is conserved in evolution as WNK1+/− mice are hypotensive (6).

Previously, we and others demonstrated that a 5′-truncated kinase-deficient isoform (WNK1-S) predominates in kidney (7), this being conserved between human and mouse (7–9). Isoform-specific probes distinguished ubiquitous low-level expression of full-length WNK1-long (WNK1-L) from abundant WNK1-S expression in distal nephron. Recent *Xenopus* oocyte studies implicate WNK4 in inhibition of NaCl reabsorption by thiazide-sensitive Na^+Cl^- co-transporter (NCC) (10,11) and/or K^+ transport *via* renal outer medullary K^+ (ROMK) (12), while WNK1-L may in turn inhibit WNK4 (11). Furthermore, very recent *in vitro* reports show that WNK1-S, the predominant isoform in kidney, may participate in regulation of electrolyte transport. In *Xenopus* oocyte studies, WNK1-S acted as a dominant negative regulator of WNK1-L (13) (thereby WNK1-S would relieve repression of WNK4). In cultures of mouse cortical collecting duct (CCD) cells, aldosterone induces WNK1-S expression, and this may mediate an increased epithelial Na channel (ENaC) conductance (14).

This evidence suggests that this WNK pathway plays a functional role in normal physiology to control electrolyte homeostasis and BP. The full renal response that maintains normal BP or compensates for altered electrolyte intake involves a substantial component that takes many hours per day to develop fully and is accompanied by significant persistent

Received November 18, 2005. Accepted June 11, 2006.

Published online ahead of print. Publication date available at www.jasn.org.

Address correspondence to: Dr. Roger W. Brown, Centre for Cardiovascular Science, Queen's Medical Research Institute, 47 Little France Crescent, Edinburgh, UK EH16 4TJ. Phone: +44-1312426739/6777; Fax: +44-1312426779; E-mail: roger.brown@ed.ac.uk

Copyright © 2006 by the American Society of Nephrology

ISSN: 1046-6673/1709-2402

Table 1. Primer and probe sequences for assays by design[a]

Gene	Forward Primer (5′-3′)	Reverse Primer (5′-3′)	Probe (5′-3′)
WNK1-T	GGGATGTACCAGAAGATGTTGCT	CCATGGTCTTGTGATCACCTTCA	CCAGACTCAACCATTTCT
WNK1-S	TGCTGCTGTTCTCAAAAGGATTGTA	TTCAGGAATTGCTACTTTGTCAAAACTG	CTGGCTTCACTCCCTCATT
WNK1-L	TGCATGCTTGAGATGGCTACAT	CTTTGTCAAAACTGGCTGGCTT	CACTCCACTGGTCACTCG
WNK4	GCGGAGGAGGTGGCT	GCCACTGGCTGGTAGTCA	CCAAGGCTACCATCTCC

[a]-L, full length; -S, short; -T, total.

changes in nephron ultrastructure and gene expression. These current studies progress from valuable insights of *Xenopus* oocyte work to investigate the physiologic role of the WNK pathway *in vivo* in mice, localizing it within the nephron and tracking WNK mRNA expression changes in response to chronic variations in dietary electrolyte intake and aldosterone status. This leads to a working model of the distal nephron, explaining the WNK pathway findings and the pathophysiology of FHHt.

Materials and Methods

Animal Treatment

All procedures were carried out under provisions of ethically approved licenses and involved adult, 25- to 30-g, male C57BL/6 mice (Charles River, Margate, UK). Modified electrolyte feeds for mice were obtained from Special Diet Services (Witham, UK).

RNA Extraction

At conclusion of treatments of mice, both kidneys were removed under terminal anesthetic, immediately frozen on dry ice, and stored at −80°C. Frozen kidneys were fragmented and immediately homogenized in TRIzol Reagent (Invitrogen, Paisley, UK), and total RNA was extracted following the manufacturer's guidelines.

Real-Time PCR

Assays used ABI PRISM 7900 relative quantification real-time methods (Applied Biosystems, Foster City, CA). PCR was performed in 384-well plates (AB Gene) and used 10-μl reactions that contained 5.0 μl of TaqMan Master Mix (Applied Biosystems), 200 nM of each primer, 5 nM of probe, and 4.5 μl of template (1:40 dilution of cDNA synthesized as described previously [7]). PCR conditions involved 95°C for 10 min, then 40 cycles of 95°C for 15 s and 60°C for 60 s. Standard template dilution curves enabled target gene quantification and normalization to the endogenous control TATA-Box Binding Protein (TBP). All group values were calibrated to their control groups.

Validation studies using mouse renal RNA established TBP as an excellent control for these studies, showing less variation than 18S, actin, and several other reputed housekeeping genes and excellent reproducibility against an exogenous control gene. Previous literature (15) reinforces TBP as a particularly good renal endogenous control gene. Real-time PCR assays used the ABI Assays-on-Demand (TBP: Mm00446973_m1) or Assays-by-Design services (all other assays, see Table 1).

In Situ *Hybridization Analysis*

RNA probes for *in situ* hybridization (ISH) were produced to specific gene regions using nested PCR methods (7,16). For primer sequences, see Table 2. ISH used renal cryostat sections (10 μm) from each mouse mounted on silane-coated glass slides, then fixed, hybridized, RNase A treated, washed, and ethanol-dehydrated as described previously (7,16,17). Slides were exposed to Kodak x-ray film (BioMax MR-1; Sigma, Poole, UK), dipped in NTB-2 photographic emulsion (Anachem Ltd., Bedfordshire, UK), exposed (within light-tight box) for up to 4 wk, and developed. Cresyl violet/eosin counterstaining with bright and dark-field illumination was used routinely to visualize and localize silver-grain distribution in emulsion-dipped slides. In counterstained slides, blue dark-field views (dark-field view in blue-filtered light) also were used to limit/eradicate counterstain dark-field artifacts. Serial sections allowed co-localizations and tracing of nephron structures beyond the plane of individual sections.

Image Analysis

Digital image analysis was performed using custom-written applications within the Image Processing Toolkit MATLABR version 7 (The Mathworks, Inc., Natick, MA) environment on 16-bit grayscale TIFF

Table 2. Primer sequences for PCR construct probes used in ISH[a]

Target	Sequence (5′-3′)	Orientation
γ-ENaC	GCCCGTCACAAACATCTACAATGCTGC	Sense
γ-ENaC	CTTGGCCAGGTCAGTCTTGTTGAGC	Antisense
NCC	GCATTCATTCCTCAAGCAGGAAGGTAG	Sense
NCC	GGTGTGCCATACTCCTGCAGTAGG	Antisense
NKCC2	AAGATGTCGGTCAGCATCCCTTCC	Sense
NKCC2	CCATCATTGAATCGCTCTCCTTAAGAAGA	Antisense
WNK4	GAACGAGAGGTTCACCATCCAGG	Sense
WNK4	CATCTGAGGCGTAGCTATCCCCAG	Antisense

[a]Primer sequences for WNK1 are detailed in reference (7). For additional information, contact the corresponding author. γ-ENaC, γ subunit of epithelial Na channel; NCC, thiazide-sensitive Na^+Cl^- co-transporter; NKCC2, $Na^+K^+2Cl^-$ co-transporter type 2.

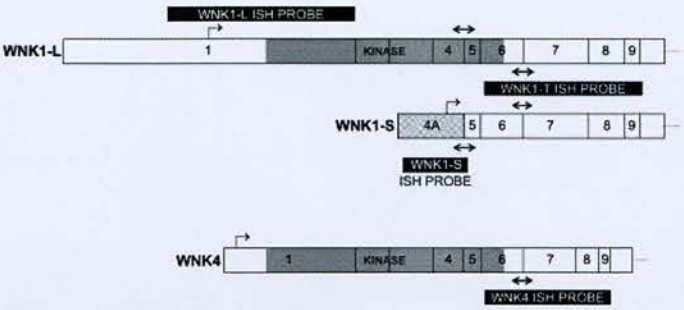

Figure 1. Schematic representation of WNK cDNA structure showing 5′-exon composition and probe positions. The cDNA structures of the 5′-regions of kinase-intact full-length WNK1 (WNK1-L; containing exons 1 through 4), kinase-deficient WNK1 short (WNK1-S; containing exon 4a in place of exons 1 through 4), and WNK4 are illustrated with vertical bars representing exon:exon boundaries. Numbers within rectangles refer to exon numbers. Black boxes specify the cDNA region probed by *in situ* hybridization (ISH). Double-headed arrows indicate the exon:exon boundary crossed by probes used in real-time PCR studies. Horizontal dashed lines indicate further exons that were not included in this illustration.

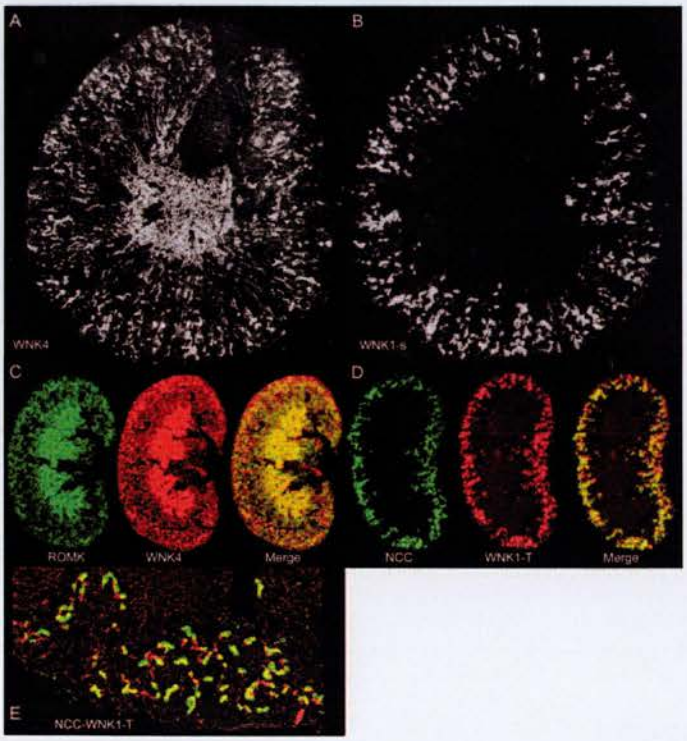

Figure 2. WNK kinase gene expression in kidney. ISH for the genes indicated in mouse kidney. (A and B) Serial transverse sections, dark-field views. (C and D) Two-color dark-field views for paired serial sagittal sections, merging showing co-localization (yellow shift). (E) Two-color merge views of D (at higher magnification). WNK1-T expression (E) encompasses the striking distal nephron cortical expression of WNK1-S (B) and additional widespread expression near background levels of WNK1-L. Note: comparing (A)+(B), major coincidence of expression of WNK1-S and WNK4 in cortex, but WNK1-S proportionately very limited in medullary rays and absent in medulla; (E) strong WNK1-S cortical (labyrinth) expression is seen beyond thiazide-sensitive Na^+Cl^- co-transporter (NCC) overlap (distal convoluted tubule [DCT]), representing particularly extension into connecting tubule (CNT; NCC being DCT restricted).

images, having an intensity range from 0 (black) to 65535 (white). This allows semiquantitative image analysis of ISH autoradiographic films and dipped emulsion slides, measuring areas and grayscale intensities (or silver grain densities) as an index of expression level. Measured grayscale levels are converted to equivalent dpm of bound radioactive probe by calibrating from co-exposed radioactive microscales (Amersham, Little Chalfont, UK) that are designed specifically for this purpose. Alignment of consecutive sections involved systematic rotation and linear displacement of one image relative to the next to calculate their normalized cross-correlation and interatively proceeding to the optimal alignment, where this value is a maximum. The aligned images can be displayed as different red and green channels of a single overlaid merged image. Autoradiographic films were scanned on a high-resolution flatbed scanner. Any damaged or inadequate sections were excluded. The software greatly facilitated selection of regions (typically complex shapes) showing expression that was highly significantly above background levels. Background was low, with sense-section backgrounds having a grayscale level that was not significantly different from zero.

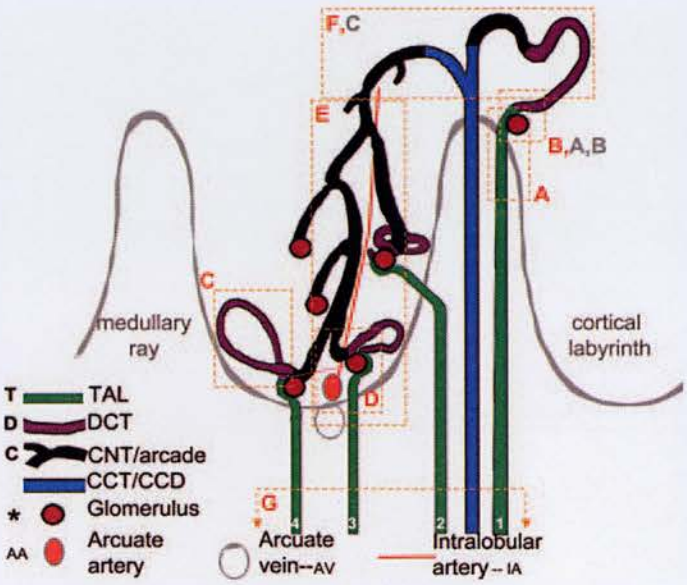

Figure 3. Nephron structure. Several distal nephrons that drain into one cortical collecting duct (CCD) are shown. Distal nephron begins in the renal medulla in thick ascending limb of the loop of Henle (TAL; numbered), which ascends into cortical medullary rays and enters the cortical labyrinth, contacting its glomerulus (specialized macula densa cells at contact point) then shortly beyond this enters DCT, CNT, and finally initial/cortical collecting tubule (ICT/CCT), which re-enters medullary rays as CCD and re-descends into medulla. Nephrons of superficial glomeruli (*e.g.*, TAL1) typically have a simple structure, with a short usually unbranched CNT. In contrast, in most species, nephrons of mid-cortical (*e.g.*, TAL2) and some juxtamedullary glomeruli (TAL3 + 4) commonly drain through well-developed branched arcades of CNT. A considerably higher proportion of nephrons form arcades in mouse than in human. Arcades are arranged around vascular axes, with CNT being close to arcuate and especially intralobular vessels. The dashed boxes and lettering delimit regional views relevant to panels of Figure 4 (red letters) and Figure 5 (gray letters).

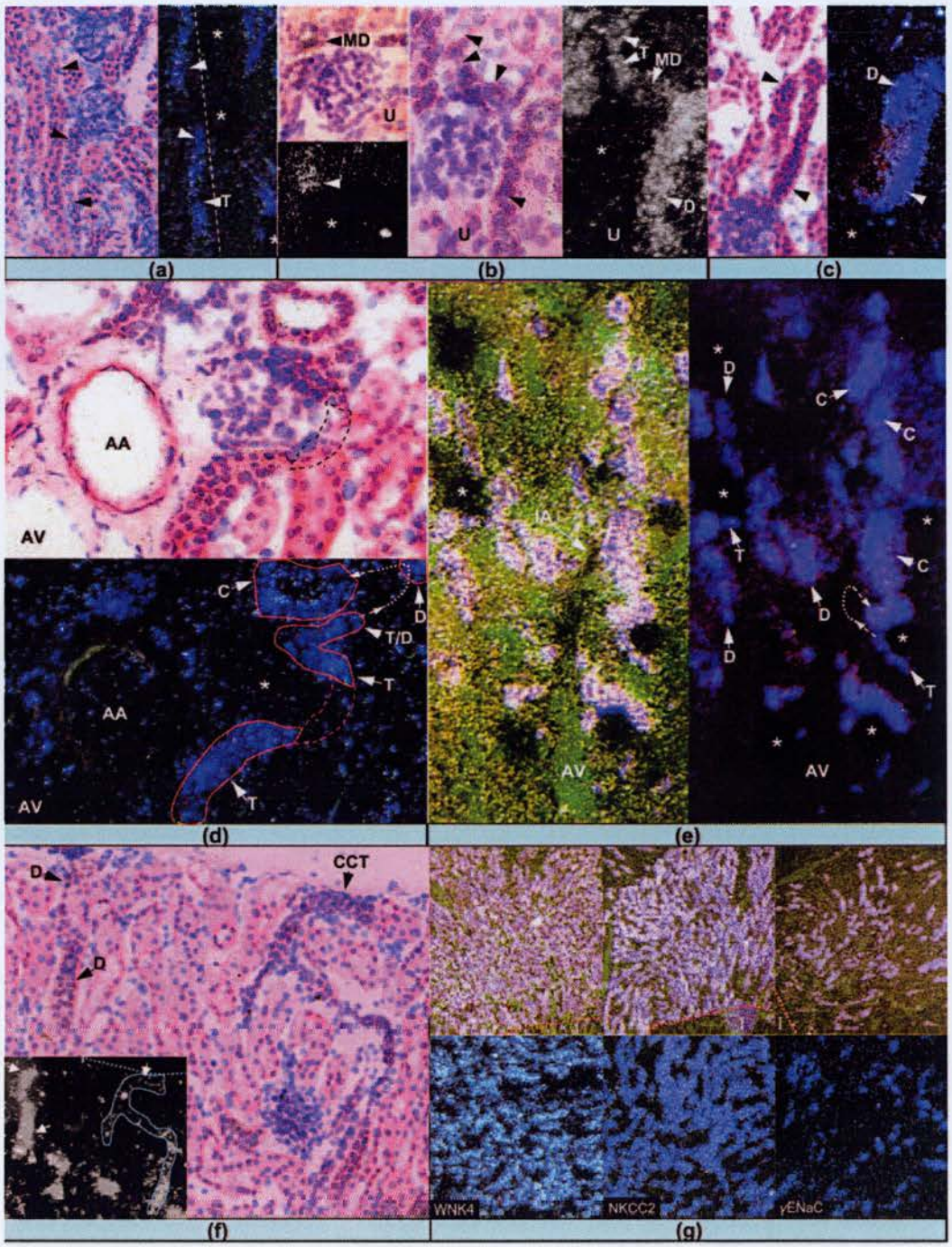

Figure 4. WNK4 gene expression in mouse kidney. ISH studies are shown in bright-field, dark-field, and blue dark-field (see *In Situ* Hybridization Analysis). Throughout a through g, similar regions of view are illustrated in Figure 3 (red labeled [A through G] boxes). (a) WNK4 expression in TAL(T) in medullary ray, crossing boundary (dashed line) to contact glomeruli (*) in cortical labyrinth. (b) Substantial expression in segment of macula densa (MD) and higher still in DCT (D), also seen in c. U, proximal tubule emerging from urinary pole of glomerulus. (d) WNK4 expression in TAL emerging from medulla, through MD segment, DCT, and CNT. DCT convolutions (dashed arrow) and a segment of TAL (red dashed outline) fall outside the plane of section. (e) Extensive WNK4 expression throughout a well-developed deep cortical arcade. Vascular axis (arcuate artery [AA] and vein [AV] and intralobular artery [IA]) and associated glomeruli are seen in left panel. Note extensive DCT loops adjacent to glomerulus (*) in left panel. Dashed arrow indicates connections of DCT convolutions (out of section plane). (f) Superficial cortex with loops of DCT and ICT/CCT passing near renal capsule. Although both segments have WNK4 expression, note that the level is strikingly higher in DCT. Dashed line indicates renal capsule. (g) Views of ISH studies for the genes indicated in inner stripe of renal outer medulla (having TAL and outer medullary CD [OMCD] as largest tubules). Note that the relative density of WNK4-positive tubules is greater than that for the γ subunit of epithelial Na channel (γ-ENaC; an OMCD marker) but similar to $Na^+K^+2Cl^-$ co-transporter type 2 (NKCC2; a TAL marker). Dashed red line indicates boundary of outer and inner medulla (I). Magnifications: ×50 in g, top (dark-field view); ×100 in G, bottom (blue dark-field view).

Statistical Analyses

Data are expressed as mean ± SEM, $P < 0.05$ was considered significant, and group comparisons were analyzed by one-way ANOVA and Neuman-Keuls *post hoc* testing, unless otherwise stated. Least significant difference *post hoc* test for planned comparisons ($ANOVA_{LSD}$) was used when Neuman-Keuls testing was borderline nonsignificant. Routine changes are expressed as %change (mean ± SEM) relative to control values. Larger scale changes are expressed as fold change (mean ± SEM), relative to control values, and 95% confidence intervals are quoted.

Results

Renal WNK1 and WNK4 Gene Expression

Renal WNK1 and WNK4 mRNA expression is illustrated in Figures 1 through 5, with WNK structure and probe positions shown in Figure 1, an overview shown in Figure 2, the structures involved (and their abbreviations) in superficial and deep distal nephrons in Figure 3, and key expression details in Figures 4 and 5. Both WNK1-S and WNK1-L are expressed in kidney (Figure 2, B, D, and E). WNK1-L shows near background seemingly ubiquitous expression. The great preponderance of WNK1 expression is due to WNK1-S and limited to renal cortex (Figure 2B). High levels of WNK1-S in distal tubules (Figure 2, D and E) fall off sharply distally from connecting tubule (CNT) to cortical collecting tubule (CCT) to CCD (Figure 5C; see Figure 3) (7) and proximally dropping 10-fold at the thick ascending limb of the loop of Henle (TAL)–distal convoluted tubule (DCT) junction (Figure 5, A and B) with expression (including the macula densa) extinguishing in the cortical TAL. Hence, WNK1-S has only a limited weak extension into medullary rays. WNK4 expression levels are lower than WNK1 (more than threefold longer exposures for WNK4 than for WNK1[-S/-T] in Figures 2, 4, and 5). WNK4 expression also is strongest in distal tubule structures (DCT/CNT) but extends beyond distal tubule, at reduced levels, more proximally into TAL, including macula densa and medullary TAL (Figure 4, A, B, D, and G) and more distally at low expression levels (compared with DCT) in collecting duct (CD; Figure 4F). Thus, substantial WNK4 expression extends into medullary rays and outer (but not inner) medulla (Figures 2A and 4G) involving much too high a proportion of tubules to be due to outer medullary CD alone (ENaC γ-subunit *versus* WNK4; Figure 4G) rather resembling the density of medullary TAL tubules (shown by $Na^+K^+2Cl^-$ co-transporter type 2 [NKCC2]; Figure 4G).

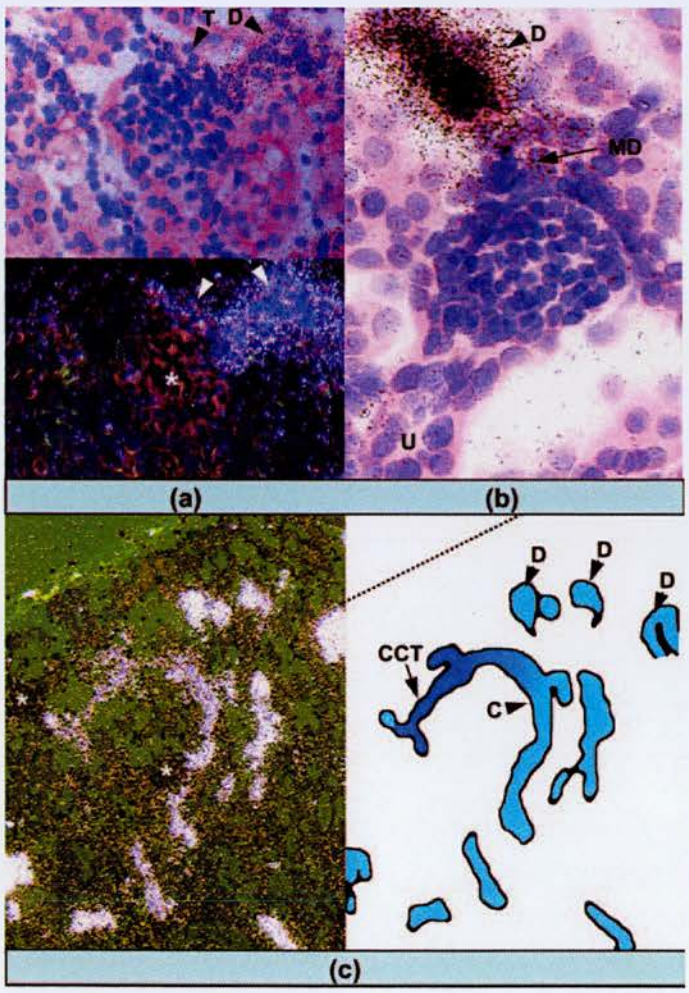

Figure 5. WNK1-S gene expression in mouse kidney. ISH studies: in bright-field view in a (top) and b, in blue dark-field view in A (bottom), and in dark-field view in c. Note that WNK1-S gene expression is present in late TAL (T) including at the macula densa (MD) but rises to much higher levels in DCT (D) and CNT (C), reducing somewhat by CCT. *Glomerulus; dashed line indicates position of renal capsule; U, proximal tubule emerging from urinary pole of glomerulus (see also Figure 3, gray-labeled boxes).

Effects of Chronic Variation in Dietary K^+ In Vivo

Body Weight, Food Intake, and Fluid Balance. Mice were given group treatments of varying dietary K^+ intake (low K^+ [LK], normal K^+ [NK], and high K^+ [HK]; see Table 3 and Figure 6, A through C). The LK group showed borderline lower weight that became significant *versus* HK (but not NK) at the end (25.6 ± 0.6 *versus* 27.3 ± 0.6 g, respectively; $P = 0.03$), but mice seemed healthy throughout. Both HK and LK groups developed a higher fluid intake and urinary output compared with the NK group (HK *versus* NK significant at conclusion: >3.4-fold higher intake [$P < 0.05$] and >4.9-fold higher output [$P < 0.01$]).

Urinary Electrolytes. Mice were allowed a period of 3 d (days 1 through 3) to acclimate to metabolic cages. After this, during the initial 3 d of active treatment with specific diets (days 4 through 6), K/Cre and Cl/Cre rose 6.8-fold and 4.9-fold, respectively, with HK; remained unchanged with NK; and K/Cre showed a dramatic 24.4-fold decrease with LK. After days 5 to 6, group K/Cre ratios did not change significantly, indicating reestablishment of appropriate electrolyte balance. The HK and LK groups demonstrated a >17-fold increase and a >14-fold decrease, respectively, in K/Na by day 6 (Figure 6, D through F).

Plasma Measurements. As expected, HK induced a small but significant increase in plasma K^+ within the normal range. Plasma aldosterone was elevated with HK but was unchanged with LK (see Table 3).

Table 3. Metabolic measurements[a]

	Low K	Normal K	High K
Initial body weight (g)	29.7 ± 0.7	28.8 ± 0.5	29.8 ± 0.6
Final body weight (g)	25.6 ± 0.5	26.9 ± 0.3	27.3 ± 0.6
Plasma K^+ (mM)[b]	4.13 ± 0.22	4.08 ± 0.22	4.85 ± 0.2
Plasma Na^+ (mM)[c]	145.4 ± 0.4	146 ± 0.6	144.3 ± 0.7
Plasma Cl^- (mM)[d]	114.4 ± 1.54	112 ± 1	114.5 ± 1.05
Plasma creatinine (μM)[e]	13.8 ± 2.24	14.4 ± 1.21	12.5 ± 1.44
Aldosterone (nM)	0.834 ± 0.297	0.793 ± 0.207	1.879 ± 0.387
Renin activity (ng/ml per h)	4.38 ± 1.12	4.45 ± 0.83	5.71 ± 0.34
Corticosterone (nmol/L)	345.8 ± 48.8	342 ± 58.2	300 ± 42.6

[a]Plasma concentrations of Na^+, K^+, Cl^-, and creatinine were measured on commercial clinical chemistry analyzers and remained within the normal range for all groups. Plasma renin activity (PRA), aldosterone, corticosterone, and plasma electrolyte measurements were performed in samples that were removed on cardiac puncture during terminal anaesthetic. Blood samples were centrifuged, and plasma was removed, put on ice, and rapidly stored at −20°C. Aliquots of plasma for assay of PRA were thawed, and buffer stabilizing renin activity was added immediately. PRA (40) and corticosterone (41) were assayed as previously described (40,41). PRA and corticosterone did not change significantly. Aldosterone levels were measured using a radioimmunoassay kit (Coat-a-Count aldosterone; DPC, Los Angeles, CA). Values are means ± SEM.

Normal plasma ranges for [b]K^+, 3.0 to 8.3 mmol/L (35), but carefully taken having a narrower range probably nearer 3.8 to 6.8 mmol/L (36–38); [c]Na^+, 139 to 157 mmol/L; [d]Cl^-, 104 to 119 mmol/L (39); [e]creatinine, 5 to 67 μmol/L (35).

WNK Expression Responses to Dietary K^+ and Na^+ Challenges

For investigation of the effect of varied dietary K^+ intake on WNK expression, mice were fed diets with a specific K^+ content (NK, LK, or HK) for 10 d. Specific real-time PCR assays indicated that renal WNK1-S was downregulated by 20 ± 9.3% with LK ($P = 0.04$) and upregulated by 30 ± 10.4% with HK ($P = 0.01$; a 50 ± 10.2% rise from LK to HK), as was total WNK1 (WNK1-T: 24 ± 7% increase; $P = 0.0009$) compared with NK (Figure 7A). WNK4 was upregulated with HK (48 ± 24.2%; $P = 0.01$) but unchanged with LK.

In regions with clear WNK1-S expression (Figure 7B), ISH analysis showed upregulation in cortex by HK (*versus* NK: 2.1 ± 0.6-fold; 95% confidence interval 1 to 3.3; $P = 0.003$). WNK1-S distribution remained cortical without striking change. Over kidney regions with clear WNK4 expression, there was a 2.3 ± 0.6-fold (1.1 to 3.5) upregulation in expression with HK ($P = 0.02$; Figure 7C); in contrast, the LK diet did not affect WNK4 mRNA significantly.

For testing whether varied dietary Na^+ induces similar WNK expression changes, mice were fed diets with a specific Na^+ content (normal Na^+ [control], low Na^+ [LNa], or high Na^+ [HNa]) for 6 d. WNK1-S showed a borderline significant downregulation, by 39 ± 16% of control levels, between HNa and LNa-diet ($P = 0.049$, $ANOVA_{LSD}$; Figure 8). Although WNK4 in particular showed a trend to similar changes, no other significant changes in WNK expression were observed across the treatment groups.

WNK Expression and Aldosterone Challenge

For examination of the effect of aldosterone levels on WNK expression, mice were given excess aldosterone *via* minipump (150 μg aldosterone/kg per d [18]) or adrenalectomized (supplemented with 0.9% saline drinking water) to abolish aldosterone production. Real-time PCR showed that aldosterone treatment induced a 32 ± 6.7% (18.9 to 45.2) WNK1-S upregulation ($P = 0.0002$) without affecting WNK1-L or WNK4 expression (Figure 9). Adrenalectomy had no significant effect on WNK expression, but WNK1-S rose significantly across the adrenalectomy-aldosterone excess range (43 ± 7.6%; $P = 0.0002$).

Discussion

In beginning to understand the WNK pathway, *Xenopus* oocyte studies provided invaluable evidence of WNK pathway regulation of key mediators of distal nephron electrolyte transport. This study is one of the first to investigate this pathway *in vivo* in a much more physiologically relevant system, the mouse, reporting detailed nephron segment localization and WNK expression responses to dietary electrolyte challenges. The relevant aspects of human physiology and their disorders are very well modeled in mice, particularly mechanisms of electrolyte handling and associated effects on long-term BP control (19,20). Very few tools that reliably differentiate WNK isoforms are currently available to quantify expression changes and examine distribution simultaneously. Moreover, this study allows examination of changes within kidney regions that are not easily accessible to micropuncture techniques and have no good, well-validated, cell-line models (*e.g.*, outer medullary CD, deep distal nephron arcades/CNT) and avoids dangers of unequal RNA degradation, a concern that is associated with microdissection.

Here we report strongest WNK1 and WNK4 expression in the distal tubule (DCT, CNT) with WNK1-S dropping to much lower levels by CD, whereas WNK4 extends somewhat diminished into TAL and CD. WNK1-L has widespread, low-level, near-background expression. Figure 10 puts the distribution of WNK pathway expression in context.

WNK4 expression in TAL and macula densa (discussed fur-

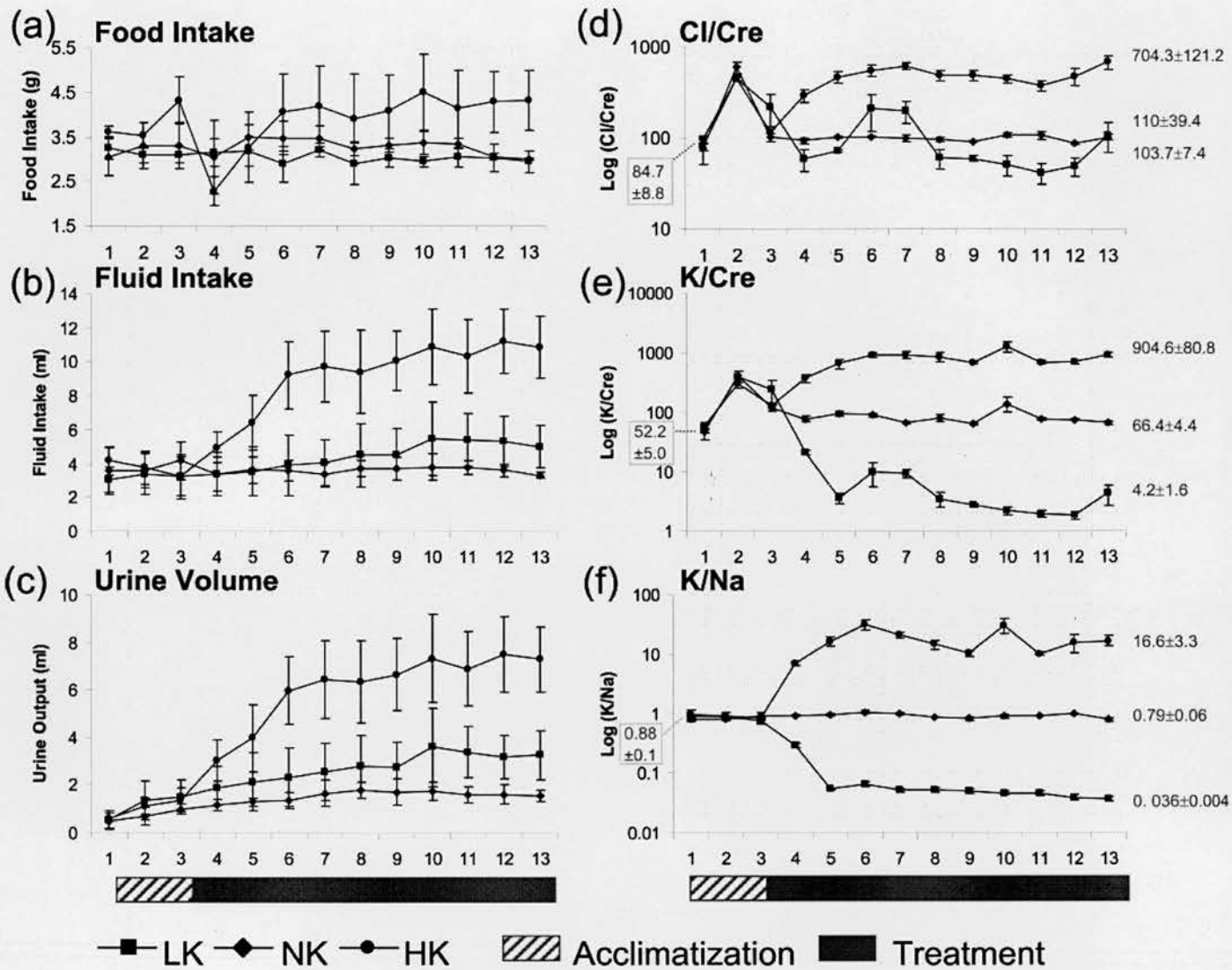

Figure 6. Effect of dietary K^+ intake on metabolic measurements. The K^+ diet study involved adult male C57BL/6 mice, housed in pairs in mouse metabolic cages (Techniplast). After 3 d of acclimation, groups (n = 6) of mice commenced specific diets: (*1*) Normal (0.33%) K^+ feed (NK; control group), (2) low (0.006%) K^+ feed (LK), and (*3*) high-KCl (3.3% K^+, 4.4% Cl^-) feed (HK). Batch analysis confirmed that diets were well matched for Na^+ (0.28 ± 0.05%; all diets) and Cl^- content (0.7 ± 0.12%; NK and LK). Mice took the specified diets for 10 d, and daily measurements of food intake (A), fluid intake (B), and urine output (C) were recorded. Urinary electrolyte excretion was measured daily, reflected changes in dietary electrolyte intake, and was expressed as a ratio of creatinine or Na^+ excretion (Cl/Cre, K/Cre, K/Na [D through F]). A transient decrease in food intake was observed in the HK group on day 4 immediately after the introduction of treatment diet.

ther below) has not been recognized before and may indicate different WNK4 isoforms or posttranslational modifications in TAL (3). These are common in transport pathways (*e.g.*, NKCC2 in TAL), whereas additional bands on WNK4 immunoblots suggest varied posttranslational modification (3). A study of transgenic mice that express a FHHt-WNK4 cDNA in TAL-CNT (and intercalated cells) reported that mutant-WNK4 protein was absent from tight junctions and apically localized in TAL (21). The lack of FHHt phenotype in these FHHt-WNK4 mice leaves some uncertainty. This may relate to transgenic WNK4 expression being driven from a cDNA and so lacking normal *in vivo* regulation and potential for transcriptional diversity of the WNK4 genomic locus.

Our studies challenged mice with varied dietary K^+ and Na^+ intake and aldosterone. All three classes of treatment showed notable WNK pathway gene expression responses *in vivo* to these physiologic determinants of electrolyte balance and BP. Changes with varied dietary K^+ intake were particularly clear. WNK1-S expression rose on HK and fell on LK diet, correlating significantly with K^+ intake, while ISH findings revealed the importance of upregulation of this isoform with HK diet, in strongly expressing segments (DCT-CNT). HK intake also increased WNK4 expression. These coordinated WNK expression changes seem functionally significant as merely heterozygous changes in WNK1 or WNK4 cause substantial BP and electrolyte abnormalities (1,3,5,6).

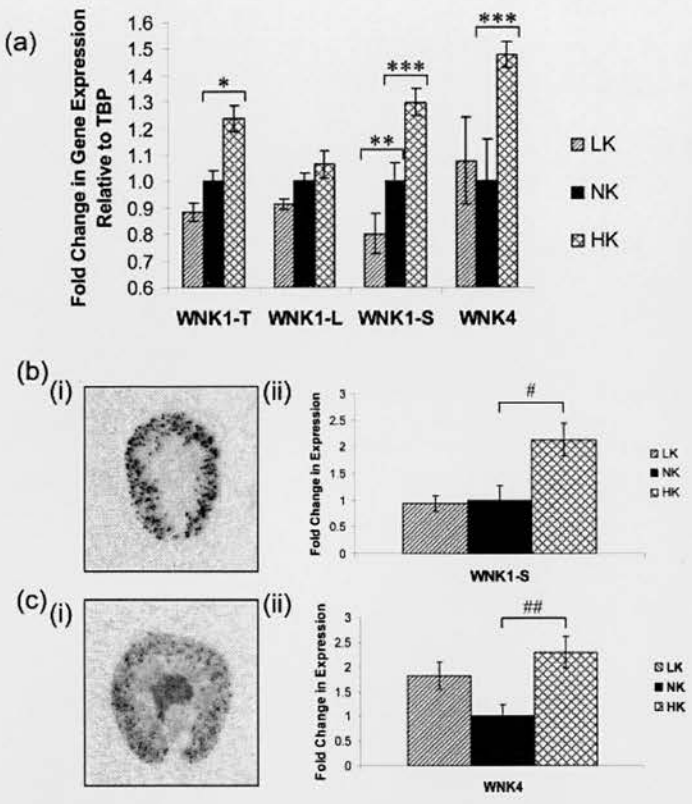

Figure 7. WNK expression in response to varied K^+ intake. (A) Real-time PCR results from renal RNA from groups of mice ($n = 6$) with variations in dietary K^+. WNK1-S expression is significantly downregulated with LK, whereas WNK1-S and WNK4 are upregulated with HK. No significant changes were observed in WNK1-L expression across the experimental groups. (B and C) ISH analysis for WNK1-S and WNK4 detected any major shifts in distribution and level of WNK expression with K^+ intake at the regional level, undiluted by any widespread, invariant low-level expression. (i) Representative sections and (ii) densitometric analysis from ISH studies. WNK1-S (B) and WNK4 (C) have different expression profiles with WNK1-S expression restricted to the cortex, and WNK4 restricted to cortex and outer medulla. WNK1-S and WNK4 expression both are upregulated with HK. $^*P = 0.009$; $^{**}P = 0.04$; $^{***}P = 0.01$; $^{\#}P = 0.003$; $^{\#\#}P = 0.02$.

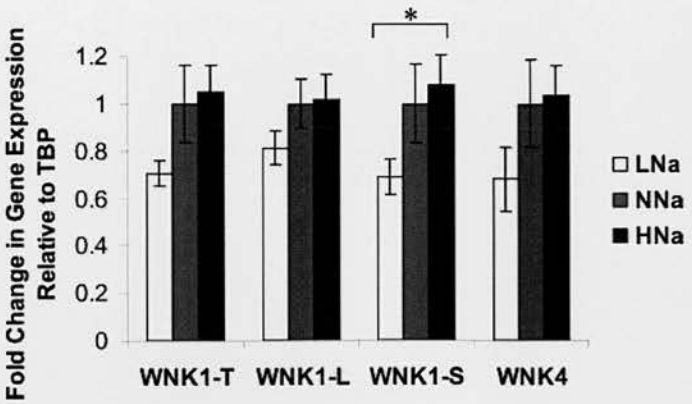

Figure 8. WNK expression in response to varied Na^+ intake. The Na^+ diet study involved adult male C57BL/6J mice, housed in pairs in mouse metabolic cages (Techniplast). Animals were allowed 1 wk to acclimate, after which they commenced specific dietary Na^+ treatments that lasted 7 d: (*1*) low Na^+ (0.03%) feed group (LNa), (*2*) normal/control Na^+ (0.3%) feed group (NNa), or (*3*) high Na^+ (3%) feed group (HNa). WNK1-S showed a marginally significant* downregulation (by $ANOVA_{LSD}$) between HNa and LNa diet. No other significant changes in WNK expression were observed across the treatment groups. $^*P = 0.049$.

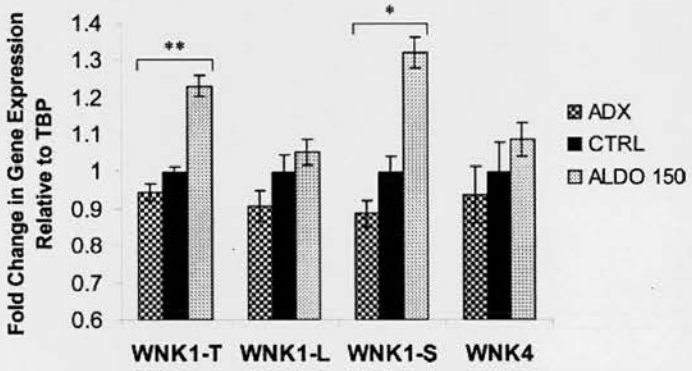

Figure 9. WNK expression in response to variations in aldosterone. The aldosterone study involved adult male C57BL/6 mice, housed in pairs in normal cages. Mice that had food and fluid intake and BP monitoring were given ($n = 6$) subcutaneous (Alzet) minipump (MP) treatments for 6 d: (*1*) Adrenalectomy (ADX): Bilateral adrenalectomy, 0.3% Na^+ feed, 0.9% saline drinking water, saline-only MP; (*2*) control (CTRL): Normal 0.3% Na^+ feed, saline-only MP; and (*3*) aldosterone excess (ALDO 150): 150 μg aldosterone/kg per d (18) by MP, 0.3% Na^+ feed. Plasma renin activity and aldosterone measurements allowed confirmation of adequacy of treatments. WNK1-S expression was upregulated by chronic aldosterone treatment (150 μg/kg per d, 6 d) but was unchanged in the absence of aldosterone after adrenalectomy. No changes in WNK1-L or WNK4 were observed across the experimental groups. $^*P = 0.0002$; $^{**}P = 0.02$.

WNK1-S was significantly upregulated with chronic aldosterone excess. There were no significant changes in WNK1-L or WNK4 across the aldosterone-adrenalectomy range. With variations in Na^+ intake, a fall in WNK1-S expression just reached significance comparing HNa and LNa groups. It is intriguing that this could represent a WNK pathway response to reductions in extracellular fluid volume as Na^+ intake falls.

Thus, K^+ intake, plasma aldosterone, and dietary Na^+ intake/extracellular volume seem to be possible *in vivo* regulators of the WNK pathway. K^+ intake seems to be a relatively robust regulator, whereas in some circumstances, the role of aldosterone may be counterbalanced or secondary to another regulator. Thus, similar WNK1-S expression accompanies very different aldosterone elevations (2.3-fold [HK] and 11.2-fold [aldosterone]) or when aldosterone fell from normal to adrenalectomized levels (Figure 9). Aldosterone-independent regulation of WNK1-S expression clearly is present across LK-HK dietary groups, with individual WNK1-S expression correlating with K^+ intake ($P < 0.001$) but not significantly with aldosterone. Moreover, reduced WNK1-S with LNa intake (lowering

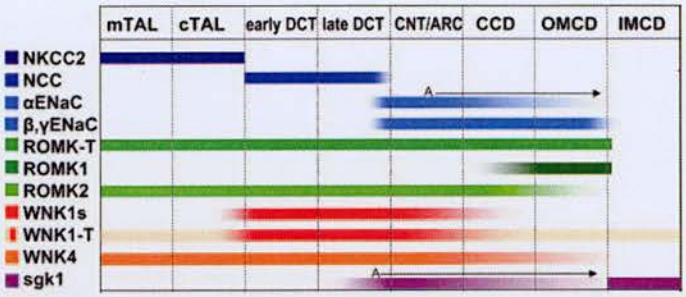

Figure 10. Distribution of gene expression of key genes involved in Na^+ and K^+ balance in distal nephron. Structure illustrated in Figure 3. mTAL, cTAL, medullary and cortical TAL; CNT/ARC, connecting tubule/arcade; CCD/OMCD/IMCD, cortical/outer medullary/inner medullary CD. $\alpha\beta\gamma$ENaC, $\alpha\beta\gamma$ subunits of ENaC; ROMK, renal outer medullary K channel; WNK1-S/-L/-T, WNK1 short (kinase deficient), long (kinase intact), and total; sgk1, serum and glucocorticoid kinase 1. For αENaC/sgk expression, arrows represent regulated expression by rising aldosterone (A).

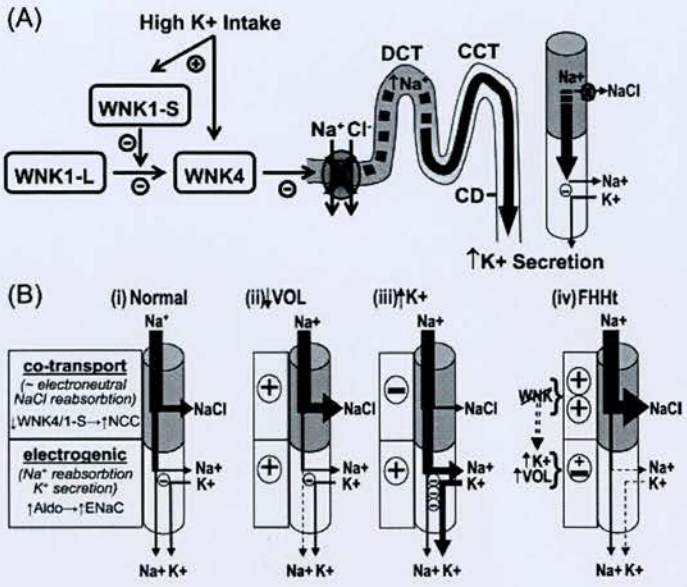

Figure 11. Potential WNK pathway and two-compartment model of distal nephron Na^+/K^+ handling. (A) The WNK pathway is suggested to regulate the extent of NaCl reabsorption in (early) DCT in the manner of the alleged molecular switch proposed in explaining familial hyperkalemic hypertension (FHHt). A high K^+ intake switches to lower Na^+ reabsorption *via* NCC in DCT, so distal Na^+ delivery rises, allowing K^+ to be cleared. (B) Two-compartment model. (i) Normally, Na reabsorption is partitioned between an upper co-transport compartment (under WNK pathway repression), driving NaCl reabsorption and a lower electrogenic compartment (stimulated by aldosterone and Na^+ delivery), where Na^+ reabsorption *via* ENaC generates a lumen-negative charge facilitating K^+ secretion. (ii) In hypovolemia, both compartments upregulate Na reabsorption, minimizing urinary NaCl loss and facilitating K^+ secretion. (iii) In high K intake, the mechanism above delivers increased Na and aldosterone, which strongly drive Na^+ reabsorption and K^+ secretion. (iv) In FHHt, there is constitutive overreabsorption of NaCl, causing hypervolemia and hypertension with low renin, which limits the distal delivery to the electrogenic compartment without renin suppression and blunted aldosterone, promoting limited K secretion and hyperkalemia. WNK pathway regulation of NCC and the extent of Na^+ delivery to the distal electrogenic compartment and inappropriate restriction of this in FHHt fits well with reported features of FHHt, including thiazide-sensitivity and NaCl dependence.

volume, stimulating secondary hyperaldosteronism) and increased WNK1-S with aldosterone (raising volume, primary hyperaldosteronism) implies that WNK1-S responds more to extracellular volume than aldosterone and suggests falling WNK1-S as a potential response to conserve volume. Further investigation is required to define fully the *in vivo* regulatory roles of K^+ intake, aldosterone, and volume acting on the WNK pathway, but integrating these findings into a more functional context is of interest. One attempt to do so is outlined in Figure 11 and discussed further next.

How do these results expand understanding of this novel WNK pathway? The FHHt phenotype and usual hyperresponsiveness to thiazide diuretics highlight the importance of DCT in electrolyte balance and BP control (1,5,22). The work above provides some of the first clues as to the role *in vivo* of WNK1-S, the predominant WNK1 isoform in kidney, and intriguingly shows that strongest WNK1-S and WNK4 expression co-localizes in DCT-CNT, where they may contribute to a mechanism that regulates K^+ homeostasis and BP. *Xenopus* oocyte work suggests that WNK4 may inhibit NCC in DCT, and WNK1-L prevents this inhibition (10,11). In a preliminary presentation of this work (see Acknowledgments), we proposed the hypothesis that both WNK1-S and WNK4 can limit NCC transport (Figure 11A). *Xenopus* oocyte work reported since supports a similar mechanism (13). We propose, especially in DCT-CNT, that WNK1-S could bind and counterbalance WNK1-L effects, so shielding WNK4 from inhibition. Although WNK1-S is kinase deficient, it retains domains (coiled-coils) that likely facilitate multimeric/tetrameric WNK1 assembly (23,24). Alternatively, WNK1-S could interact directly with a WNK-binding site on WNK4 or another regulatory kinase to repress NCC.

Figure 11 incorporates this WNK pathway in a two-compartment model. In the upper co-transport compartment, increased WNK1-S or WNK4 (as in our *in vivo* studies) downregulates NCC-mediated NaCl reabsorption, increasing Na^+ delivery to the lower electrogenic compartment (from late DCT distally), where ENaC reabsorbs Na^+, facilitating K^+ secretion (19) (itself augmented by high distal flow-mediated Maxi-K channel activation). The two compartments will normally overlap in late DCT. LNa diet/hypovolemia and HK diet both will stimulate aldosterone, activating the lower compartment. The *in vivo* studies above indicate that LNa diet/hypovolemia also will stimulate the upper compartment (Figure 11B[ii]), producing appropriate Na^+ retention, whereas HK diet will repress it, producing appropriate K^+ secretion (Figure 11B[iii]). The upper co-

transport compartment thus interconverts the same aldosterone response between Na^+ retention and K^+ excretion. We propose that the molecular switch that is alleged to explain FHHt (12) is based on distal delivery of Na^+. This hypothesis is supported by careful ultrastructural studies showing that HK diet (25), NCC−/− Gitelman mice, and high-dosage thiazide diuretics (19) all predispose to extensive hypertrophy and increased Na^+/K^+-ATPase (25) in early CNT (indicating higher Na^+ delivery) and predispose to greater K^+ clearance and reduced BP (19). In WNK1+/− mice, global WNK1 reduction would repress NaCl reabsorption (in DCT, unopposed WNK4) and promote lower extracellular volume, in keeping with their lower BP.

FHHt jams the switch in the opposite direction (Figure 11B[iv]), inappropriately engaging a response (reducing distal Na^+ delivery and K^+ secretion) that these studies suggest is normal when body K and/or Na/extracellular volume fall and require conservation. Although aldosterone level is low to normal, its contribution to FHHt pathophysiology and hypertension should not be underestimated (26). Both aldosterone-dependent and -independent mechanisms contribute to K^+ secretion (19,27); blunting of both seems likely in FHHt. Thus, distal Na^+ delivery is blunted and hypervolemic suppression of renin will restrain circulating aldosterone, blunting the aldosterone response to levels that are inadequate to restore normokalemia despite hyperkalemic drive (28). Thus, FHHt causes hypertension *and* hyperkalemia.

In vitro evidence suggests the WNK pathway also may directly (i) reduce surface ROMK (12), (ii) promote ENaC conductance (14), and (iii) increase paracellular Cl^- flux (29,30) (depleting electrogenic lumen-negative charge). Although the pathway in Figure 11 seems not to require these effects, these processes could impair K^+ secretion, promote Na^+ reabsorption, or both if they contributed significantly. Effect (ii) depends on WNK1-S and was demonstrated in CCD cells; it is unresolved if it extends to late DCT-CNT, where the expression of WNK1-S and ENaC and the potential physiologic influence all are stronger. The roles and significance *in vivo*, and in FHHt, of effects (i) through (iii) are not yet clear.

It is intriguing that we have found previously unexpected gene expression of WNK4 in TAL and macula densa. WNK4 potentially could influence TAL NaCl transport *via* regulation of ROMK, NKCC2, CLC-Kb, or Barttin, because inactivation of any causes severe NaCl wasting in Bartter's syndromes. ROMK surface localization was unaffected in transgenic mice that expressed FHHt-mutant WNK4 protein, which was apically distributed in TAL (21). *In vitro*, WNK4 can interact directly or with other kinases (*e.g.*, OSR1, SPAK, other WNK), to regulate proteins of key importance in TAL-DCT transport, including NCC (11,12), ROMK (12), and, it seems, NKCC2 (31,32). Hence, WNK4 might influence NKCC2 co-transport and expand the co-transport compartment (Figure 11) to more powerful proportions. Overactivity of TAL-DCT NaCl reabsorption seems compatible with FHHt. Certainly, increased BP is reported with activating mutation of CLC-Kb (T481S) (33). Moreover, considering phenotypes of Gitelman plus Bartter syndromes (DCT+TAL salt-wasting hypokalemic alkalosis), it seems that the inverse of these may encompass hyperkalemia, acidosis, and low-renin hypertension, all FHHt features. Other WNK4-FHHt features (*e.g.*, degree of thiazide sensitivity, hypercalcuria [34]) might depend on the spectrum of overactivation within DCT-TAL. Clearly, this makes WNK4 expression in TAL of interest, but much needs to be clarified before a role in physiology or FHHt pathophysiology could be attributed.

Acknowledgments

We acknowledge The Wellcome Trust (grant 065616 PhD Studentship to M.D.), British Heart Foundation (grant PG2 0/01075), and Scottish Hospitals Endowment Research Trust (grant 77/00) for support. The Wellcome Trust Clinical Research Facility enabled real-time PCR and image analysis studies.

Portions of this work were presented at the 24th British Hypertension Society Meeting, September 13 through 15, 2004, Cambridge, UK; the 37th annual meeting of American Society of Nephrology, October 29 through November 1, 2004, St. Louis, MO; and the 24th British Endocrine Societies' Meeting, April 4 through 6, 2005, Harrogate, UK; and appear in abstract form (*Endocr Abstr* 9: 138, 2005).

References

1. Gordon RD: Syndrome of hypertension and hyperkalemia with normal glomerular filtration rate. *Hypertension* 8: 93–102, 1986
2. Paver WK, Pauline GJ: Hypertension and hyperpotassaemia without renal disease in a young male. *Med J Aust* 35: 305–306, 1964
3. Wilson FH, Disse-Nicodeme S, Choate KA, Ishikawa K, Nelson-Williams C, Desitter I, Gunel M, Milford DV, Lipkin GW, Achard JM, Feely MP, Dussol B, Berland Y, Unwin RJ, Mayan H, Simon DB, Farfel Z, Jeunemaitre X, Lifton RP: Human hypertension caused by mutations in WNK kinases. *Science* 293: 1107–1112, 2001
4. Lifton RP, Gharavi AG, Geller DS: Molecular mechanisms of human hypertension. *Cell* 104: 545–556, 2001
5. Bonny O, Rossier BC: Disturbances of Na/K balance: Pseudohypoaldosteronism revisited. *J Am Soc Nephrol* 13: 2399–2414, 2002
6. Zambrowicz BP, Abuin A, Ramirez-Solis R, Richter LJ, Piggott J, BeltrandelRio H, Buxton EC, Edwards J, Finch RA, Friddle CJ, Gupta A, Hansen G, Hu Y, Huang W, Jaing C, Key BW Jr, Kipp P, Kohlhauff B, Ma ZQ, Markesich D, Payne R, Potter DG, Qian N, Shaw J, Schrick J, Shi ZZ, Sparks MJ, Van S, I, Vogel P, Walke W, Xu N, Zhu Q, Person C, Sands AT: Wnk1 kinase deficiency lowers blood pressure in mice. *Proc Natl Acad Sci U S A* 100: 14109–14114, 2003
7. O'Reilly M, Marshall E, Speirs HJ, Brown RW: WNK1, a gene within a novel blood pressure control pathway, tissue-specifically generates radically different isoforms with and without a kinase domain. *J Am Soc Nephrol* 14: 2447–2456, 2003
8. Delaloy C, Lu J, Houot AM, Disse-Nicodeme S, Gasc JM, Corvol P, Jeunemaitre X: Multiple promoters in the WNK1 gene: One controls expression of a kidney-spe-

cific kinase-defective isoform. *Mol Cell Biol* 23: 9208–9221, 2003
9. Xu Q, Modrek B, Lee C: Genome-wide detection of tissue-specific alternative splicing in the human transcriptome. *Nucleic Acids Res* 30: 3754–3766, 2002
10. Wilson FH, Kahle KT, Sabath E, Lalioti MD, Rapson AK, Hoover RS, Hebert SC, Gamba G, Lifton RP: Molecular pathogenesis of inherited hypertension with hyperkalemia: The Na-Cl cotransporter is inhibited by wild-type but not mutant WNK4. *Proc Natl Acad Sci U S A* 100: 680–684, 2003
11. Yang CL, Angell J, Mitchell R, Ellison DH: WNK kinases regulate thiazide-sensitive Na-Cl cotransport. *J Clin Invest* 111: 1039–1045, 2003
12. Kahle KT, Wilson FH, Leng Q, Lalioti MD, O'Connell AD, Dong K, Rapson AK, Macgregor GG, Giebisch G, Hebert SC, Lifton RP: WNK4 regulates the balance between renal NaCl reabsorption and K+ secretion. *Nat Genet* 35: 372–376, 2003
13. Subramanya AR, Yang CL, Zhu X, Ellison DH: Dominant-negative regulation of WNK1 by its kidney-specific kinase-defective isoform. *Am J Physiol Renal Physiol* 290: F619–F624, 2006
14. Naray-Fejes-Toth A, Snyder PM, Fejes-Toth G: The kidney-specific WNK1 isoform is induced by aldosterone and stimulates epithelial sodium channel-mediated Na+ transport. *Proc Natl Acad Sci U S A* 101: 17434–17439, 2004
15. Vandesompele J, De Preter K, Pattyn F, Poppe B, Van Roy N, De Paepe A, Speleman F: Accurate normalization of real-time quantitative RT-PCR data by geometric averaging of multiple internal control genes. *Genome Biol* 3: RESEARCH0034, 2002
16. MacDonald P, MacKenzie S, Ramage LE, Seckl JR, Brown RW: Corticosteroid regulation of amiloride-sensitive sodium-channel subunit mRNA expression in mouse kidney. *J Endocrinol* 165: 25–37, 2000
17. Brown RW, Chapman KE, Kotelevtsev Y, Yau JL, Lindsay RS, Brett L, Leckie C, Murad P, Lyons V, Mullins JJ, Edwards CR, Seckl JR: Cloning and production of antisera to human placental 11 beta-hydroxysteroid dehydrogenase type 2. *Biochem J* 313: 1007–1017, 1996
18. Hou J, Speirs HJ, Seckl JR, Brown RW: Sgk1 gene expression in kidney and its regulation by aldosterone: Spatiotemporal heterogeneity and quantitative analysis. *J Am Soc Nephrol* 13: 1190–1198, 2002
19. Malnic G, Bailey MA, Giebisch G: Control of renal potassium excretion. In: *Brenner and Rector's The Kidney*, 7th Ed., edited by Brenner BM, Levine SA, Philadelphia, Saunders, 2004, pp 453–497
20. Brown RW, Mullins JJ, Webb DJ: Mechanisms and molecular pathways in hypertension. In: *The Molecular Basis of Cardiovascular Disease, A Companion to Braunwald's Heart Disease*, 2nd Ed., edited by Chien KR, Philadelphia, Elsevier/Mosby, 2004, pp 566–649
21. Yamauchi K, Yang SS, Ohta A, Sohara E, Rai T, Sasaki S, Uchida S: Apical localization of renal K channel was not altered in mutant WNK4 transgenic mice. *Biochem Biophys Res Commun* 332: 750–755, 2005
22. Schambelan M, Sebastian A, Rector FC Jr: Mineralocorticoid-resistant renal hyperkalemia without salt wasting (type II pseudohypoaldosteronism). *Kidney Int* 19: 716–727, 1981
23. Xu B, English JM, Wilsbacher JL, Stippec S, Goldsmith EJ, Cobb MH: WNK1, a novel mammalian serine/threonine protein kinase lacking the catalytic lysine in subdomain II. *J Biol Chem* 275: 16795–16801, 2000
24. Xu BE, Min X, Stippec S, Lee BH, Goldsmith EJ, Cobb MH: Regulation of WNK1 by an autoinhibitory domain and autophosphorylation. *J Biol Chem* 277: 48456–48462, 2002
25. Kaissling B: Structural aspects of adaptive changes in renal electrolyte excretion. *Am J Physiol* 243: F211–F226, 1982
26. Dahlmann A, Pradervand S, Hummler E, Rossier BC, Frindt G, Palmer LG: Mineralocorticoid regulation of epithelial Na+ channels is maintained in a mouse model of Liddle's syndrome. *Am J Physiol Renal Physiol* 285: F310–F318, 2003
27. Hebert SC, Desir G, Giebisch G, Wang W: Molecular diversity and regulation of renal potassium channels. *Physiol Rev* 85: 319–371, 2005
28. Farfel Z, Iaina A, Levi J, Gafni J: Proximal renal tubular acidosis: Association with familial normaldosteronemic hyperpotassemia and hypertension. *Arch Intern Med* 138: 1837–1840, 1978
29. Kahle KT, Macgregor GG, Wilson FH, Van Hoek AN, Brown D, Ardito T, Kashgarian M, Giebisch G, Hebert SC, Boulpaep EL, Lifton RP: Paracellular Cl- permeability is regulated by WNK4 kinase: Insight into normal physiology and hypertension. *Proc Natl Acad Sci U S A* 101: 14877–14882, 2004
30. Yamauchi K, Rai T, Kobayashi K, Sohara E, Suzuki T, Itoh T, Suda S, Hayama A, Sasaki S, Uchida S: Disease-causing mutant WNK4 increases paracellular chloride permeability and phosphorylates claudins. *Proc Natl Acad Sci U S A* 101: 4690–4694, 2004
31. Vitari AC, Deak M, Morrice NA, Alessi DR: The WNK1 and WNK4 protein kinases that are mutated in Gordon's hypertension syndrome phosphorylate and activate SPAK and OSR1 protein kinases. *Biochem J* 391: 17–24, 2005
32. Moriguchi T, Urushiyama S, Hisamoto N, Iemura S, Uchida S, Natsume T, Matsumoto K, Shibuya H: WNK1 regulates phosphorylation of cation-chloride-coupled cotransporters via the STE20-related kinases, SPAK and OSR1. *J Biol Chem* 280: 42685–42693, 2005
33. Jeck N, Waldegger S, Lampert A, Boehmer C, Waldegger P, Lang PA, Wissinger B, Friedrich B, Risler T, Moehle R, Lang UE, Zill P, Bondy B, Schaeffeler E, Asante-Poku S, Seyberth H, Schwab M, Lang F: Activating mutation of the renal epithelial chloride channel ClC-Kb predisposing to hypertension. *Hypertension* 43: 1175–1181, 2004
34. Mayan H, Munter G, Shaharabany M, Mouallem M, Pauzner R, Holtzman EJ, Farfel Z: Hypercalciuria in familial hyperkalemia and hypertension accompanies hyperkalemia and precedes hypertension: Description of a large family with the Q565E WNK4 mutation. *J Clin Endocrinol Metab* 89: 4025–4030, 2004
35. Meneton P, Ichikawa I, Inagami T, Schnermann J: Renal physiology of the mouse. *Am J Physiol Renal Physiol* 278: F339–F351, 2000
36. Takaya J, Matsusaka T, Katori H, Tamura M, Miyazaki Y, Homma T, Ichikawa I: In situ demonstration of angioten-

sin-dependent and independent pathways for hyperaldosteronism during chronic extracellular fluid volume depletion. *Mol Endocrinol* 15: 2229–2235, 2001

37. Wang Z, Wang T, Petrovic S, Tuo B, Riederer B, Barone S, Lorenz JN, Seidler U, Aronson PS, Soleimani M: Renal and intestinal transport defects in Slc26a6-null mice. *Am J Physiol Cell Physiol* 288: C957–C965, 2005
38. Zhou X, Hansson GK: Effect of sex and age on serum biochemical reference ranges in C57BL/6J mice. *Comp Med* 54: 176–178, 2004
39. Canadian Council on Animal Care: Clinical biochemistry reference values, appendix V. In: *Guide to the Care and Use of Experimental Animals*, 2nd Ed., Ottawa, Canadian Council on Animal Care, 2005
40. Millar JA, Leckie BJ, Morton JJ, Jordan J, Tree M: A microassay for active and total renin concentration in human plasma based on antibody trapping. *Clin Chim Acta* 101: 5–15, 1980
41. Kotelevtsev Y, Brown RW, Fleming S, Kenyon C, Edwards CR, Seckl JR, Mullins JJ: Hypertension in mice lacking 11beta-hydroxysteroid dehydrogenase type 2. *J Clin Invest* 103: 683–689, 1999